Structure-function studies on the stereochemical promiscuity of ThDP-dependent enzymes

Inaugural-Dissertation

zur Erlangung des Doktorgrades
der Mathematisch-Naturwissenschaftlichen Fakultät
der Heinrich-Heine-Universität Düsseldorf

vorgelegt von

Anna Baierl
aus Duisburg

Ratingen, März 2018

aus dem Institut für Bio- und Geowissenschaften 1 (IBG-1: Biotechnologie)
des Forschungszentrums Jülich GmbH

Gedruckt mit der Genehmigung der
Mathematisch-Naturwissenschaftlichen Fakultät der
Heinrich-Heine-Universität Düsseldorf

Berichterstatter:
1. Prof. Dr. Martina Pohl
2. Prof. Dr. Vlada Urlacher

Tag der mündlichen Prüfung: 04.06.2018

SELBSTSTÄNDIGKEITSERKLÄRUNG

Hiermit versichere ich an Eides statt, dass die vorgelegte Dissertation „Structure-function studies on the stereochemical promiscuity of ThDP-dependent enzymes“ von mir selbstständig verfasst und unter ausschließlicher Verwendung der angegebenen Literatur und Hilfsmittel gemäß der „Grundsätze zur Sicherung guter wissenschaftlicher Praxis an der Heinrich-Heine-Universität Düsseldorf“ erstellt wurde.

Bisher habe ich keine erfolglosen Promotionsversuche unternommen und diese Dissertation an keiner anderen Fakultät vorgelegt.

_____ _____

Ort, Datum Anna Baierl

„Je mehr man schon weiß, desto mehr hat man noch zu lernen. Mit dem Wissen nimmt das Nichtwissen in gleichem Grade zu oder vielmehr das Wissen des Nichtwissens.“

Friedrich Schlegel, Athenaeum 1798

ACKNOWLEDGEMENTS

A PhD-thesis is never just the result of a single person's efforts, but also of the help of many. Therefore, I would like to thank all the people that made this thesis possible.

First of all, my deepest gratitude goes to my supervisor Prof. Dr. Martina Pohl for the possibility to work on this interesting and challenging project, and for her guidance and support, both scientifically and non-scientifically. Difficulties always appeared much easier after discussions with her.

I would also like to thank Prof. Dr. Vlada Urlacher, who has kindly agreed to be the co-referee of this thesis.

Further, I thank Prof. Dr. Wolfgang Wiechert for the opportunity to work under outstanding conditions at the IBG-1. In that respect I would also like to thank Dr. Iris Eggeling, Marianne Hess, Maria Lauer, Nina Böckmann and Marion Dreßen-Combach for their support regarding any organisational or administrative problem.

This project was part of the DFG research consortium FOR 1296 "Diversity of Asymmetric Thiamine Catalysis". I like to thank all the members for very inspiring and pleasant meetings and all the constructive discussions. Special thanks go to:

- Prof. Dr. Jürgen Pleiss together with Dr. Constantin Vogel, Dr. Silvia Fademrecht and Michaela Häcker for their input on the four-state stereoselectivity model and to Patrick Buchholz for developing a transketolase standard numbering scheme.
- Prof. Dr. Michael Müller and Jan-Patrick Steitz for their advice on the *Pp*YerE studies.
- Prof. Dr. Kai Tittmann together with Fabian Rabe von Pappenheim and Fabienne Libuda for discussions regarding the details of the transketolase reaction mechanism.
- Prof. Dr. Dörte Rother and Saskia Bock for their interest in my project, their valuable input in many fruitful discussions, and for sharing my enthusiasm to go swimming before breakfast.

Also outside the DFG-group I would like to thank all cooperation partners who have contributed to the progress of this work.

- Axel Theorell and Dr. Katharina Nöh for the cooperation regarding the Bayes-analysis of the results obtained with transketolase variants and for the patient introduction to the mysteries of statistical analysis.
- Dr. Jan Marienhagen for his advice regarding the design of the *Pp*YerE library.
- Prof. Dr. Helen Hailes for her interest in my project and helpful advice.
- Prof. Dr. Jörg Fitter for the possibility to measure CD-spectra at his institute and Dr. Tina Züchner for her assistance.
- Rainer Goldbaum and Laura Öhler for measuring NMR-spectra.

I was fortunate to be part of a great work group. Here, I want to thank all my colleagues for the excellent working atmosphere, productive discussions, and many joyful moments. Particularly, I would like to thank:

- Philipp Marquardt, Friederike Hoffmann, and Stephanie Moers for their performances in the course of their master theses, during which they generated and tested many transketolase variants.
- Lilia Arnold, Ilona Frindi-Wosch, Doris Hahn, Ursula Mackfeld, and Heike Offermann for their skilful assistance in the lab and for keeping the labs running smoothly by organising so many things in the background.
- Special thanks go to Ursula Mackfeld, for being my hands in the lab during the last months of my PhD project, during which she finalised many measurements, and for her ingenuity and persistence in developing analytical methods for the *Pp*YerE study.
- Dr. Zaira Maugeri for helping me with all chemistry problems.
- All other members of the "ivory tower" office: Dr. Victoria Steffen, Dr. Aischarya Brahma, Vanessa Erdmann, Julia Otten, and Reinhard Oeggl for making our office a delightful place and for providing new motivation whenever needed.
- The members of our carpool, Saskia Bock and Ramona Kloß and later also Jennifer Aschenbrenner and Christoph Westerwalbesloh, for many enjoyable riding hours that often gave creative and/or scientific input.

Last but not least, I want to thank my parents Petra and Thomas Baierl for their trust and constant support in all circumstances and my boyfriend Lucas Koijen, whose love and care always helped me to keep my spirits high.

ABSTRACT

Thiamine diphosphate (ThDP)-dependent enzymes are versatile tools catalysing the stereoselective formation of chiral building blocks such as α-hydroxy ketones. They can be categorised in nine structural superfamilies, which all share two conserved domains that form the active site with ThDP bound at the domain interface. Of these, the family of ThDP-dependent decarboxylases (DCs) has been studied most extensively. In previous studies, a highly predictive two-state model has been developed that explains the stereoselectivity of DCs for the 1,2-additions of (decarboxylated) α-ketoacids (donor substrate) and aldehydes (acceptor substrate) by the relative orientation of the substrate side chains prior to C-C-bond formation. This model enables the stereoinversion of the predominantly *R*-selective DCs with few amino acid substitutions that open a pocket as an alternative binding site of the acceptor side chain (antiparallel to the donor side chain), which is a prerequisite for *S*-selectivity. The aim of this thesis was to evaluate the model for further ThDP-dependent DCs (1) and to transfer the model on another structural family of ThDP-dependent enzymes, the transketolases (TKs) (2).

(1*) Evaluation of the stereoselectivity model for YerE from Pseudomonas protegens (PpYerE)*
*Pp*YerE catalyses the *R*-selective carboligation of (decarboxylated) pyruvate with non-activated ketones besides aldehydes as acceptor substrates, which increases the product platform that is accessible with ThDP-dependent DCs. An antiparallel acceptor binding pocket could be opened by a single amino acid substitution (V479A), but the size of this pocket was restricted by the backbone of an α-helix. Several attempts to enlarge the pocket to host a phenylring did not succeed in creating *S*-selective variants for the formation of phenylacetylcarbinol (PAC) from pyruvate (donor) and benzaldehyde (acceptor). However, for the smaller acceptor substrates n-pentanal and propanal the stereoselectivity could be shifted towards the *S*-product, even though no high enantiomeric excess was achieved. The stereoselectivity with hexan-3,4-dion as acceptor was as well influenced. This shows that the stereoselectivity model is also valid for *Pp*YerE, but not generally applicable for stereoinversion with large acceptor substrates.

(2) Transfer of the stereoselectivity model on transketolases (TKs)
Transketolases are *S*-selective even though no antiparallel acceptor binding pocket could be found within the active site. To explain this natural *S*-selectivity, the existing stereoselectivity model was extended based on literature data, yielding a four-state model that includes the relative orientation of the substrate functional groups. As a consequence, two strategies may be followed to create TK variants with inverted stereoselectivity: i. opening of an antiparallel acceptor binding pocket as described for DCs and ii. changing the orientation of the acceptor carbonyl group relative to the donor hydroxy group. Both strategies were investigated by site-directed mutagenesis studies with *Escherichia coli* TK (*Ec*TK). Overall, the four-state model proved to be far more complex and less predictive than the two-state model. Nevertheless, it provides a first framework to understand the mechanism steering the stereoselectivity of TKs. Thereby, H26, H261 and F434 were identified as key-residues to influence the stereoselectivity.

ZUSAMMENFASSUNG

Thiamindiphosphat (ThDP)-abhängige Enzyme sind vielseitige Werkzeuge, welche die stereoselektive Bildung chiraler Bausteine, wie z.B. α-Hydroxyketone, katalysieren. Sie lassen sich in neun strukturelle Familien einteilen. Diese haben zwei konservierte Domänen gemeinsam, welche das aktive Zentrum bilden in dem ThDP an der Grenzfläche der Domänen gebunden ist. Von diesen wurde die Familie der ThDP-abhängigen Decarboxylasen (DCs) am intensivsten untersucht. In früheren Studien wurde ein sehr vorhersagekräftiges 2-Zustands-Modell entwickelt, das die Stereoselektivität von DCs für 1,2-Additionen von (decarboxylierten) α-Ketosäuren (Donorsubstrat) und Aldehyden (Akzeptorsubstrat) durch die relative Orientierung der Substratseitenketten vor der C-C-Bindungsknüpfung erklärt. Dieses Modell ermöglicht die Stereoinversion der vorwiegend *R*-selektiven DCs durch Substitution weniger Aminosäuren, wodurch eine Tasche als alternative Bindestelle für die Akzeptorseitenkette geöffnet wird (antiparallel zur Donorseitenkette), was eine Voraussetzung für *S*-Selektivität ist. Das Ziel dieser Arbeit war es, das Modell für weitere ThDP-abhängige DCs zu evaluieren (1) und auf eine andere strukturelle Familie von ThDP-abhängigen Enzymen, die Transketolasen, zu übertragen (2).

(1) Evaluierung des Stereoselektivitätsmodells für YerE aus Pseudomonas protegens (PpYerE)
*Pp*YerE katalysiert die *R*-selektive Carboligation von Pyruvat und nicht aktivierten Ketonen, zusätzlich zu Aldehyden, als Akzeptorsubstrate, wodurch die Produktplattform von ThDP-abhängigen DCs vergrößert wird. Eine antiparallele Akzeptor-Bindetasche konnte durch Substitution einer einzelnen Aminosäure (V479A) geöffnet werden, aber die Größe dieser Tasche wurde durch das Rückgrat einer α-Helix begrenzt. In verschiedenen Ansätzen zur Vergrößerung der Tasche für die Aufnahme eines Phenylrings gelang es nicht, *S*-selektive Varianten für die Bildung von Phenylacetylcarbinol aus Pyruvat (Donor) und Benzaldehyd (Akzeptor) zu erzeugen. Für die kleineren Akzeptorsubstrate n-Pentanal und Propanal konnte die Stereoselektivität jedoch in Richtung des *S*-Produkts verschoben werden, obwohl kein hoher Enantiomerenüberschuss erzielt wurde. Die Stereoselektivität mit Hexan-3,4-dion wurde ebenfalls beeinflusst. Dies zeigt, dass das Stereoselektivitätsmodell zwar auch für *Pp*YerE gültig ist, aber nicht generell für die Stereoinversion mit großen Akzeptorsubstraten anwendbar ist.

(2) Übertragung des Stereoselektivitätsmodells auf Transketolasen (TKs)
Transketolasen sind *S*-selektiv, obwohl keine antiparallele Akzeptor-Bindetasche im aktiven Zentrum gefunden werden konnte. Um diese natürliche *S*-Selektivität zu erklären, wurde das bestehende Stereoselektivitätsmodell basierend auf Literaturdaten zu einem 4-Zustands-Model zu erweitert, das zusätzlich die relative Orientierung der funktionellen Gruppen der Substrate beinhaltet. Demnach können zwei Strategien verfolgt werden, um TK-Varianten mit umgekehrter Stereoselektivität zu erzeugen: i. die Öffnung einer antiparallelen Akzeptor-Bindetasche, wie es für DCs beschrieben ist, und ii. die Änderung der Orientierung der Akzeptor-Carbonylgruppe relativ zur Donor-Hydroxygruppe. Beide Strategien wurden durch ortsspezifische Mutagenesestudien mit *Escherichia coli* TK (*Ec*TK) untersucht. Insgesamt erwies sich das 4-Zustands-Modell als weitaus komplexer und weniger vorhersagekräftig als das 2-Zustands-Modell. Dennoch bietet es einen ersten Rahmen, um den Mechanismus, der die Stereoselektivität von TKs steuert, zu erklären. Dabei wurden H26, H261 und F434 als Schlüsselstellen identifiziert, um die Stereoselektivität zu beeinflussen.

TABLE OF CONTENT

LIST OF ABBREVIATIONS

Abbreviations for enzymes

*Ap*PDC	pyruvate decarboxylase from *Acetobacter pasteurianus*
*Bs*MenD	2-succinyl-5-enolpyruvyl-6-hydroxy-3-cyclohexene-1-carboxylate synthase from *Bacillus subtilis*
*Ec*AHAS	acetohydroxyacid synthase from *Escherichia coli*
*Ec*MenD	2-succinyl-5-enolpyruvyl-6-hydroxy-3-cyclohexene-1-carboxylate synthase from *Escherichia coli*
*Ec*TK	transketolase from *Escherichia coli*
*Gst*TK	transketolase from *Geobacillus stearothermophilus*
*Pf*BAL	benzaldehyde lyase from *Pseudomonas fluorescens*
*Pp*BFD	benzoylformate decarboxylase from *Pseudomonas putida*
*Pp*YerE	YerE from *Pseudomonas protegens*
*Sc*PDC	pyruvate decarboxylase from *Saccharomyces cerevisiae*
*Sc*TK	transketolase from *Saccharomyces cerevisiae*
*Yp*YerE	YerE from *Yersinia pseudotuberculosis*

Abbreviations for chemical compounds

3-FBA	3-formylbenzoic acid
3-HBA	3-hydroxybenzaldehyde
3-HH	3-hydroxyheptan-2-one
3-HP	3-hydroxypentan-2-one
4-FBA	4-formylbenzoic acid
ADP	adenosine diphosphate
AMP	adenosine monophosphate
ATP	adenosine triphosphate
DHH	1,3-dihydroxyheptan-2-one
DHP	1,3-dihydroxypentan-2-one
DMSO	dimethyl sulfoxide
E4P	erythrulose-4-phosphate
EDTA	ethylenediaminetetraacetic acid
EHH	3-ethyl-3-hydroxyhexan-2,4-dion
F6P	fructose-6-phosphate
FAD	flavin adenine dinucleotide
G3P	glyceraldehyde-3-phosphate
HMH	3-hydroxy-3-methylheptan-2-one
HMP	3-hydroxy-3-methylpentan-2-one
HPA	3-hydroxypyruvate
HPP	2-hydroxypropiophenon
IPTG	isopropyl-b-D-1-thiogalactopyranoside
MTBE	methyl *tert*-butyl ether
PAC	phenylacetylcarbinol
R5P	ribose-5-phosphate
S7P	sedoheptulose-7-phosphate
SDS	sodium dodecyl sulfate
SEPHCHC	2-succinyl-5-enolpyruvyl-6-hydroxy-3-cyclohexene-1-carboxylate

ThDP	thiamine diphosphate
Tris	tris-(hydroxymethyl)-aminomethane
TTC	2,3,5-triphenyl tetrazoliumchloride
X5P	xylulose-5-phosphate

Further abbreviations

AI-medium	auto-induction medium
aKADH1	α-ketoacid dehydrogenase 1
aKADH2	α-ketoacid dehydrogenase 2
aKGDH	α-ketoglutarate dehydrogenase
bp	base pairs
BSA	bovine serum albumin
CCE	crude cell extract
CD	circular dichroism
ddH_2O	deionised water
DC	decarboxylase
DFG	Deutsche Forschungsgemeinschaft
DNA	deoxyribonucleic acid
DXPS	1-deoxy-D-xylulose-5-phosphate synthase
e.g.	example given
ee	enantiomeric excess
FD	fast digest
FID	flame ionisation detector
GC	gas chromatography
HPLC	high-performance liquid chromatography
i.e.	in explicit
KP_i-buffer	potassium phosphate buffer
LB-medium	lysogeny broth medium
MS	mass spectrometry
NMR	nuclear magnetic resonance
OR	oxidoreductase
PAGE	polyacrylamide gel electrophoresis
PCR	polymerase chain reaction
PDB	Protein Data Base
PPDC	phosphonopyruvate decarboxylase
PP-domain	pyrophosphate binding domain
Pyr-domain	pyrimidine binding domain
SPDC	sulfopyruvate decarboxylase
TEED	ThDP-dependent Enzyme Engineering Database
TK	transketolase
UV	ultraviolet
wt	wildtype

1 INTRODUCTION

1.1 Enzyme catalysis

Although the existence of microorganisms and enzymes was not yet known, both were already used biotechnologically to produce bread, cheese, beer and wine thousands of years ago. Up to today more than 60 % of the total enzyme market are still dedicated to food and beverage processing, including animal feed (Sheldon and Pereira, 2017). However, in the past 30 years enzymes also got more and more recognised as catalysts for organic synthesis. Two driving forces behind that process were the development of recombinant DNA technologies (Bornscheuer, 2016) and an understanding for the impact of chirality on the properties of pharmaceutically active compounds. The latter resulted in stronger regulations by the FDA, which required separate testing of both enantiomers of chiral drugs by the manufacturers. In praxis the production of enantiomerically pure products is therefore preferred, which creates a need for effective asymmetric synthesis methods (Sheldon and Pereira, 2017). Moreover, the upcoming issues of sustainability and eco friendliness encourage the use of enzymes. In that regard, the twelve principles of green chemistry have become a popular guideline to rate the sustainability of a process. These principles address all steps of the process line, including the process efficiency, the choice of substrates, reagents, and solvents, the process safety, and the properties of the products (Anastas and Zimmerman, 2007; Poliakoff and Licence, 2007; Tang et al., 2005). A condensed version of the twelve principles is shown in Figure 1-1.

Figure 1-1: Twelve principles of green chemistry according to Poliakoff and Licence, 2007

Enzyme catalysis meets the requirements of green chemistry in many aspects that are summarised in the following according to Sheldon, 2016:

- Being catalysts themselves, enzymes already fulfil one of the twelve criteria of green chemistry. They are characterised by a **high efficiency** and enhance the reaction rate 10^7- to 10^{19}-fold compared to non-catalysed reactions, which is more than chemical catalyst typically achieve (Faber, 2011; Wolfenden and Snider, 2001). Therefore, lower catalyst loads are required in

enzyme catalysis. In contrast to organometallic catalysts that are frequently used for cross-coupling reactions, enzymes are non-hazardous, degradable, and can be produced from renewable resources.

- Enzyme-catalysed reactions can usually be performed under **mild reaction conditions** concerning pH, temperature and pressure. This intrinsically leads to a safer and more environmental friendly process and decreases the amount of energy that is needed to maintain the reaction conditions, e.g. the temperature or the pressure. Moreover, the formation of side products, for example due to isomerisation or racemisation, is less likely under mild reaction conditions, which increases the atom efficiency. The comparable conditions of many enzyme-catalysed reactions also increase the compatibility of multiple reactions in cascade processes.

- An important characteristic of enzymes is their **high selectivity** regarding the specific reactivity for one type of functional groups (chemoselectivity), the distinction of the relative position of (identical) functional groups (regioselectivity), and the preference for one specific stereoisomer in both product formation and substrate specificity (stereoselectivity). In contrast, chemical synthesis often suffers from low selectivity. Frequently, it requires auxiliary reactions, like activation, protection, or deprotection of functional groups that can be omitted in enzyme catalysis. Especially high stereoselectivity is difficult to obtain in chemical synthesis. Other options are the separation of racemates, which is limited to 50 % yield, and the isolation of enantiomerically pure compounds from natural sources, which usually contain only low concentrations of the desired product. Therefore, enzyme catalysis increases the step-and atom efficiency of a process and helps to prevent wastes.

1.1.1 Limitations of enzyme catalysis

Despite their high potential, the use of enzymes entails certain disadvantages, which are in some way related to their supposed environmental friendliness.

Most biocatalytic processes use water as a solvent. Even though water is often regarded an environmentally compatible solvent, the use of water as solvent entails certain disadvantages (Ni et al., 2014). Due to its high polarity, the solubility of organic compounds in water is usually low, which reduces the substrate load and thereby the attainable product yield. Moreover, the product retrieval from water is often laborious and may for example require the extraction with organic solvents. This, as well as contamination with microorganisms, necessitates follow up treatment of the waste water, lowering the eco-efficiency and increasing the costs of a process (Burton et al., 2002).

Natural evolution has shaped enzymes as highly efficient and specialised catalysts that operate best under natural, above mentioned mild reaction conditions. However, evolution has not optimised enzymes for the conditions of an industrial process, which may vary greatly from the conditions found in nature. As a consequence, enzymes do not always meet the process demands regarding their activity, stability and selectivity. Further, an efficient process requires high product- and thereby also high substrate concentrations. This is often as well limiting, since typical concentrations at process conditions are inhibitory for many enzymes. (Huisman and Collier, 2013; Otte and Hauer, 2015; Woodley, 2013).

There are different possibilities to overcome these limitations. Besides the adaptation of the process, which includes optimisation of reaction conditions and the choice of the appropriate process design, e.g. of a continuous or discontinuous process, the adaptation of the catalyst by enzyme engineering is an efficient approach, which was followed in this thesis.

1.1.2 Enzyme Engineering

A precondition for the development of enzyme engineering was the discovery of recombinant DNA technology, which initiated the so-called first wave of protein engineering around 1985. This phase was characterised by rational protein design based on site-directed mutagenesis but also site-saturation mutagenesis (Bommarius, 2015). This approach requires a fundamental understanding of the targeted enzyme, e.g. regarding its structure and its functional mechanism (Li and Cirino, 2014). The following second wave of enzyme engineering was the phase of directed evolution, employing random mutagenesis and recombination protocols. In contrast to rational design, directed evolution requires no prior knowledge but instead high-performing selection or screening systems, which can be a limiting factor depending on the screened parameter and on the available resources (Porter et al., 2016). Therefore, rational design and directed evolution were combined to semi rational protein engineering in the third wave of enzyme engineering (Bommarius, 2015). This approach aims to create data-driven, "smart" libraries by utilising knowledge, for example from the enzyme structure or mutagenesis studies, to decrease the library size. Thereby, the coverage of a bigger sequence space is retained, and the size of a library is ultimately dependent on the available knowledge and the screening capacity. Typical techniques are the use of restricted libraries, in which positions in a target enzyme are not fully saturated but replaced by a reduced set of amino acids, combinatorial active-site saturation testing (CASTing), and iterative saturation mutagenesis (ISM), which both address several positions of an enzyme, either simultaneously or consecutively (Reetz et al., 2008, 2006). Recently, computational approaches, like molecular dynamics modelling or quantum mechanical modelling, have gained more and more impact for enzyme engineering. This can support established enzyme engineering techniques but also led to the first successes in de novo design of artificial enzymes (Hilvert, 2013).

Overall, enzyme engineering has been established as a potential tool for example to improve the turnover, alter functionalities and (stereo-) selectivities, enable the conversion of non-natural substrates, as well as to increase the stability and/or activity especially with respect to non-physiological reaction conditions including micro-aqueous and organic media (Burton et al., 2002). Moreover, the engineering of enzymes catalysing non-natural reactions that were exclusively accessible by chemical synthesis before, is possible (Hammer et al., 2017). However, a major drawback of enzyme engineering is that it is often very time consuming and thus does not meet the short development times demanded by the pharmaceutical industry as a key requirement (Truppo, 2017).

1.1.3 Toolbox concept

The establishment of enzyme toolboxes is one way to address the issue of time-consuming enzyme development. Such toolboxes comprise enzymes that catalyse the same reaction type but differ in their substrate scope and selectivity, and thus provide access to a broad (enantio-complementary) product platform. Besides above described means of enzyme engineering, the mining of databases and

metagenomes and the exploration of the catalytic promiscuity of enzymes are further tools to build up and to extend enzyme toolboxes (Davids et al., 2013).

A toolbox of ThDP-dependent enzymes has been developed by Pohl and co-workers which up to know contains 20 wildtype enzymes and more than 150 variants (Gocke, 2007; Gocke et al., 2010). This toolbox gives access to chiral α-hydroxy ketones, which are valuable building blocks in chemical synthesis due to their chiral centre with a vicinal prochiral group (Sukumaran and Hanefeld, 2005). With a single reducing step using alcohol dehydrogenases or amination step using transaminases 1,2-diols and amino alcohols can be formed, respectively, which are building blocks of pharmaceutically active compounds or even pharmaceutically active themselves (Sehl et al., 2015, 2014; Wachtmeister et al., 2016). While chemical synthesis of α-hydroxy ketones suffers from many steps resulting in lower yields and high waste production, ThDP-dependent enzymes offer an alternative route in which α-hydroxy ketones are synthesised from inexpensive aldehydes in one single step with high stereoselectivity (Hoyos et al., 2010).

1.2 ThDP-dependent enzymes

ThDP-dependent enzymes catalyse the formation and cleavage of C-C, C-O, C-S, C-N, and C-P bonds and thus play an essential role for different reactions in the anabolic and catabolic metabolism. For example, ThDP-dependent enzymes are involved in the tricarboxylic acid cycle, the pentose phosphate pathway and the biosynthesis of amino acids and neurotransmitters (Frank et al., 2007). They are classified as oxidoreductases, transferases and lyases and can be found in all organisms (Widmann et al., 2010). The ThDP-dependent Enzyme Engineering Database (TEED, https://teed.biocatnet.de/), which is part of the BioCatNet database, offers a comprehensive overview over ThDP-dependent enzymes and currently contains 119566 sequence and 308 structure entries (January 2018) (Buchholz et al., 2016; Widmann et al., 2010)

1.2.1 The cofactor ThDP

ThDP is the biologically active derivative of thiamine, which is also known as vitamin B_1. The phosphorylation of thiamine to ThDP is catalysed by a thiamine diphosphokinase and consumes ATP (Figure 1-2 A, Leuthardt and Nielsen, 1952; Steyn-Parvé, 1952). Thiamine is exclusively synthesised by bacteria, fungi and plants, making it an essential nutrient for humans and animals (Frank et al., 2007). As thiamine is needed in the carbohydrate metabolism as well as for the function of nerves and heart, thiamine deficiency leads to severe diseases. The most commonly known of them is beriberi, which is a collective name for several symptoms that affect the peripheral nervous system, the cardiovascular system and the digestive system, but also Alzheimer's disease and Parkinson's disease have been related to thiamine deficiency (Costantini et al., 2013; Gibson et al., 2016; Kerns and Gutierrez, 2017; Stewart, 1990; Williams et al., 1940).

Already in 1943 ThDP was shown to be a catalyst for acyloin condensations on the example of the benzoin condensation from two benzaldehyde molecules (Hönig et al., 2017; Ukai et al., 1943). However, outside the globular protein environment ThDP exhibits only minor catalytic activity compared to the protein-bound form. This can be explained by the highly conserved V-conformation

that ThDP adopts when it is bound in enzymes (Andrews et al., 2013; Muller et al., 1993). This conformation enables the activation of ThDP by deprotonation of the C2-carbon atom of the thiazolium ring, forming a nucleophilic ylide that can attack electrophilic moieties (Figure 1-2 B) (Breslow, 1958, 1957). The activation of ThDP is supported by a highly conserved glutamate residue that abstracts a proton from the N1'-nitrogen atom of the pyrimidine ring and thereby induces the formation of a 1',4'-imino tautomer in the pyrimidine ring. Due to the V-conformation, the 4'-imino group is in reactive distance to the thiazolium ring and can thus abstract a proton from the C2 atom (Hübner et al., 1998; Kern et al., 1997). This activation is essential for the catalytic activity of ThDP, which is described in the following chapter.

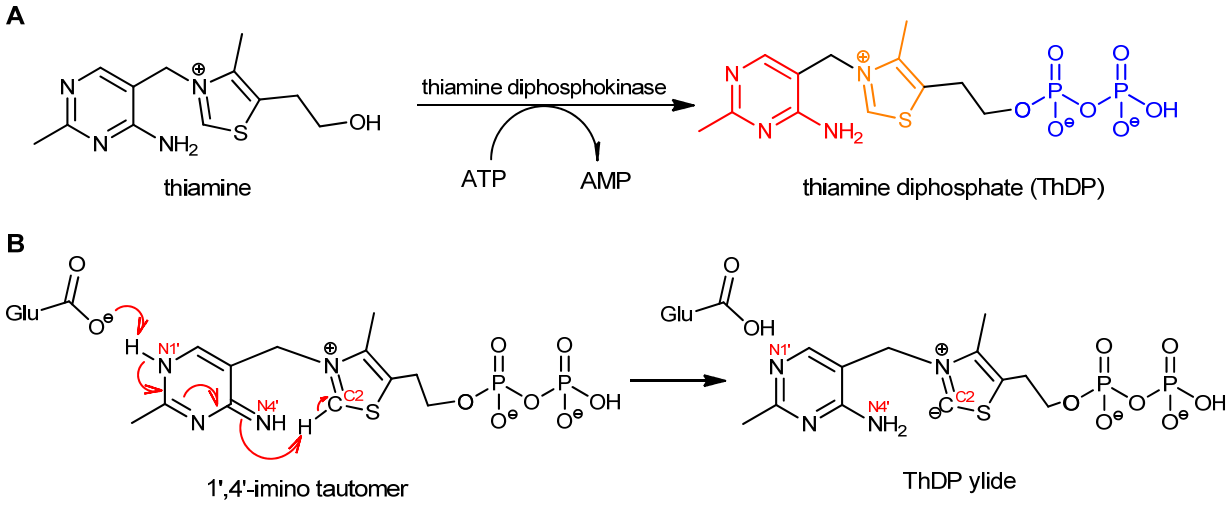

Figure 1-2: Synthesis, structure and activation of thiamine diphosphate (ThDP). A: Thiamine diphosphokinase phosphorylates thiamine under ATP consumption (Steyn-Parvé, 1952). ThDP is composed of an aminopyrimidine ring (red), a thiazolium ring (orange) and a diphosphate group (blue). ATP=adenosine triphosphate, AMP=adenosine monophosphate; **B:** Activation of ThDP according to Frank et al., 2007. From the N1'-nitrogen of the imino-form a proton is abstracted from by a glutamate residue, leading to the deprotonation of the C2 atom of the thiazolium ring by the N4'-nitogen via a relay system.

1.2.2 Catalytic cycle of ThDP-dependent enzymes

In Figure 1-3 the reaction mechanism is exemplarily shown for C-C bond forming or cleaving reactions. The reaction starts with a nucleophilic attack of the ThDP C2-atom on the carbonyl C-atom of the donor substrate, which may amongst others be an α-keto acid, an aldehyde, an α-hydroxy ketone or a ketose. During the nucleophilic attack the donor is covalently bound to C2-ThDP (**b**). After elimination of a leaving group from the ThDP-donor adduct (**c**), a carbanion-enamine is formed, which is also called "active aldehyde" or "Breslow-intermediate". This leaving group is CO_2, a proton, an aldehyde, or an aldose for the donor substrate named above, respectively. The carbanion-enamine exhibits a nucleophilic activity at the previously electrophilic carbon atom of the former donor substrate (Kluger and Tittmann, 2008). This reversal of the polarity is called *Umpolung* and allows a second nucleophilic attack on the carbonyl C-atom of an acceptor substrate, e.g. an aldehyde (**d**). After deprotonation the product is released (**e**) and the cofactor is regenerated. Besides aldehydes, also other molecules, like aldoses, α-keto acids, or ketones, can serve as acceptor substrate. In the case of C-C bond cleavage the acceptor is a proton and the respective aldehyde is released.

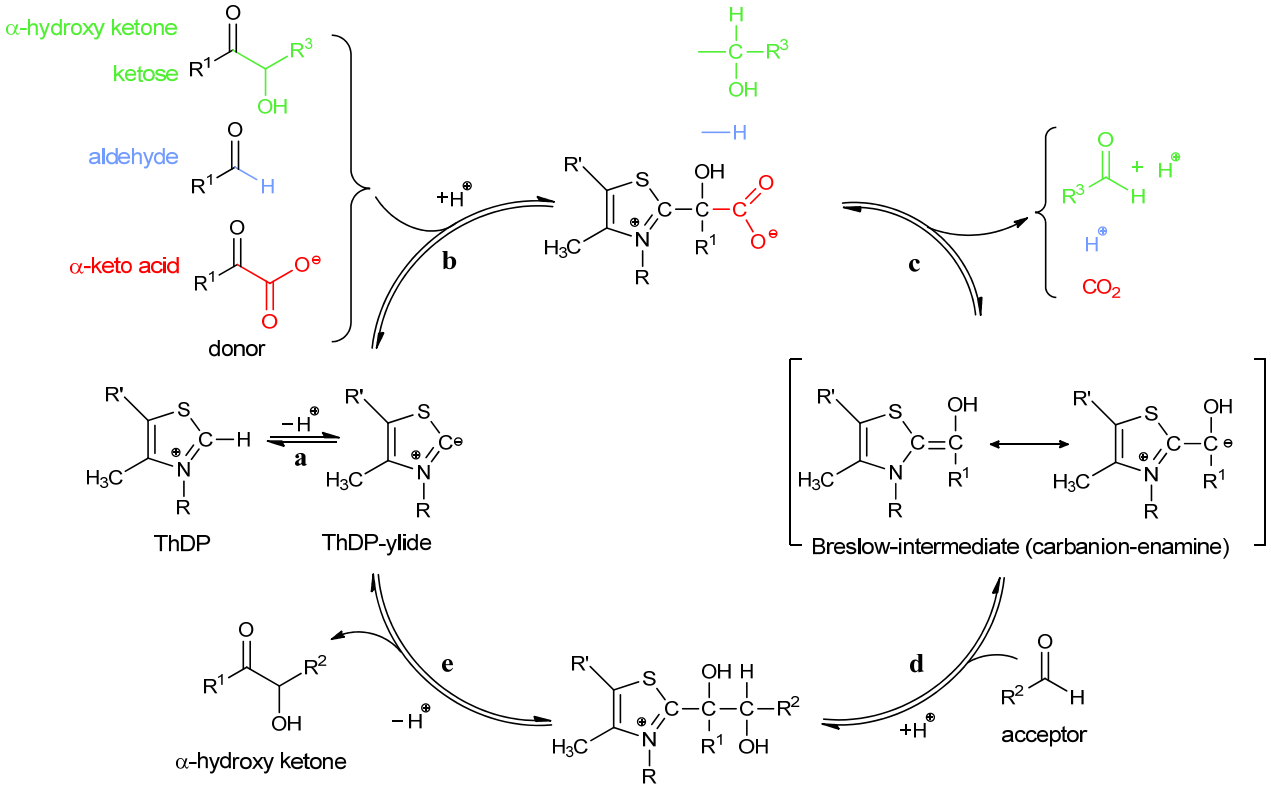

Figure 1-3: Catalytic cycle for the formation of α-hydroxy ketones by ThDP-dependent enzymes. a: activation of the cofactor ThDP. b: nucleophilic attack of the ylide on the donor substrate, c: elimination of a leaving group from the ThDP-donor adduct, d: nucleophilic attack of the carbanion-enamine on the acceptor substrate, e: product release and regeneration of ThDP. R: ThDP-pyrimidine ring; R': ThDP-diphosphate group. Typical donor substrates in this thesis were: pyruvate (R^1=CH_3), 3-hydroxypyruvate (R^1=CH_2-OH) and benzaldehyde (R^1=C_6H_5), typical acceptor substrates were benzaldehyde (R^2=C_6H_5), n-pentanal (R^2=C_4H_9), propanal (R^2=C_2H_5), and acetaldehyde (R^2=CH_3).

Even though the cofactor is the catalytically active component of ThDP-dependent enzymes, the amino acid residues surrounding ThDP in the active site are decisive for the catalysed reaction. Besides maintaining the V-conformation of the cofactor, the enzyme provides the residues for a proton relay system to support the protonation and deprotonation steps during the catalytic cycle (Figure 1-3). Further, active site residues probably play a role in the stabilisation of reaction intermediates like the carbanion-enamine (Frank et al., 2007; Huang et al., 2001). Apart from that, factors like substrate specificity, chemoselectivity or stereoselectivity are determined by the enzyme structure and the architecture of the active site (Vogel and Pleiss, 2014).

1.2.3 Structure of ThDP-dependent enzymes

On the level of the primary structure ThDP-dependent enzymes show only low homology with usually less than 20 % sequence identity even between enzymes catalysing similar reactions (Frank et al., 2007). However, the tertiary structure of ThDP-dependent enzymes contains several conserved folds and the architecture of the active site is highly conserved which originates from a similar binding pocket for the cofactor ThDP (Vogel and Pleiss, 2014). This structural homology indicates a divergent evolution from a common ancestor, in which selective pressure on the ThDP-binding residues maintained their geometrical position while other substitutions were tolerated (Frank et al., 2007).

The cofactor is always bound on the interface of two catalytic domains that have been described for all ThDP-dependent enzymes:

- The **Pyr-domain** interacts with the pyrimidine ring of ThDP. It also contains the highly conserved glutamate residue involved in cofactor activation (Duggleby, 2006; Muller et al., 1993).
- The **PP-domain** contains a $GDGX_{25\text{-}30}N$ motif that binds a divalent cation (i.e. Mg^{2+}) which serves as an anchor for the ThDP diphosphate group (Duggleby, 2006; Hawkins et al., 1989; Muller et al., 1993; Schenk et al., 1997).

Both domains have the same ThDP-binding fold that consists of six central parallel β-strands, flanked by α-helices in an α–β–α sandwich structure, which hints to their evolutionary relationship (Duggleby, 2006; Muller et al., 1993; Vogel and Pleiss, 2014). Additionally, ThDP-dependent enzymes often feature one or more additional domains, like the TKC-domain, the TH3-domain or the ATN-domain, that were assumedly recruited later in the evolutionary process (Table 1-1). They are not involved in cofactor binding and the function is hitherto mostly unknown, although regulatory functions have been proposed (Lindqvist et al., 1992). For the TKC-domain this is supported by the observation that deletion of the entire domain increases the specific activity of *Escherichia coli* transketolase (*Ec*TK) (Costelloe et al., 2008). Also for the TH3-domain examples for binding of allosteric activators have been described (König et al., 2009; Kutter et al., 2009). In some enzymes the TH3-domain binds additional cofactors like FAD or ADP (Lindqvist and Schneider, 1993; Werther et al., 2010).

Based on their modular structure, ThDP-dependent enzymes can be classified in nine different structural superfamilies, which are summarised in Table 1-1 (Vogel and Pleiss, 2014; Widmann et al., 2010). These families are characterised by four aspects:

- **Encryption of the Pyr- and the PP-domain on gene level:** While the Pyr-domain and the PP-domain are the common structural elements of all ThDP-dependent enzymes, they differ in how the domains are encoded on their genes (Widmann et al., 2010). For two structural superfamilies (aKADH2, SPDC) the catalytic domains are encoded on different genes. For all other families both domains are encoded on a single gene with either an N-terminal Pyr-domain and a C-terminal PP-domain (DC, OR, PPDC) or vice versa (TK, DXPS, aKADH1, aKGDH)

- **ThDP-binding mode:** ThDP is always bound at the interface of the Pyr- and the PP-domain. For all structural superfamilies in which both domains are encoded in one gene, the cofactor can consequently either be bound at the interface of the Pyr- and PP-domain from the same monomer (intra-monomer type), or at the interface of two monomers that form a dimer (inter-monomer type) (Vogel and Pleiss, 2014). Four structural families (DC, TK, aKADH1, aKGDH) belong to the inter-monomer type and two families (DXPS, OR) belong to the intra-monomer type. For the PPDC structural family the type is unknown, as no structural information are available.

- **Additional domains:** The number of additional domains to the Pyr- and the PP-domain varies from no (SPDC, PPDC) up to five (OR) additional domains, which are located C- or N-terminally or in between the catalytical domains. The TKC domain is represented in most superfamilies (TK, DXPS, OR, aKADH1, aKADH2, aKGDH), while the TH3-domain is specific for the DC-family. The aKGDH-family encompasses 2-oxoglutarate dehydrogenases

(OGDH) and 2- oxoglutarate decarboxylases (OGDC), of which only OGDCs contain the ATN-domain (Vogel and Pleiss, 2014).

- **Differentiation on the sequence level:** The superfamilies of TKs, aKADH1s and aKGDH share the same specific domain arrangement. Nevertheless, they were assigned to different superfamilies, as they clearly differ on sequence level (Vogel and Pleiss, 2014).

Table 1-1: Structural families of ThDP-dependent enzymes according to Widmann et al., 2010. The numbers of sequences and structures a given for the BioCatNet TEED in January 2018.

structural family	structural domain arrangement	ThDP-binding	№ of sequences	№ of structures
decarboxylases (DC)		inter-monomer	39289	138
transketolases (TK)		inter-monomer	22617	43
1-deoxy-D-xylulose-5-phosphate synthase (DXPS)		intra-monomer	9259	2
oxidoreductases (OR)	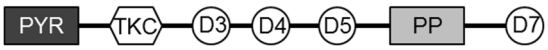	intra-monomer	16994	14
α-ketoacid dehydrogenases 1 (aKADH1)		inter-monomer	4966	12
α-ketoacid dehydrogenases 2 (aKADH2)		-	17776	85
sulfopyruvate decarboxylases (SPDC)		-	439	0
phosphonopyruvate decarboxylases (PPDC)	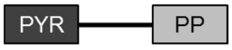	unknown	791	0
α-ketoglutarate dehydrogenases (aKGDH)	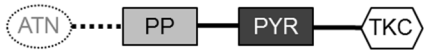	inter-monomer	7435	14

The smallest functional units found for ThDP-dependent enzymes are dimers. For all structural families of the inter-monomer type this is directly related to the requirement of two monomers to form the active site, with ThDP bound at the interface of the monomers. However, also for the intra-monomer type no monomeric enzymes have been found, yet. Also enzymes of the structural families with their PP- and PYR domain separated on different chains form $\alpha_2\beta_2$- heterotetrametric complexes (aKADH2) or $\alpha_6\beta_6$-heterododecameric complexes (SPDC), so that always at least two active sites are present in an enzyme (Vogel and Pleiss, 2014).

ThDP-dependent enzymes of the DC-family were most frequently observed as homodimers or homotetramers, whereas the latter are best described as dimers of dimers (Duggleby, 2006). Besides

also higher-order oligomers, like octamers, have been described in solution (Mücke et al., 1995; Pohl et al., 1994). Members of the TK-family are predominantly homodimers, but a minority of transketolases was found to have the PP and PYR domains split to different protein chains and are thus heterotetramers (Vogel and Pleiss, 2014).

1.2.4 Standard-numbering schemes

Despite high structural similarity, the sequence identity of ThDP-dependent enzymes is generally low. This hinders the identification of homologous amino acids in sequences of different proteins and thus the comparison of results and the assignment of functional or structural roles to specific residues. Standard numbering schemes provide a useful tool for the unambiguous identification of amino acid residues and have therefore been employed for several protein families. A standard numbering scheme for ThDP-dependent decarboxylases was developed by Pleiss and co-workers (Vogel et al., 2012). The scheme was derived from structure-guided multi-sequence alignments of 16 representative ThDP-dependent decarboxylases, using the sequence of the pyruvate decarboxylase form *Saccharomyces cerevisiae* (*Sc*PDC) as a reference for numbering of the amino acid positions. In the course of this thesis an analogous numbering scheme for the structural family of transketolases became available (Baierl et al., 2018). Here, the sequence of the transketolase from *Escherichia coli* (*Ec*TK) was used as the reference. Both numbering schemes are implemented as work tools within the BioCatNet TEED-database (Buchholz et al., 2016; Widmann et al., 2010). In the following chapters standard positions of amino acids in ThDP-dependent enzymes other than *Sc*PDC and *Ec*TK are indicated by numbers in brackets after the protein specific amino acid position at the first mention.

1.3 ThDP-dependent decarboxylases (DCs)

ThDP-dependent DCs are the best characterised structural superfamily with the highest number of sequences and structures within the TEED-database (Table 1-1, Widmann et al., 2010). In the following, ThDP-dependent DCs relevant for this thesis are briefly introduced.

1.3.1 Description of specific DCs

Benzaldehyde lyase from Pseudomonas fluorescens (PfBAL)

Benzaldehyde lyase (BAL) was first isolated from *Pseudomonas fluorescens* in 1989 (González and Vicuña, 1989). The *bznB* gene (former name *bzl*) from *Pseudomonas fluorescens*, which encodes for *Pf*BAL, was cloned and sequenced in 1994, allowing more detailed characterisation of the enzyme (Hinrichsen et al., 1994). While the physiological function of BAL is still unknown, it catalyses the cleavage of (*R*)-benzoin and (*R*)-benzoin derivatives to two molecules of benzaldehyde or the respective derivatives (Figure 1-4 A). Thereby, it enables *Pseudomonas fluorescens* to grow on benzoin and anisoin (4,4'-dimethoxybenzoin) as the single carbon and energy source, which can probably further metabolise the respective aldehydes via the β-ketoadipate pathway (Stainer and Ornston, 1973). Further, *Pf*BAL also catalyses carboligation reactions, i.e. the formation of (*R*)-benzoin from benzaldehyde and the formation of (*R*)-2-hydroxypropiophenon (HPP) from acetaldehyde and benzaldehyde with excellent

stereoselectivity (Figure 1-4 B). Thereby, *Pf*BAL can also utilise several *ortho*-, *meta*-, and *para*-substituted benzaldehydes yielding (*R*)-HPP derivatives and (mixed) (*R*)-benzoin derivatives (Demir et al., 2002; Dünkelmann et al., 2002). Besides, (*R*)-HPP can also be formed from (*R*)-benzoin and acetaldehyde as starting substrates. Since (*S*)-benzoin is not accepted by wild type (wt) *Pf*BAL, this can be exploited for the chiral resolution of racemic benzoins (Figure 1-3 C, Demir et al., 2001).

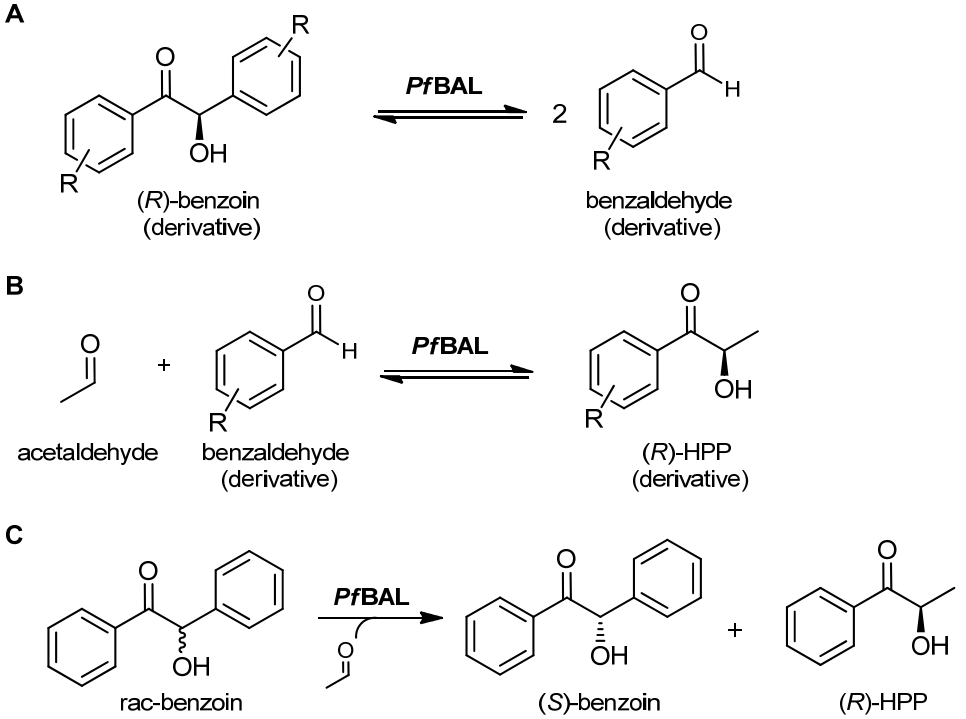

Figure 1-4: *Pf*BAL catalysed reactions. A: Reversible cleavage of (*R*)-benzoin to two benzaldehyde molecules; **B:** Mixed carboligation of acetaldehyde and benzaldehyde to (*R*)-HPP; **C:** Chiral resolution of racemic benzoin in the presence of acetaldehyde to (*S*)-benzoin and (*R*)-HPP

Benzoylformate decarboxylase from Pseudomonas putida (PpBFD)

*Pp*BFD was first described in 1966 (Hegeman, 1966) and the encoding gene *mdlC* was first cloned in 1990 (Tsou et al., 1990). Its physiological reaction, the non-oxidative decarboxylation of benzoylformate (Figure 1-5 A), is part of the mandelate pathway. In this pathway mandelic acid is converted to benzoic acid which is then further metabolised in the β-ketoadipate pathway and the tricarboxylic acid (TCA) cycle. Due to this pathway, *Pseudomonas putida* is able to grow on (*R*)-mandelic acid as a sole carbon source. Regarding non-physiological reactions *Pp*BFD shows similar reactivity to *Pf*BAL. It catalyses the formation of HPP from benzaldehyde and acetaldehyde, but in contrast to *Pf*BAL with an excess of the *S*-enantiomer, which is untypical for ThDP-dependent decarboxylases (Figure 1-4 B, Wilcocks and Ward, 1992). Thereby, *Pp*BFD has a wide substrate range that comprises *meta*- and *para*-substituted benzaldehydes, as well as other heteroaromatic, cyclic aliphatic, and olefinic aldehydes (Dünnwald et al., 2000; Iding et al., 2000). By directed evolution, also *Pp*BFD variants accepting ortho-substituted substrates became available (Lingen et al., 2003). Further, also a range of benzoin-derivatives can be prepared by *Pp*BFD catalysed reactions. In this case the respective products are in *R*-configuration (Demir et al., 1999).

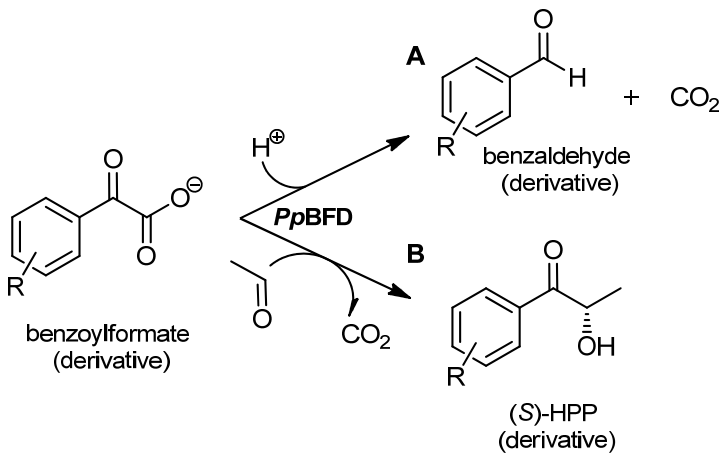

Figure 1-5: *Pp*BFD catalysed reactions. A: Physiological decarboxylation of benzoylformate to benzaldehyde; **B**: Mixed carboligation of (decarboxylated) benzoylformate and acetaldehyde to (*S*)-HPP

Pyruvate decarboxylase from Acetobacter pasteurianus (ApPDC)

*Ap*PDC was first cloned and described in 2001 (Raj et al., 2001). It catalyses the non-oxidative decarboxylation of pyruvate to acetaldehyde in the oxidative metabolism of lactic acid (Figure 1-6 A). This contrasts with all known PDCs from other organisms, which exclusively function in anaerobic metabolism as a part of the fermentative ethanol production and not in the oxidative metabolism (Raj et al., 2001). In addition to the decarboxylation, PDCs catalyse a non-physiological carboligation of pyruvate or acetaldehyde and benzaldehyde to (*R*)-phenylacetylcarbinol (PAC, Figure 1-6 B). This reaction has been employed in one of the first biotransformations used at industrial scale for the production of PAC, as a precursor for ephedrine and ephedrine analogues (Hildebrandt and Klavehn, 1934; Shukla and Kulkarni, 2000).

The substrate scope for the formation of (*R*)-PAC-derivatives was investigated with *Ap*PDC. Besides acetaldehyde, *Ap*PDC also accepts larger, not-branched aliphatic aldehydes (up to C_5) as well as the respective α-keto acids as substrates (Baraibar et al., 2014; Rother neé Gocke et al., 2011). Also benzaldehyde derivatives can be converted by *Ap*PDC, with a preference for *meta*- and *para*-substitutions (Sehl et al., 2017).

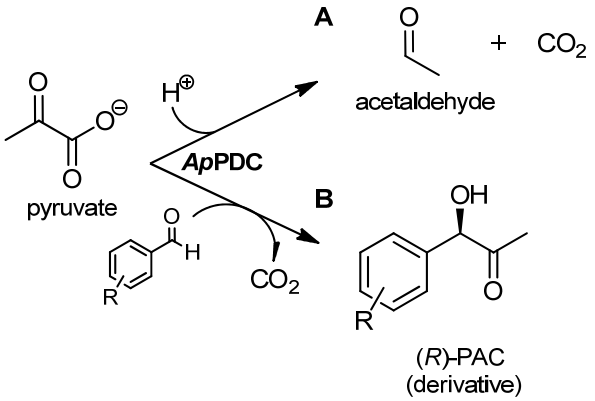

Figure 1-6: *Ap*PDC catalysed reactions. A: Physiological decarboxylation of pyruvate to acetaldehyde; *B*: Mixed carboligation of (decarboxylated) pyruvate and benzaldehyde to (*R*)-PAC

Acetohydroxyacid synthase from Escherichia coli (EcAHAS)

*Ec*AHAS catalyses the decarboxylation of pyruvate and the transfer of the hydroxyethyl unit on a second pyruvate or ketobutyrate in the biosynthesis of the branched-chain amino acids valine, leucine, and

isoleucine, yielding (*S*)-acetolactate or (*S*)-acetohydroxy butyrate, respectively (Vinogradov et al., 2006). Thereby, *Ec*AHAS cannot catalyse the transfer of the ThDP-bound hydroxyethyl group to a proton as acceptor, thus aldehyde cannot be released and *Ec*AHAS does not function as a decarboxylase (Chipman et al., 1998).

In contrast to most other ThDP-dependent decarboxylases, AHAS needs flavin adenine dinucleotide (FAD) as additional cofactor and possess two additional regulatory subunits, which form a $\alpha_2\beta_2$-heterotetramer with the two catalytic subunits (Weinstock et al., 1992). In *E. coli* three AHAS isozymes were found (*Ec*AHAS I-III) which all catalyse the formation of (*R*)-PAC from pyruvate and benzaldehyde with high stereoselectivity, but different efficiency (Figure 1-6 B, Engel et al., 2003). The most efficient isozyme, *Ec*AHAS-I, was further characterised regarding its substrate scope. It also catalyses the carboligation of pyruvate with mono-substituted benzaldehydes, pyridine carboxaldehydes, naphthaaldehydes as well as furan, thiophene, and pyrrole carboxaldehydes to the respective PAC-derivatives (Engel et al., 2004). Recently it has been shown that *Ec*AHAS-I and -II also accept acetaldehyde and propanal besides pyruvate as donor substrates and can also catalyse the self-ligation of the aldehydes to acetoin and propioin, respectively (Westphal, 2013).

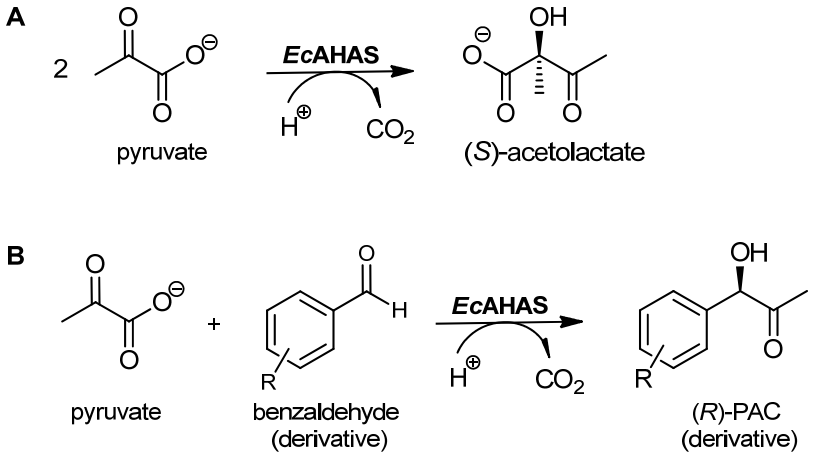

Figure 1-7: *Ec*AHAS catalysed reactions. A Formation of (*S*)-acetolactate from pyruvate as example for the physiological AHAS reactions; **B**: Mixed carboligation of pyruvate and benzaldehyde to (*R*)-PAC

YerE from Yersinia pseuodotuberculosis (YpYerE) and Pseudomonas protegens (PpYerE)

YerE from *Yersinia pseudotuberculosis* (*Yp*YerE) was first described and cloned in 1998 (Chen et al., 1998). It is part of the biosynthetic pathway of yersiniose A, a branched-chain sugar, which is part of the O-antigen of the *Yersinia pseudotuberculosis* and other bacteria (Gorshkova et al., 1984). Here, *Yp*YerE catalyses the decarboxylation of pyruvate and the transfer of the hydroxyethyl group onto cytidine-5'-diphosphate -3,6-dideoxy-4-keto-D-glucose (Figure 1-7 A, Chen et al., 1998).

Like AHAS, *Yp*YerE catalyses the formation of (*S*)-acetolactate from pyruvate and of (*R*)-PAC (derivatives) from pyruvate and benzaldehyde (derivatives, Figure 1-7). Further, it catalyses the carboligation of pyruvate and acetaldehyde to (*S*)-acetoin (Lehwald et al., 2010). Moreover, *Yp*YerE was the first ThDP-dependent decarboxylase that was described to accept non-activated ketones besides aldehydes as acceptor substrates. Among these were (methylated) cyclic ketones and –diketones, tetralone, phenoxypropan-2-one derivatives, and linear diketones (Lehwald et al., 2010). The resulting α-hydroxy ketones are tertiary alcohols (Figure 1-8 B), which are promising targets for chemical

synthesis as they are building blocks for many pharmaceuticals. However, an enzymatic synthesis of enantiopure tertiary alcohols is more challenging than of primary or secondary alcohols (Müller, 2014).

The *Yp*YerE homologue *Pp*YerE from *Pseudomonas protegens* was identified by BLAST analysis with 59 % sequence identity to *Yp*YerE. Both enzymes share a similar catalytic activity. *Pp*YerE also catalyses the formation of phenylacetylcarbinol (PAC) derivatives from pyruvate and substituted benzaldehydes but with a lower excess of *R*-product compared to *Yp*YerE (68-84 % *ee*). Upon incubation with pyruvate, acetolactate is formed followed by a probably non-enzymatic decarboxylation to almost racemic acetoin. Further, also ketones can serve as acceptor substrates, even though the acceptance is lower compared to *Yp*YerE. Recently, the crystal structure of *Pp*YerE was solved (Loschonsky *et al*., submitted to ChemBioChem).

Like AHAS, YerE requires FAD as additional cofactor, although no catalytical function could be assigned.

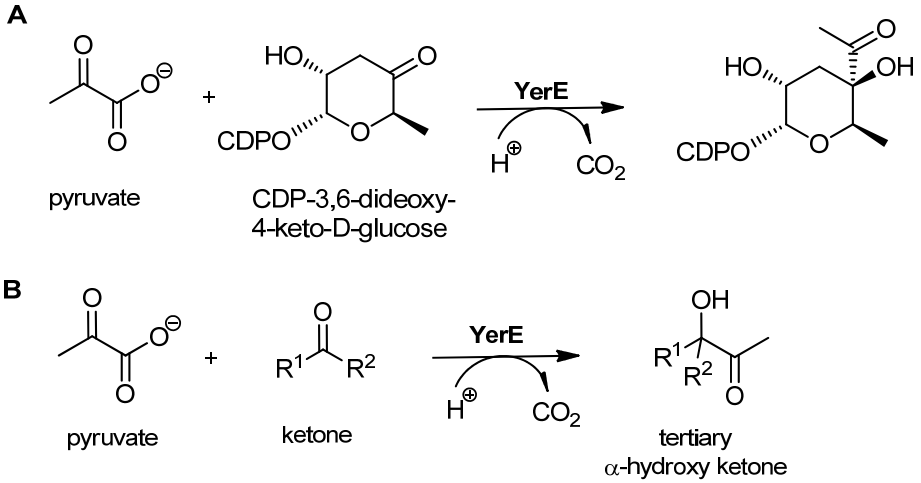

Figure 1-8: YerE catalysed reactions. A: Physiological reaction of YerE in the biosynthetic pathway of yersiniose A. CDP=cytidine-5'-diphosphate; **B:** Formation of tertiary α-hydroxy ketones by the carboligation of pyruvate with non-activated ketones as acceptor substrates.

MenD from Escherichia coli (EcMenD) and Bacillus subtilis (BsMenD)

MenD from *Escherichia coli* (*Ec*MenD) catalyses the synthesis of 2-succinyl-5-enolpyruvyl-6-hydroxy-3-cyclohexene-1-carboxylate (SEPHCHC) from α-ketoglutarate and isochorismate, which is the second step in the menaquinone (vitamin K_2) biosynthetic pathway, starting from chorismate (Figure 1-8 A, Jiang et al., 2007). Thereby, the utilisation of α-ketoglutarate as natural substrate and the catalysis of an Stetter-like 1,4-addition are exceptional among ThDP-dependent decarboxylases (Beigi et al., 2014). Apart from the physiological reaction, the formation of 5-hydroxy-4-oxo-5-arylpentanoates (PAC-derivatives) from α-ketoglutarate and various benzaldehyde derivatives has been shown with an excellent stereoselectivity towards the *R*-enantiomer (Figure 1-8 B, Beigi et al., 2013). Also further 1,4-additions of α-ketoglutarate and different Michael acceptors have been described (Beigi et al., 2014). MenD from *Bacillus subtilis* (*Bs*MenD) shows a similar substrate scope and stereoselectivity like *Ec*MenD regarding the formation of PAC-derivatives (Westphal et al., 2014a).

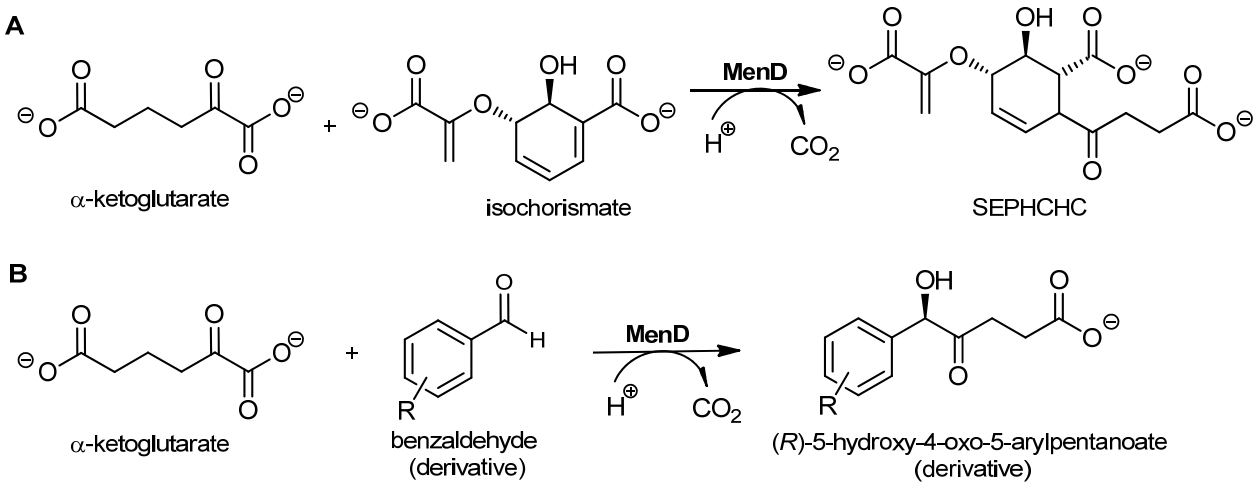

Figure 1-9: MenD-catalysed reactions. A: Physiological reaction of MenD in menaquinone biosynthetic pathway; **B:** Non-physiological of (*R*)-5-hydroxy-4-oxo-5-arylpentanoates (PAC-derivatives) from α-ketoglutarate and benzaldehyde.

1.3.2 Non-physiological benzoin-condensation like reactions

Despite a highly conserved reaction mechanism, the physiological activity of ThDP-dependent DCs varies broadly. However, all described enzymes catalyse a non-physiological, benzoin condensation-like 1,2-addition. Therefore, the 1,2-addition of acetaldehyde and benzaldehyde is used as a model-reaction to characterise the carboligation potential of ThDP-dependent DCs. This reaction can yield eight different carboligation products, which are shown in Figure 1-10: The self-ligation products acetoin and benzoin as well as the mixed ligation products HPP and PAC. Since a new stereocenter is formed during the reaction, each of these products can be formed in two configurations.

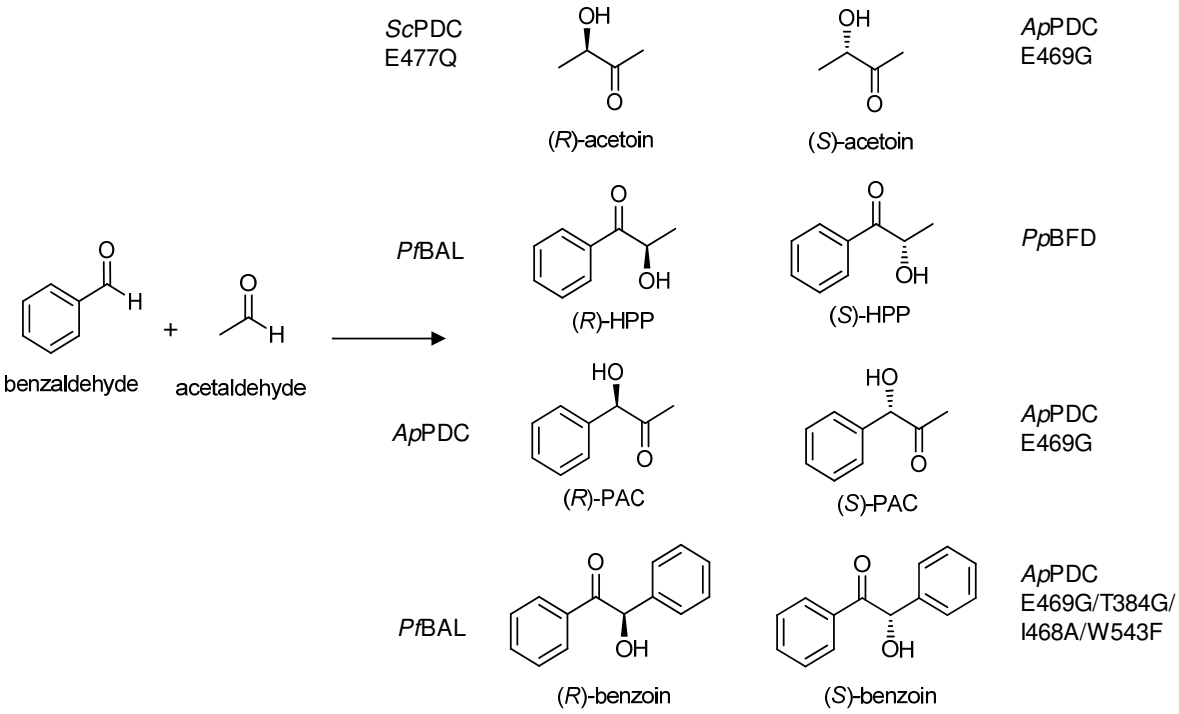

Figure 1-10: Model reaction to characterise the carboligation potential of ThDP-dependent decarboxylases. All eight possible products of the carboligation of benzaldehyde and acetaldehyde are accessible with ThDP-decarboxylases and variants thereof.

ThDP-dependent DCs usually show high selectivity for the formation of one to two of these products. Using the enzymes from this toolbox all eight products, as well as derivatives thereof, were made

accessible with high chemo- and stereoselectivity. In order to generate suitable variants, a fundamental understanding of the mechanisms controlling region- and stereoselectivity was required. The underlying principles are described in the following chapters.

1.3.3 Regioselectivity

The regioselectivity depends on the binding order of the substrates (Pohl et al., 2010). For the example given in Figure 1-10, the mixed carboligation product HPP is formed when benzaldehyde acts as the donor substrate and acetaldehyde is the acceptor substrate. The isomeric product PAC is obtained from acetaldehyde as the donor and benzaldehyde as the acceptor.

This donor- and acceptor selectivity is determined by the architecture of the respective binding sites. For instance, *Pf*BAL and *Pp*BFD have a large donor binding sites that provide enough space for benzaldehyde and thus these enzymes catalyse the formation of HPP from acetaldehyde and benzaldehyde. In contrast, *Ap*PDC prefers small, aliphatic donor substrates because of a small donor binding site and PAC is formed (Figure 1-11, Pohl et al., 2010).

Besides steric hindrance the optimal stabilisation of the substrates in the binding sites plays a decisive role for stereoselectivity. Despite offering enough space for acetaldehyde as the donor substrate, neither *Pf*BAL nor *Pp*BFD catalyse the formation of PAC or acetoin, when benzaldehyde is present in the reaction mixture (Gerhards et al., 2012; Gocke et al., 2009). This shows that the better stabilisation of benzaldehyde, which is correlated with a higher affinity for this substrate, makes it the preferred donor over acetaldehyde.

Due to this dependency on optimal substrate stabilisation the choice of substrates can shift the regioselectivity in favour the one or the other product. The 2-ketoacid decarboxylase from *Lactococcus lactus Ll*KdcA catalyses the formation of both PAC and HPP in a ratio of 60:40 from acetaldehyde and benzaldehyde (Gocke et al., 2007). The use of bigger aliphatic aldehydes like propanal or n-butanal fully shifts this ratio toward the PAC-derivative while the use of 3,5-dichlorobenzaldehyde results in the selective formation of the HPP-derivative. This indicates that larger substrates are better stabilised by the *Ll*KdcA donor binding site compared to the acceptor binding site.

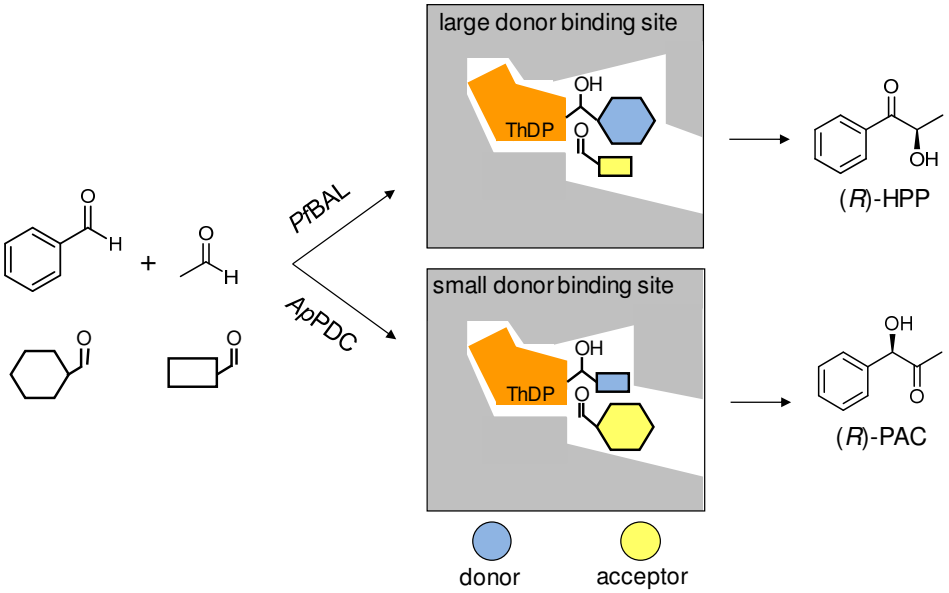

Figure 1-11: Regioselectivity model for ThDP-dependent decarboxylases according to (Gocke, 2007): The binding order of the substrates and thereby the size of the donor binding site determines the regioselectivity. The large donor binding site of *Pf*BAL offers enough space to stabilise the benzaldehyde side chain and with acetaldehyde as acceptor HPP is formed. Due to the restricted size of the *Ap*PDC donor binding site only acetaldehyde can serve as donor substrate and benzaldehyde acts as acceptor substrate, yielding PAC.

Provided that the employed enzyme can function as a decarboxylase, another way to control the regioselectivity by the choice of substrate is to use the corresponding α-ketoacid instead of aldehydes as the donor substrates. In most cases, these must be decarboxylated prior to the carboligation reaction and, thus, do not serve as acceptors. Nevertheless, certain ThDP-dependent enzyme can also utilise α-ketoacid as acceptors. For example, AHAS catalyses the formation of acetolactate from two pyruvate molecules, the corresponding α-ketoacid to acetaldehyde. Here, pyruvate serves as donor and as acceptor.

1.3.4 Stereoselectivity

The stereoselectivity depends on whether the nucleophilic attack of the carbanion-enamine-intermediate on the acceptor substrate occurs from the re- or the *si*-face of the acceptor (Baykal et al., 2006; Iding et al., 2000) For the here described model reaction, an attack from the *si*- and the *re*-face result in formations of *R*- and *S*- product, respectively. The orientation of the donor hydroxy group and the acceptor carbonyl group is supposably the same, because these functional groups are assumed to interact with the same histidine residue in ThDP-dependent DCs (Knoll et al., 2006) Therefore, a *si*-attack requires a parallel arrangement of the acceptor side chain relative to the donor side chain (binding state *I*, Figure 1-12) before the new C-C-bond is formed. The *re*-attack on the other hand requires an antiparallel arrangement of both side chains (binding state *II*).

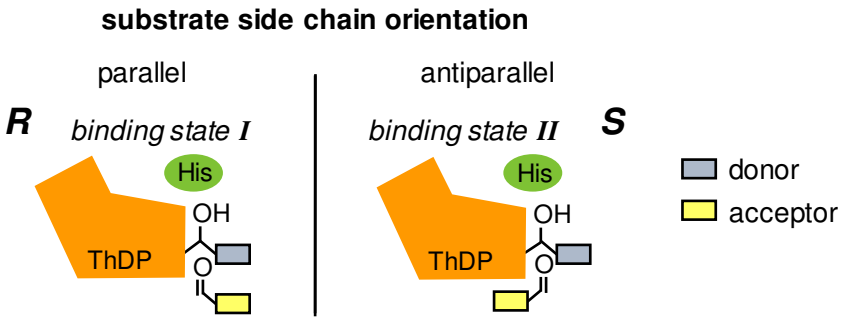

Figure 1-12: Schematic representation of the relative substrate side chain orientation for a *si*-attack (binding state *I*) and a *re*-attack (binding state *II*) of the carbanion-enamine-intermediate on the acceptor substrate, resulting in *R*- and *S*-selective product formation, respectively.

ThDP-dependent decarboxylases are predominantly *R*-selective in the mixed carboligation of aromatic and aliphatic aldehydes. One exception is the *Pp*BFD, which catalysed the formation of (*S*)-HPP derivatives from substituted benzaldehydes (donor) and acetaldehyde (acceptor) with *ee*-values ranging from 74 % to >99 % (Dünnwald et al., 2000). When larger aliphatic aldehydes like propanal or n-butanal were used as acceptors, the *R*-product was produced in excess with *ee*-values of 21 % and 66 %, respectively (Gocke et al., 2008). Additionally, the reactions with these aliphatic aldehydes also yielded the regioisomeric PAC-derivatives with the aliphatic aldehyde acting as the donor and benzaldehyde as the acceptor substrate. Here, high *R*-selectivity with *ee*-values of 98 % and 99 % for propanal and n-butanal, respectively, were obtained. Also, low amounts of (*R*)-benzoin were formed with 99 % *ee* (Gocke et al., 2008).

Superimposition of the active site structures of *Pp*BFD and *Pf*BAL, which both form HPP but with opposite stereoselectivity, revealed a binding pocket in *Pp*BFD that allows antiparallel binding of the acceptor side chain in relation to the donor side chain and thereby enables the *re*-attack according to binding state *II* on the acceptor and the formation of the *S*-product (Knoll et al., 2006, Figure 1-13). This binding pocket, which is often referred to as an *S*-pocket, is not present in *Pf*BAL. The small size of the antiparallel binding pocket also explains the increasing relative amount of *R*-product with increasing acceptor size: The size of the pocket is ideal for the stabilisation of the methyl side chain of acetaldehyde in antiparallel orientation to the phenyl group of benzaldehyde, while the antiparallel orientation is not preferred over the parallel orientation for propanal and n-butanal as acceptor. Antiparallel binding of benzaldehyde is sterically impossible, thus all products resulting from benzaldehyde as acceptor are formed selectively in *R*-configuration (Figure 1-13).

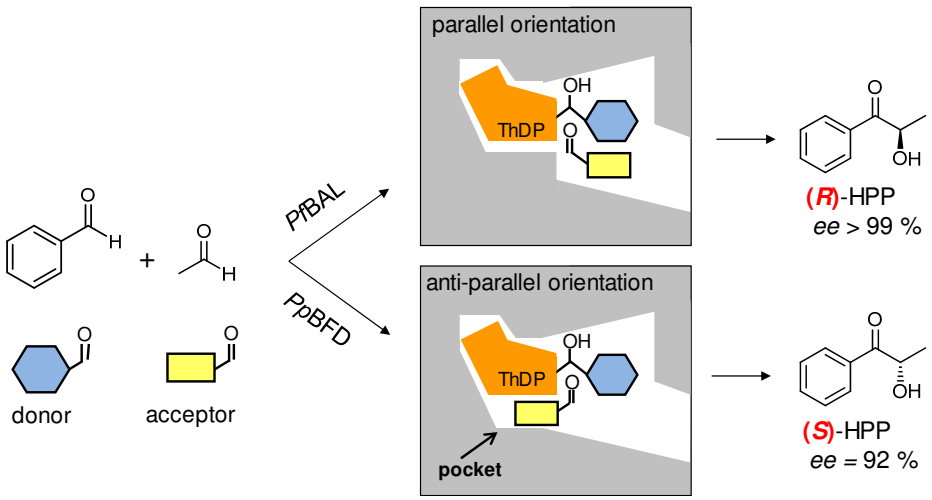

Figure 1-13: Stereoselectivity model for ThDP-dependent decarboxylases according to Knoll et al., 2006: The stereoselectivity is dependent on the relative orientation of the donor- and the acceptor side chain. In contrast to *Pf*BAL, the active site of *Pp*BFD features an antiparallel acceptor binding pocket, which is also known as "*S*-pocket". *Pf*BAL catalyses the formation of (*R*)-HPP and *Pp*BFD catalyses the formation of (*S*)-HPP from benzaldehyde and acetaldehyde.

1.3.5 Engineering of ThDP-dependent decarboxylases with altered stereoselectivity

Opening of an antiparallel acceptor binding pocket ("S-pocket")

The first attempt to engineer *S*-selective variants of ThDP-dependent decarboxylases was done with the *Pp*BFD, which already shows *S*-selectivity, but only with the small acceptor substrate acetaldehyde. Enlargement of the pocket by replacement of L461(477) by glycine and alanine increased the enantiomeric excess for the formation of (*S*)-HPP from benzaldehyde (donor) and acetaldehyde (acceptor) from 92 % to 98 % (Gocke et al., 2008). Further, the L461A mutation enabled the formation of (*S*)-HPP derivatives using propanal and n-butanal as acceptors with *ee*-values of 93 % and 63 %, respectively. Nevertheless, *Pp*BFD variant L461A also catalysed the formation of benzoin and the PAC-derivative from benzaldehyde and n-butanal with high enantiomeric excess of the respective *R*-products. This indicates that the formed pocket was not big enough to stabilise benzaldehyde as acceptor substrate (Gocke et al., 2008).

Superimposition of the crystal structure of *Pp*BFD, *Ap*PDC and the PDC from *Zymomonas mobilis* (*Zm*PDC) revealed potential alternative acceptor binding pockets for all three enzymes that in contrast to *Pf*BAL are not blocked by the protein backbone. However, for *Ll*KdcA, *Ap*PDC and *Zm*PDC the entrance to the *S*-pocket is completely blocked by bulky amino acid residues, explaining the strict *R*-selectivity of these enzymes (Gocke, 2007). Since *Ap*PDC has the largest antiparallel acceptor binding pocket with respect to the protein backbone, it was subjected to site-directed mutagenesis of E469(477) to glycine to open and further enlarge the pocket and enable acceptor binding according to binding state *II* (Figure 1-12, Figure 1-14). The obtained E469G variant showed almost no decarboxylation activity due to the mutation of the glutamate residue, which is necessary for decarboxylation (Pohl et al., 1998; Rother neé Gocke et al., 2011). The carboligation activity on the other hand was not affected and the E469G variant catalysed the formation of (*S*)-PAC (*ee*: 61 %) from acetaldehyde as the donor and benzaldehyde as acceptor, which was not enzymatically accessible before (Rother neé Gocke et al., 2011). The *ee*-value could later be improved to 87 % (*S*) by optimisation of the reaction conditions (Gerhards et al., 2012).

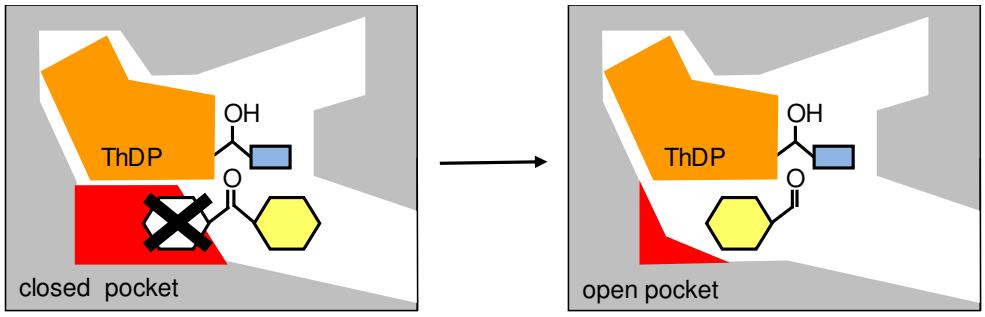

Figure 1-14: Opening of an antiparallel acceptor binding pocket in ThDP-dependent DCs. The pocket enables the antiparallel orientation of the acceptor substrate side chain (yellow) relative two the donor substrate side chain (light blue), which is a prerequisite for *S*-selectivity according to the stereoselectivity model for ThDP-dependent decarboxylases. The pocket is typically blocked by the residue in standard position 477.

Subsequently, the concept of opening an antiparallel acceptor binding pocket (Figure 1-14) was transferred to the MenDs from *Escherichia coli* (*Ec*MenD) (Westphal et al., 2013a, 2013b) and *Bacillus subtilis* (*Bs*MenD) (Westphal et al., 2014a) using the carboligation of α-ketoglutarate (donor) and benzaldehyde (acceptor) to 5-hydroxy-4-oxo-5-phenylpentanoate as a model reaction. Both wt *Ec*MenD and *Bs*MenD are highly *R*-selective for this reaction with *ee*-values higher 99 %. In contrast to *Ap*PDC, with *Ec*MenD an analogous single amino acid exchange of F475(477), was here not sufficient to invert the stereoselectivity (*ee* 83 % (*R*)). However, combined site-directed mutagenesis of F475 and the adjacent I474(476) to glycine and alanine resulted in *S*-selective variants with an *ee* between 34% and 75%. The highest stereoselectivity was obtained with the I474A/F475G variant (*ee* 75 % (*S*)) (Westphal et al., 2013b). This also shows that besides pocket size also the stabilisation in the pocket is important for antiparallel binding of the acceptor side chain, as variant I474G/F475G offers the most space in the pocket but nevertheless results in a lower *ee*-value for the 5-hydroxy-4-oxo-5-phenylpentanoate of 34 % (*S*). In this case the additional methyl group of alanine in position 474 stabilises the benzaldehyde side chain by hydrophobic interactions.

For *Bs*MenD structural comparison with *Ec*MenD showed that the access to the antiparallel acceptor binding pocket is blocked by the same residues as for *Ec*MenD, F490(477) and I489(476) (Westphal et al., 2014a). Here, a combined exchange of both residues by alanine and glycine successfully inverted the stereoselectivity for all variants except I489G/F490A, which could not be produced solubly in *E. coli* BL12 and was therefore not further characterised. The other three variants showed ee-values between 67 % (*S*) and 92 % (*S*), which is remarkably higher than for the analogous *Ec*MenD variants. The best stereoselectivity was found for I489A/F490A.

Destabilisation of parallel side chain orientation

The availability of an open antiparallel acceptor binding pocket is a necessary but not sufficient condition for antiparallel binding of the acceptor side chain according to binding state *II*, as it does not restrict the possibility of parallel acceptor side chain binding (binding state *I,* Figure 1-12). Additional measures to destabilise the parallel acceptor side chain binding were first investigated for *Ec*MenD (Figure 1-15, Westphal et al., 2013a). The *ee*-value of 75 % (*S*) for variant I474A/F475G shows that still an eighth of the benzaldehyde molecules bound with parallel orientation of the side chain. R395(393) was identified as a residue that might contribute to the parallel stabilisation of the benzaldehyde side chain by cation-π interactions. In order to supress the parallel side chain orientation R395 was subjected to site-saturation mutagenesis using the variant I474A/F475G as a starting point.

Most of the triple variants showed only low activity, which can be explained by the role that R395 has for the stabilisation of the donor substrate α-ketoglutarate by interaction with its terminal carboxylate group. However, one *Ec*MenD variant - I474A/F475G/R395Y – was found to catalyse the formation of (*S*)-5-hydroxy-4-oxo-5-phenylpentanoate with an increased *ee*-value of 85 %. This confirms the concept of supressing the stabilisation of the parallel acceptor side chain orientation, as the exchange of arginine to tyrosine prohibits cation-π interactions. Additionally, the tyrosine hydroxy group might destabilise the parallel orientation (Westphal et al., 2013a)

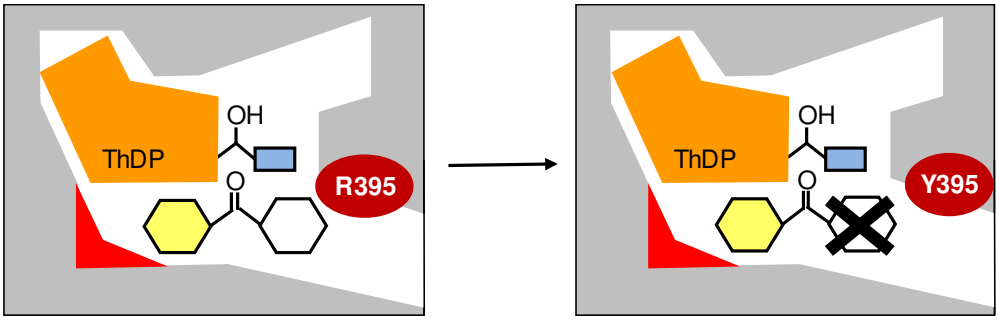

Figure 1-15: Destabilisation of the parallel acceptor substrate orientation relative to the ThDP-bound donor side chain. The opening of an antiparallel acceptor binding pocket is a necessary, but not sufficient condition for antiparallel binding of the acceptor side chain. The *S*-selectivity can be enhanced by destabilisation of the parallel orientation of acceptor side chain (yellow) relative to the donor side chain (light blue). In the given example, this was obtained by an R395Y substitution in *Ec*MenD (Westphal et al., 2013a).

Following the same strategy also the *S*-selective formation of PAC from (decarboxylated) pyruvate (donor) and benzaldehyde (acceptor) with *Ap*PDC variants could be further improved. Here, W543(559), which might stabilise the parallel orientation of the benzaldehyde side chain via π–π stacking interactions, and I468(476), which probably stabilises the parallel orientation of benzaldehyde by hydrophobic interactions with the phenyl ring and additionally might block the entrance of the antiparallel acceptor binding pocket, were chosen as target positions for site-saturation mutagenesis studies with the *Ap*PDC E469G variant as a starting point. The triple variant E469G/I468A/W543F showed the highest *S*-selectivity in the formation of PAC from pyruvate and benzaldehyde with an *ee*-value of 97 % (*S*) (Sehl et al., 2017).

Influence of second shell residues

Apart from amino acid residues in the active site that can immediately interact with the substrate molecules, also second shell residues may have a considerable influence on the stereoselectivity. This was first demonstrated for the position L476(488) in *Pp*BFD, which is located on a loop at the surface of the monomer near the active site cavity and might interact with the α-helix that defines the antiparallel acceptor binding pocket (Figure 1-16, Lingen et al., 2002). Several *Pp*BFD variants with replacements of L476 showed an up to 15 percent points improved *ee*-value for the formation of (*S*)-HPP from benzaldehyde and acetaldehyde. This indicates structural changes in the area of the antiparallel binding pocket, probably induced by changes of the flexibility of the loop region L476 is located in (Lingen et al., 2002).

Similarly, the difference in stereoselectivity of *Ec*MenD and *Bs*MenD variants might be explained. Here, opening of an antiparallel acceptor binding pocket by replacement of the corresponding amino acids resulted in considerably higher *ee*-values for the formation of (*S*)-5-hydroxy-4-oxo-5-phenylpentanoate with *Bs*MenD (Westphal et al., 2014a). Comparison of the α-helix defining the antiparallel acceptor

binding pocket showed that most amino acid residues on the helix are strictly conserved. One exception is the residue in standard position 475, which is a glutamine in *Ec*MenD and a glycine in *Bs*MenD. The glutamine lies adjacent to the two amino acids that were exchanged to open the antiparallel acceptor binding pocket (Westphal et al., 2013b), but its side chain is not orientated towards the pocket (Figure 1-16). Nevertheless, it might impact the position or flexibility of the α-helix and thereby have a direct influence on the stereoselectivity. Replacement of the respective glycine (G488(475)) by glutamine in the *S*-selective *Bs*MenD variant I189G/F190G restored the original *R*-selectivity of wildtype *Bs*MenD with an *ee*-value of 77 % for (*R*)-5-hydroxy-4-oxo-5-phenylpentanoate. This indicates a structural change of the antiparallel acceptor binding pocket, for example due to a shift of the α-helix into the pocket area or due to decreased flexibility of the α-helix after removal of one of three adjacent glycine residues, and underlines the importance of second shell residues on the architecture of the antiparallel acceptor binding pocket (Westphal et al., 2014a).

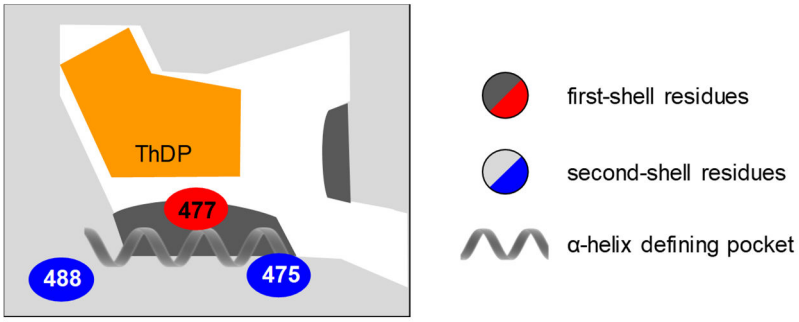

Figure 1-16: Schematic representation of the positions of second shell residues that were shown to influence the stereoselectivity by interactions with first-shell residues that are in contact with the substrate. The residues are assigned by their standard number. The first-shell residue in standard position 477 is mainly blocking the antiparallel acceptor binding pocket. Substitution of the second-shell residue L476(488) in *Pp*BFD was shown to increase the *S*-selectivity (Lingen et al., 2002). Substitution of the second-shell residue G488(475) by glutamine in the *S*-selective *Bs*MenD variant I189G/F190G was shown restored the original *R*-selectivity of wildtype *Bs*MenD (Westphal et al., 2014a).

Hybridisation: Combining features of different ThDP-dependent DCs

The asymmetric synthesis of (*S*)-benzoins starting from benzaldehyde was a longstanding challenge in enzymatic catalysis. Two essential requirements for (*S*)-benzoin formation with ThDP-dependent decarboxylases are a large donor binding site providing enough space for benzaldehyde binding and an antiparallel acceptor binding pocket with space to accommodate the phenylring of the benzaldehyde acceptor and thus enables *S*-selectivity. *Pf*BAL and *Pp*BFD both provide a large donor binding site and can thus utilise benzaldehyde as donor substrate (Figure 1-11). However, *Pf*BAL lacks an antiparallel binding pocket and the respective pocket in *Pp*BFD is limited in size and cannot stabilise the benzaldehyde side chain in antiparallel orientation (Figure 1-13). As described above an antiparallel acceptor binding pocket could be opened in *Ap*PDC by exchange of E469(477) to glycine, but *Ap*PDC has a small donor binding site that can stabilise aliphatic aldehydes but not benzaldehyde. Consequently, a rational hybridisation approach was investigated to combine the desired features of *Pf*BAL and *Ap*PDC (Westphal et al., 2014b). Introduction of the large donor binding site of *Pf*BAL into the *Ap*PDC variant E469G by an additional T384(388)G substitution enabled the formation of (*S*)-benzoin from benzaldehyde with 59 % *ee*. The *ee* was subsequently further increased by destabilisation of the parallel side chain orientation (see Figure 1-15). Biotransformations with *Ap*PDC E469G/T384G/I468A gave (*S*)-benzoin 87 % *ee*. Additional substitution of W543 by phenylalanine increased the *ee*-value to 95 % (*S*) (Westphal et al., 2014b).

1.3.6 Summary

Due to their versatility but also their high stereo- and regioselectivity, ThDP-dependent enzymes of the structural DC family are valuable tools for the asymmetric synthesis of α-hydroxy ketones, starting from inexpensive substrates, like pyruvate, acetaldehyde, and benzaldehyde (derivatives). A comprehensive understanding of the mechanisms controlling the regio- and stereoselectivity of DCs enabled the engineering of enzyme variants to extend the available product platform and especially gave access to enantioenriched (*S*)-α-hydroxy ketones.

Tools for the generation of such variants are:

- Opening or enlarging of substrate binding pockets to either enable antiparallel binding of the acceptor substrate according to binding state *II* (Figure 1-12) resulting in the formation of *S*-products ("*S*-pocket", Figure 1-14) or to allow binding of larger substrates in the donor binding site in order to change the donor substrate specificity.
- Suppression of the parallel binding of the acceptor side chain according to binding state *I* (Figure 1-12) in order to increase the *S*-selectivity after opening of an antiparallel acceptor binding pocket (Figure 1-15).
- Modification of second shell residues to induce structural changes that might influence the architecture of the antiparallel acceptor binding pocket (Figure 1-16).

1.4 Transketolases

The term transketolase was first used in 1953 to describe an enzyme isolated from baker's yeast, *E. coli*, spinach and rat liver that catalyses the cleavage of pentose phosphate and the formation of glyceraldehyde-3-phospahte and seduheptulose-7-phosphate when ThDP and Mg^{2+} ions are present (Horecker and Smyrniotis, 1953; Racker et al., 1953). More than 60 years later transketolase is well characterised as an enzyme which plays a key role in the non-oxidative branch of the pentose phosphate pathway (Horecker, 2002, 1953). Here, it catalyses the cleavage of the C2-C3-bond of the ketose xylulose-5-phosphate (X5P) and the transfer of the resulting dihydroxyethly moiety to the C1 position of the aldoses ribose-5-phosphate (R5P) or eryhtulose-4-phosphate (E4P), yielding glyceraldehyde-3-phosphate (G3P) and sedoheptulose-7-phosphate (S7P) or fructose-6-phosphate, (F6P), respectively (Figure 1-17). Further, transketolase catalyses the reverse reactions in the Calvin cycle of photosynthesis (Flechner et al., 1996; van den Bergh et al., 1996). For all reactions, the new stereocenter is formed in *S*-configuration with high stereoselectivity (*ee*>99 %).

Besides TKs, the structural TK superfamily also comprises phosphoketolases and dihydroxyacetone synthase. But as these were not part of this thesis, they are not described here.

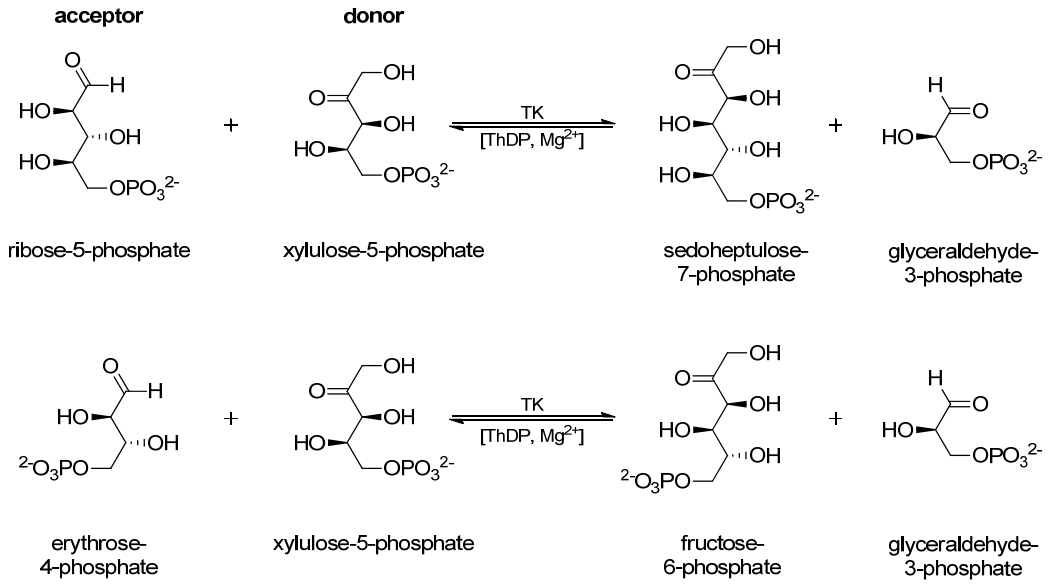

Figure 1-17: Physiological transketolase reaction: A C2-ketol group is transferred from xylulose-5-phospahte to either ribose-5-phosphate or erythrose-4-phosphate, yielding sedoheptulose-7-phosphate or fructose-6-phosphate, respectively. Both reactions are part of the non-oxidative branch of the pentose phosphate pathway. The reverse reactions are as well catalysed by transketolases within the Calvin-cycle of photosynthesis.

1.4.1 Transketolase active site structure

The crystal structure of *Saccharomyces cerevisiae* transketolase (*Sc*TK) was elucidated in 1992 (Lindqvist et al., 1992), as the first 3D structure of a ThDP-dependent enzyme. In the following years the structure was further refined (Nikkola et al., 1994) and structures of *Sc*TK in complex with the acceptor substrate erythrose-4-phosphate (Nilsson et al., 1997) and with the carbanion intermediate (Fiedler et al., 2002) became available. Up to now 47 entries for transketolase structures are listed in the protein data base (PDB, January 2018, www.rcsb.org (Berman et al., 2000)), among these are human transketolase (Mitschke et al., 2010), *E. coli* transketolase (*Ec*TK) (Asztalos et al., 2007; Littlechild et

al., 1995), and several other eukaryotic and prokaryotic transketolases. For simplicity, all here mentioned amino acid positions refer to *Ec*TK, if not otherwise stated. An overview over all described residues is given in Table 1-2.

ThDP-binding

Also in TKs ThDP is bound in a deep cleft at the interface of the PP- and the Pyr-domain from the two different subunits (Lindqvist et al., 1992). While the rest of the molecule is buried inside the protein, the C2 atom of the thiazolium ring is solvent exposed (Nikkola et al., 1994). Interactions with the residues lining the active site are shown in Figure 1-18. The pyrimidine ring is bound in a hydrophobic pocket formed by F434, F437 and Y440 from the Pyr-domain. The pyrimidine ring can form π-π stackings with the aromatic ring of F437 and its methyl group is orientated orthogonal towards the ring plane of Y440. Further, the pyrimidine ring is bound via hydrogen bonds between H473 and G114 and the 4'-NH_2 group, L116 and the N3' nitrogen as well as E411 and the N1' nitrogen (Lindqvist et al., 1992; Nikkola et al., 1994). The latter is responsible for the deprotonation of N1', which induces the activation of the cofactor ThDP. The diphosphate group is anchored via a divalent cation, which is a Ca^{2+} in most transketolase crystal structures. It forms an octahedral complex with the side chains of D155 and N185, the main oxygen atom of I187, a water molecule and two oxygen atoms of the diphosphate group. Additionally, the diphosphate group is bound by hydrogen bonds with H66, G156, H261 and several water molecules (Lindqvist et al., 1992; Nikkola et al., 1994). The thiazolium ring is mainly stabilised via hydrophobic interactions with L116, I189 and L382 (not shown in Figure 1-18). Additionally D381 might neutralise the positive charge of the thiazolium ring (Lindqvist et al., 1992; Nikkola et al., 1994).

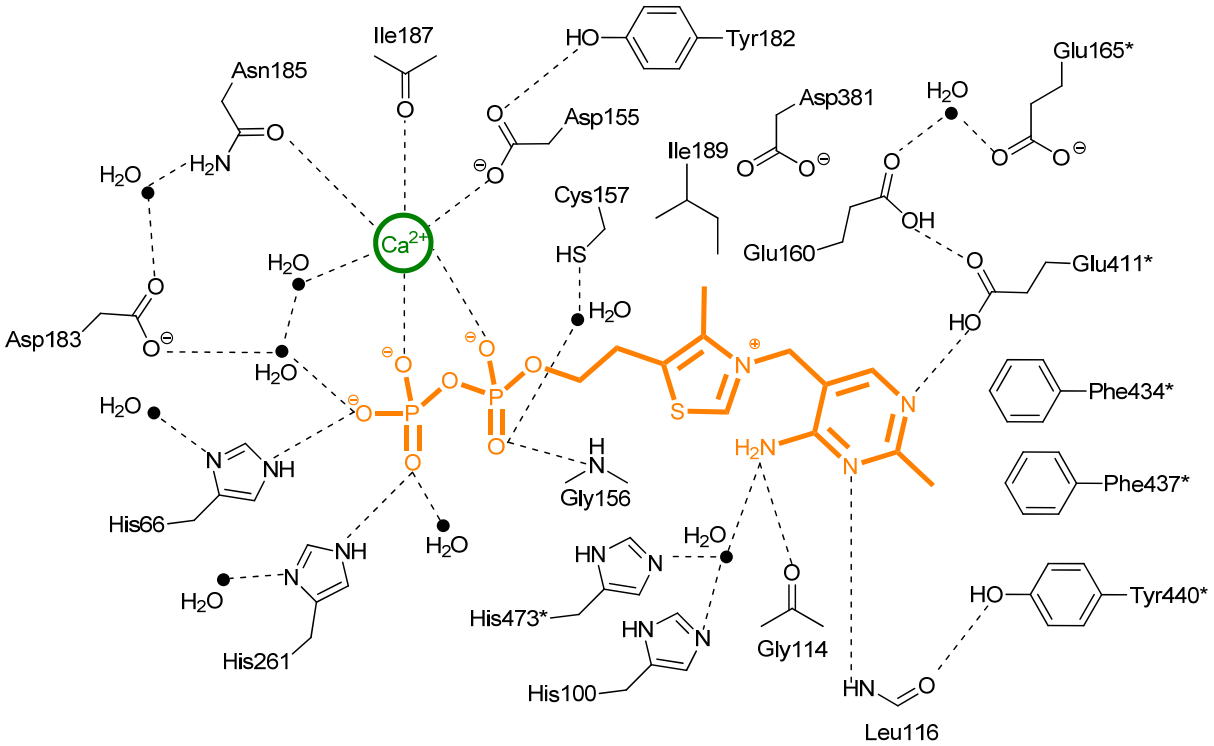

Figure 1-18: Interactions between the cofactors and the active site amino acid residues of transketolase according to Schneider and Lindqvist, 1998. Amino acids positions refer to *Ec*TK. Residues from the second subunit are marked with an asterisk; orange: ThDP, green: divalent cation, e.g. Ca^{2+}

Substrate binding

The active site is accessible by a narrow substrate channel located at the interface of the two subunits. Interactions of the active site residues with the substrates are shown in Figure 1-19. At the entrance of the channel R358, S385, H461 and R520 form a binding site for the substrate's phosphate group (Asztalos et al., 2007; Nikkola et al., 1994; Nilsson et al., 1997). Replacement of any of the four residues in *Sc*TK by alanine increased the K_m-value of the donor (X5P) and the acceptor (R5P) substrate 2.2- to 11.4-fold and 12- to 48-fold, respectively (Nilsson et al., 1997). Another conserved residue in the substrate channel is D469, which forms hydrogen bonds with the C4-hydroxy group of the donor and the C2-hydroxy group of the acceptor (Asztalos et al., 2007; Nilsson et al., 1997). This makes D469 a key residue for the recognition of the proper stereochemistry at the donor ketose C4-position (4*S*) and the acceptor aldose C2 position (2*R*). For *Sc*TK is was observed that replacement of the corresponding aspartate (D477) by alanine reduced k_{cat}/K_m by 2-3 orders of magnitude for the physiological acceptor substrates R5P and E4P, while it was less than 2-fold decreased for the respective (2*S*)- or the 2-deoxy-substrates (Nilsson et al., 1998). At the bottom of the substrate channel there is a cluster of five highly conserved histidine residues (H26, H66, H100, H261, H473) in vicinity of the thiazolium ring (Nikkola et al., 1994), which have been probed my mutagenesis studies.

The side chains of H66 and H100 form hydrogen bonds with the C1-hydroxy group of the donor substrate (Asztalos et al., 2007; Schneider and Lindqvist, 1998). Exchange of the respective histidine residues H69 and H103 in *Sc*TK led to a 6- and 12-fold increased K_m-value for the donor substrate X5P, respectively. The same variants showed an only 1.3-fold increased K_m value (*Sc*TK H69A) or even 1.5-fold decreased K_m-value (*Sc*TK H103A) for the acceptor substrate R5P, which underlines that H66 and H100 are involved into donor- but not acceptor binding (Wikner et al., 1997, 1995). Further, a role in the stabilisation of reaction intermediates after binding of the donor substrate has been proposed for both residues (Wikner et al., 1997, 1995).

The H473 side chains can form hydrogen bods with the C1- and the C2-hydroxy group of the donor substrate (Asztalos et al., 2007; Ranoux and Hanefeld, 2013). Also for this residue replacement by alanine in *Sc*TK (H481A) increased the K_m for the donor substrate (X5P) 18-fold, while it did not affect the K_m for the acceptor substrate (R5P) (Wikner et al., 1997). Further H473 has been proposed as a proton donor during the nucleophilic attack on the donor substrate (step **b**, Figure 1-3) (Schneider and Lindqvist, 1993). However, *Sc*TK H481A still showed 5 % residual specific activity compared to wildtype *Sc*TK which points against an essential role of this residue in acid-base catalysis (Wikner et al., 1997). Instead, the 4'-imino group of ThDP might be responsible for this protonation step (Schneider and Lindqvist, 1998). In contrast to the other four histidines, H473 is not conserved in transketolases from mammalian sources. Here, the corresponding residue is a glutamine, which also rules out the possibility that this residue acts as an acid-base catalyst (Mitschke et al., 2010; Singleton et al., 1996).

H26 and H261 can form hydrogen bonds to the donor C3-hydroxy group (Asztalos et al., 2007; Wikner et al., 1997) and to the acceptor carbonyl oxygen (Asztalos et al., 2007; Nilsson et al., 1997). Exchange of the corresponding residues H30 and H263 in *Sc*TK against alanine increased the K_m for the donor X5P and the acceptor R5P 14-fold and 2-fold, respectively, for *Sc*TK H263A. In contrast, for *Sc*TK H30A the K_m for donor and acceptor was decreased 2- to 3-fold. However, the variant still showed low residual activity of 0.5 % compared to wildtype *Sc*TK (Wikner et al., 1997). Both residues are candidates

as proton acceptors from C3 of the bound donor intermediate before the carbanion-enamine is formed (step **c**, Figure 1-3) and as proton donors for C1 of the acceptor during the nucleophilic attack on the acceptor (step **d**, Figure 1-3) (Fiedler et al., 2001; Wikner et al., 1997). It has been proposed that both residues act in concert during proton abstraction. H261 forms an additional hydrogen bond to the ThDP diphosphate group and its second unprotonated nitrogen atom is thereby optimally positioned to abstract the proton from the donor. A hydrogen bond to H26 could support this step by positioning the donor C3-hydroxy group in the proper orientation and by stabilising the transition state (Wikner et al., 1997).

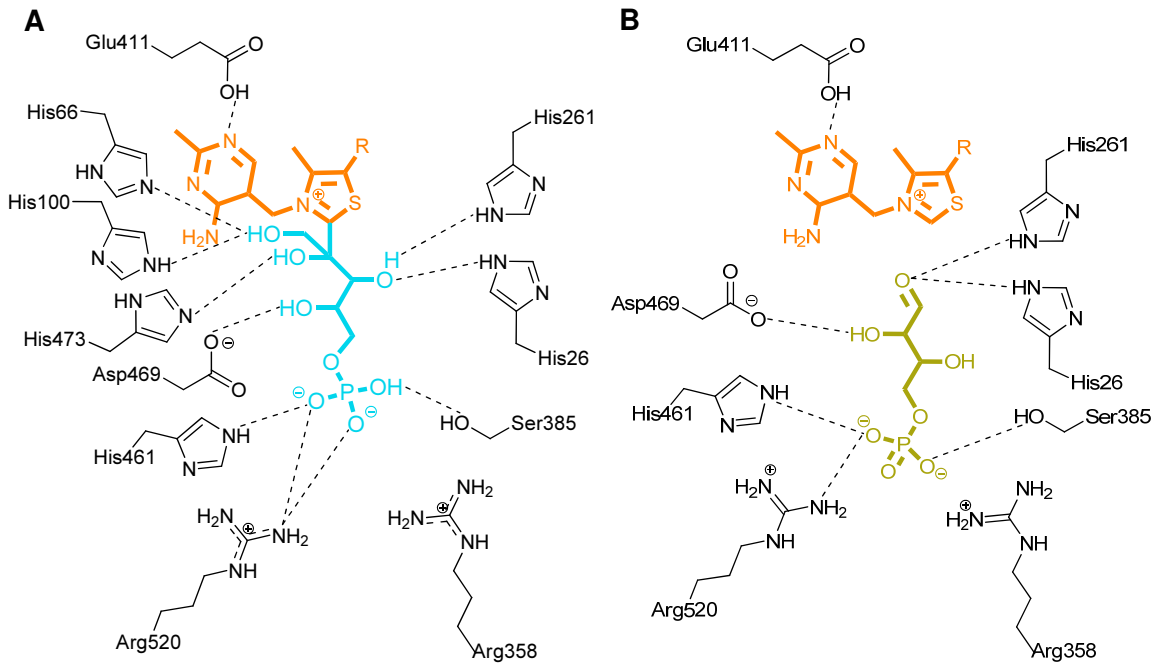

Figure 1-19: A: Model of the interactions of the covalent donor substrate-ThDP adduct (light blue) with active site residues of transketolase according to Schneider and Lindqvist, 1998; B: Schematic view of the interactions of the acceptor substrate erythrose-4-phosphate (yellow) with transketolase active side residues according to Nilsson et al., 1997; orange: ThDP, R=diphosphate group

Table 1-2: Function of transketolase active site residues and standard position according to the standard numbering scheme for transketolases (Baierl et al., 2018)

function	standard №	*Ec*TK	*Sc*TK	*Gst*TK
ThDP-binding				
pyrimidine ring (via water molecule)	100	H100	H103	H102
pyrimidine ring	114	G114	G116	G116
pyrimidine ring	116	L116	L118	L118
pyrimidine ring + ThDP activation	411	E411	E418	E412
pyrimidine ring	434	F434	F442	F435
pyrimidine ring	437	F437	F445	F438
pyrimidine ring	440	Y440	Y448	Y441
pyrimidine ring (via water molecule)	473	H473	H481	H474
thiazolium ring	189	I189	I191	L191
thiazolium ring	382	L382	L383	L382
diphosphate group	66	H66	H69	H68
diphosphate group	156	G156	G158	G158
diphosphate group (via water molecule)	183	D183	D185	D185
diphosphate group	261	H261	H263	H263
divalent cation	155	D155	D157	D157
divalent cation	185	N185	N187	N187
divalent cation	187	I187	I189	I189
donor substrate binding				
C1-hydroxy group	66	H66	H69	H68
C1-hydroxy group	100	H100	H103	H102
C2-hydroxy group	473	H473	H481	H474
C3-hydroxy group	26	H26	H30	H28
C3-hydroxy group	261	H261	H263	H263
C4-hydroxy group	469	D469	D477	D470
phosphate group	358	R358	R359	R358
phosphate group	385	S385	S386	S385
phosphate group	461	H461	H469	H462
phosphate group	520	R520	R528	R521
acceptor substrate binding				
C1-carbonyl group	26	H26	H30	H28
C1-carbonyl group	261	H261	H263	H263
C2-hydroxy group	469	D469	D477	D470
phosphate group	358	R358	R359	R358
phosphate group	385	S385	S386	S385
phosphate group	461	H461	H469	H462
phosphate group	520	R520	R528	R521

1.4.2 Non-physiological reactions

Donor substrates

The donor scope of transketolase is narrow (Ranoux and Hanefeld, 2013). Besides the physiological substrate X5P, S7P and F6P also other, non-phosphorylated ketoses like erythrulose can serve as donors (Hecquet et al., 1993; Wohlgemuth, 2009), which all share the common feature of a keto group vicinal to the splitting C2-C3 bond and a hydroxy group on the C1 atom. Further, a *trans*-configuration of the hydroxy groups at the C3 and the C4 atom is preferred (Kochetov and Sevostyanova, 2005). A widely used artificial donor substrate is 3-hydroxypyruvate (HPA), which after decarboxylation gives the carbanion-enamine (step **c**, Figure 1-3). This step was earlier assumed to render the reaction irreversible and was therefore regarded as the thermodynamic driving force of the reaction (Hobbs et al., 1993). However, a recent study gave evidence that TK can catalyse a reverse reaction in which the initial product is cleaved back into glycolaldehyde and the respective acceptor aldehyde. Consequently, carboligation reactions with HPA are initially kinetically controlled rather than thermodynamically controlled (Marsden et al., 2017).

Besides, it was also demonstrated that the glycolaldehyde, the corresponding aldehyde of HPA, can act as a donor substrate. This was shown for a one-substrate reaction, in which the self-ligation product of glycolaldehyde, erythrulose, was formed (Bykova et al., 2001; Sevostyanova et al., 2004).

All above mentioned donor substrates have a hydroxy group adjacent to the carbonyl group in common, meaning that in all cases a 1,2-dihydroxy ethyl group is transferred to the acceptor molecule. In contrast, pyruvate is not accepted as a donor substrate by TKs. This preference for hydroxylated substrates might be explained on a molecular basis by the recognition of the hydroxy group through interaction with H66 and H100 (see chapter 1.4.1) (Schneider and Lindqvist, 1998). Nevertheless, one study showed that also C3-halogenated derivatives of pyruvate can be donor substrates for *Sc*TK (Esakova et al., 2009). Here, H66 and H100 presumably form a bond to the respective halogen atom.

Acceptor substrates

Especially with HPA as a donor, a broad range of non-phosphorylated acceptor substrates were converted with TKs. Among these are aldehydes with hydroxylated and non-hydroxylated aliphatic, araliphatic, unsaturated as well as branched side chains and those containing (thio-)ethers of different lengths (C_1 to C_8) (Hailes et al., 2013; Schörken and Sprenger, 1998). Among the tested TKs from *E. coli*, yeast, and spinach, the reaction rate for α-hydroxylated aldehydes is significantly higher compared to non-hydroxylated substrates. Thereby, TKs are strictly selective for (2*R*)-hydroxylated aldehydes and can also be used for the chiral resolution of racemic α-hydroxy aldehydes (Effenberger et al., 1992; Kobori et al., 1992). Only for *Sc*TK, also conversion of aromatic acceptor aldehydes like benzaldehyde and benzaldehyde derivatives has been shown, although the formation of the corresponding products was not confirmed (Demuynck et al., 1991).

Overall, the affinity for the non-physiological acceptor substrates is about 10 to 100 times lower and also the excellent stereoselectivity of the physiological reaction is not met with these substrates (Ranoux and Hanefeld, 2013). Exemplarily, *ee*-values for the *Ec*TK catalysed carboligation of HPA and linear, aliphatic aldehydes are shown in Table 1-3.

1.4.3 Engineering of transketolases

The ability of TKs to catalyse asymmetric syntheses with high stereoselectivity and their wide range of acceptor substrates makes them interesting for preparative applications. To address the lower activity and stereoselectivity with non-physiological substrates, improved TK variants were developed. Thereby, most mutagenesis studies concerned the transketolases from *E. coli* (*Ec*TK) and *Geobacillus stearothermophilus* (*Gst*TK).

Substrate scope and stereoselectivity of EcTK

*Ec*TK variants with higher activity towards non-physiological acceptor substrates were developed by Helen Hailes, Paul Dalby, John Ward and co-workers using active-site targeted directed evolution. For that purpose, 19 different *Ec*TK libraries were created by site-saturation mutagenesis of single amino acid residues within a 10 Å distance from ThDP (Figure 1-20). As 52 residues lie within in this perimeter, a selection of target residues was made based on two criteria (Hibbert et al., 2007):

- **Phylogenetically defined sites** located within 10 Å distance from ThDP. They vary through the evolutionary history of transketolase, as assigned based on 52 verified transketolase sequences from bacteria, fungi and plants. This group comprised nine residues which showed maximum residue identities of 25 % to 67 % within these 52 sequences.

- **Structurally defined sites** located within 4 Å distance from ThDP. This group comprised ten residues of which nine were highly conserved with more than 91 % of the equivalent residues in bacterial and yeast sequences being identical to those in *Ec*TK.

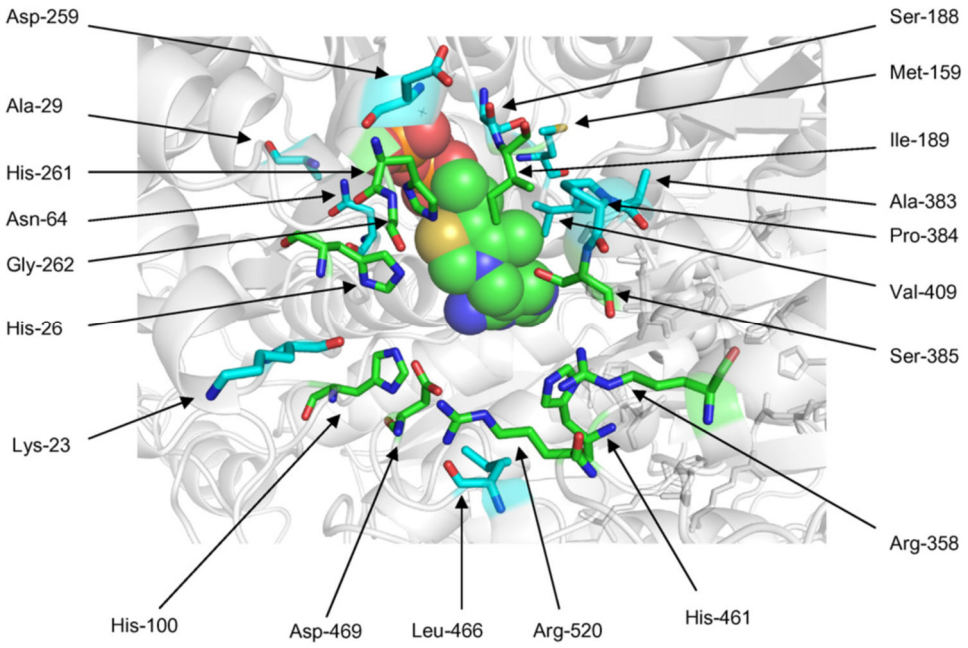

Figure 1-20: Location of the residues targeted by site-saturation mutagenesis in the active-site of *Ec*TK (PDB: QGD) according to Hibbert et al., 2007. Structurally defined sites: green, stick representation, phylogenetically defined sites: cyan, stick representation, ThDP: green, ball representation.

The libraries were first screened aiming at increasing the *Ec*TK activity for non-phosphorylated substrates using 3-HPA and glycolaldehyde as donor and acceptor, respectively. This and all following screenings were performed in microtiter plates using crude cell extracts (CCE). Specific activities were

estimated from endpoint determinations. In total twelve *Ec*TK variants with 1.5- to 4.8-fold faster product formation compared to the wt enzyme were found (Hibbert et al., 2007). For a majority of the variants the exchanged amino acids were originally involved in interactions with the phosphate group of the physiological substrate.

Subsequently, the libraries were screened for further substrates with stepwise less similarity to the physiological substrates, starting with non α-hydroxylated acceptors. For this purpose, the libraries were screened with propanal as acceptor aldehyde (Hibbert et al., 2008). In all screenings HPA served a donor substrate. 13 *Ec*TK variants showed 1.2-4.9-fold increased activity towards propanal compared to wt. Besides residues that interact with the phosphate group and two second shell residues, three further residues were identified, whose exchange promoted the activity with propanal: H26, H100 and D469. All three residues interact with the C2-hydroxy group of the physiological acceptor. Consequently, most of the respective variants in these positions showed lower activity towards glycolaldehyde compared to wt *Ec*TK, while the variants in the other positions increased the activity toward glycolaldehyde to the same or a higher degree as propanal (Hibbert et al., 2008).

The libraries H26X, H100X and D469X were additionally screened for the carboligation of HPA and propanal with the focus on the stereoselectivity of the variants (Table 1-3 Smith et al., 2008). Wt *Ec*TK catalyses the formation of the corresponding reaction product 1,3-dihydroxypentan-2-one (DHP) with 58% *ee* (*S*). For 44 % of the screened variants (as crude cell extracts) of library H26X stereoinversion with more than 10 % *ee* of the (*R*)-enantiomer was found. The highest *ee*-value of 88 % (*R*) was found for variant H26Y, which additionally showed a 4-fold increased activity towards propanal compared to wt *Ec*TK, although a second study reported lower activity of this variant (Yi et al., 2012). Variants from other samples of this library were not sequenced. In contrast, 72 % of the samples from the D469X library were *S*-selective and the highest *ee*-value of 90 % (*S*) as well as 8-fold increased activity was found for *Ec*TK D469E. Another variant of this library, D469Y catalyses the formation of (*R*)-DHP with 68 % *ee*. The combination of that substitution with R520V increased the *R*-selectivity to 85 % *ee* (Strafford et al., 2012). Variants of the library H100X showed only moderate stereoselectivities and comparably low activities and were therefore not further analysed (Smith et al., 2008).

Subsequently the stereoselectivity of *Ec*TK variants H26Y and D469E was also tested with longer aliphatic acceptor aldehydes (C_3-C_8) (Cázares et al., 2010). For all substrates both variants showed comparably high stereoselectivity with *ee*-values between 78 % (*R*) and 92 % (*R*) for variant H26Y and 86 % (*S*) and 98 % (*S*) for variant D469E (Table 1-3). *Ec*TK D469E additionally gave excellent stereoselectivities (>97 % (*S*)) with cyclic, aliphatic acceptor aldehydes (Cázares et al., 2010).

As a next step the similarity of the acceptor substrates to the physiological substrates was further reduced by using aromatic aldehydes in the screening. For that purpose, the D469X library was screened with HPA as a donor and benzaldehyde as an acceptor, which is not converted by wt *Ec*TK (Galman et al., 2010). Three variants D469E, D469K and D469E gave the respective product 1,3-dihydroxyphenylpropan-2-one, albeit with low yields of 2 %. Additionally, the rationally designed variant F434A was also tested, as the amino acid substitution was predicted to improve conversion of larger, aromatic substrates by removal of steric and hydrophobic interactions within the active site. This variant gave 10 % yield for the same reaction. Subsequently, all four variants were also tested with the heteroaromatic substrates furan-2-carbaldehyde and thiophene-2-carbaldehyde, for which in contrast to

wt *Ec*TK also conversion with yields <5 % were found. The stereoselectivity was not determined. Higher yields of 50 % were achieved with 2-phenylacetaldehyde as acceptor substrate with all four variants, which was 10-fold increased compared to wt *Ec*TK. Thereby, the product was formed with good stereoselectivity (>90 % *ee* (*S*), Table 1-3 ,Galman et al., 2010).

In order to re-establish electrostatic and hydrogen bonding interactions comparable to those with the physiological phosphorylated substrates, the carboxylated or hydroxylated analogues 3-formylbenzoic acid (3-FBA), 4-formylbenzoic acid (4-FBA), and 3-hydroxybenzaldehyde (3-HBA) were used instead of benzaldehyde for further engineering of variants with higher activity towards aromatic acceptors (Payongsri et al., 2012). Since *Ec*TK D469T gave up to 30- fold higher yields with these substrates compared to benzaldehyde, this variant was used as a starting point for a next round of mutagenesis, which targeted the phosphate binding site for the physiological TK substrates. D469T was combined with R520Q, because this substitution was described to improve the soluble production of *Ec*TK variants, to double the specific activity of variant D469T towards propanal, and to retain most of the activity of D469T towards 3-FBA and 4-FBA (Payongsri et al., 2012; Strafford et al., 2012). Subsequently, the libraries R358X/D469T/R520Q and S385X/D469T/R520Q were created and screened with 3-FBA, 4-FBA and 3-HBA (Payongsri et al., 2015). While no improved variants were found for the R358X/D469T/R520Q library, the S385X/D469T/R520Q library gave various variants with 1.8- to 5.5-fold increased conversion of the three acceptor substrates compared to *Ec*TK D469T. Among the best variants was S385Y/D469T/R520Q, which showed 3.4- and 12.4-fold increased activity towards 4-FBA and 3-HBA, respectively, but halved activity towards 3-FBA compared to *Ec*TK D469E. With 3-FBA the best variant was S385E/D469T/R520Q with 3.5-fold increased activity. This variant also showed 6-fold increased activity with 3-HBA but 5-fold decreased activity with 4-FBA (Payongsri et al., 2015). Stereoselectivities for these reactions were not determined.

Table 1-3: Stereoselectivity of selected, literature described *Escherichia coli* transketolase (*Ec*TK) variants for the carboligation of HPA (donor) and (ar-)aliphatic aldehydes (acceptor). Measurements were performed in CCE.

*Ec*TK variant	acceptor substrate	*ee*-value	literature
wildtype	propanal	58 % (*S*)	(Smith et al., 2008)
	n-butanal	75 % (*S*)	(Cázares et al., 2010)
	n-pentanal	84 % (*S*)	(Cázares et al., 2010)
	n-hexanal	85 % (*S*)	(Cázares et al., 2010)
	n-heptanal	74 % (*S*)	(Cázares et al., 2010)
	n-octanal	66 % (*S*)	(Cázares et al., 2010)
	2-phenylacetaldehyde	93 % (*S*)	(Galman et al., 2010)
H26Y	propanal	88 % (*R*)	(Smith et al., 2008)
	n-butanal	92 % (*R*)	(Cázares et al., 2010)
	n-pentanal	84 % (*R*)	(Cázares et al., 2010)
	n-hexanal	84 % (*R*)	(Cázares et al., 2010)
	n-heptanal	78 % (*R*)	(Cázares et al., 2010)
	n-octanal	83 % (*R*)	(Cázares et al., 2010)
F434A	2-phenylacetaldehyde	97 % (*S*)	(Galman et al., 2010)
D469Y	propanal	68 % (*R*)	(Strafford et al., 2012)
D469Y/R520V	propanal	85 % (*R*)	(Strafford et al., 2012)
D469E	propanal	90 % (*S*)	(Smith et al., 2008)
	n-butanal	98 % (*S*)	(Cázares et al., 2010)
	n-pentanal	97 % (*S*)	(Cázares et al., 2010)
	n-hexanal	97 % (*S*)	(Cázares et al., 2010)
	n-heptanal	86 % (*S*)	(Cázares et al., 2010)
	n-octanal	86 % (*S*)	(Cázares et al., 2010)
	2-phenylacetaldehyde	90 % (*S*)	(Galman et al., 2010)
D469K	2-phenylacetaldehyde	95 % (*S*)	(Galman et al., 2010)
D469T	2-phenylacetaldehyde	96 % (*S*)	(Galman et al., 2010)
D469T/R520Q	propanal	68 % (*S*)	(Strafford et al., 2012)

Substrate scope and stereoselectivity of GstTK

In a similar approach also *Geobacillus strearothermophilus* transketolase (*Gst*TK) variants with an improved activity towards aliphatic aldehydes as acceptor substrates were developed (Yi et al., 2015; Zhou et al., 2017). This thermostable transketolase was first reported in 2013 and shows 28-fold reduced activity for the non-hydroxylated aliphatic aldehyde n-butanal compared to the α-hydroxylated glycolaldehyde (Abdoul-Zabar et al., 2013). In contrast to the directed evolution of *Ec*TK, the libraries were created by combined site-saturation mutagenesis of two residues in this case. One of these residues was always D470(469), as it is involved into binding of the physiological transketolase substrates via hydrogen bonding to the α-hydroxy group. Further, L191(189), L382(382) and F435(434) form a non-polar pocket that contributes to substrate binding via hydrophobic interactions. Consequently, each of these residues was chosen as the second target residue in the combined site-saturation mutagenesis. The three resulting libraries where screened as CCE for activity with HPA as the donor and propanal as the acceptor substrate (Yi et al., 2015; Zhou et al., 2017). Positive hits were purified by a one-step heat shock protocol and characterised in detail. The specific activity was determined via a colorimetric assay

that follows the pH-shift upon the release of carbon dioxide from HPA (Yi et al., 2012). An overview over the *ee*-value of selected variants is shown in Table 1-4.

Screening of library L382X/D470X resulted in 34 *GstTK* variants with unique sequences and up to 16-fold improved activity towards propanal (D470I). Seven of the variants also showed increase *S*-selectivity compared to wt *Gst*TK. Six of those had a L382F substitution, including the L382F single variant, which additionally showed the highest activity of these seven variants. Most of the variants showed similar stereoselectivity like wt *Gst*TK and only 17 % showed clearly reduced excess of the *S*-enantiomer (*ee*<15 %) or even excess of the *R*-enantiomer for one variant, albeit with low *ee* of 9 % (*R*). The latter variants had a bulky residue in position 470 in common (Yi et al., 2015).

Variants from the library F435X/D470X showed up to 5-fold increased activity (variant F435L/D470E). The stereoselectivity ranged from almost racemic variants (D470W and F435V/D470W) up to an *ee* of 81 % (*S*) (F435Y), but none of the variants gave an excess of the *R*-enantiomer. As observed for the L382X/D470X library, variants with low stereoselectivity had a bulky residue in position 470. Variants with a high *S*-selectivity generally showed a lower activity (Zhou et al., 2017).

With variants from the library L191X/D470X up to 7.4-fold increased activity compared to wt *Gst*TK was achieved (L191I/D470L). In contrast to the other two libraries, 64 % of the variants formed an excess of the *R*-enantiomer up to 85 % *ee* (*R*) (L191V/D470R) and no variants showed increased *S*-selectivity. In the three variants with the highest *R*-selectivity L191 was substituted by valine. Again, lower activity was observed for variants with higher stereoselectivity (Zhou et al., 2017).

Besides propanal as a representative for aliphatic aldehydes, also benzaldehyde and 3-phenylpropanal were used as acceptor substrates to screen the library L382X/D470X in order to evolve *Gst*TK for aromatic acceptor substrates (Saravanan et al., 2017b). For that a reduced subset of 198 transformants was screened, which were previously identified in a screening with propanal as acceptor. Four variants were identified with benzaldehyde, two of them with a D470T substitution. The corresponding D469T substitution in *Ec*TK was also found earlier in screenings with benzaldehyde. The other two variants had a D470S substitution. L382 was exchanged for the polar or charged amino acids asparagine, aspartate and glutamate. Stereoselectivities could not be determined for this reaction, as the reaction products racemised due to C–H acidity of the ketone and the benzylic activation. From a further screening of the library with 3-phenylpropanal 15 variants with 8-fold to 28-fold (L382M/D470L) improved activity were selected. Most of these variants gave an *ee* between 54 % (*S*) and 81% % (*S*), which was increased compared to wt *Gst*TK (22 % *ee* (*S*)). The highest stereoselectivity with >99 % *ee* (*S*) was achieved with variant L382F/D470S, which also showed 19-fold increased activity. Further variants with high *S*-selectivity were L382M/D470T and L382N/D470S (Table 1-4). No variant with inverted stereoselectivity was found, but *Gst*TK L382A/D470I catalysed the formation of almost racemic product. The five best performing variants also showed increased conversion with several other arylated aldehydes as acceptor substrates (Saravanan et al., 2017b).

As described above, TK prefers (2*R*)-hydroxylated aldehydes as acceptor substrates. This stereospecificity was addressed in another screening of library L382X/D470X using the (2*S*)-hydroxylated acceptor L-glyceraldehyde (Abdoul Zabar et al., 2015). In contrast to other TKs, a slight activity towards this acceptor was found for *Gst*TK. From the library 72 variants were identified with at

least 2-fold increased activity towards L-glyceraldehyde. After re-screening for low activity towards D-glyceraldehyde, four variants with 2-fold to 5-fold increased activity towards L-glyceraldehyde and 5-fold to 13-fold decreased activity towards D-glyceraldehyde were selected. Similar effects on the activity were also observed with L- and D-lactaldehyde. The best performing variant was L382D/D470S. Here, the L382D substitution probably established a polar contact in favour of a (2*S*)-hydroxylated acceptor aldehyde, while the substitution of D470 removes interactions with (2*R*)-hydroxy groups. A serine in position 470 might support the binding of the 3-hydroxy group of L-glyceraldehyde, instead (Abdoul Zabar et al., 2015). The use of (2*S*)-hydroxylated acceptor aldehydes was subsequently demonstrated for the synthesis of naturally rare L-erythro (3*S*,4*S*)-ketoses (Lorillière et al., 2017).

Also the donor specificity was addressed in mutagenesis studies with *Gst*TK. For that purpose, *Gst*TK libraries in position H102(100) and H474(473), and combined libraries thereof were screened with pyruvate, as well as with the branched-chain oxoacids 3-methyl-2-oxobutanonate and 4-methyl-2-oxopentanonate (Saravanan et al., 2017a). Both residues are in direct contact to the CH_2OH moiety of HPA. Among the best performing variants were H102L/H474S for pyruvate as the donor and H102T for 3-methyl-2-oxobutanonate as the donor. In contrast, no variants with activity towards 4-methyl-2-oxopentanonate could be found. Further studies of the identified variants with other donor substrates demonstrated that H102L/H474S also showed high activity towards 2-oxobutanoate.

Table 1-4: Stereoselectivity of selected, literature described *Geobacillus stearothermophilus* transketolase (*Gst*TK) variants for the carboligation of HPA (donor) and propanal or 3-phenylpropanal (acceptor)

***Gst*TK variant**	**acceptor substrate**	***ee*-value**	**literature**
wildtype	propanal	79 % (*S*)	(Yi et al., 2015)
wildtype	propanal	70 % (*S*)	(Zhou et al., 2017)
L191V	propanal	69 % (*R*)	(Zhou et al., 2017)
L191V/D470R	propanal	84 % (*R*)	(Zhou et al., 2017)
L191V/D470I	propanal	74 % (*R*)	(Zhou et al., 2017)
L191A/D470L	propanal	44 % (*R*)	(Zhou et al., 2017)
L382F	propanal	94 % (*S*)	(Yi et al., 2015)
L382F/D470S	propanal	95 % (*S*)	(Yi et al., 2015)
L382F/D470V	propanal	95 % (*S*)	(Yi et al., 2015)
L382F/D470N	propanal	94 % (*S*)	(Yi et al., 2015)
L382F/D470T	propanal	94 % (*S*)	(Yi et al., 2015)
L382F/D470P	propanal	93 % (*S*)	(Yi et al., 2015)
L382E/D470S	propanal	92 % (*S*)	(Yi et al., 2015)
F435Y	propanal	81 % (*S*)	(Zhou et al., 2017)
F435T/D470V	propanal	81 % (*S*)	(Zhou et al., 2017)
wildtype	3-phenylpropanal	22 % (*S*)	(Saravanan et al., 2017b)
L382A/D470I	3-phenylpropanal	4 % (*S*)	(Saravanan et al., 2017b)
L382F/D470S	3-phenylpropanal	>99 % (*S*)	(Saravanan et al., 2017b)
L382M/D470L	3-phenylpropanal	43 % (*S*)	(Saravanan et al., 2017b)
L382M/D470T	3-phenylpropanal	80 % (*S*)	(Saravanan et al., 2017b)
L382N/D470S	3-phenylpropanal	81 % (*S*)	(Saravanan et al., 2017b)

1.4.4 Summary

TKs enlarge the product platform that is accessible with ThDP-dependent enzymes, as they catalyse the asymmetric synthesis of dihydroxy ketones. They differ from members of the DC superfamily with respect to their structure and their stereoselectivity. The active site structure and the function of the residues lining the active site have been studied thoroughly. Moreover, many variants with few substitutions within or close to the active site have been generated with increased activity towards various non-physiological substrates and/or increased or reversed stereoselectivity. All variants were found by active-site targeted directed evolution. A stereoselectivity model comparable to the model for ThDP-dependent DCs (see Figure 1-13) has not been developed before this thesis was started.

2 AIM OF THE THESIS

This project was embedded in the DFG research consortium FOR1296 with the topic "Diversity of asymmetric Thiamine Catalysis". The main goal of this research group was the elucidation of new thiamine-catalysed reactions based on a comprehensive understanding of thiamine catalysis. Here, the investigation of structure-function relationships with respect to the stereoselectivity of ThDP-dependent enzymes is an important issue. In this context, the aim of the project was to evaluate the applicability of the stereoselectivity model, which was developed for the structural decarboxylase (DC)-superfamily, for further ThDP-dependent DCs and to transfer this model to the structural superfamily of transketolases (TKs). Thereby, analytical methods should be selected to provide the highest possible information content about the (relative) quantities of the enantiomers in order to enable mechanistic conclusions.

For the evaluation of the stereoselectivity model for further DCs, YerE from *Pseudomonas protegens* (*Pp*YerE) was chosen. The crystal structure of *Pp*YerE has recently been solved (Loschonsky *et al.*, submitted to ChemBioChem). In contrast to most other ThDP-dependent DCs, *Pp*YerE catalyses 1,2-additions with non-activated ketones as acceptor substrate. Thereby, it broadens the product platform of ThDP-dependent enzymes by tertiary α-hydroxy ketones, which are usually difficult to access by enzymatic synthesis (Müller, 2014). The possibility to create *S*-selective *Pp*YerE variants should first be investigated for the formation of phenylacetylcarbinol (PAC) from pyruvate and benzaldehyde, which is a typical reaction for ThDP-dependent DCs. Later on, the stereoselectivity of *Pp*YerE variants should also be characterised with ketones as acceptor substrates.

For the investigations regarding the transfer of the stereoselectivity model on TKs, the TK from *Escherichia coli* (*Ec*TK) was chosen. TKs show a different domain arrangement and active-site structure compared to the DC superfamily and are moreover naturally *S*-selective. *R*-selective variants of *Ec*TK and also *Geobacillus stearothermophilus* TK (*Gst*TK) have already been generated by active-site targeted directed evolution (Hailes et al., 2013; Yi et al., 2015; Zhou et al., 2017). However, a structure-based stereoselectivity model comparable to the model described for DCs was still missing. In this thesis, structural knowledge, literature data of published TK-variants and results from comprehensive site-directed mutagenesis studies should be combined to develop an extended stereoselectivity model that comprises DCs and TKs. Thereby, the primary goal was a profound understanding of the mechanism that enable the formation of *R*-enantiomers rather than just a stereoselectivity switch, which could also be achieved by a reduction of the *S*-enantiomers.

3 RESULTS AND DISCUSSION

3.1 Evaluation of the stereoselectivity model for a further decarboxylase: YerE from *Pseudomonas protegens*

3.1.1 Identification of target residues

As shown in Figure 1-14, opening of an antiparallel acceptor binding pocket can invert the stereoselectivity of ThDP-dependent DCs by enabling binding state *II* according to Figure 1-12. Here, this principle was evaluated for YerE from *Pseudomonas protegens* (*Pp*YerE). Important residues for the opening of a potential antiparallel acceptor binding pocket in *Pp*YerE were identified based on the amino acid sequence as well as the crystal structure (PDB: 5AHK, Loschonsky *et al.*, submitted to ChemBioChem). For sequence-based analysis the standard numbering scheme for ThDP-dependent decarboxylases of the BioCatNet databases system was applied (Buchholz et al., 2016; Vogel et al., 2012). According to this, the pocket is defined by the amino acid residues L22(25), I23(26), G24(27), G25(28), and V479(477) (numbers in parentheses indicate the respective standard position). Further, F482 (480) lines the pocket and M478(476) defines the entrance to the pocket. Generally, most of these side chains are consistent with the amino acids defining the potential antiparallel acceptor binding pockets of *Ec*AHAS-I and *Ec*AHAS-II (Westphal, 2013) and are mostly smaller than for other ThDP-dependent DCs. Standard position 477, which was decisive for the inversion of stereoselectivity of *Pp*BFD, *Ap*PDC, *Ec*MenD and *Bs*MenD (see chapter 1.3.5), is in *Pp*YerE occupied by valine, whereas glutamate and phenylalanine are found in *Ap*PDC and the MenDs in this position, respectively. Thus, the space of the potential antiparallel acceptor binding pocket in *Pp*YerE is smaller compared to the other enzymes, were such a pocket was successfully opened.

The structure-based analysis identified V479 as the main residue defining the potential pocket besides L22, I23, G24, G25 and L476(474) (Figure 3-1 A). M478 is located at the entrance of the pocket but at least in the crystal structure appears to be in a conformation that does not restrict accessibility of the pocket. F482 is located in the substrate channel and seems to have only minor influences of the pocket architecture. From the crystal structure it further becomes evident that the potential pocket size is restricted by the backbone of an α-helix (helix 22, amino acids 477-486), which is shifted by about 1.6 Å into the area of the potential pocket in comparison to *Ap*PDC (Figure 3-1 B).

In this thesis, *Pp*YerE variants were created by amino acids substitutions of residues defining the antiparallel acceptor binding pocket and their stereoselectivity in 1,2-additions was investigated. Thereby, the stereoselectivity was not only evaluated based on relative *ee*-values but also based on the absolute concentrations of both enantiomers. This provides deeper insights into the mechanisms by which amino acid substitutions affect the stereoselectivity since it allows to distinguish whether the stereoselectivity changed because of an increased formation of one enantiomer, a decreased formation of the other enantiomer, or a combination of both.

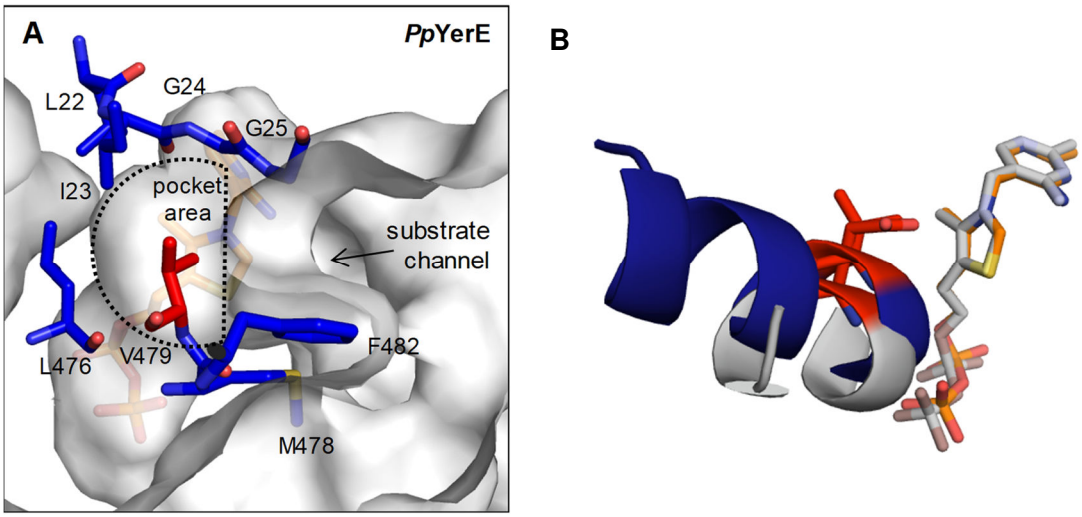

Figure 3-1: A: Active-site structure of *Pp*YerE. Residues defining the potential antiparallel acceptor binding pocket are shown in stick representation. V479(477) is displayed in red, further residues lining the pocket are displayed in blue. ThDP is depicted in orange. **B: Structure alignment of *Pp*YerE (blue, PDB: 5AHK) and *Ap*PDC (grey, PDB: 2VBI).** Compared to *Ap*PDC the helix lining the antiparallel acceptor binding pocket of *Pp*YerE is shifted into the area of the pocket, decreasing the potential pocket size. The amino acid at standard position 477 is highlighted in red. ThDP bound in *Pp*YerE and *Ap*PDC is depicted in orange and grey, respectively. The figures were generated with the PyMOL Molecular Graphics System (Schrödinger, LLC).

3.1.2 Opening of an antiparallel acceptor binding pocket

As shown in Figure 3-2, manual docking of benzaldehyde into a pocket that was opened by a single amino acid exchange of V479(477) to glycine indicated that the available space is not sufficient for binding and stabilisation of benzaldehyde according to binding state *II* (Figure 1-12), as it clashes with α-helix 22. This was also confirmed by experimental results (Figure 3-3) in which the *ee* of (*R*)-PAC was >99 % in biotransformations with wt *Pp*YerE and variant V479G. With variant V479A the *ee*-value was only slightly reduced to 95 %. After 24 h the *ee*-values were lowered by four to five percent points. Wt *Pp*YerE gave excellent yields with full conversion within 30 min. Variant V479G was almost as fast as the wt enzyme, giving full conversion after 1 h, while variant V479A was slower.

Even though the lowered *ee* with variant V479A shows that relative amount of benzaldehyde that binds in antiparallel orientation before C-C bond formation could be slightly increased, an inversion of the stereoselectivity could not be achieved by a single amino acid exchange. This is consistent with results obtained with *Ec*AHAS-II before, for which the size of the antiparallel acceptor binding pocket is as well restricted by the backbone of an α-helix and single amino acid substitutions of the residue in standard position 477 could not invert the stereoselectivity for PAC-formation (Westphal, 2013). The reduced *ee*-value of (*R*)-PAC obtained with variant V479A shows that the productive antiparallel binding of the benzaldehyde side chain is in principle possible but rather unlikely, probably because of the restricted space within the antiparallel acceptor binding pocket. Therefore, additional strategies were needed to optimise the size and the architecture of the pocket.

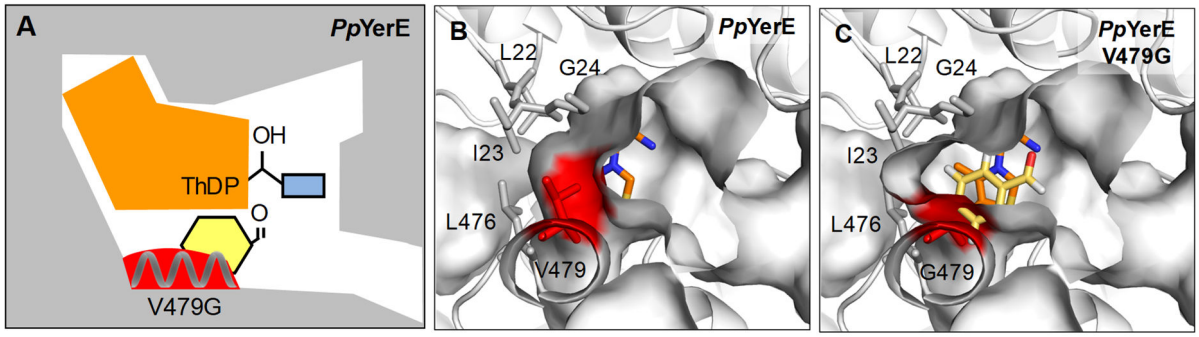

Figure 3-2: Opening of an antiparallel acceptor binding pocket in *Pp*YerE by substitution of V479(477) which blocks the antiparallel orientation of the acceptor side chain (highlighted in red). **A** and **B**: Schematic and PyMOL representation of the antiparallel binding pocket area including α-helix 22, which restricts the size of the pocket. **C**: Despite opening of an antiparallel acceptor binding pocket by exchange of V479 by glycine, the pocket does not fit benzaldehyde (yellow) as it collides with the backbone of α-helix 22. Figures B and C were generated with the PyMOL Molecular Graphics System (Schrödinger, LLC) based on the crystal structure of *Pp*YerE (PDB: 5AHK).

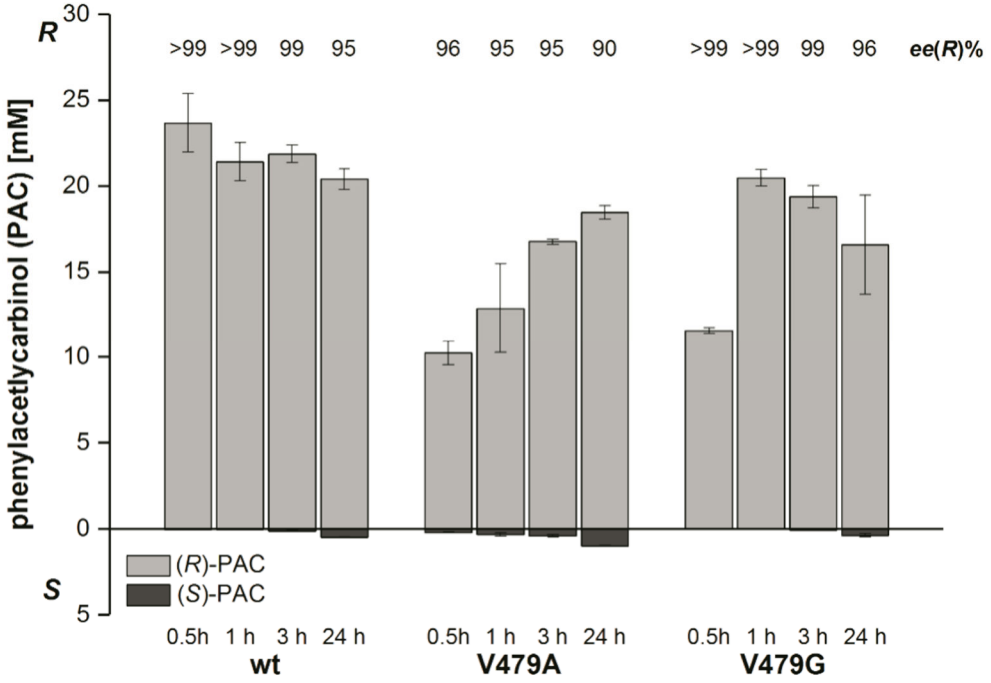

Figure 3-3: *Pp*YerE catalysed carboligation of (decarboxylated) pyruvate (donor) and benzaldehyde (acceptor) to phenylacetylcarbinol (PAC) after opening of an antiparallel acceptor binding pocket by substitution of V479(477). Reaction conditions: 50 mM KP_i-buffer pH 8, 0.5 mM ThDP, 3 mM $MgCl_2$ and 1 mg·mL^{-1} *Pp*YerE variant, 50 mM pyruvate and 20 mM benzaldehyde; 30 °C. Samples were analysed via chiral phase HPLC (see chapter 5.4.2). Error bars represent the standard error of biological triplicates.

3.1.3 Site-saturation mutagenesis on second shell residues to displace α-helix 22

As described in chapter 1.3.5 exchange of second shell residues can influence the stereoselectivity despite any direct interaction with the substrate molecules. Probably the exchange influences the architecture of the active site and especially the antiparallel acceptor binding pocket which might be induced by a shift or increased flexibility of the α-helix. Therefore, the potential of an exchange of second shell residues by site-saturation mutagenesis was investigated for the stereoinversion of *Pp*YerE and variant V479(477)G was chosen as a starting point. T494(486.2)* is located on a flexible loop in proximity to α-helix 22 (Figure 3-4). Exchange of the corresponding residue L476(488) in *Pp*BFD increased the stereoselectivity for (*S*)-PAC formation up to 15 percent points (Lingen et al., 2002). It

*Standard number 468 is assigned to several residues in *Pp*YerE, because its sequence is longer than the reference *Sc*PDC sequence. These residues are distinguished by the decimal number.

might influence the position of α-helix 22 by interactions with Q483(481), which is 2.6 Å apart. Consequently, both residues were subjected to combined site-saturation mutagenesis (chapter 5.2.3).

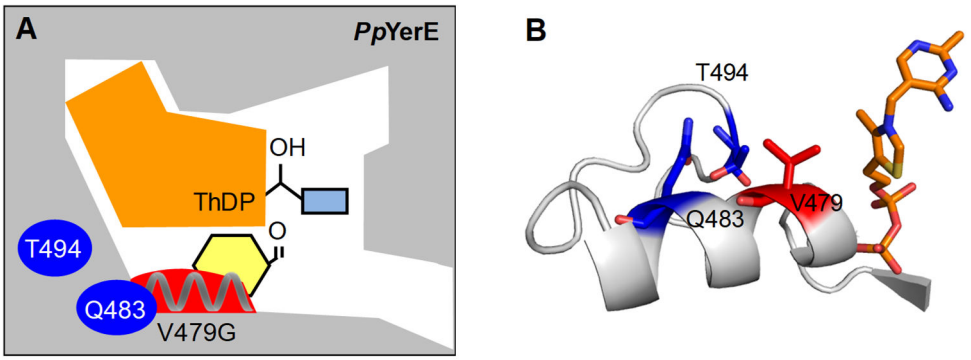

Figure 3-4: Position of the second shell residues Q483(481) and T494(486.2) (blue) that were addressed in combined site saturation mutagenesis in order to displace α-helix 22 in schematic (A) and PyMOL (B) representation. V479 (477) is depicted in red, ThDP in orange, the donor in light blue, and the acceptor in yellow. Figure B was generated with the PyMOL Molecular Graphics System (Schrödinger, LLC) based on the crystal structure of *Pp*YerE (PDB: 5AHK).

In order to reduce the amount of *Pp*YerE variants which must be screened for adequate sequence coverage NDT-codons were used (chapter 5.2.3). Thereby, codons for twelve different proteogenic amino acids can be inserted during the mutagenesis protocol, yielding 144 possible sequences by combinatorial mutagenesis at two sites. To cover >95 % of the possible sequences at least 430 *Pp*YerE variants have to be screened (Firth and Patrick, 2008; Patrick and Firth, 2005). However, after the site-saturation mutagenesis was carried out according to the protocol described in chapters 5.2.3 and 5.2.4, only 188 colonies were obtained, which correlates with a sequence coverage of 73 % so that 105 distinct *Pp*YerE variants were expected (Firth and Patrick, 2008; Patrick and Firth, 2005). Supported by a robotic platform, the library was screened for the formation of (*S*)-PAC starting from pyruvate and benzaldehyde using crude cell extracts (CCE) in microtiter plates as described in chapter 5.3.8. *Pp*YerE V479G and wt *Pp*YerE were included as controls. Figure 3-5 shows that for none of the screened variants the fraction of (*S*)-PAC was higher than for the V479G control (dark red), which also gave the highest overall yield. However, absolute yields have to be interpreted very carefully in this type of screening, because the amount of active enzyme is not comparable. Neither cell growth, nor expression levels were monitored in this system. Since even silent codon exchanges in recombinant genes can greatly influence the metabolism of *E. coli* (Rahmen et al., 2015) the amount of recombinant enzyme variants produced in different clones cannot be assumed to be the same. Further, the completeness of the cell disruption step could vary between different wells. Through pipetting inaccuracies of the robotic platform parts of the cell pellet containing enzyme variants were often removed together with the medium. Consequently, different product yields are likely to result from different *Pp*YerE concentrations in different samples. This also explains that the product yield with the wt *Pp*YerE control (green in Figure 3-5) was more than seven times lower than with *Pp*YerE V479G control, even though the yield for PAC after 24 h were comparable for both variants with purified enzymes (see chapter 3.1.2).

The stereoselectivity was not affected for most of the screened variants. 80 % of the variants showed a stereoselectivity ≥95 % (*R*). 25 samples showed a clear shift of the stereoselectivity with up to 40 °% ee for the *S*-enantiomer. This shift, however, was not due to an increase of (*S*)-PAC concentration, but to a strong decrease of (*R*)-PAC concentration. Sequencing of the respective isolated plasmids showed that for all these 25 samples at least 84 % of the *ilvB* gene, which encodes for *Pp*YerE, as well as the T7-promotor sequence were deleted from the plasmid. Thus, a functional production of *Pp*YerE variants

was not possible with the respective transformants and the observed product formation was most likely due to background reactions of the crude cell extract.

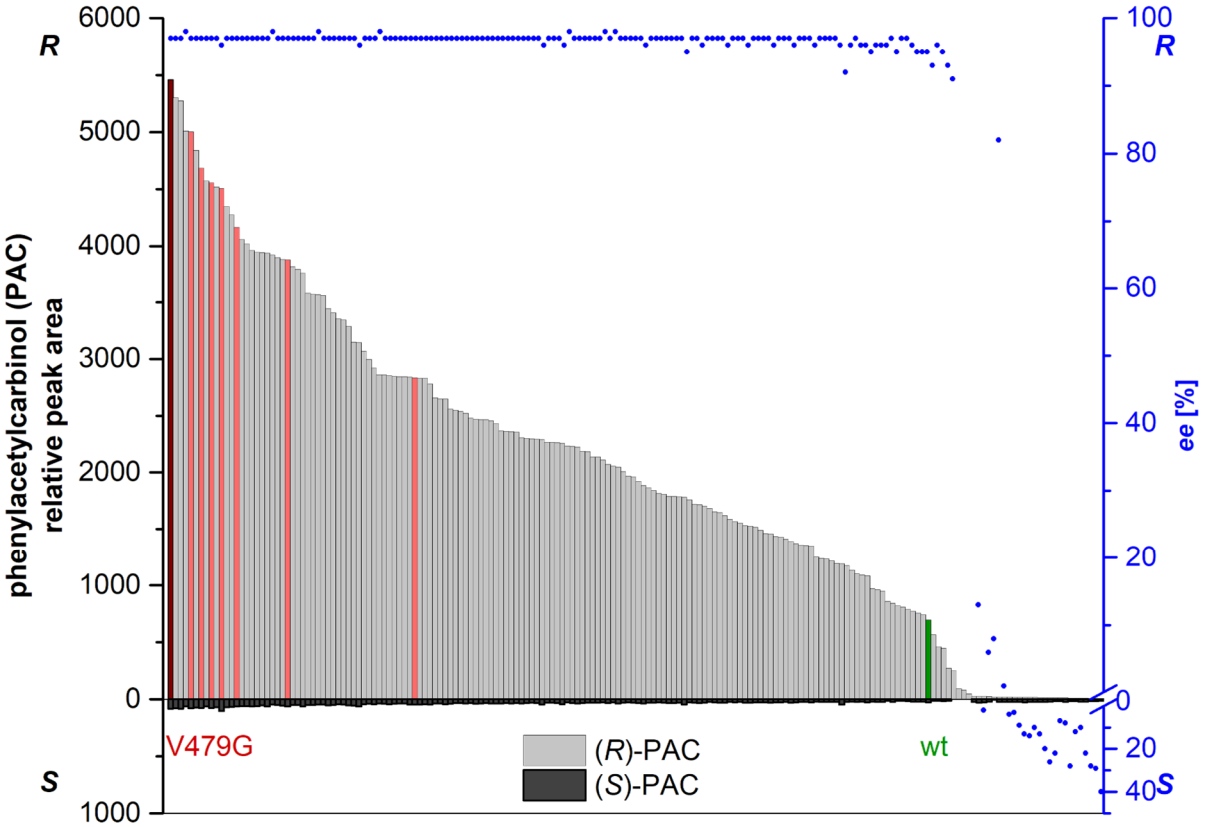

Figure 3-5: Screening results of the *Pp*YerE V479(477)G/Q483(481)X/T494(486.2)X library for the formation of phenylacetlycarbinol (PAC) from pyruvate and benzaldehyde. (*R*)- and (*S*)-PAC are represented by columns on the positive and negative ordinate, respectively. The *ee*-values are given as dots above or underneath each column, depending on which enantiomer is in excess. The results are sorted by the amount of (*R*)-PAC formed under the tested conditions. The wt *Pp*YerE control is displayed in green and the *Pp*YerE V479G control in dark red. Sequencing identified variants without a substitution of Q483 and T494, thus being replicas of the V479G control. These variants are highlighted in light red. Blue dots represent the *ee* with each variant. Reaction conditions: 50 mM KP_i-buffer pH 8, 0.5 mM ThDP, 3 mM $MgCl_2$, 50 mM pyruvate and 20 mM benzaldehyde in crude cell extracts, 30 °C, 24 h. The screening was performed semi-automated with a robotic liquid handling system (see chapter 5.3.8). Samples were analysed via chiral phase HPLC (see chapter 5.4.2).

To evaluate the quality of the library 55 further variants were sequenced. For seven of these variants no amino acid substitutions were found for Q483 and T494 (light red in Figure 3-5). This indicates that the *Dpn*I-digestion to remove parental DNA was not complete, since NDT-codons do not include the codons for glutamine or threonine. Among the other sequenced mutants, at both positions eleven of in total twelve possible amino acid substitutions were found, suggesting that the mutation rate was good, and the full range of possible substitutions was covered for each individual position. Nevertheless, in total only 28 of 144 possible combinations of the two amino acid substitutions were found. Statistically 41 different combinations were expected in that number of sequences (Firth and Patrick, 2008; Patrick and Firth, 2005). This indicates a biased mutagenesis procedure, for example due to primer synthesis or primer binding.

Overall the quality of the library was impaired by a combination of a small number of transformants, incomplete *Dpn*I digestion, deletion of the *ilvB* gene sequence and the biased mutagenesis procedure. Nevertheless, the results still show that *Pp*YerE is very robust with respect to amino acid substitutions in positions 483 and 494. The stereoselectivity was not affected and differences in the product formation were more likely to be due to the non-standardised screening conditions than a consequence of different

activities of the variants. Here it is also noteworthy that the substitution of three amino acid residues in or near the active side did apparently not have a significant impact on the activity. Therefore, this approach to increase the size of the antiparallel acceptor binding pocket was not further followed, even though the sequence coverage was low so that most likely not all possible *Pp*YerE variants were tested in the screening.

3.1.4 Deletion of α-helix 22

Since the possibilities to open an antiparallel binding pocket through mutagenesis in the area were limited, the α-helix 22 causing the sterical limitation was deleted in the next step. The crystal structure of *Pp*YerE shows that the C_α-atoms of G477(475), which is the first amino acid in α-helix 22, and T494(486.2), which is located on a loop eight amino acids C-terminal of the helix, have a spatial distance of 7.1 Å. Thus, the 16 amino acids* between G477 and T494 (red in Figure 3-6) were deleted by ligase free cloning (chapter 5.2.3). As both residues are located on flexible loops, no additional linker was inserted. The deletion of the sequence creates space for aromatic substrates like benzaldehyde in anti-parallel binding conformation (Figure 3-6 D)

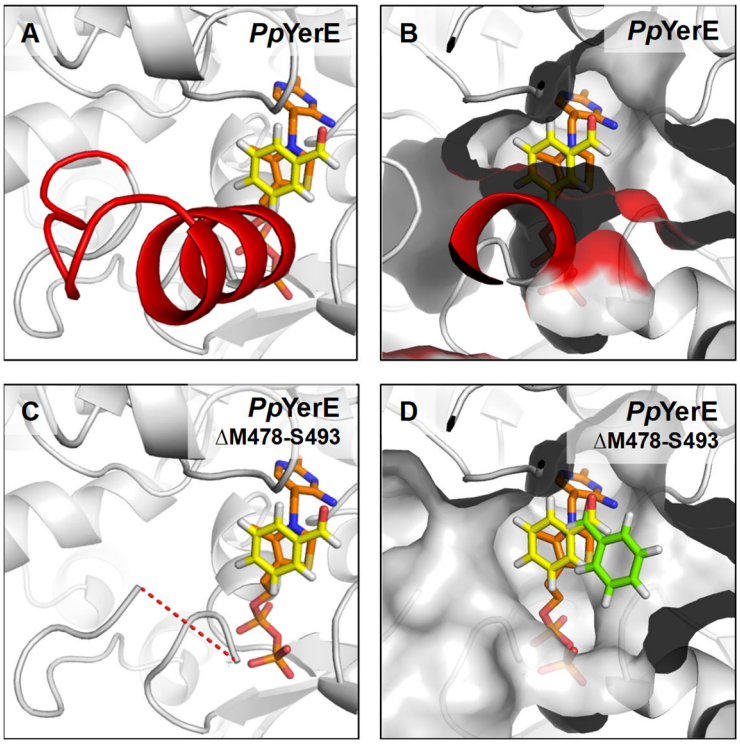

Figure 3-6: Deletion of α-helix 22. The deleted sequence in wt *Pp*YerE (**A** and **B**) is displayed in red. The distance of 7.1 Å between the amino acids N- and C-terminal of the deletion is illustrated by a red, dashed line in **C**. Deletion of the helix provides enough space for antiparallel binding of the benzaldehyde site chain (**D**). Figures were generated with the PyMOL Molecular Graphics System (Schrödinger, LLC) based on the crystal structure of *Pp*YerE (PDB: 5AHK). A and C show the cartoon representation, B and D display the surface. Yellow: Benzaldehyde in antiparallel binding orientation; Light green: Benzaldehyde in parallel binding orientation Orange: ThDP.

The carboligation potential of the resulting variant *Pp*YerE ΔM478-S493 was investigated using crude cell extracts according to the conditions described in Table 5-29. Since the deletion of α-helix 22 probably led to an increased solvent exposition of the active site, the concentrations of ThDP and $MgCl_2$ where increased to 2.5 mM and 9 mM respectively, in order to avoid diffusion of the cofactors out of the active site. Despite the deletion of 16 amino acids close to the active site, *Pp*YerE ΔM478-S493 still showed residual activity, even though the PAC-formation within 24 h was 24-fold reduced compared to

*The difference according to the standard numbering scheme is lower, as the helix and the loop are shorter in the reference *Sc*PDC sequence and therefore some standard numbers are assigned to several residues.

wt *Pp*YerE. Although the deletion of α-helix 22 probably provided enough space for the antiparallel binding of the benzaldehyde side chain (Figure 3-6 D), the *R*-enantiomer was still produced in excess (40 % *ee*). Possible reasons are that the formed antiparallel acceptor binding pocket was too big to optimally stabilise benzaldehyde and that the parallel binding of the benzaldehyde side was not destabilised to supress reaction via the *R*-pathway (light green in Figure 3-6 D). Nevertheless, the lowered *ee*-value indicated that the probability for benzaldehyde to bind in the antiparallel side chain orientation increased. However, due to the low activity of *Pp*YerE ΔM478-S493, the absolute amount of (*S*)-PAC produced with the variant was lower than with wt *Pp*YerE, therefore this approach was not further followed. Subsequent studies to invert the stereoselectivity of the enzyme concerned further residues in the active site.

3.1.5 Combinatorial mutagenesis of residues lining the pocket to increase its size

As already pointed out in chapter 1.3.5 the residue in standard position 477 is mainly blocking the antiparallel acceptor binding pocket and its exchange was found to be decisive to invert the stereoselectivity of *Ap*PDC, *Ec*MenD and *Bs*MenD. However, the example of MenD shows that a single amino acid exchange may not be sufficient for complete stereoinversion. This was only possible in combination with the exchange of the residue in standard position 476, which blocks the entrance to the pocket. Judging from the crystal structure the corresponding residue in *Pp*YerE, M478(476), does not restrict the access to the pocket (see chapter 3.1.1). However, among the other residues lining the pocket exchange of I23(26) and L476(474) might increase the pocket size (Figure 3-7).

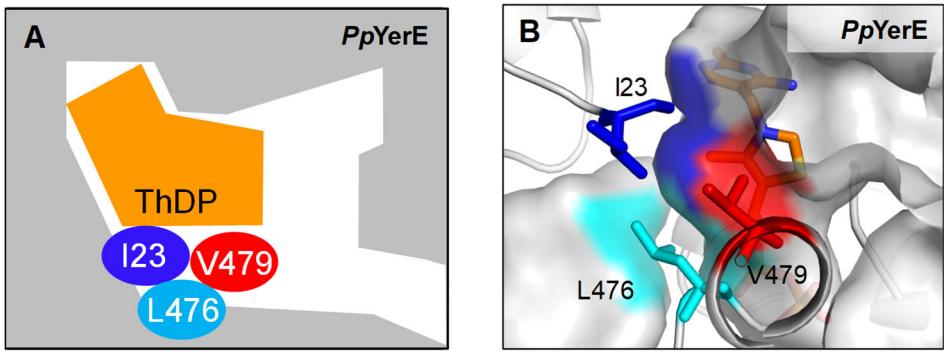

Figure 3-7: Positions of the residues I23 (26), L476 (474), and V479 (477) in the active site of *Pp*YerE that were exchanged by alanine and glycine in a combinatorial library to increase the size and to optimise the architecture of the antiparallel acceptor binding pocket, shown in schematic (**A**) and PyMOL (**B**) representation. Figure B was generated with the PyMOL Molecular Graphics System (Schrödinger, LLC) based on the crystal structure of *Pp*YerE (PDB: 5AHK).

Therefore, a combinatorial library in which I23, L476, and V479 were substituted by alanine and glycine was created by site-directed mutagenesis (chapter 5.2.3). The resulting 27 *Pp*YerE variants (including wt *Pp*YerE) were screened for the carboligation of pyruvate and benzaldehyde as described in chapters 3.1.3 and 5.3.8. Since the library was not constructed by site-saturation mutagenesis the plasmid sequence of each transformant was known and it was possible to perform the screening in triplicate. The results of these biological triplicates underline that absolute yields cannot be compared in this screening system, as they fluctuate drastically between some of the samples within one triplicate (see Figure 3-8). This can probably be deduced to differences in cell growth and expression levels as well as inaccurate pipetting as pointed out in chapter 3.1.3. Nevertheless, some trends concerning the productivity of the variants could be deduced from the results:

Substitution of I23 or V479 by alanine and glycine as well as combinations thereof did not impair the PAC-formation under the tested conditions, although the end point determination does not allow conclusions concerning the respective reaction velocities. Exchange of L476 especially in combination with substitution of V479 on the other hand resulted in variants with a lower PAC-forming activity, as could be deduced from the significantly lower product concentration after 24 h (Figure 3-8). However, at that point a lower stability of these variants could lead to a similar result. The stereoselectivity could not be inverted for any of the variants. Variants with an exchange of L476 gave lower excess of (*R*)-PAC (between 38 % and 89 % *ee* (*R*)) but that was due to a decreased formation of the *R*-enantiomer rather than an increase of the *S*-enantiomer. Overall the results show that also combined substitution of I23, L476, and V479 was not sufficient to create enough space for stabilisation of the benzaldehyde side chain in the antiparallel acceptor binding pocket of *Pp*YerE according to binding state *II* (Figure 1-12).

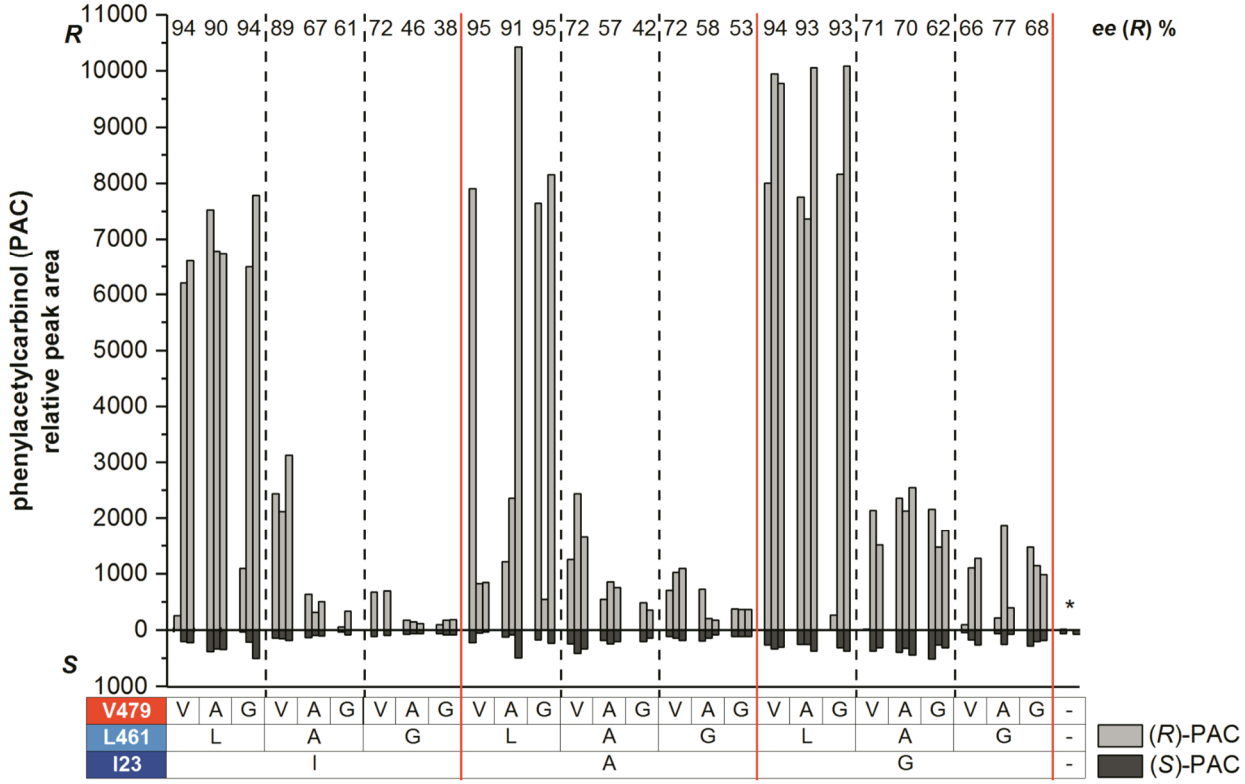

Figure 3-8: Screening of the combinatorial library of I23 (26) L476 (474) and V479 (477) for the carboligation of pyruvate and benzaldehyde to phenylacetylcarbinol (PAC). Due to high fluctuations, triplicates are shown as individual measurements. Reaction conditions: 50 mM KP_i-buffer pH 8, 0.5 mM ThDP, 3 mM $MgCl_2$, 50 mM pyruvate and 20 mM benzaldehyde in crude cell extracts, 30 °C, 24 h. The screening was performed semi-automated with a robotic liquid handling system (see chapter 5.3.8). Samples were analysed via chiral phase HPLC (see chapter 5.4.2). Full conversion roughly corresponds to a peak area of 17000. *Empty vector control with *E. coli* BL21 carrying the pET28a (+) vector without insertion of the *ilvB* gene encoding for *Pp*YerE.

3.1.6 Smaller acceptor substrates

Opening of an antiparallel acceptor binding pocket by substitution of V479(477) as well as different approaches to increase the size of the pocket were not successful in terms of inverting the stereoselectivity for PAC-formation from pyruvate as donor and benzaldehyde as acceptor substrate. In order to evaluate the applicability of the stereoselectivity model for *Pp*YerE, the use of smaller aliphatic acceptor aldehydes like n-pentanal and propanal was investigated. The respective products of the carboligation of pyruvate and n-pentanal or propanal, 3-hydroxyheptan-2-one (3-HH) and

3-hydroxypentan-2-one (3-HP) (Figure 3-9), are nature-identical flavour ingredients and used for aroma production (Neuser et al., 2000; van der Schaft et al., 1997). Manual docking of both substrates into a pocket that was opened by exchange of V479 with glycine indicated that the available space should be sufficient for antiparallel binding of the side chains of both acceptors (Figure 3-10).

Since no reference compounds or applicable synthesis protocols for reference compounds were available, the corresponding peaks were initially identified based on their mass fragmentation pattern using a chiral GC-MS. The identity of the products was subsequently confirmed by ^{1}H- and ^{13}C-NMR (see chapter 5.4.4) and the configuration at the stereocenter was determined by CD-spectroscopy (see chapter 5.4.5).

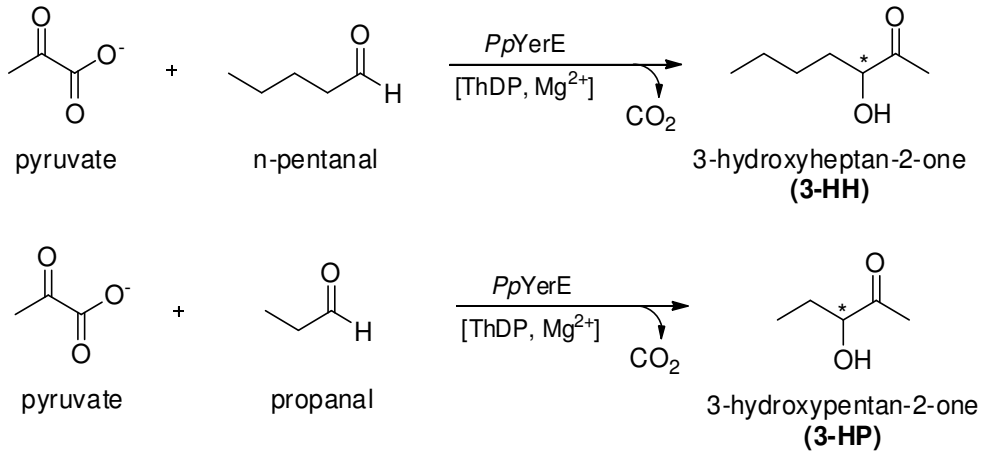

Figure 3-9: *Pp*YerE catalysed carboligations of pyruvate (donor) and the aliphatic aldehydes n-pentanal and propanal (acceptors).

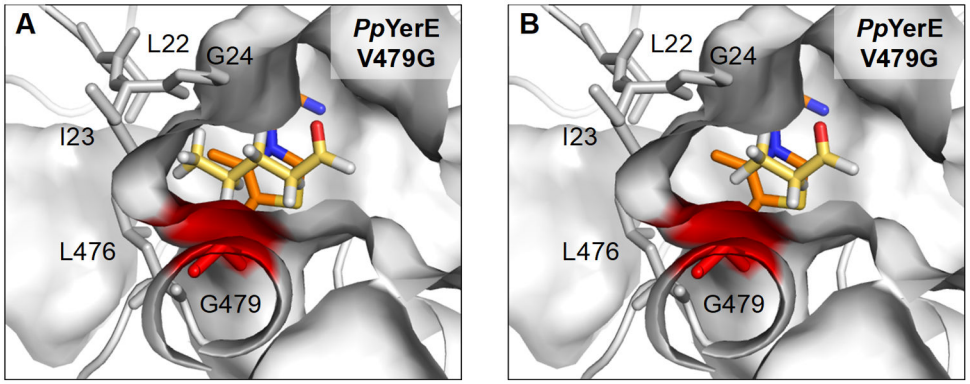

Figure 3-10: Manual docking of binding of n-pentanal (A) and propanal (B) in an antiparallel binding pocket in *Pp*YerE opened by a V479(477) substitution (red). The pocket provides enough space to enable antiparallel binding of the smaller aliphatic acceptor substrates. The figures were generated with the PyMOL Molecular Graphics System (Schrödinger, LLC) based on the crystal structure of *Pp*YerE (PDB: 5AHK). Yellow: acceptor aldehyde; orange: ThDP.

Biotransformations with PpYerE variants V479A and V479G

As shown in Figure 3-11 wt *Pp*YerE catalysed the formation of (*R*)-3-HH from pyruvate and n-pentanal with a low *ee* of 16 %. This indicates that the antiparallel acceptor side chain orientation according to binding state *II* (Figure 1-12) was already possible without opening of a pocket. Substitution of V479 by alanine inverted the stereoselectivity with a low *ee*- value of about 30 % (*S*). Substitution by glycine, on the other hand, increased the *ee* of (*R*)-3-HH to 30 %. With propanal as the acceptor wt *Pp*YerE yielded an excess of (*S*)-3-HP (*ee* 40 %). This is consistent with the results with pentanal, since a smaller

substrate side chain is more likely to be bound in antiparallel orientation when no pocket is opened. Opening of the pocket in the V479A variant increased the *S*-selectivity after 1 h to an *ee*-value of 57 % for (*S*)-3-HP. As with n-pentanal, variant V479G showed a shift of the stereoselectivity toward the *R*-enantiomer of 3-HH, which was in this case formed with 54 % *ee*.

As shown in Figure 3-3 with benzaldehyde as the acceptor, a slightly lower *R*-selectivity of variant V479A compared to wt and variant V479G was observed. Here, this effect is more pronounced as variant V479G even gave a higher relative amount of the *R*-enantiomer as wt *Pp*YerE, while variant V479A showed inversion of the stereoselectivity or increased *S*-selectivity for n-pentanal or propanal as acceptor, respectively. Since the size of the opened antiparallel acceptor binding pocket is theoretically bigger for the V479G substitution, these results are counter-intuitive on the first sight. However, it is likely that the introduction of a glycine destabilises the secondary structure in the area of the pocket, especially since four other glycine residues are present in position 477(475) and 481(479) in α-helix 22 as well as in position 24(27) and 25(28), lining the pocket area. Therefore, it can be assumed that the antiparallel acceptor binding pocket disintegrates upon introduction of another glycine residue, resulting in increased *R*-selectivity.

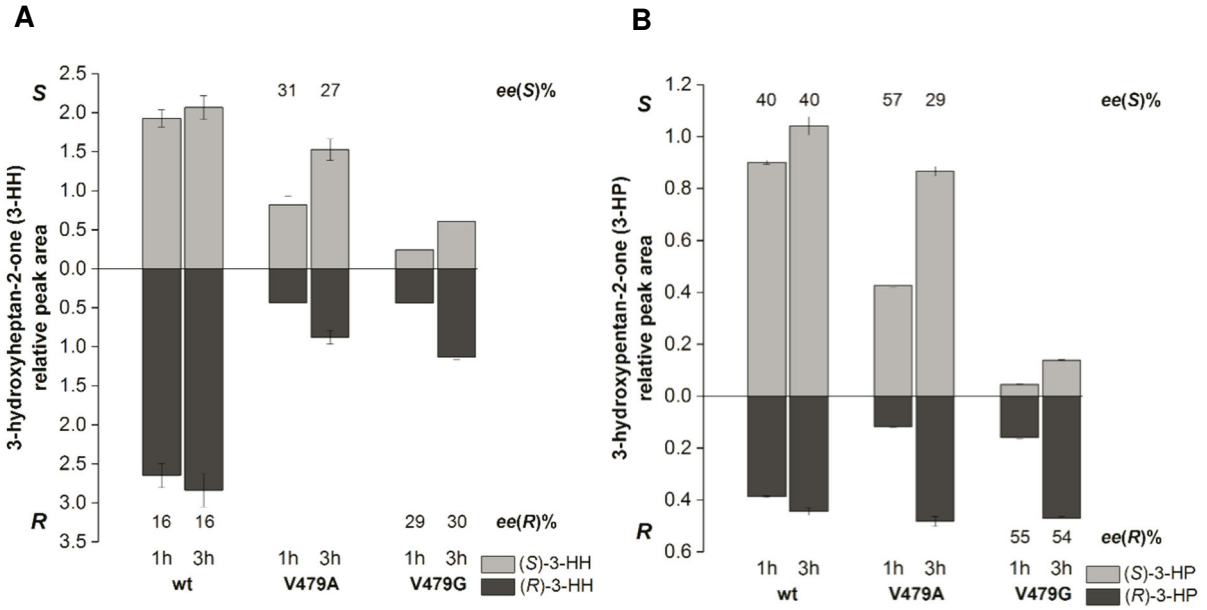

Figure 3-11: *Pp*YerE-catalysed carboligation of pyruvate (donor) and the aliphatic acceptor aldehydes n-pentanal (A) and propanal (B) to 3-hydroxyheptan-2-one (3-HH) and 3-hydroxypentan-2-one (3-HP), respectively, after opening of an antiparallel acceptor binding pocket by substitution of V479 (477). Reaction conditions: 100 mM KP_i-buffer pH 8, 2.4 mM ThDP, 3 mM $MgCl_2$, 0.05 mM FAD and 1 mg·mL^{-1} *Pp*YerE variant, 50 mM pyruvate and 50 mM n-pentanal or propanal, 30 °C. Samples were analysed via chiral phase GC-MS (see chapter 5.4.3). Error bars represent the standard error of biological triplicates.

Screening of the combinatorial library with aliphatic acceptor aldehydes

As single substitution of V479(477) by alanine and glycine did not results in highly *S*-selective variants, the combinatorial library of I23(26), L476(474) and V479 (see chapter 3.1.5) was also screened with n-pentanal and propanal as acceptors (chapter 5.3.8, donor: pyruvate) with the intention to find the optimal architecture of the antiparallel acceptor binding pocket for stabilisation of the n-pentanal and propanal side chains, respectively.

In addition to the 27 *Pp*YerE variants, a control for the background reaction of the crude cell extract was included. As shown in Figure 3-12 and Figure 3-13, a comparatively high amount of (*S*)-3-HH and (*S*)-3-HP, respectively, was formed in the samples of the control reactions with high *ee*, This is surprising, because the stereoselectivity of a enzymatic benzoin condensation-like 1,2-addition is usually lower, if not at least one of the substrate is aromatic. A similar formation of aliphatic α-hydroxy ketones from pyruvate and n-hexanal has been shown before with crude cell extracts from different yeast strains, although no stereoselectivity was determined (Neuser et al., 2000). Regarding the screening results this background reaction of the crude cell extract distorted the *ee,* resulting in a shift towards the *S*-enantiomer. This can be seen for the measured *ee*-values of wt *Pp*YerE as well as variants V479A and V479G, which are generally shifted towards the (*S*)-enantiomer for crude cell extract (Figure 3-12 and Figure 3-13) compared to the results with purified enzyme (Figure 3-11). Therefore, it has to be assumed that the amount of the (*S*)-enantiomer is also overestimated for all other measurements. The resulting effect on the *ee*-value depends on the activity and stereoselectivity of a respective variant and is greater the lower the activity and/or the higher the *R*-selectivity of a variant is. This and the fluctuations in the enzyme concentration (see chapter 3.1.3) make it difficult to correct the *ee*-value for the background reaction. Hence, the *ee*-values given in the following section represent the values measured under the screening conditions in CCE and do not display the stereoselectivity of the *Pp*YerE variants with full accuracy. Anyway, these initial studies provide a good basis to identify variants for further tests with purified enzyme. The following conclusion can be deduced from Figure 3-12:

Concerning the formation of 3-HH from pyruvate and n-pentanal replacement of I23 with alanine and glycine unexpectedly increased the formation of (*R*)-3-HH and resulted in an inversion of the stereoselectivity of the wt enzyme with low to moderate *ee*-values of 18 % (*R*) and 40 % (*R*), respectively. Probably the substitution of I23 influenced the structure of the active site in such a way that the available space for antiparallel binding of the acceptor side chain decreased, although isoleucine was replaced by smaller amino acids (alanine and glycine). It is possible that the exchange of I23 leads to the disintegration of substructures in the pocket area like described above for the introduction of an additional glycine residue in position 479, as it might remove stabilising effects of the isoleucine side chain. With an additional substitution of V479 by alanine or glycine the amount of (*R*)-3-HH decreased with the decreasing size of the amino acid in this position. This corresponds to the opening of an antiparallel acceptor binding pocket that compensates for the probably reduced space due to the I23 substitution. Exchange of L476 generally reduced the formation of (*R*)-3-HH independent of the combination with other amino acid substitutions in position 23 or 479. Thereby *ee*-values between 83 % (*S*) and 95 % (*S*) were observed with crude cell extracts (Figure 3-12).

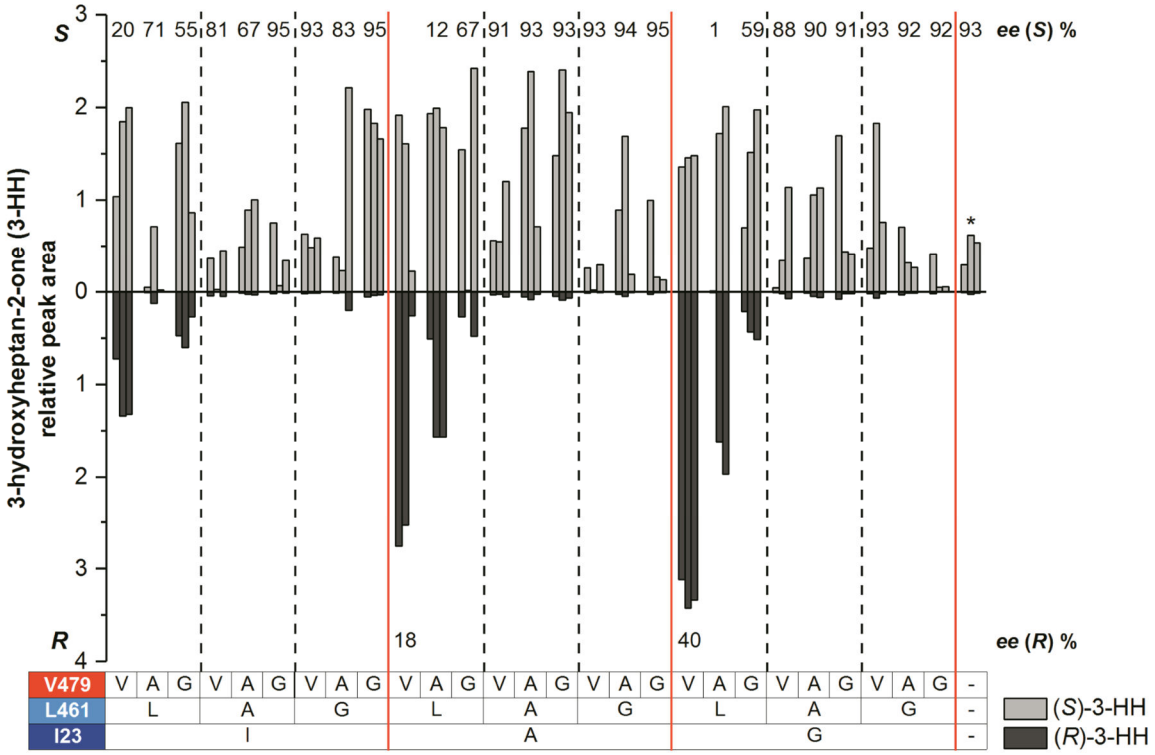

Figure 3-12: Screening of the combinatorial library of I23 (26) L476 (474) and V479 (477) for the carboligation of pyruvate and n-pentanal to 3-hydroxyheptan-2-one (3-HH). Due to high fluctuations, triplicates are shown as individual measurements. Reaction conditions: 100 mM KP_i-buffer pH 8, 2.4 mM ThDP, 3 mM $MgCl_2$, 50 mM pyruvate and 50 mM n-pentanal in crude cell extracts, 30 °C, 24 h. The screening was performed semi-automated with a robotic liquid handling system (see chapter 5.3.8). Samples were analysed via chiral phase HPLC (see chapter 5.4.3). *Empty vector control with *E. coli* BL21(DE3) carrying the pET28a (+) vector without insertion of the *ilvB* gene encoding for *Pp*YerE.

Similar results were obtained for the screening with propanal as the acceptor (Figure 3-13). Substitution of I23 by alanine and glycine also increased the formation of (*R*)-3-HP, but additionally the formation of (*S*)-3-HP was increased, so that only a minor effect on the *ee* was observed in this case. The combined exchange of I23 and V479 resulted in a decrease of both enantiomers with decreasing size of the residue in position 479. Again, substitution of L476 with alanine and glycine reduced the formation of (*R*)-3-HP. Independent of the combination with other amino acid exchanges *ee*-values between 82 % (*S*) and 94 % (*S*) were reached using crude cell extracts.

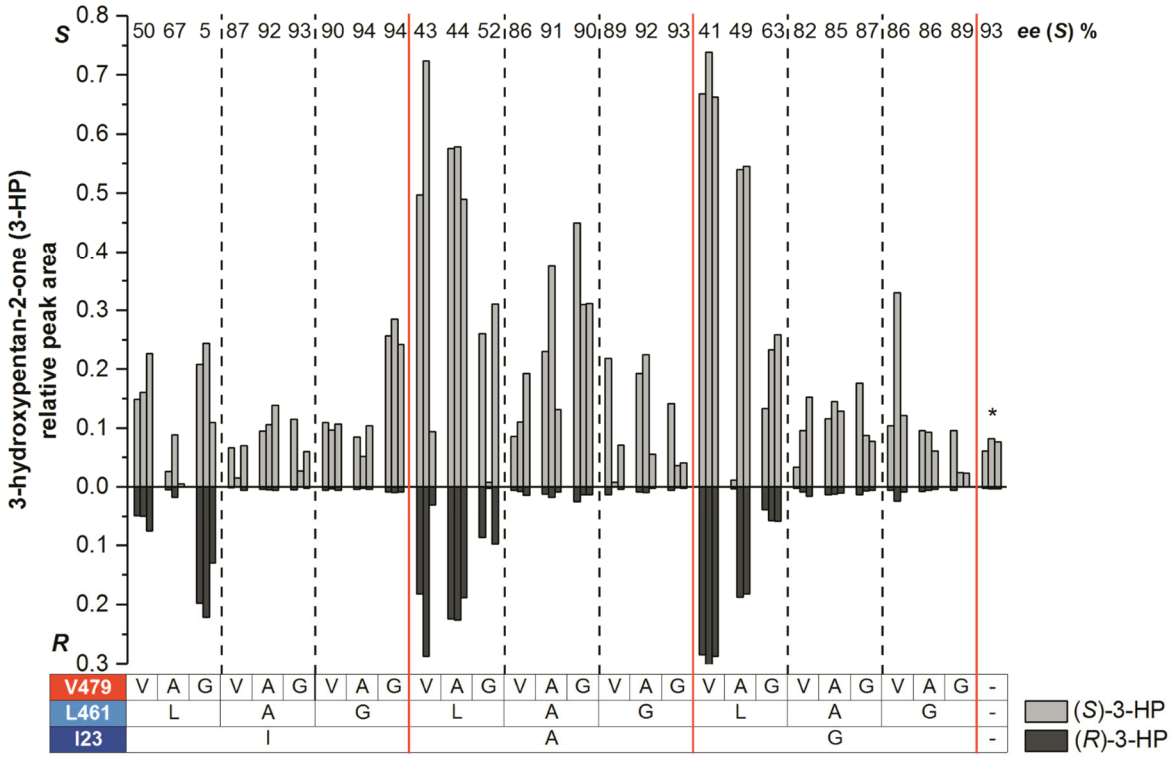

Figure 3-13: Screening of the combinatorial library of I23 (26) L476 (474) and V479 (477) for the carboligation of pyruvate and propanal to 3-hydroxypentan-2-one (3-HP). Due to high fluctuations, triplicates are shown as individual measurements. Reaction conditions: 100 mM KP_i-buffer pH 8, 2.4 mM ThDP, 3 mM $MgCl_2$, 50 mM pyruvate and 50 propanal in crude cell extracts, 30 °C, 24 h. The screening was performed semi-automated with a robotic liquid handling system (see chapter 5.3.8). Samples were analysed via chiral phase GC-MS (see chapter 5.4.3). *Empty vector control with *E. coli* BL21(DE3) carrying the pET28a (+) vector without insertion of the *ilvB* gene encoding for *Pp*YerE.

Based on the results with crude cell extracts, variants L476G/V479G, I23A/L476A, I23A/L476A/V479A, and I23A/L476A/V479G were chosen for more detailed characterisation in purified form. However, after purification none of these variants showed any activity for the carboligation of pyruvate and n-pentanal or propanal, which might be explained by the low stability of the variants in purified form. Therefore, the reactions were repeated with crude cell extracts. In contrast to the first screenings, the conditions for these reactions were more defined, as the total protein concentration of the crude cell extracts was standardised. As shown in Figure 3-14 carboligations of pyruvate with n-pentanal and propanal, respectively, in crude cell extracts of the *E. coli* BL21 (DE3) empty vector control gave the respective products 3-HH and 3-HP with high excess of the *S*-enantiomer (*ee*: 98 %). Especially after 3 h the amount of the *S*-enantiomer formed in this background reaction was in a similar range or even exceeded the amount of *S*-enantiomer formed with the crude cell extract from *E. coli* BL21 (DE3) containing the respective *Pp*YerE variants. This indicates that the *S*-enantiomer in these reactions as well as in the samples of L476 variants during the initial screening was formed by other enzymes in the CCE rather than by the *Pp*YerE variants. Thereby, the background reaction of the CCE was probably underestimated due to fluctuating protein concentrations in the samples as described in chapter 3.1.3. Using n-pentanal as acceptor substrate the variants I23A/L476A, I23A/L476A/V479A, and I23A/L476A/V479G gave a 21- to 25-fold higher amount of (*R*)-3-HH than the empty vector control reaction after 3 h, suggesting that these variants in fact form the *R*-enantiomer in excess but that the reaction rate is lower than for the background reaction of the crude cell extract.

The L476 variants were probably either inactive or had a very low reaction rate. Possibly, the loss of the side chain in position 476 affects the backbone conformation at the Mg^{2+} binding site and thus disturbs cofactor binding. This also explains why no carboligation activity was found for the purified L476 variants. Further, the screening results underline that measurements and especially screenings with crude cell extracts have to be interpreted very carefully when the investigated reactions are not bio-orthogonal to the host metabolism. Overall, the highly *S*-selective formation of 3-HH and 3-HP with comparable yields to *Pp*YerE catalysed biotransformations was surprising, but also offered an easy synthesis protocol for aliphatic (*S*)-α-hydroxy ketones. In this thesis, this was used for the preparative synthesis of (*S*)-3-HH and (*S*)-3-HP references for CD-spectroscopy (see chapter 5.4.5)

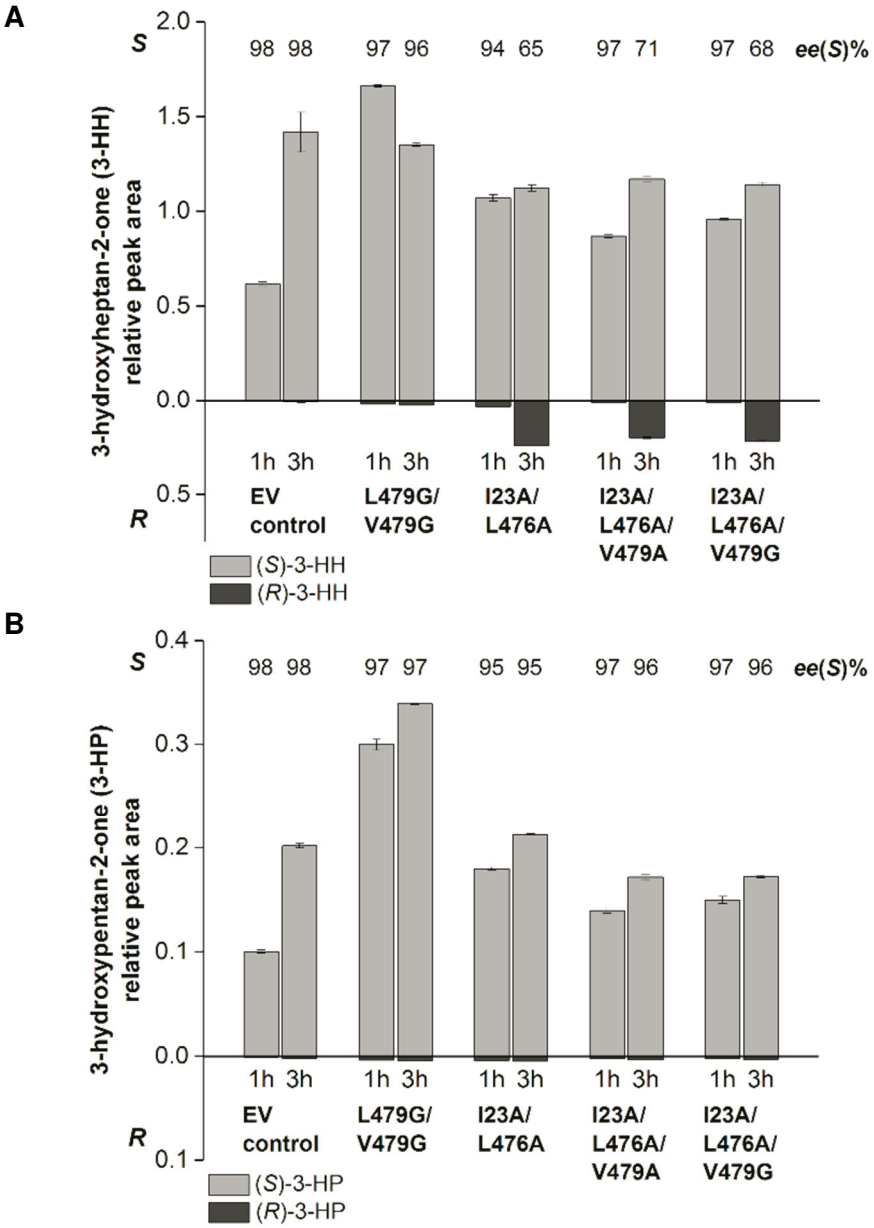

Figure 3-14: Biotransformation of pyruvate and n-pentanal (A) or propanal (B) with selected *Pp*YerE-variants in crude cell extracts. Reaction conditions: 100 mM KP_i-buffer pH 8, 2.4 mM ThDP, 3 mM $MgCl_2$, 0.05 mM FAD, 50 mM pyruvate, and 50 mM n-pentanal or propanal, 30 °C. The protein concentrations of the crude cell extracts were determined according to Bradford and adjusted to a final concentration of 10 mg·mL^{-1}. EV control = empty vector control with *E. coli* BL21(DE3) carrying a pET28a (+) vector without insertion of the *ilvB* gene encoding for *Pp*YerE. Samples were analysed via chiral phase GC-MS (see chapter 5.4.3). Error bars represent the standard error of biological triplicates.

3.1.7 Ketones as acceptor substrates

Unlike most ThDP-dependent decarboxylases YerE accepts also non-activated ketones as acceptor substrates. For *Pp*YerE the carboligation of (decarboxylated) pyruvate with cyclohexanone, cyclohexan-1,2-dione, β-tetralone, hexan-3,4-dione, and 1-phenoxy-2-propanone has been shown (Loschonsky, 2014). From these, only the smallest acceptor hexane-3,4-dione was selected for further investigations with the *Pp*YerE variants, as it could theoretically fit into the opened antiparallel acceptor binding pocket. Due to the nomenclature based on the Cahn-Ingold-Prelog priority rules (Cahn et al., 1966), the *parallel* orientation of the donor side chain and the longer acceptor side chain of hexane-3,4-dione (-CO-CH_2-CH_3) before C–C bond formation according to binding state *I* (Figure 1-12) results in the formation of the *S*-enantiomer of the reaction product 3-ethyl-3-hydroxyhexan-2,4-dione (EHH), although this parallel orientation of the substrates usually yields the (*R*)-enantiomer. In fact, an excess of the *S*-enantiomer was determined for *Pp*YerE as was deduced from the optical rotation of the reaction product, which was opposite compared to the published specific rotation of (*R*)-EHH (personal communication with Jan-Patrick Steitz, Albert-Ludwigs-Universität Freiburg, Giovannini et al., 2011). The *ee*-value of the *Pp*YerE product has not been determined before. It was thus expected that opening of the antiparallel acceptor binding pocket increases the formation of the *R*-enantiomer. Additionally, the conversion of hexan-2-one and butan-2-one, as the corresponding ketones to n-pentanal and propanal, with wt *Pp*YerE and the two *Pp*YerE variants V479(477)A and V479(477)G was investigated. The respective reaction products are shown in Figure 3-15.

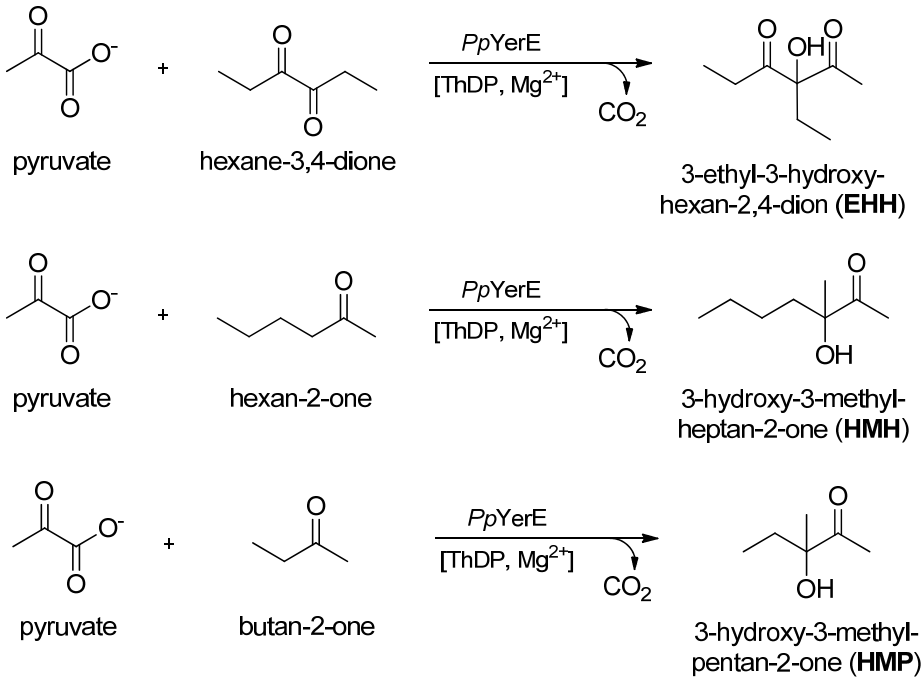

Figure 3-15: Investigated biotransformations of pyruvate as donor and different non-activated ketones as acceptors using *Pp*YerE variants.

As shown in Figure 3-16, carboligation of pyruvate and 3,4-hexandion with wt *Pp*YerE resulted in EHH formation with an *ee* of 19 %, which is considerably lower than the *ee* of 84 % obtained with *Yp*YerE (Lehwald et al., 2010). The enantiomeric excess was inverted with variant V479A (27 % *ee*). Variant V479G showed almost racemic product formation. The absolute stereoselectivity was determined for none of the variants, here, but since *S*-selective product formation with wt *Pp*YerE was observed before (see above) it can be assumed that also here the *S*-enantiomer was formed in excess with wt *Pp*YerE,

whereas the variants V479A and V479G formed a (slight) excess of the *R*-enantiomer. This also fits the expectations of the stereoselectivity model, that opening of an antiparallel acceptor binding pocket promotes *R*-selectivity for this reaction. The stereoselectivity shift was more pronounced for the V479A variant, which underlines the hypothesis that introduction of a glycine in position 479 leads to disintegration of the antiparallel acceptor binding pocket (chapter 3.1.6). Overall, only low stereoselectivities could be achieved which is probably due to the rather symmetric structure of hexan-3,4-dione.

With the other two tested ketones, hexan-2-one and butan-2-one, no conversion was observed by chiral GC-MS under the applied conditions (chapter 5.3.7) with wt *Pp*YerE and the two variants V479A and V479G.

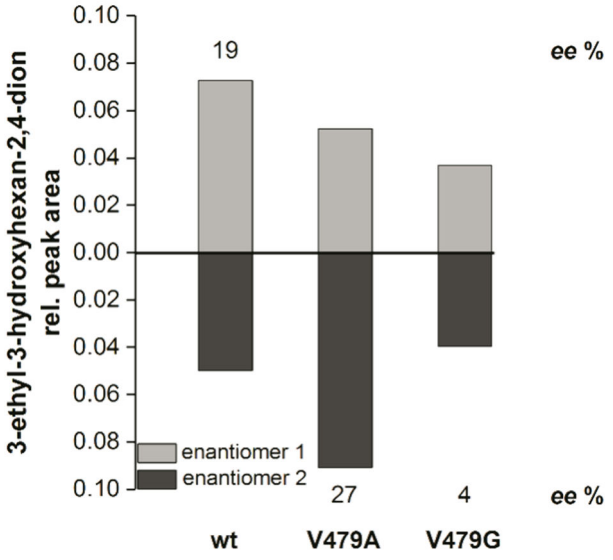

Figure 3-16: *Pp*YerE-catalysed carboligation of pyruvate (donor) and hexan-3,4-dion (acceptor) to 3-ethyl-3-hydroxyhexan-2,4-dion (EHH) after opening of an antiparallel acceptor binding pocket by substitution of V479(477). Reaction conditions: 100 mM KP_i-buffer pH 7, 2.4 mM ThDP, 3 mM $MgCl_2$, 0.05 mM FAD, and 1 mg·mL^{-1} *Pp*YerE variant, 50 mM pyruvate and 20 mM hexan-3,4-dion, 30 °C, 24 h. Samples were analysed via chiral phase GC-MS (see chapter 5.4.3).

3.1.8 Summary

Because of its potential for the carboligation with non-activated ketones as acceptor substrates, *Pp*YerE was chosen as a target for the evaluation of the stereoselectivity model on further ThDP-dependent DCs. The opening of an antiparallel acceptor binding pocket proved to be challenging, as its size was restricted by the backbone of an α-helix. Consequently, single amino acid substitution of the residue in standard position 477 (V479) was not sufficient to invert the stereoselectivity for the formation of PAC from pyruvate and benzaldehyde. Several attempts to increase the size of the pocket, i.e. to displace or remove the α-helix and combined substitution of residues lining the pocket, did only result in variants for that the stereoselectivity was hardly affected or variants that lost their activity/stability, as deduced from very low product yields. With the smaller acceptor substrates n-pentanal, propanal, and hexan-3,4-dion the stereoselectivity could be shifted in favour of the *S*-product (or *R*-product in case of hexan-4,5-dion), but only low *ee*-values could be achieved. Overall, the results are in agreement with the stereoselectivity model, but its applicability for the inversion of the stereoselectivity is limited for *Pp*YerE.

3.2 Transfer of the structural stereoselectivity model from the decarboxylase superfamily to the transketolase superfamily*

3.2.1 Extension of the stereoselectivity model

According to the two-state model described for ThDP-dependent DCs the antiparallel acceptor binding pocket (Figure 1-13) is a prerequisite for *S*-selectivity (see chapter 1.3.4). Nevertheless, despite the natural *S*-selectivity of TKs no evidence for such a pocket could be found in the crystal structures of *Ec*TK (PDB: 2R3O, Asztalos et al., 2007), *Sc*TK (PDB: 1GPU, Fiedler et al., 2002), or *Bacillus anthracis* TK (which served as a template for a homology model of *Gst*TK, since no crystal structure is available yet (Yi et al., 2015); PDB: 3M49), particularly with regard to the large physiological substrates of TKs (Figure 3-17). Thus, there must be an alternative mechanism for the control of stereoselectivity in TKs and the existing model for DCs had to be extended.

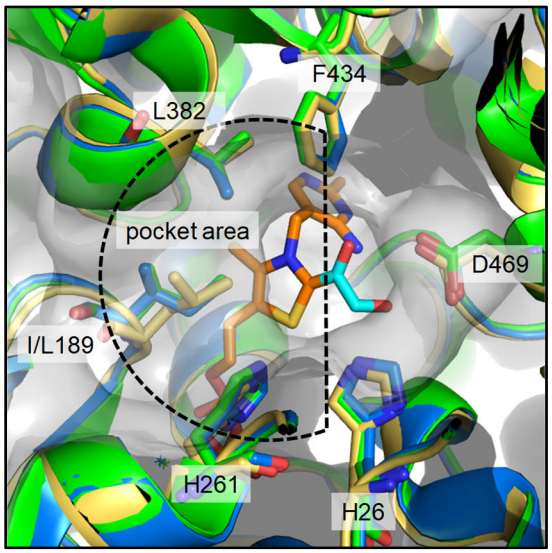

Figure 3-17: Structural alignment of *Ec*TK (blue, PDB: 2R8O), *Sc*TK (green, PDB: 1GPU) and *Bacillus anthracis* transketolase (yellow, PDC: 3M49), the latter serves as a template for a homology model of *Gst*TK. The surface is depicted in transparent grey. ThDP (orange) and the bound donor dihydroxyethyl- intermediate (light blue) are taken from the *Sc*TK structure. The standard position of the residues shown in stick representation are given according to the transketolase standard numbering scheme. For all three transketolases the potential pocket is blocked by amino acid side chains. The figure was generated with the PyMOL Molecular Graphics System (Schrödinger, LLC).

To understand the factors controlling the stereoselectivity in TK, the active site structures of DCs and TKs were compared. For both families the active site is formed at the interface of the PP- and Pyr-domain, but the sequences of those domains differ for DCs and TKs (see chapter 1.2.3). It is therefore possible that an analogues mechanistic model as the two-state model developed for the DC-family (Figure 1-13) could also explain the TK stereoselectivity. But in contrast to DCs, whose active sites contain predominantly hydrophobic and only few charged residues (Knoll et al., 2006; Pohl et al., 2010b), TKs feature several charged amino acids within the active site that serve for substrate stabilisation and proton transfer. This is in accordance with the highly hydrophilic nature of the phosphorylated physiological TK substrates (Figure 1-17). Among these residues, the histidines in standard position 26 and 261 have been described to stabilise the C1-carbonyl group of the acceptor substrate and to mediate proton transfer during the catalytic cycle (Nilsson et al., 1998, 1997; Ranoux and Hanefeld, 2013; Schneider and Lindqvist, 1993; Wikner et al., 1997) (see chapter 1.4.1).

* Large parts of this chapter were taken with changes from the manuscript Baierl et al., 2018, see appendix 7.4).

Accordingly, the carbonyl group of the acceptor is orientated in an antiparallel manner to the hydroxy group of the carbanion-enamine (Figure 3-18 A). The stereoselectivity model for ThDP-dependent decarboxylases only comprises substrate orientations with a parallel alignment of the acceptor carbonyl and the donor hydroxy group corresponding to binding state *I* and *II* in Figure 1-12, which is in agreement with the existence of only one to two histidine residues that stabilise the functional groups and function as proton-relay system during the catalytic cycle (Figure 1-3). Consequently, the model for TKs was extended by the orientation of the acceptor carbonyl group resulting in four possible substrate orientations prior to C-C bond formation (binding states *I-IV*, Figure 3-19). According to the extended model, the ratio of *R*- and *S*-products is dependent on the probability for four different binding states of which two lead to *R*- and two lead to *S*-selective product formation.

Considering the natural *S*-selectivity of TKs, the interaction of the acceptor carbonyl group with H26 and H261 and the sterical restriction of antiparallel binding of the acceptor side chain, it was assumed that binding state *III* (Figure 3-19) is most prominent for wt TK. Consequently, two strategies could be followed in order to invert the stereoselectivity. The first strategy was to open an antiparallel acceptor binding pocket analogously to the successful examples of DCs (Gocke et al., 2008; Rother neé Gocke et al., 2011; Sehl et al., 2017; Westphal et al., 2014a, 2013a, 2013b). Opening a pocket should enhance binding state *IV* and thus result in preferred formation of the *R*-enantiomer. Amino acids that block potential antiparallel binding pockets are I189, H261, L382 and F434 (Figure 3-18). The second strategy to produce the *R*-enantiomer in excess is to promote binding state *I* by destabilisation of the antiparallel orientation of the acceptor carbonyl group. The second strategy concerned the replacement of these histidine residues, since H26 and H261 are described to stabilise the acceptor carbonyl group in orientation *III*. Thereby, H261 has a double function, as it contributes to the interactions with the acceptor carbonyl group and blocks the area of the antiparallel acceptor binding pocket. Both strategies were addressed by studying the function of key residues around the active site and are discussed in the following sections.

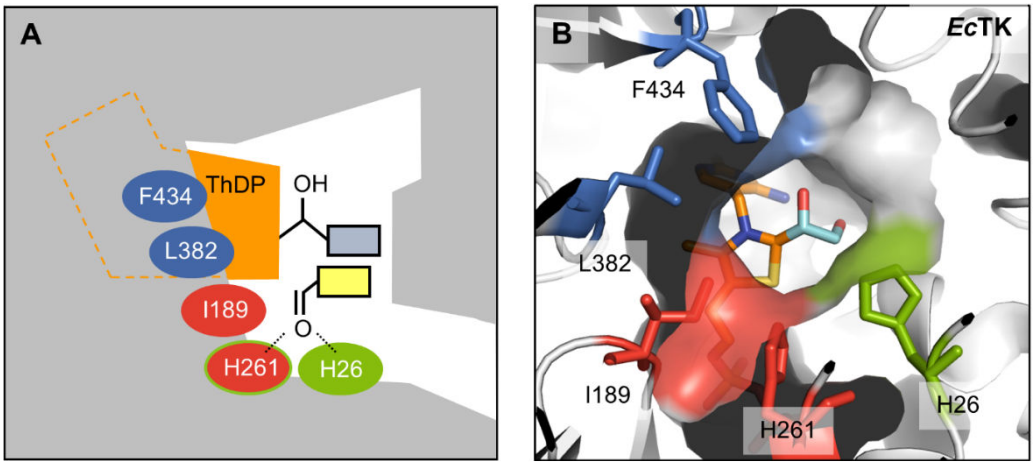

Figure 3-18: Schematic active site map (A) and structure (B) of the active site with the location of all amino acids targeted by site-directed mutagenesis to evaluate the extended stereoselectivity model. Figure B was generated with the PyMOL Molecular Graphics System (Schrödinger, LLC) based on the crystal structure of *Ec*TK (PDB: 2R8O (Asztalos et al., 2007)). Orange: ThDP, light blue: ThDP-bound donor dihydroxy ethyl-intermediate, yellow: acceptor substrate (not shown in B), green: residues that predominantly interact with the acceptor carbonyl group. Replacing the residues depicted in blue and red represents two different possibilities to open a potential antiparallel acceptor binding pocket. H261 has a double function, as it contributes to the interactions with the acceptor carbonyl group and blocks the area of the potential pocket.

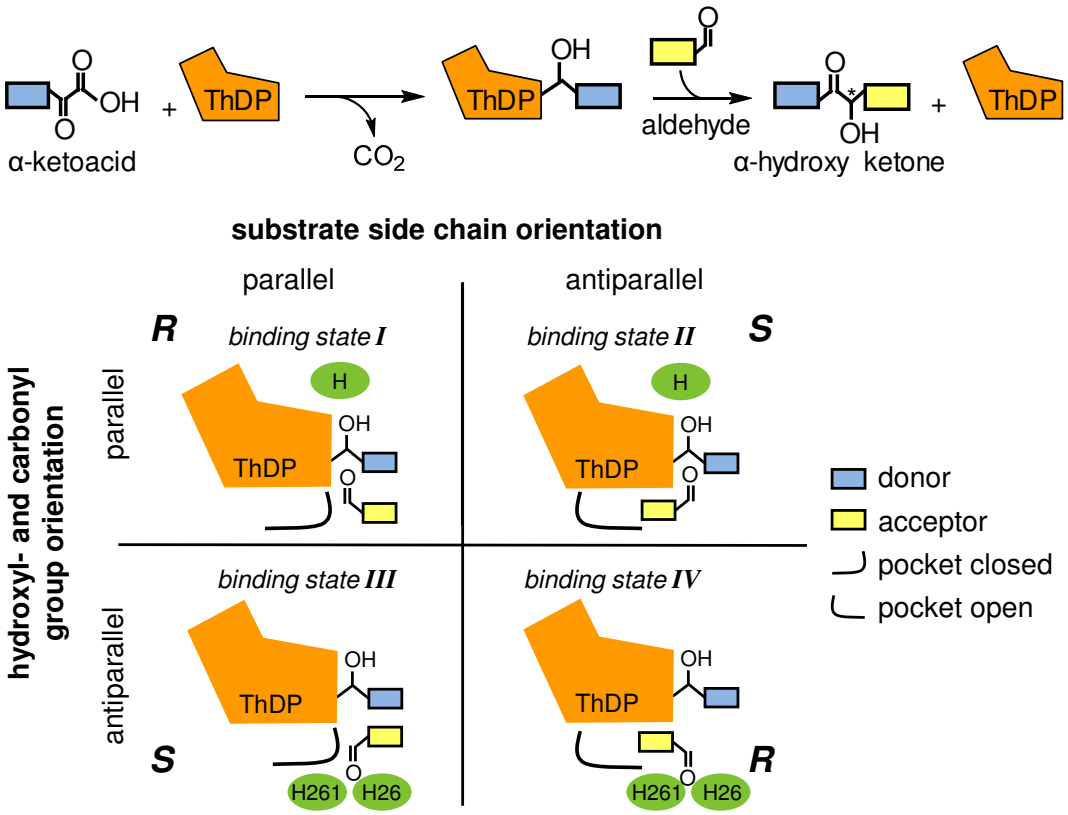

Figure 3-19: Extended stereoselectivity model for ThDP-dependent enzymes. The model was extended from two to four binding states prior to C-C bond formation that are defined by the orientation of the acceptor side chain relative to the donor side chain and by the orientation of the acceptor carbonyl group relative to the ThDP-bound donor hydroxy group. Binding states *I* and *IV* result in the formation of the *R*-enantiomer and binding states *II* and *III* result in the formation of the *S*-enantiomer

3.2.2 Model reactions for the evaluation of the extended stereoselectivity model

For the evaluation of the extended stereoselectivity model and the two strategies to generate *R*-selective TK variants, comprehensive mutagenesis studies have been conducted with active site residues of *Ec*TK. The amino acid substitutions were introduced by site-directed mutagenesis (chapter 5.2.3) and the variants were produced by heterologous expression of the respective genes in *E. coli* BL21 (DE3) (chapter 5.3.1). All tested carboligation reactions were conducted with purified enzymes. For that purpose, the *Ec*TK variants were purified by Ni-NTA affinity chromatography (chapter 5.3.3) with typical yields between 10 mg and 20 mg purified protein per gram wet cells.

The carboligations of 3-hydroxypyruvate (HPA) as the donor substrate and n-pentanal as well as propanal as acceptor substrates were chosen as model reactions for the investigation of these variants. The products of these reactions 1,3-dihydroxyheptan-2-one (DHH) and 1,3-dihydroxypentan-2-one (DHP), respectively, are shown in Figure 3-20. The conversion of both acceptor aldehydes by *Ec*TK has been shown before. Molecular docking studies suggest that n-pentanal and propanal adopt different confirmations in the active site (Cázares et al., 2010). Therefore, it is likely that effects caused by different amino acid substitutions vary for both acceptor aldehydes. The substrates were always used equimolar at 50 mM and 100 mM final concentration for n-pentanal and propanal as acceptor, respectively. The lower concentration with n-pentanal was due to its lower solubility in the reaction buffer.

ee-Values and product yields measured with wildtype *Ec*TK under the standard reaction conditions applied in this study are given in Figure 3-20. The yields given here and in all following chapters refer to the amount of product formed in the course of the reactions as determined by GC-MS in the reaction solution.

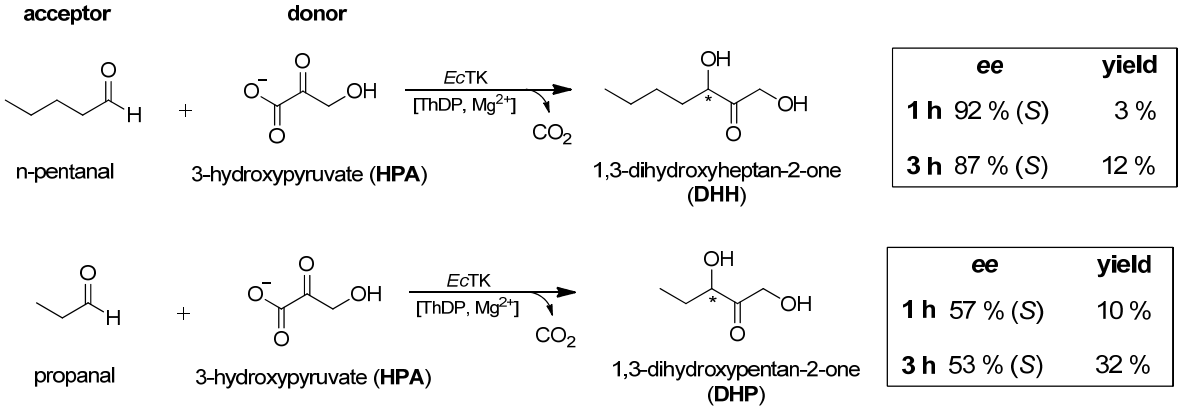

Figure 3-20: Carboligations of artificial substrates as investigated in this study with 3-hydroxypyruvate (HPA) as the donor and n-pentanal as well as propanal as acceptors. The denoted *ee*-values and product yields were measured with wildtype *E. coli* transketolase (*Ec*TK). The yields refer to the product concentrations measured by GC-MS immediately after the reactions without any product purification. Reaction conditions: 100 mM KPi-buffer, pH 7, 2.4 mM ThDP, 3 mM $MgCl_2$ and 0.9 mg·mL^{-1} *Ec*TK. The donor substrate HPA and the acceptor substrates were always used equimolar with final concentrations of 50 mM and 100 mM for n-pentanal and propanal, respectively. Samples were incubated at 25°C for 1 h and 3 h before analysis via chiral phase GC-MS

3.2.3 Opening of an antiparallel acceptor binding pocket

Substitution of I189 and H261

Given that the acceptor carbonyl group is orientated antiparallel to the donor hydroxy group, opening of an antiparallel acceptor binding pocket, should shift the distribution of possible substrate binding states in favour of binding state *IV* (Figure 3-19) and thus enable a preferred *R*-selective carboligation. The side chains of I189 and H261 block a potential pocket in *EcTK* (Figure 3-22 A) that has a comparable position relative to ThDP as the pocket in DCs, which was opened by substitution of the residue in standard position 477 (see chapter 1.3.5). According to studies on *Gst*TK, exchange of L191 (189) influenced the stereoselectivity in a double variant with additional exchange of D470 (469). Here, effects on the orientation of the acceptor side chain were already discussed (Zhou et al., 2017). For *Ec*TK *Hibbert et al*. created I189X library, but screening with glycolaldehyde and n-pentanal as acceptors gave no variants with greater activity than wt *Ec*TK (Hibbert et al., 2008, 2007).

In this study, a combined exchange of both I189 and H261 to the smaller amino acids glycine, alanine and valine was performed with the aim to test different sizes of the resulting pocket and to optimise the architecture of the antiparallel acceptor binding pocket for the respective acceptor side chains. In total 11 *Ec*TK variants were produced, purified and tested for their potential to catalyse the formation of DHH and DHP (see Figure 3-21). Variant I189V/H261G could not be purified and was therefore not further characterised. As H261 fulfils a double function, results with single variants in position 261 are shown and discussed in chapter 3.2.4.

Regarding the formation of DHH most variants, including those with a single amino acid exchange of I189, showed a 2-fold to 3-fold lower product formation after 3 h compared to wt *Ec*TK. Only for variants carrying a H261V exchange a 2-fold to 4-fold increased product formation was observed (Figure 3-21 A). Among these, variants with a combined exchange of I189 to glycine, alanine, or valine and H261 to valine showed 2.4- to 3.7-fold increased formation of DHH compared to the single variant H261V (see appendix, Table 7-1). This indicates cooperative effects of the two exchanges, as the single exchange of I189 decreased the product formation for all other respective variants. With *ee*-values for DHH between 20 % (*S*) and 81 % (*S*) none of the variants showed inversion of the stereoselectivity. A reduced *S*-selectivity resulted from a decreased formation of the *S*-enantiomer rather than an increased formation of the *R*-enantiomer (Figure 3-21 A). With propanal as the acceptor substrate the reduced productivity of the variants was more pronounced with up to 15-fold reduced final amount of DHP compared to wt *Ec*TK (see appendix, Table 7-1). Here, the *ee*-values ranged from 4 % (*R*) to 63 % (*S*) but again this shift toward *R*-selectivity was caused by a decreased formation of the *S*-enantiomer. Only variant I189V/H261V catalysed the formation of an increased amount of the *R*-enantiomer but nevertheless the *S*-enantiomer was in excess (*ee*-value: 17 %) (Figure 3-21 B).

The results show that both positions influence the stereoselectivity. However, stereoinversion by combined substitution of I189 and H261 was not successful for the tested reactions. Especially exchange of I189 appeared to be detrimental for the activity as deduced from the low product yields. This is consistent with the results of Hibbert *et al.*, who did not find variants with higher activity than wt within a I189X library (Hibbert et al., 2008, 2007). Besides the loss of stability and/or activity due to the exchange of I189, the presumed double function of H261 might have negative effects on the reversion of the stereoselectivity. Here the aim of exchanging H261 was to open an antiparallel acceptor binding pocket that promotes binding state *IV* (Figure 3-19). But the exchange probably also destabilised the antiparallel orientations of the acceptor carbonyl group and thus increase the probability for binding states *I* and *II* (Figure 3-19), which explains the overall lower stereoselectivity of the *Ec*TK variants. Detailed investigations on the effects induced by substitution of H261 are discussed in chapter 3.2.4.

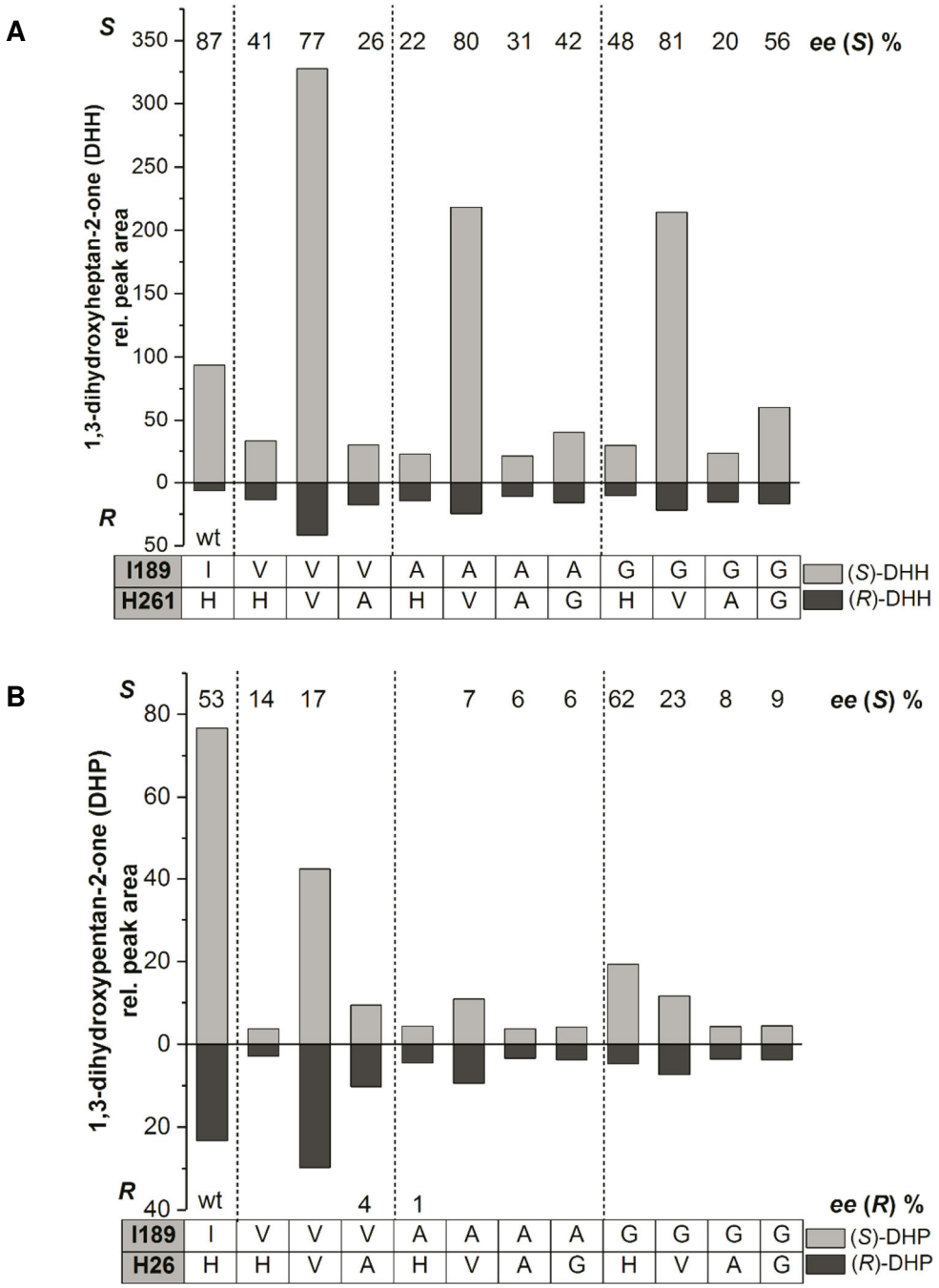

Figure 3-21: Opening an antiparallel acceptor binding pocket in *Ec*TK according to binding state *IV* in Figure 3-19 by combinatorial amino acid exchange of I189 and H261 - Carboligation of 3-hydroxypyruvate (HPA) n-pentanal (**A**) or propanal (**B**) to 1,3-dihydroxyheptan-2-one (DHH) or 1,3-dihydroxypentan-2-one (DHP), respectively. Reaction conditions: 100 mM KP_i-buffer pH 7, 2.4 mM ThDP, 3 mM $MgCl_2$ and 0.9 mg·mL^{-1} *Ec*TK variant, 50 mM HPA and 50 mM n-pentanal or 100 mM HPA and 100 mM propanal. Samples were incubated at 25°C for 3 h before analysis via chiral phase GC. Most variants were prepared by Friederike Hoffmann in the course of her master thesis (Hoffmann, 2016).

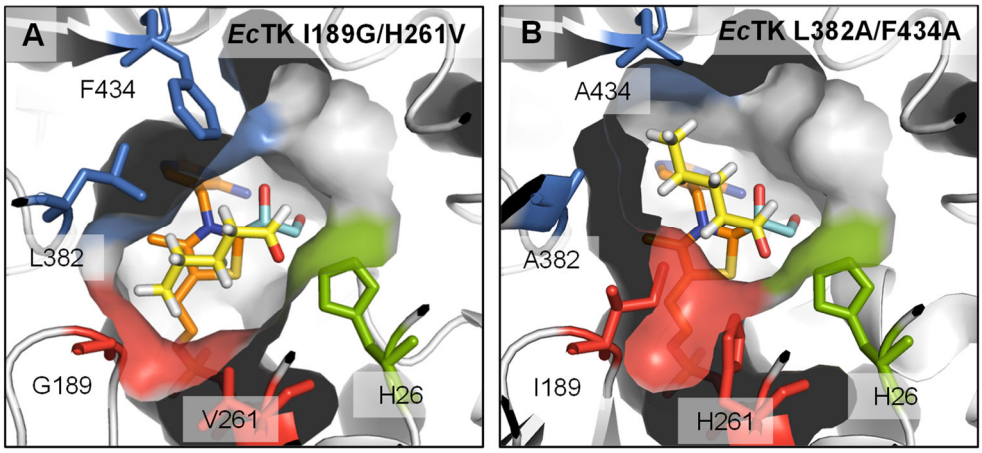

Figure 3-22: Opening of an antiparallel acceptor binding pocket according to binding state *IV* (**Figure 3-19**) by amino acid exchange of I189 and H261 (red) (**A**) as well as exchange of L382 and F434 (blue) (**B**). Exemplarily, n-pentanal is shown as the acceptor substrate. Figures were generated with the PyMOL Molecular Graphics System (Schrödinger, LLC) based on the crystal structure of *Ec*TK (PDB: 2R3O (Asztalos et al., 2007)). Orange: ThDP, light blue: ThDP-bound donor-intermediate, yellow: n-pentanal. Substrates were placed manually in the active side, considering the reactive distance of the substrates and the Bürgi-Dunitz angle for the nucleophilic attack.

Substitution of L382 and F434

As shown in Figure 3-18 and Figure 3-22 B, substitution of L382 and F434 offers an alternative way to open an antiparallel acceptor binding pocket. Thereby substitution of I189, which seemed to be detrimental for the enzyme activity or stability, and H261, which has a double function that complicates the prediction of effects on the stereoselectivity, was avoided. Even though the spatial location of this pocket relative to ThDP differs from the pockets described for DCs and the other pocket in *Ec*TK described above, the characteristics of binding according to state *IV* are still fulfilled (Figure 3-19, Figure 3-22B). The equivalent positions in *Gst*TK were subjected to side saturation mutagenesis in combination with full saturation of D470 (469). Thereby, the stereoselectivity was influenced by substitutions in both positions but no highly *R*-selective variants were found (Yi et al., 2015; Zhou et al., 2017). In *Ec*TK exchange of F434 was addressed with respect to an improved acceptance of aromatic acceptor aldehydes (Payongsri et al., 2012). In the present study, the amino acid exchanges L382A, F434L, and F434A as well as combinations thereof were investigated.

Surprisingly, *Ec*TK variant L382A showed an increased formation of the *S*-enantiomer for both DHH and DHP and in the latter case an additional decrease of the *R*-enantiomer. After 1 h product yields for DHH and DHP were 59 % and 21 % with *ee*-values of 97 % (*S*) and 91 % (*S*), respectively (Figure 3-23). After 3 h the yield of DHP was increased to 48 % while the yield of DHH as not further increased. The *ee*-values did not change in between 1 h and 3 h for both products.

Variants F434L and F434A showed increased formation of both (*S*)- and (*R*)-DHH, resulting in increased yields of 57 % and 69 % and reduced *ee*-values of 74 % (*S*) and 53 % (*S*) after 1 h, respectively. Even though both variants still catalysed the formation of a clear excess of (*S*)-DHH, the increased formation of the *R*-enantiomer was a first indicator for the opening of an antiparallel acceptor binding pocket, which enabled substrate orientation according to binding state *IV* (Figure 3-19, Figure 3-23 A). Interestingly, after 3 h the *ee*-value dropped to 57 % (*S*) (F434L) and 33 % (*S*) (F434A) which could be attributed to an increasing amount of the *R*-enantiomer and accompanied by decreasing amount of the *S*-enantiomer, so that the overall yield stayed roughly constant. This indicates a transformation of

(*S*)-DHH to (*R*)-DHH, which is most likely catalysed by the respective *Ec*TK variants, as other variants did not show that behaviour under the applied reaction conditions. Further investigations regarding this observation are described in chapter 3.2.5.

Combination of the exchanges F434L and L382A decreased the formation of (*S*)-DHH and increased the formation of (*R*)-DHH compared to variant F434L and thus resulted in the lowest enantiomeric excess of (*S*)-DHH (10 %) among all variants that were created with the aim to open an antiparallel acceptor binding pocket. Variant L382A/F434A also catalysed the formation of less (*S*)-DHH than variant F434A but the amount of (*R*)-DHH was decreased as well, resulting in an *ee*-value of 66 % (*S*). Except for variant L382A/F434A the relative amount of (*R*)-DHH increased with increasing size of the opened antiparallel acceptor binding pocket. These results indicate that for the tested variants the pocket opened by the combined amino acid exchanges L382A and F434L is best suited to stabilise the side chain of n-pentanal in antiparallel orientation, while the pocket opened by the combined exchanges L382A and F434A is probably too big for optimal binding of n-pentanal.

With respect to the product DHP the variant F434L showed an increased formation of the *R*- and the *S*-enantiomer, relative to the wt enzyme. But as the increase was relatively higher for (*S*)-DHP, the *ee*-value was increased to 65 % (*S*) after 1 h (yield: 41 %, Figure 3-23 B). In contrast, the formation of both DHP enantiomers was decreased for variant L434A resulting in a yield of 5 % and an *ee*-value of 65 % (*S*) after 1 h. The combination of the L382A and the F434L exchanges resulted in an almost inactive variant. *Ec*TK L382A/F434A, however, gave a yield of 24 % after 1 h. As shown in Figure 5, this variant showed an increased formation of the *R*-enantiomer and a slightly decreased formation of the *S*-enantiomer compared to variant L382A yielding in an *ee*-value of 31 % (*S*). A correlation of the pocket size and the relative amount of the *R*-enantiomer, as described for DHH, could not be found for DHP, especially as biotransformations with variants F434A and L382A/F434L gave only low product yields (Figure 3-23 B). Variant L382A/F434A catalysed the formation of the highest relative amount of (*R*)-DHP. This was surprising, because n-pentanal was best stabilised in the pocket of variant L382A/F434L and thus the pocket of variant L382A/F434A was assumed to be too big for optimal stabilisation of n-pentanal. Consequently, the pocket size of L382A/F434A should also not be ideal for the smaller acceptor propanal and a reduced formation of (*R*)-DHP was expected. This shows that apart from pure steric properties also other factors influence the orientation of the acceptor substrate before C-C-bond formation. Besides, it should be noted that not all effects of an amino acid exchange can be predicted based on the crystal structure, since it does not reflect the flexible nature of enzyme active sites.

In addition, all five variants of the second approach to open an antiparallel acceptor binding pocket according to binding state *IV* (Figure 3-19) were also tested in combination with an additional I189A substitution, because I189 lies adjacent to L382 in the active site and might also influence the architecture of the antiparallel acceptor binding pocket (Figure 3-18). However, as also shown for single I189 variants or combined substation of I189 and H261 the I189A substitution decreased the activity, which can be deduced from the decreased product formation for all tested variants. Besides the influence on the stereoselectivity was only minor and caused by a stronger decrease of the *S*-enantiomer instead of an increase of the *R*-enantiomer (see appendix, Table 7-1).

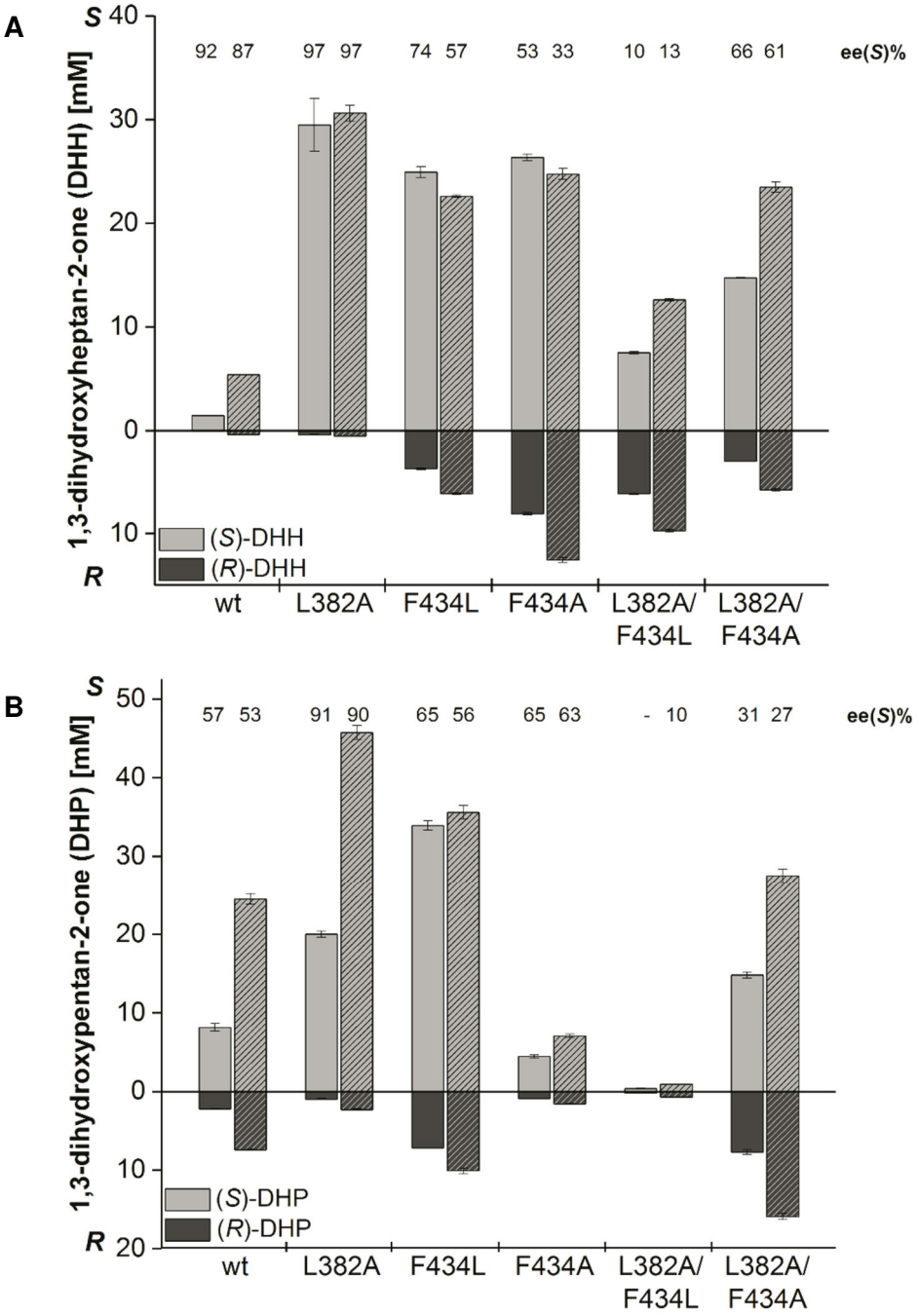

Figure 3-23: Opening an antiparallel acceptor binding pocket according to binding state *IV* in Figure 3-19 by replacement of L382 and F434 in order to invert the *Ec*TK stereoselectivity. The variants are ordered by the potential size of the pocket. **A**: Carboligation of 3-hydroxypyruvate (HPA) and n-pentanal to 1,3-dihydroxyheptan-2-one (DHH); **B:** Carboligation of HPA and propanal to 1,3-dihydroxypentan-2-one (DHP); Reaction conditions: 100 mM KP_i-buffer, pH 7, 2.4 mM ThDP, 3 mM $MgCl_2$ and 0.9 mg·mL^{-1} *Ec*TK variant. The donor substrate HPA and the acceptor substrates were always used equimolar with final concentrations of 50 mM and 100 mM for n-pentanal and propanal, respectively. Samples were incubated at 25°C for 1 h (open columns) and 3 h (hatched columns) before analysis via chiral phase GC-MS. Error bars display the standard error from biological triplicates. Most of the variants were prepared by Stephanie Moers in the course of her master thesis (Moers, 2017).

3.2.4 Destabilisation of the acceptor carbonyl group

The second strategy followed to invert the stereoselectivity of *Ec*TK was to promote binding state *I* (Figure 3-19) by destabilising the antiparallel acceptor carbonyl group orientation. The conserved residues H26 and H261 are structurally adjacent and their stabilising effect on the acceptor carbonyl group are well described in literature (Nilsson et al., 1998, 1997; Ranoux and Hanefeld, 2013; Schneider and Lindqvist, 1993; Wikner et al., 1997). Therefore, they have a potential influence on catalysis and stereoselectivity and mutagenesis studies were performed in both positions.

Single substitution of H26

For H26 Hailes and co-workers showed that replacement with tyrosine inverts the stereoselectivity (Cázares et al., 2010; Smith et al., 2008). According to the extended stereoselectivity model, this can be explained by the loss of the respective directing hydrogen bond between H26 and the acceptor carbonyl increasing the probability for binding state *I* (Figure 3-19). In the present study, the purified variant H26Y catalysed the formation of (*R*)-DHH with an *ee*-value of 98 % and a yield of 8 % after 1 h (Figure 3-24 A). The *ee*-value for this reaction was 14 % higher than described by Hailes and co-workers, which can be explained by their different reaction conditions, i.e. measurements with crude cell extracts and longer reaction times of 24 h. Replacement of H26 by alanine also resulted in stereoinversion for the formation of DHH, but with a considerably lower *ee*-value of 18 % (*R*). Comparison of the individual amounts of *S*-and *R*-product instead of the relative *ee*-values revealed that the formation of (*R*)-DHH catalysed by both variants was vastly increased compared to wildtype *Ec*TK. Their different stereoselectivity was caused by the formation of different amounts of the (*S*)-enantiomer relative to the wt enzyme. With variant H26Y the formation of (*S*)-DHH was decreased, whereas reactions with variant H26A resulted in a higher concentration of (*S*)-DHH compared to wt *Ec*TK. As a consequence, biotransformations with variant H26A gave an increased overall DHH yield (17 %) compared to wt *Ec*TK and a low enantiomeric excess of (*R*)-DHH (Figure 3-24 A). As replacement of H26 by tyrosine did not affect the size of the residue and could therefore not open an additional acceptor binding pocket, it can be assumed that the high *R*-selectivity results from a preference for of binding state *I* (Figure 3-19). In variant H26A, on the other hand, histidine was replaced by a smaller residue and could open a pocket that enables antiparallel binding of the acceptor side chain. Thus, the high amount of (*S*)-DHH formed by variant H26A might be explained by enhanced population of binding state *II* in addition to binding state *I* (Figure 3-19). Consequently, it was tested next, whether replacement of H26 by the largest amino acid tryptophan could further repress the formation of the *S*-product. However, compared to variant H26Y variant H26W showed an 8-fold decreased formation of (*R*)-DHH but a 4-fold increased formation of (*S*)-DHH, resulting in an *ee*-value of 30 % (*S*) after 1 h reaction time. Consequently, the larger residue in position 26 reduced the catalytic activity and did not improve the *R*-selectivity.

With respect to the formation of DHP the variants behaved similar, except that biotransformations with variant H26A gave a higher *ee* of (*R*)-DHP (73 %) than (*R*)-DHH (Figure 3-24 B). This suggests that orientation according to binding state *II* (Figure 3-19) is less likely for propanal compared to n-pentanal. These results suggest that the pocket opened by the H26A substitution stabilises n-pentanal better than propanal.

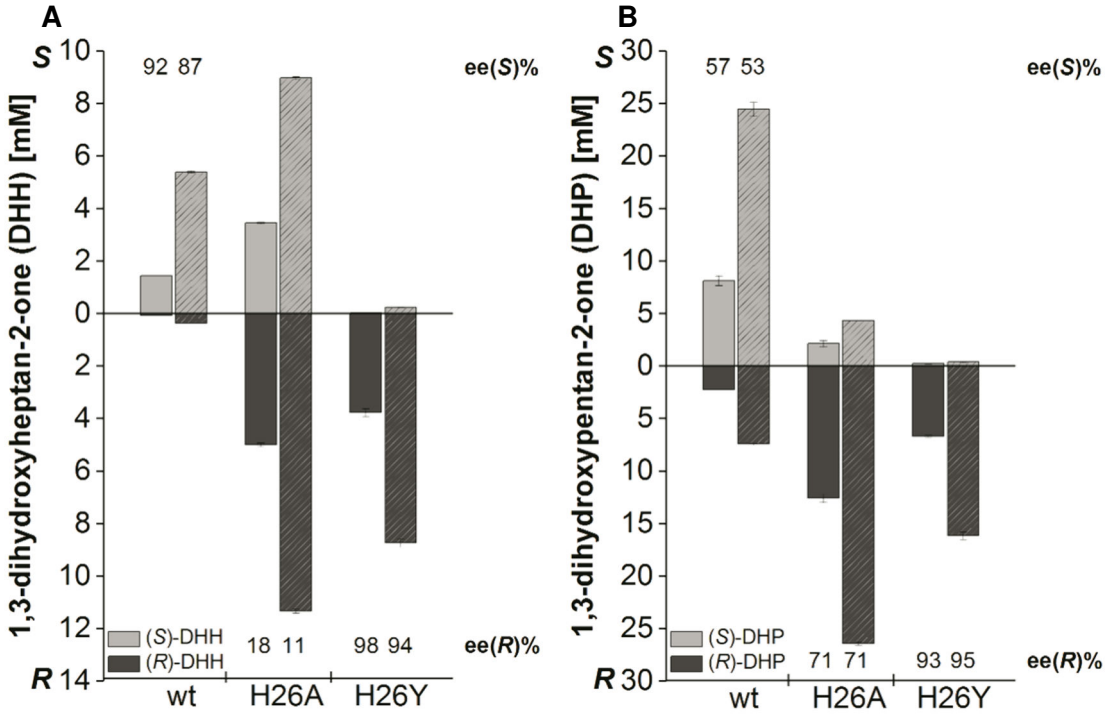

Figure 3-24: Influence of substitution of H26 on the *Ec*TK stereoselectivity. **A:** Carboligation of 3-hydroxypyruvate (HPA) and n-pentanal to 1,3-dihydroxyheptan-2-one (DHH); **B:** Carboligation of HPA and propanal to 1,3-dihydroxypentan-2-one (DHP); Reaction conditions: 100 mM KP_i-buffer pH 7, 2.4 mM ThDP, 3 mM $MgCl_2$ and 0.9 mg·mL^{-1} *Ec*TK variant. The donor substrate HPA and the acceptor substrates were always used equimolar with final concentrations of 50 mM and 100 mM for n-pentanal and propanal, respectively. Samples were incubated at 25°C for 1 h (open columns) and 3 h (hatched columns) before analysis via chiral phase GC-MS. Error bars display the standard error from biological triplicates. The variants were prepared by Philipp Marquardt in the course of his master thesis (Marquardt, 2015).

Single substitution of H261

As shown in Figure 3-18, substitution of H261 can potentially have two effects: destabilisation of the antiparallel orientation of the acceptor carbonyl group and opening of an antiparallel acceptor binding pocket. Here, replacement with phenylalanine and leucine, as uncharged amino acids with comparable size to histidine, as well as with smaller residues (valine, alanine and glycine) was investigated. Concerning the formation of DHH, all five variants showed increased formation of the *R*-enantiomer but no inversion of the stereoselectivity with *ee*-values ranging from 33 % to 75 % (*S*) and yields comparable to wildtype *Ec*TK (Figure 3-25 A). Except for variant H261G, the relative amount of *R*-product decreased with decreasing size of the residue at position 261. This corresponds to the opening of an antiparallel acceptor binding pocket as described above and enhancement of binding state *II* (Figure 3-19) due to replacement of H261 by smaller amino acids.

Also, for propanal as the acceptor substrate the *ee* for (*S*)-DHP obtained with the variants was lowered to values between 6 % (*R*) and 24 % (*S*). But in contrast to the formation of DHH, this was mainly attributed to a decreased amount of the *S*-enantiomer instead of an increasing amount of the *R*-enantiomer (Figure 3-25 B). Consequently, the yields for DHP were decreased up to 8-fold in comparison to wildtype *Ec*TK. The highest relative amount of (*R*)-DHP was reached with *Ec*TK H261V.

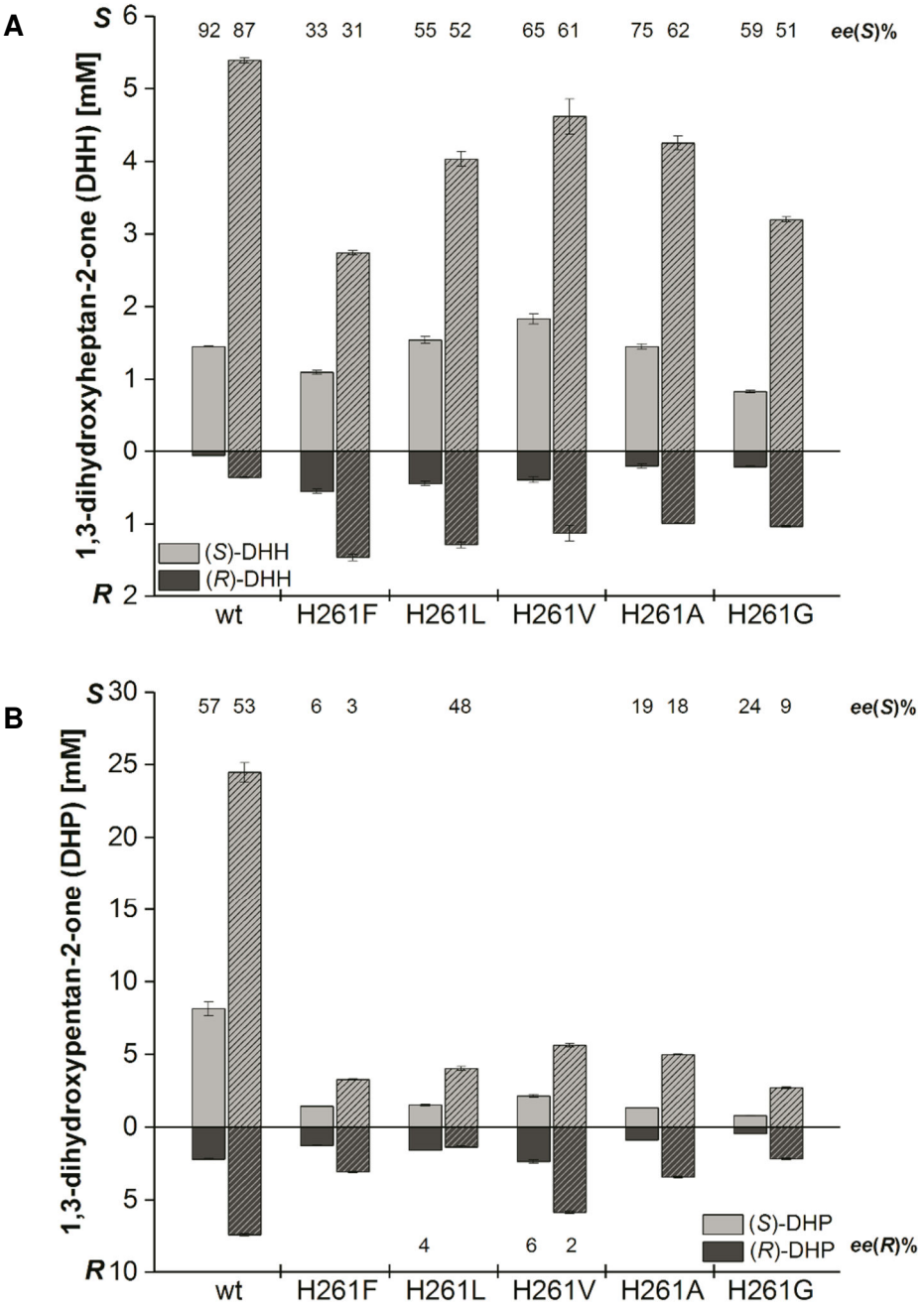

Figure 3-25: Influence of substitution of H261 on the *Ec*TK stereoselectivity. The variants are ordered by the size of the residue in position 261. **A:** Carboligation of 3-hydroxypyruvate (HPA) and n-pentanal to 1,3-dihydroxy-2-heptanone (DHH); **B:** Carboligation of HPA and propanal to 1,3-dihydroxy-2-pentanone (DHP); Reaction conditions: 100 mM KP_i-buffer pH 7, 2.4 mM ThDP, 3 mM $MgCl_2$ and 0.9 mg·mL^{-1} *Ec*TK variant. The donor substrate HPA and the acceptor substrates were always used equimolar with final concentrations of 50 mM and 100 mM for n-pentanal and propanal, respectively. Samples were incubated at 25°C for 1 h (open columns) and 3 h (hatched columns) before analysis via chiral phase GC-MS. Error bars display the standard error from biological triplicates.

Combined substitution of H26 and H261

Even though H26 and H261 are probably responsible for proton transfer during the carboligation reaction, variant H26A/H261A still gave a yield of 7 % DHH after 3 h reaction time, which is still 60 % of the product amount obtained with wildtype *Ec*TK under identical conditions. This indicates that the proton transfer can also be mediated by other amino acids or water molecules. As stabilising interactions with H26 and H261 are not possible in variant H26A/H261A, the acceptor carbonyl group could be stabilised by other histidine residues in the active site, for example H461 or H473, which would imply a parallel orientation of the acceptor carbonyl group according to states *I* and *II* in Figure 3-19. Nevertheless, biotransformations with variant H26A/H261A resulted in an excess of the *S*-enantiomer (DHH) with an *ee*-value of 57 % (Figure 3-26 A). Again, this can be explained by the opening of an antiparallel acceptor binding pocket, which in that case would promote binding state *II* (Figure 3-19). To prevent opening of a pocket, the substitution H26A was also combined with replacement of H261 by leucin and phenylalanine, but this resulted in a further decrease in activity, as could be deduced from the reduced yield of 2-3% for DHH after 3 h and low *ee*-values (H26A/H261L: 22 % (*S*); H26A/H261F: 8 % (*R*), Figure 3-26 A). Combination of the H26Y substitution with a H261A exchange yielded an almost inactive variant. With respect to the formation of DHP the yields were even further decreased compared to wildtype *Ec*TK and *ee*-values were within the same range (see also appendix, Table 7-1)

Summarised, an inversion of the stereoselectivity could solely be achieved by exchange of H26, while replacement of H261 only lowered the excess of the *S*-enantiomer. This suggests that H26 has the major role in the stabilisation of the acceptor carbonyl group. Expectedly, the effect strongly depends on the inserted amino acid (Figure 3-24). The results with the H261 variants further show that effects on the stereoselectivity also depend on the applied acceptor substrate (Figure 3-25).

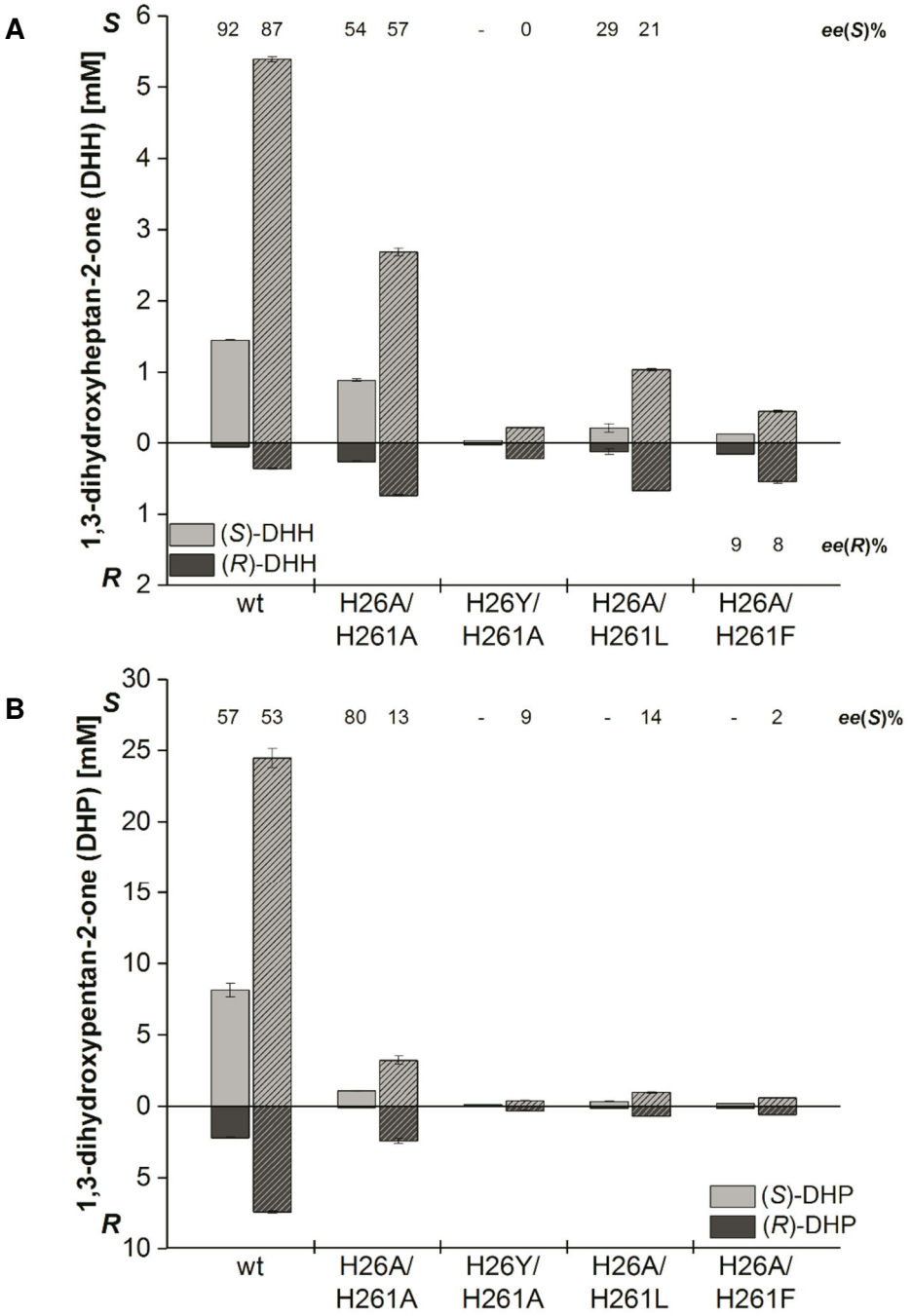

Figure 3-26: Influence of combined substitution of H26 and H261 on the *Ec*TK stereoselectivity. **A:** Carboligation of 3-hydroxypyruvate (HPA) and n-pentanal to 1,3-dihydroxy-2-heptanone (DHH); **B:** Carboligation of HPA and propanal to 1,3-dihydroxy-2-pentanone (**DHP**); Reaction conditions: 100 mM KP_i-buffer pH 7, 2.4 mM ThDP, 3 mM $MgCl_2$ and 0.9 mg·mL^{-1} *Ec*TK variant. The donor substrate HPA and the acceptor substrates were always used equimolar with final concentrations of 50 mM and 100 mM for n-pentanal and propanal, respectively. Samples were incubated at 25°C for 1 h (open columns) and 3 h (hatched columns) before analysis via chiral phase GC-MS. Error bars display the standard error from biological triplicates.

3.2.5 Influence of the D469E substitution

The substitution D469E has been reported to increase the activity and the *S*-selectivity of *Ec*TK towards aliphatic acceptor aldehydes (Cázares et al., 2010; Hibbert et al., 2008; Smith et al., 2008). These results have recently been confirmed for the analogous substitution D477E in *Sc*TK (Marsden et al., 2017). Therefore, it was investigated whether the activity of variants H26A and H261A could also be increased by combination with the D469E substitution and how this would affect the stereoselectivity. While the increased activity of *Ec*TK D469E towards DHH and DHP formation could be reproduced, as deduced from 21-fold and 4.6-fold higher yields compared to wt *Ec*TK after 1 h, respectively, the double variants with a D469 substitution gave comparabley lower product yields (Figure 3-27). For *Ec*TK H26A/D469E the stereoselectivity was shifted towards the *R*-enantiomers compared to wt *Ec*TK but shifted towards the *S*-enantiomers compared to *Ec*TK H26A. Similarly, the yields were as well reduced and the stereoselectivity was also shifted towards the *S*-enantiomer with *Ec*TK H26Y/D469E compared to variant H26Y (see appendix Table 7-1). *Ec*TK H261A/D469E showed comparable stereoselectivites and yields as *Ec*TK H261A. Overall, combination of amino acid substitution with a D469E substitution did not help to create further variants with increased acivity and to maintain high stereoselectivities.

In silico docking studies with *Sc*TK D477(469)E indicated that the substituion might improve the *S*-selectivity with aliphatic acceptor aldehydes by interactions of the carboxyl group with the acceptor substrate carbonyl group via a coordinated water molecule. Thereby, it stabilises the reactive orientation of the acceptor substrate and the formation of a oxyanion during the nucleophilic attack of the dihydroxyethyl-ThDP intermediate (Marsden et al., 2017). In the context of the extended stereoselectivity model, this translates to a increased population of binding state *III* (Figure 3-19). Hence, a likely reason for the shift of the stereoselectivity toward the *S*-enatiomers with the H26A/D469E and H26Y/D469E variants is that the D469E substitution compensates for the loss of the intercation between the acceptor carbonyl group and H26. The reason for the reduced product formation with the D469E double variants might be that H26, H261 and D469 are part of different co-evolved amino acid clusters that were identified by statistical coupling analysis by Strafford et al., 2012. According to this study the combined substitution of amino acids from these clusters can destabilise networks of co-evolved residues and therefore impair the enzyme activity.

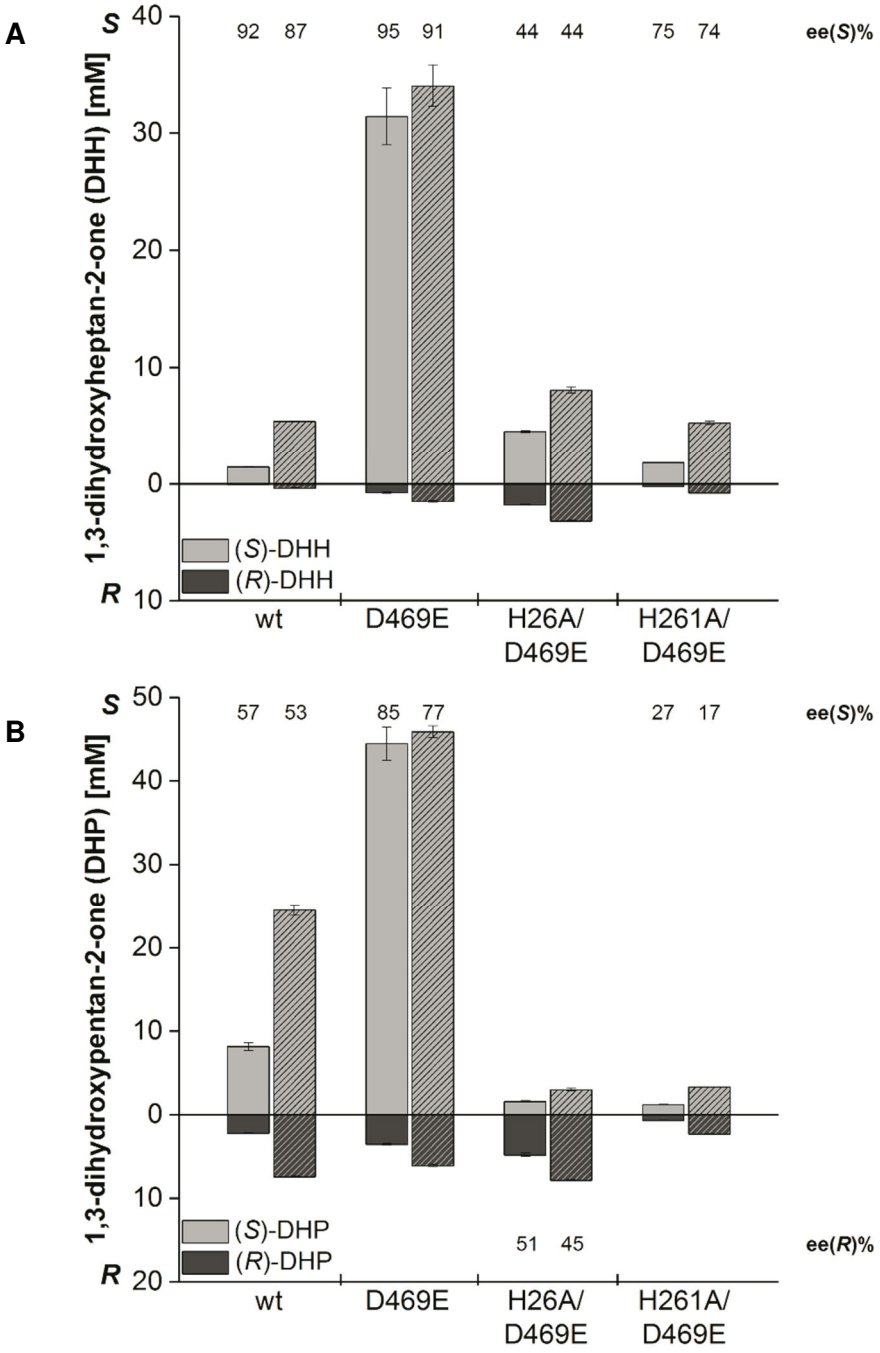

Figure 3-27: Influence of an additional D469E substitution on *Ec*TK variants. Reaction conditions: 100 mM KP_i-buffer pH 7, 2.4 mM ThDP, 3 mM $MgCl_2$ and 0.9 mg·mL^{-1} *Ec*TK variant. The donor substrate HPA and the acceptor substrates were always used equimolar with final concentrations of 50 mM and 100 mM for n-pentanal and propanal, respectively. Samples were incubated at 25°C for 1 h (open columns) and 3 h (hatched columns) before analysis via chiral phase GC-MS. Error bars display the standard error from biological triplicates. The variants were prepared by Philipp Marquardt in the course of his master thesis (Marquardt, 2015).

3.2.6 Time-dependent decline of the enantiomeric excess of DHH

The *Ec*TK variants F434L and F434A showed a comparably great drop (17 and 20 percent points) of the *ee*-value for DHH between 1 h and 3 h reaction time. In contrast to the other tested variants, only the amount of (*R*)-DHH increased between 1 h and 3 h while the amount of (*S*)-DHH decreased (Figure 3-23 A). This effect was investigated in more detail for variant F434A by following the reaction over 3 h as shown in Figure 3-29 A. Wildtype *Ec*TK, which was used as a control, showed a constant increase of DHH over 3 h reaction time. The *ee*-value fluctuated between 84 % (*S*) and 91 % (*S*) but showed no increasing or decreasing tendency. In contrast, with variant F434 the majority of the product was formed within the first 30 min of the reaction. At that time point the product amount formed by *Ec*TK F434A catalysis exceeded the amount formed by wt *Ec*TK about 20-fold (Figure 3-29 A). Afterwards, the amount of DHH stayed roughly constant. However, residual n-pentanal showed that the reaction was not completed. The *ee*-value decreased over the whole measuring period, starting from 72 % (*S*) after 10 min to 32 % (*S*) after 3 h. This shows that the *ee*-value of 53 % (*S*) measured with *Ec*TK F434A after 1 h (Figure 3-23 A) was already impaired by the time-dependent decline of the stereoselectivity. The amount of (*S*)-DHH started to decrease after 30 min (*S*), while the amount of (*R*)-DHH constantly increased. This indicates a transformation of (*S*)-DHH to (*R*)-DHH, which is probably enzyme catalysed.

The dihydroxy ketone DHH formed in the carboligation of 3-hydroxypyruvate and aldehydes resembles xylulose-5-phosphate, the physiological donor of transketolases (Figure 3-28 A). Especially the first three carbon atoms are functionalised in the same way. This suggests that the dihydroxy ketone product DHH can serve as a donor and could be cleaved by the enzyme variant according to steps **e** and **d** (Figure 1-3). In this case R^1 is CH_2OH and R^3 is $(CH_2)_3CH_3$, meaning that n-pentanal would be cleaved from the product to form the carbanion-enamine. A similar reverse reactivity has recently been shown for *Sc*TK with glycolaldehyde as acceptor substrate (Marsden et al., 2017). In our studies only n-pentanal was present as an acceptor substrate. Thus, only DHH could be formed as a new carboligation product. Besides, glycolaldehyde, the decarboxylated form of HPA, might be released from the active site, but TK does typically not catalyse decarboxylation reactions without transfer of the decarboxylated donor on an acceptor molecule. Transketolases are highly selective for the configuration of the hydroxyl group at the C3-atom of the donor, which has to be *S*-configurated (Nilsson et al., 1998), at least with respect to the natural substrates. Therefore, only (*S*)-DHH can serve as a donor while the formed product is a mixture of (*S*)- and (*R*)-DHH depending on the stereoselectivity of the respective variant (Figure 3-28 B). Consequently, the *R*-product would accumulate while the *S*-product is (partly) transformed to the *R*-product, which would explain the decreasing *ee*-value. Similarly, *Pp*BFD was shown to catalyse the racemisation of enantiopure HPP by the same mechanism as proposed here for *Ec*TK (Berheide et al., 2015). However, for *Pp*BFD this racemisation was described starting from both HPP enantiomers instead of selectively only one enantiomer.

To test this hypothesis, (*S*)-DHH was synthesised from HPA and n-pentanal using the highly *S*-selective *EcTK* variant D469E (Smith et al., 2008) and incubated with *Ec*TK F434A as described in chapter 5.3.9. The *ee*-value was followed over several hours (Figure 3-29 B). Samples without enzyme and with wt *Ec*TK were prepared as controls in parallel. Within 20 h the *ee*-value of DHH in the reaction with variant F434A decreased from 96 % (*S*) to 78 % (*S*), thereby showing the strongest decrease within the first hour. With wt *Ec*TK and without enzyme the *ee*-value only decreased to 91 % (*S*) and 95 % (*S*), respectively (Figure 3-29 B). This result strongly supports the theory that (*S*)-DHH was transformed to

(*R*)-DHH by variant F434A. However, the strong decrease of the *ee*-value of 40 percent points within 3 h could not be reproduced, here. This can probably be explained by the low concentration of (*S*)-DHH (<5 mM, Figure 3-29 B) and thus a lower reaction rate in the setup of this control experiment compared to the concentration of (*S*)-DHH formed by the variant F434A during the reactions in which the time-dependent decay of the *ee* was first observed (>25 mM, Figure 3-23 A). The low concentration of (*S*)-DHH in the control experiment was caused by the incubation with the MP-carbonate resin (cation exchanger) to remove excess HPA, which reduced the initial concentration of (*S*)-DHH formed by *Ec*TK D469E from 40 mM to 5 mM. Thus, also DHH is adsorbed to the resin despite the lack of a carboxyl group to facilitate the adsorption.

Overall, the results support the hypothesis that the (*S*)-enantiomer of the carboligation product can act as a donor substrate. Since also with wildtype *Ec*TK the *ee*-value of (*S*)-DHH dropped by 5 percent points within 20 h, it seems likely that also other variants can accept (*S*)-DHH as a donor substrate. Probably the exchange of F434 lowered the K_m-value for (*S*)-DHH and/or increased the activity for the cleavage of (*S*)-DHH as a donor. Further, for highly *S*-selective variants (like L382A or D469E) the cleavage of (*S*)-DHH on the *ee*-value should be less pronounced, as (*S*)-DHH is formed with high excess from (*S*)-DHH as a donor and n-pentanal as the acceptor and the transfer rate from (*S*)- to (*R*)-DHH is lower. Additionally, the effect should also be more pronounced for variants with high activity for the formation of DHH starting from HPA and n-pentanal, because a high concentration of DHH and a low concertation of the competing donor substrate HPA should favour the use of (*S*)-DHH as donor substrate. Thus, even though probably all *Ec*TK variants can use (*S*)-DHH as a donor substrate this does not always result in an observable effect on the *ee*-value within the measurement parameters applied in this study.

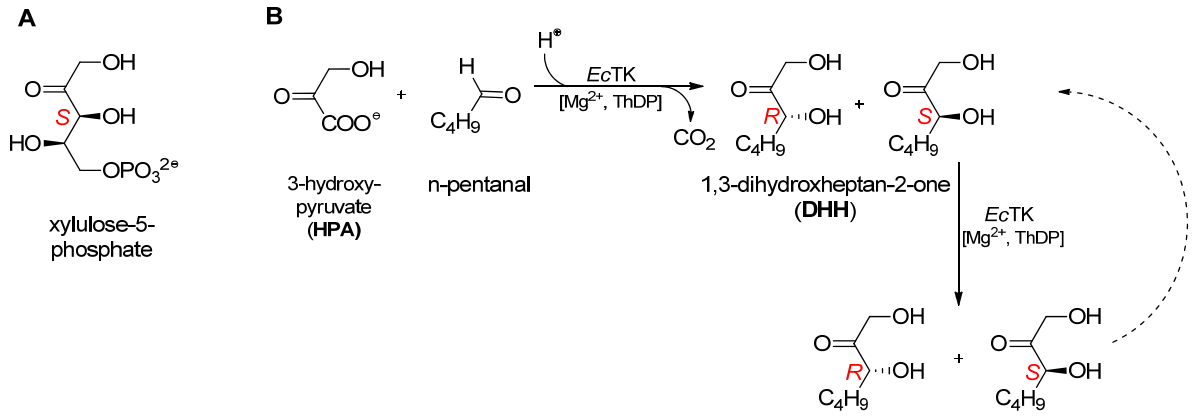

Figure 3-28: A: Donor of the physiological transketolase reaction. B: Proposed mechanism for the time-dependent decline of the *ee*-value observed for the *Ec*TK variants F434A and F434L with n-pentanal as acceptor substrate.

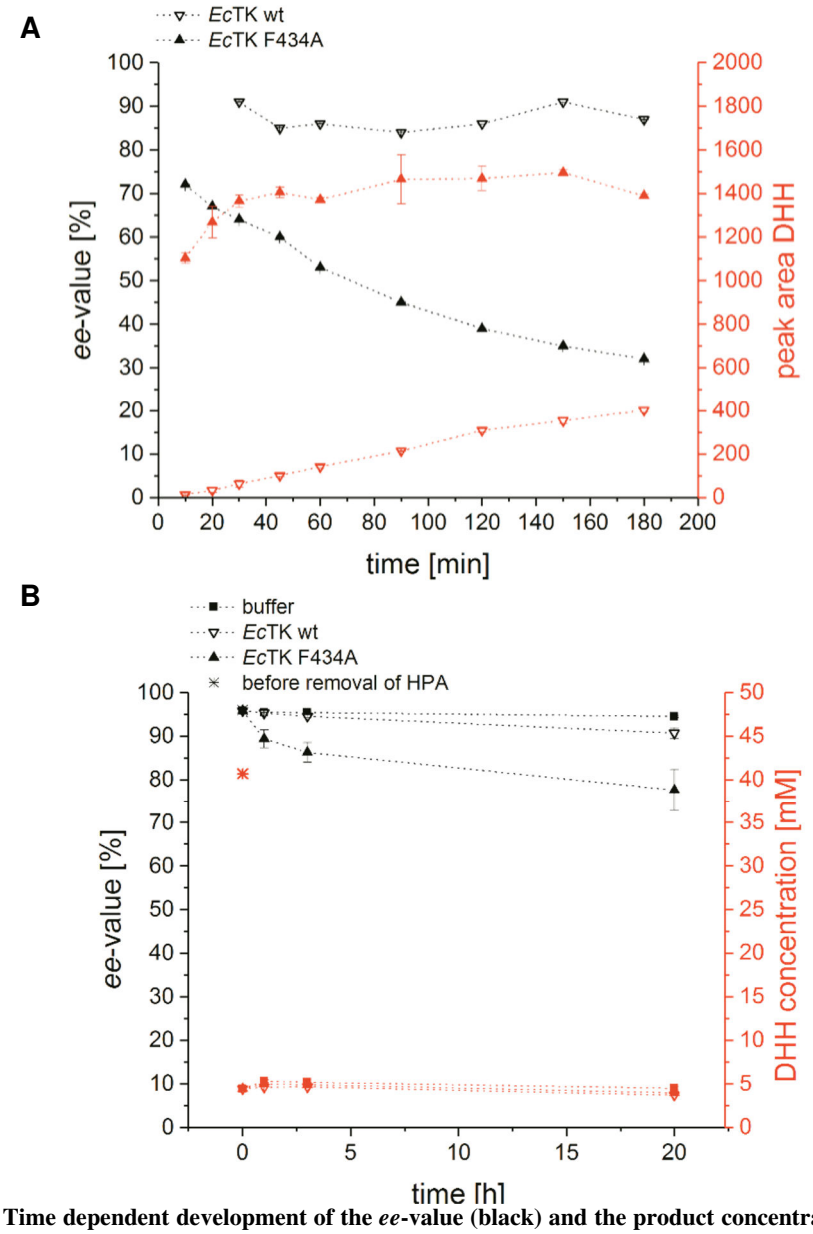

Figure 3-29: A: Time dependent development of the *ee*-value (black) and the product concentration given as the peak area (red) for the carboligation of 3-hydroxypyruvate (HPA) and n-pentanal to 1,3-dihydroxy-2-heptanone (DHH) with wildtype *Ec*TK and the variant F434A. Reaction conditions: 100 mM KP_i-buffer, pH 7, 2.4 mM ThDP, 3 mM $MgCl_2$ and 0.9 mg·mL^{-1} *Ec*TK variant, 50 mM HPA and 50 mM n-pentanal. Measurements were performed by Stephanie Moers in the course of her master thesis (Moers, 2017). **B: Change of the ee-value (black) and the concentration (red) of (*S*)-DHH (synthesised with EcTK D469E) due to incubation with wildtype *Ec*TK and variant F434A.** *Ec*TK D469E and residual HPA of the DHH synthesis were removed before the other *Ec*TK variants were added. Excess n-pentanal from the synthesis was still present in the reaction. As a control a sample of (*S*)-DHH was incubated in buffer without additional enzyme. Conditions: 100 mM KP_i-buffer, pH 7, 2.4 mM ThDP, 3 mM $MgCl_2$. Error bars represent the standard error of biological duplicates.

3.2.7 Assessment of the extended stereoselectivity model

The extension of the existing two-state stereoselectivity model for ThDP-dependent decarboxylases to a four-state model including the relative orientation of the substrates' functional groups (Figure 3-19) intrinsically hindered its predictability, as the enantiomeric excess results from the relative population of four binding states. While for a two-state model the distribution can only be shifted along one vector (*I*↔*II*, Figure 3-19), for the four-state model it can be shifted along six vectors (I↔*II*; I↔*III*; I↔IV; *II*↔*III*; *II*↔IV; *III*↔IV). This becomes especially evident for variants like H261A or H26A that potentially both destabilise the antiparallel orientation of the acceptor carbonyl group (promotes state *I* and *II*, Figure 3-19) and open an antiparallel binding pocket for the acceptor side chain (promotes state *II* and *IV,* Figure 3-19). Here, this effect is even more pronounced with propanal as the acceptor substrate as wt *Ec*TK showed only moderate stereoselectivity for this reaction. It can be assumed that a high stereoselectivity results from predominantly one preferred binding state, while a lower stereoselectivity indicates that more binding states are populated. Hence with low stereoselectivity, it is more difficult to rule out vectors as it would be possible for high stereoselectivity for which not all binding states are occupied. For example, opening an antiparallel acceptor binding pocket exclusively promotes binding state *IV*, given that initially only binding state *III* is occupied, which means a stereoselectivity of 100 %. At a lower initial stereoselectivity, like for the formation of DHP by wt *Ec*TK, it must be assumed that binding state *I* is occupied in addition to binding state *III*. Under this condition opening a pocket would enhance binding state *II* and *IV*. Along the same lines destabilisation of the acceptor carbonyl group can promote binding state *I* and *II*.

Concerning a potential stereoselectivity switch by opening a pocket according to binding states *II* and *IV* in Figure 3-19, it also must be considered that opening of a pocket is a necessary but not sufficient condition for antiparallel binding of the acceptor side chain. Thus, it cannot be assumed that opening a pocket fully shifts the distribution of the binding states to state *II* and *IV* (Figure 3-19). In that regard, studies on different ThDP-dependent decarboxylases showed that the stereoselectivity can further be increased when the parallel orientation of the acceptor side chain is destabilised in addition to opening an antiparallel acceptor binding pocket (Sehl et al., 2017; Westphal et al., 2013a).

Another difficulty of the four-state model is that the underlying binding states cannot be deduced directly from the observed stereoselectivities. As two binding states result in the formation of *S*- and *R*-product, respectively, the measured *ee*-values only reveal information about the ratio of *I* and *IV* compared to *II* and *III* (Figure 3-19). Therefore, the information obtained by stereoselectivity measurements is incomplete regarding the four-state model. A conclusion concerning the predominant substrate binding orientation responsible for an observed stereoselectivity is however possible based on the structure using the assumptions of the extended stereoselectivity model. Bayesian statistics provide a tool to combine the structural knowledge from the extended stereoselectivity model and the measured *ee*-values (Gelman et al., 2013). In cooperation with Axel Theorell (IBG-1, Forschungszentrum Jülich GmbH) first prior probability distributions of the affinities of the binding states were formulated based on the stereoselectivity model, which were subsequently updated with the information from the measured *ee*-values, to obtain substrate specific posterior probability distributions for the four binding states (Baierl et al., 2018). The results showed that in some cases, the posterior has the potential to resolve the binding state affinities with some certainty or to update the initial assumption of the affinities. However, in other cases, only partial or no affinity resolution is possible. This is the case when either the prior

does not contain enough information to resolve the binding states, for example when the experimental results differ from the prior perception, or when the experimental results, i.e. very low stereoselectivity, contributes very little to distinguish the posterior from the prior.

On the example of the DHH-formation with *Ec*TK F434A and F434L it has been shown that the *S*-product of the carboligation may serve as the donor substrate for further carboligation reactions, resulting in an accumulation of the *R*-enantiomer (chapter 3.2.6). This shows that effects of amino acid substitutions on micro reaction rates, in this case cleavage of the dihydroxy ketone product according to steps **e** and **d** in Figure 1-3, can directly influence the observed stereoselectivity. However, incorporation of this mechanism into the stereoselectivity model is not possible, especially since the effect appears to vary greatly depending on specific amino acid substitutions and on the employed substrate, which influence the kinetic properties. Regarding micro-reaction constants and K_m-values also the applied substrate concentrations are relevant. This might contribute to the observed differences with n-pentanal and propanal as acceptor, as they were not used at the same final concentration. Similarly, inactivating and/or destabilising effects of amino acid substitutions are difficult to predict and were so far not included in the model. Therefore, both effects hinder the model evaluation.

Generally, TKs that are not of mammalian origin show a high degree of sequence identity (>45 % identical amino acids) and also the active site structures are closely related (Mitschke et al., 2010; Schenk et al., 1997). However, comparison of the results for the here tested *Ec*TK variants with variants of *Gst*TK described by Zhou *et al.* (Zhou et al., 2017) shows that effects of amino acid exchanges can also differ for TKs from different organisms. For *Gst*TK exchange of L191, the corresponding residue to I189 in *Ec*TK, was found to be decisive to create *R*-selective variants with *ee*-values up to 84 % for the formation of DHP (Table 1-4) and could additionally increase the specific activity at least 3-fold when replaced by glycine, alanine or valine. The corresponding exchanges distinctly reduced the product formation for *Ec*TK, which could at least partly result from a negative influence of amino acid exchanges in this position on the enzyme stability. The differences might be explained by the thermostability of *Gst*TK, which is likely to also entail higher robustness towards replacement of amino acids. Further, I189 substitutions were combined with an exchange of D470(469), especially to leucine, for *Gst*TK which was not tested for *Ec*TK, here. By exchange of L382 to alanine also *Gst*TK showed increased activity for the formation of DHP but unlike *Ec*TK no increased *S*-selectivity. The exchanges F435(434)A and F435(434)L increased the activity and the *S*-product formation for the transketolases from both organisms.

3.2.8 Summary

In order to explain the natural *S*-selectivity of transketolases the existing stereoselectivity model for ThDP-dependent decarboxylases was extended by the antiparallel orientation of the acceptor carbonyl group, resulting in a model with four instead of two possible substrate binding states prior to C-C-bond formation (Figure 3-19). Evaluation of the model by extensive mutagenesis studies showed that the extension of the model significantly increased its complexity. With the tested reactions in this thesis, the model could partly be verified. Two strategies were followed to invert the TK stereoselectivity: Enhancement of binding state *IV* (Figure 3-19) by opening of an antiparallel acceptor binding pocket could be shown for replacement of F434 and most likely also H261 but did not lead to inversion of the

stereoselectivity for the tested reactions. Enhancement of binding state *I* (Figure 3-19) by destabilisation of the acceptor carbonyl group through substitution of H261 and H26 increased the formation of the *R*-enantiomer and could result in full stereoinversion in the latter case. For both strategies, the stereoselectivity probably resulted from the population of more than one binding state. This impairs the predictability since every substitution might influence the stereoselectivity via several mechanisms and the relative population of the four states cannot be fully resolved by the observe *ee*-values. Consequently, the application of the model for the prediction of amino acid exchanges for the inversion of stereoselectivity for the tested reactions is not possible, yet. However, the model provides a first framework to understand the structure-function relationships of transketolases with respect to their stereoselectivity.

3.3 Evaluation of the applicability of the extended stereoselectivity model for ThDP-dependent decarboxylases

The extended stereoselectivity model is based on the fact that the acceptor carbonyl group in transketolases is stabilised by H26 and H261 in an antiparallel orientation compared to the donor hydroxy group. This allows *S*-selective product formation according to binding state *III* without an antiparallel orientation of the substrate side chains (binding state *II*, Figure 3-19). As already pointed out in chapter 1.3.4, there are only a few histidine residues in the active site of ThDP-dependent decarboxylases, suggesting that the donor hydroxy group and the acceptor carbonyl group are stabilised by the same side chain and are therefore oriented in the same direction. Transferring the extended model to decarboxylases implies that the stereoselectivity can be influenced by the insertion of additional histidine residues in the active site. Consequently, a second approach to evaluate the extended stereoselectivity model was to investigate the possibility of creating *S*-selective variants of ThDP-dependent decarboxylases by changing the orientation of the acceptor carbonyl group instead of opening an antiparallel acceptor binding pocket.

Benzaldehyde lyase from *Pseudomonas fluorescens* (*Pf*BAL) was chosen for this approach, because the acceptor binding side is relatively big and probably provides enough room for an additional histidine side chain. Further, *Pf*BAL has a high reaction rate and the potential antiparallel acceptor binding pocket is blocked by the protein backbone, thereby reducing the likelihood that amino acid substitutions in the active site unintentionally open a pocket and enable antiparallel side chain binding. Based on the crystal structure of *Pf*BAL (PDB: 3D7K (Brandt et al., 2008), Figure 3-30) A480(476) was identified as a good position to insert a histidine side chain. Besides inserting a residue that facilitates antiparallel stabilisation of the carbonyl group, the amino acid originally responsible for stabilisation of the acceptor carbonyl group and proton transfer during the reaction cycle had to be removed. For *Pf*BAL this amino acid is most probably H29(29), which was consequently replaced by phenylalanine (Kneen et al., 2005; Knoll et al., 2006; Westphal, 2013).

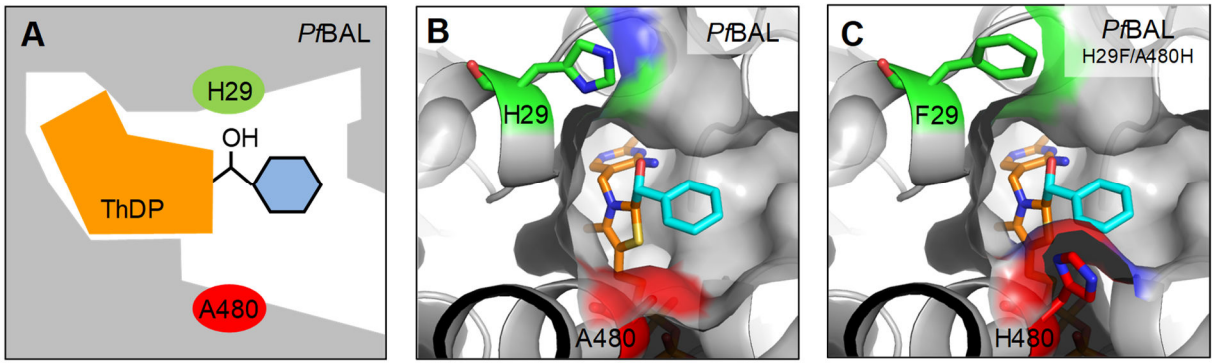

Figure 3-30: Schematic representation (A) and PyMOL structure (B) of *Pf*BAL with the location of H29(29, green) and A480(476, red) that were subjected to site-directed mutagenesis. A model of the structure after the mutagenesis is shown in C. B and C were generated with the PyMOL Molecular Graphics System (Schrödinger, LLC) based on the crystal structure of *Pf*BAL (PDB: 3D7K (Brandt et al., 2008)). Orange: ThDP, light blue: ThDP-bound donor-intermediate

Variants with the single substitutions H29F and A480H, as well as the combination thereof, were created by site-directed mutagenesis (chapter 5.2.3), produced by heterologous expression of the respective genes in *E. coli* (BL21)DE3 (chapter 5.3.1), and purified by Ni-NTA affinity chromatography (chapter 5.3.3). The yield of the protein purification was typically around 10 mg purified *Pf*BAL variant per gram

wet biomass. Subsequently, the variants where investigated regarding their stereoselectivity for the formation of benzoin and HPP.

3.3.1 Benzoin formation

The carboligation potential and stereoselectivity of the *Pf*BAL variants was first tested for the self-ligation of benzaldehyde to benzoin. Figure 3-31 shows that the product formed by the single variants A480H and H29F was reduced about three-fold compared to wt and only traces of (*R*)-benzoin could be detected for the carboligation with variant H29F/A480H. Thereby, the variants showed no increased formation of (*S*)-benzoin compared to wt *Pf*BAL and ee-values >99 % were measured with all variants.

*Pf*BAL H29F showed still reasonable activity suggesting that this histidine is not solely responsible for proton transfer during the catalytic cycle. Probably, the proton transfer is mediated by a water molecule, which was found within the active site in the crystal structure of *Pf*BAL and is stabilised by H29. Besides, also Q113(115) might be involved into proton transfer by stabilisation of water molecules. It was shown that substitution of Q113 by alanine reduces the carboligation activity of *Pf*BAL (Westphal, 2013).

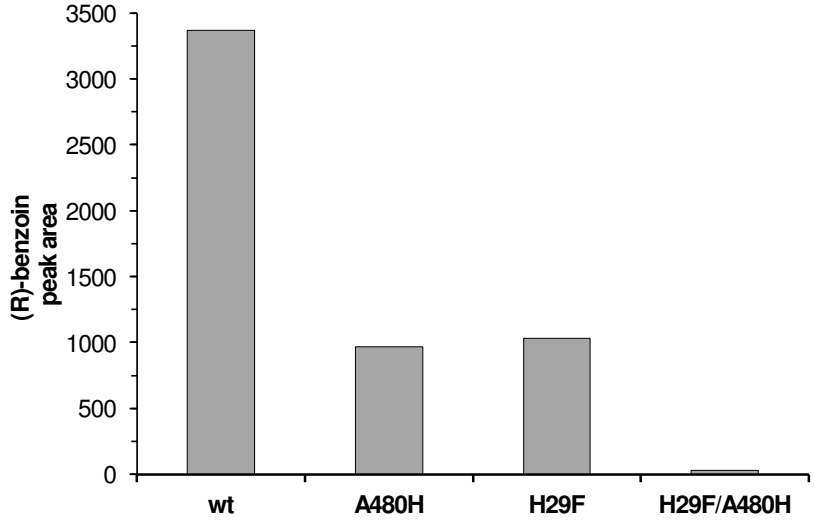

Figure 3-31: Self-ligation of benzaldehyde to benzoin with *Pf*BAL variants. Reaction conditions: 50 mM KP_i-buffer pH 7.8, 0.1 mM ThDP, 2.5 mM $MgCl_2$, 0.1 mg·mL^{-1} purified *Pf*BAL variant, and 25 mM benzaldehyde. Samples were incubated at 22°C for 15 min before analysis via chiral phase HPLC.

3.3.2 Mixed carboligation

Subsequently, the mixed carboligation of acetaldehyde and benzaldehyde was investigated with the *Pf*BAL variants (Figure 3-32). Biotransformations with wt *Pf*BAL gave full conversion of benzaldehyde to (*R*)-HPP with >99 % *ee*. Only traces of (*R*)-PAC and no benzoin were detected. As observed before for the self-ligation of benzaldehyde, the conversion with the single variants was reduced and with the double variant only traces of the products could be detected. The stereoselectivity was not lowered for all three *Pf*BAL variants, which also produced (*R*)-HPP with >99 % *ee*. However, the chemoselectivity was greatly affected when the variants were used for the carboligation of acetaldehyde and benzaldehyde. *Pf*BAL A480H gave 3-fold reduced (*R*)-HPP formation but 26-fold increased (*R*)-PAC

formation compared to wt and additionally traces of benzoin. Since the peak areas of HPP, PAC, and benzoin result from different extinction coefficients, the peak areas of the three products cannot be compared to each other and the overall productivity of a variant can only be concluded from the benzaldehyde conversion. Variant H29F showed 11-fold reduced (*R*)-HPP formation compared to wt. In contrast to variant A480H, biotransformations with variant H29F did not give any (*R*)-PAC at all but (*R*)-benzoin, which was not detected with wt *Pf*BAL.

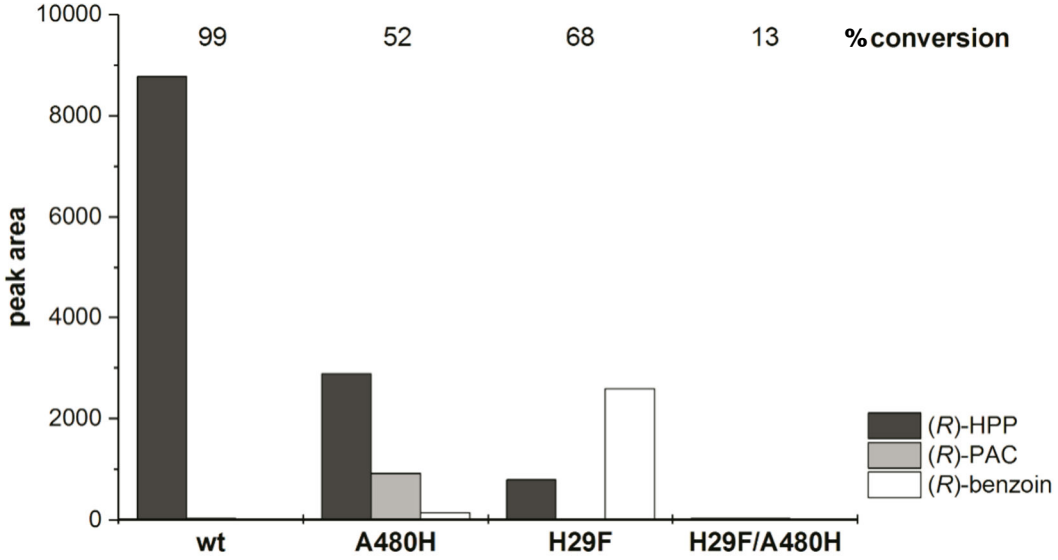

Figure 3-32: Mixed carboligation of acetaldehyde and benzaldehyde with *Pf*BAL variants Reaction conditions: 50 mM KP_i-buffer pH 7.8, 0.1 mM ThDP, 2.5 mM $MgCl_2$, 0.1 mg·mL^{-1} purified *Pf*BAL variant, 25 mM acetaldehyde, and 12.5 mM benzaldehyde. Samples were incubated at 22°C for 22 min before analysis via chiral phase HPLC.

These changes of the chemoselectivity can probably be explained by two different effects:

The formation of benzoin in carboligation reactions containing a twofold excess of acetaldehyde over benzaldehyde might directly result from **altered micro-reaction rates** of these variants. In a wt *Pf*BAL-catalysed reaction with acetaldehyde and benzaldehyde (*R*)-HPP is the final product, but (*R*)-benzoin is formed as an intermediate. When a certain concentration of (*R*)-benzoin is reached, the intermediate product is cleaved by the enzyme and the hydroxyphenyl-group is transferred to acetaldehyde as the acceptor, which results in (*R*)-HPP formation (Demir et al., 2001). With lower reaction rates, it can be expected that benzoin accumulates also over longer reaction times. Here, possibly the benzoin cleavage reaction was slowed down or the affinity for benzoin as a substrate was lowered. Mainly variant H29F showed benzoin formation, as this residue is probably involved into proton transfer during the reaction cycle. Also interactions of the introduced phenylalanine residue with benzaldehyde or benzoin might affect the reaction mechanism. For further clarification, the time course of HPP and benzoin formation should be investigated with the *Pf*BAL variants.

PAC-formation requires a change of the donor specificity from benzaldehyde to acetaldehyde (see chapter 1.3.3). Here, the substitution of A480 by the bigger amino acid histidine might result in a **restricted accessibility and/or size of the donor binding site** (Figure 3-30). Thereby, acetaldehyde can serve as a donor substrate for variants containing an A480H substitution but not for wt *Pf*BAL or variant H29F, as acetaldehyde is not well stabilised in the large donor binding site. However, also for

*Pf*BAL variant L112(114)A formation of (*R*)-PAC was described (Westphal, 2013). This shows that a reduced size of the donor binding site cannot be the exclusive reason for PAC-formation, as for the L112A variant the size of the donor binding site was increased rather than reduced. Further investigations with another DC, where the introduction of an additional histidine had less influence on the active site architecture, might help to elucidate this aspect. A candidate for this could be *Pp*YerE, which carries a methionine instead of an alanine at standard position 476.

3.3.3 Summary

The *Pf*BAL variants H29(29)F, A480(476)H, and H29(29)F/A480(478)H were created with the aim to investigate whether the four-state stereoselectivity model (Figure 3-19) could be transferred from TKs to DCs and whether *S*-selective enzyme variants could be generated by the re-orientation of the acceptor carbonyl group instead of opening an antiparallel acceptor binding pocket. However, all three variants still showed excellent stereoselectivities toward the *R*-products in all tested carboligation reactions. Instead, the chemoselectivity of the variants was affected, which can probably be explained by combined effects of altered micro- reaction rates and a restricted accessibility of the donor binding site. This shows that even single amino acid substitutions can have a strong impact on the mechanisms steering chemo- and stereoselectivity.

4 CONCLUSION AND PERSPECTIVES

The validity and applicability of the stereoselectivity model for ThDP-dependent decarboxylases (DCs) has been demonstrated in several studies. This work shows the limitations of the model but also explores new mechanisms that still need further elucidation.

For *Pp*YerE, it could be confirmed that the two-state stereoselectivity model is valid, but in consideration of the restricted size of the potential antiparallel acceptor binding pocket not applicable for the stereoinversion of *Pp*YerE, especially with larger acceptor substrates.

The extension of the stereoselectivity model for transketolases (TKs) added new mechanisms to the model that on the one hand significantly increase the complexity of the model but on the other hand offer new strategies to influence the stereoselectivity of ThDP-dependent enzymes. For further evaluation of the extended model, it is essential to develop strategies that help to distinguish the four substrate binding states despite the limited information that can be obtained from the stereoselectivity measurements. In this work, this was mainly attempted by suitable combination of amino acid substitutions, which in an ideal case would only increase one binding state and supress the other three. However, prediction of effects of amino acid substitution on crystal structures can be difficult, as these do not reflect the flexible nature of enzymes in solution. Another factor in this regard is the choice of the acceptor substrate. Here, it is desirable to find a reaction system with excellent stereoselectivities, as this halves the amount of possible binding states and thereby facilitates the interpretation, also with respect to changes of the stereoselectivity upon mutagenesis. Further, computational tools can help to resolve the probability for the four binding states. Here, especially molecular dynamics simulations could offer a framework to predict effects of amino acid substitutions. Another point that should be addressed is the effects of amino acid substitutions on the micro-reaction constants of the reaction mechanism. For *Ec*TK and *Pf*BAL H29F an influence of altered micro-reaction constants on the stereo- and chemoselectivity was observed. The current model, however, is mainly based on steric aspects. Determination of the ThDP-bound reaction intermediates by NMR (Kluger and Tittmann, 2008; Kokova et al., 2009) provides more information that measurements of the *ee*-values and could help to elucidate the effect of amino acid substitutions.

Interestingly, the four-state model offers a second possibility for the stereoinversion of *Pp*YerE, as well as *Ec*AHAS or any other ThDP-dependent enzyme for which opening of an alternative acceptor binding pocket is not successful, by re-orientating the acceptor carbonyl group. Even though, a first proof-of-principle study with *Pf*BAL did not succeed in creating *S*-selective *Pf*BAL variants, it might be worthwhile to further study this possibility with other enzymes, for example *Pp*YerE.

Furthermore, the transfer of the model on other structural superfamilies might expand the scope of ThDP-dependent enzymes and additionally help to clarify the current model. Here, the aKGDH superfamily might be a good starting point, since the domain structure is similar to TKs (see Table 1-1) but the α-ketoglutarate dehydrogenases SucA from *Escherichia coli* or Kdg from *Mycobacterium tuberculosis* share the *R*-selectivity of DCs for 1,2-additions (Beigi et al., 2013).

5 MATERIALS AND METHODS

5.1 Materials

5.1.1 Devices

Table 5-1: List of devices. Devices not listed met the usual laboratory standards

device	specifications	manufacturer
analytic		
CD spectrophotometer	J-1100	Jasco Inc., Gross-Umstadt, Germany
microplate reader	Infinite M200	Tecan Group AG, Mennedorf, Switzerland
NanoDrop spectrophotometer	ND-1000	Peqlab GmbH, Erlangen, Germany
NMR spectrometer	Advance DRX 600	Bruker Corporation, Billerica, USA
pH meter	691	Metrohm AG, Herisau, Switzerland
pH electrode	inLab® Micro pH	Mettler Toledo, Columbus, USA
SDS electrophoresis system	Mini-Cell CE-mark	Thermo Fisher Scientific Inc., Waltham, USA
submarine gel tank (agarose gels)	AGT2	VWR, Radnor, USA
UV-Vis spectrophotometer	UV-1800	Shimadzu, Kyoto, Japan
cell positioner	CPS-240A	Shimadzu, Kyoto, Japan
UV-Vis spectrophotometer	Biophotometer® plus	Eppendorf AG, Hamburg, Germany
balances		
balance	PCB	Kern, Balingen-Frommern, Germany
balance	BP 2100 S	Satorius, Göttingen, Germany
precision weighing balance	CPA225D	Satorius, Göttingen, Germany
cell cultivation		
incubator	Heracell	Heraeus, Haunau, Germany
flask shaker	Multitron Standard	Infors HT, Bottmingen, Switzerland
microplate shaker	TiMix	Edmund Bühler GmbH, Hechingen, Germany
culture flask	Duran, Erlenmeyer shape with baffles, 100 mL-5 L	DWK Life Science, Wertheim, Germany
cell disruption		
ultrasound processor	U200S/H	Hielscher, Teltow, Germany
sonotrode	S14D	Hielscher, Teltow, Germany
sonotrode	S3	Hielscher, Teltow, Germany
sonotrode	S1	Hielscher, Teltow, Germany

device	specifications	manufacturer
centrifuges		
mini centrifuge	Sprout	Biozym, Oldendorf, Germany
table top centrifuge	Universal 32R	Hettich, Tuttlingen, Germany
table top centrifuge	5424	Eppendorf AG, Hamburg, Germany
table top centrifuge	Minispin®	Eppendorf AG, Hamburg, Germany
centrifuge	Avanti J-20 XP	Beckmann Coulter Inc., Fullerton, USA
rotor	JLA 8.100	Beckmann Coulter Inc., Fullerton, USA
rotor	JA-10	Beckmann Coulter Inc., Fullerton, USA
rotor	JA-14	Beckmann Coulter Inc., Fullerton, USA
rotor	JA-20	Beckmann Coulter Inc., Fullerton, USA
centrifuge beakers	Polypropylen 50 mL-1 L	Beckmann Coulter Inc., Fullerton, USA
consumables		
air permeable membranes	AeraSeal™	EXCEL Scientific Inc., Victorville, USA
deep-well plates	Round wells, 1 mL-2 mL	Nerbe plus, Winsen, Germany
flowerplates®	48-well	m2p-Labs GmbH, Baesweiler, Germany
microwell plates	96-well, flat bottom, Nunclon surface	Thermo Fisher Scientific Inc., Waltham, USA
PMMA cuvettes	Semi-micro. 1.5 m	Brand, Wertheim, Germany
pipette tips	10 µL-5000 µL	Eppendorf, Hamburg, Germany
SDS-PAGE gels	NuPAGE 4-12% Bis-Tris gel, 1mm	Thermo Fisher Scientific Inc., Waltham, USA
GC		
injector	Combi PAL	CTC Analytics AG, Zwingen, Switzerland
gas chromatograph	6890 Series	Agilent Technologies, Santa Clara, USA
column	CP-Chirasil Dex CB 25 m, 0.25 mm, 0.25 µM	Agilent Technologies, Santa Clara, USA
GC-MS 1		
injector	AI 1310	Thermo Fisher Scientific Inc., Waltham, USA
gas chromatograph	Trace 1310	Thermo Fisher Scientific Inc., Waltham, USA
column	CP-Chirasil Dex CB 25 m, 0.25 mm, 0.25 µM	Agilent Technologies, Santa Clara, USA
mass-spectrometer	ISQ LT	Thermo Fisher Scientific Inc., Waltham, USA
GC-MS 2		
injector	Combi PAL	CTC Analytics AG, Zwingen, Switzerland
gas chromatograph	GCCP 3800	Agilent Technologies, Santa Clara, USA
column	CP-Chirasil Dex CB 25 m, 0.25 mm, 0.25 µM	Agilent Technologies, Santa Clara, USA
mass-spectrometer	Saturn 2000	Agilent Technologies, Santa Clara, USA
HPLC		
HPLC 1 (*Pp*YerE studies)	1100 Series	Agilent Technologies, Santa Clara, USA
column	Chiralpak IE	Daicel Cooperation, Tokyo, Japan
HPLC 2 (*Pf*BAL studies)	1260 Infinity	Agilent Technologies, Santa Clara, USA
column	Chiralpak IE	Daicel Cooperation, Tokyo, Japan

device	specifications	manufacturer
kits		
plasmid extraction	QIAprep Spin Miniprep	Qiagen GmbH, Hilden, Germany
PCR-purification	MinElute PCR Purification	Qiagen GmbH, Hilden, Germany
gel-extraction	Gene Jet Gel extraction	Thermo Fisher Scientific Inc., Waltham, USA
organic synthesis		
rotary evaporator	Rotavapor R-100	Büchi, Essen, Germany
heating bath	B-100	Büchi, Essen, Germany
vacuum pump	Vacuum Controller B-721	Büchi, Essen, Germany
circulation chiller	WKL 230	Lauda-Brinkamnn, Delran, USA
protein purification		
Äkta purifier pump	P-900	GE Healthcare, Solingen, Germany
Äkta purifier UV-Vis monitor	UV-900	GE Healthcare, Solingen, Germany
Äkta purifier pH monitor	pH/C-900	GE Healthcare, Solingen, Germany
Äkta purifier fraction collector	Frac-950	GE Healthcare, Solingen, Germany
1 mL Ni-NTA column	Superflow Cartridges	Qiagen GmbH, Hilden, Germany
5 mL Ni-NTA column	Superflow Cartridges	Qiagen GmbH, Hilden, Germany
desalting columns	PD-10	GE Healthcare, Solingen, Germany
miscellaneous		
autoclave	DX-65	Systec, Lindern, Germany
clean bench	UVF 6.12 S	BDK Luft-und Reinraumtechnik, Sonnebühl, Germany
lyophiliser	Alpha 1-4 LD plus	Christ, Osterode am Harz, Germany
magnetic stirrer	IKA-Combigac RET-G	IKA, Staufen, Germany
PCR thermal cycler	Biometra	Analtytik Jena, Jena, Germany
pipettes	Research® plus	Eppendorf AG, Hamburg, Germany
pipetting robot	Freedom EVO 200	Tecan Group AG, Mennedorf, Switzerland
thermomixer	Comfort	Eppendorf, Hamburg, Germany
ultrapure water system	Milli-Q	Merck Millipore, Billerica, USA
vortex mixer	Vortex-Genie®-2	Scientific Industries Inc., Bohemia, USA

5.1.2 Chemicals

Table 5-2: List of chemicals

substance	molecular formula	CAS №	manufacturer
acetaldehyde	C_2H_4O	75-07-0	Sigma-Aldrich Chemie GmbH, Traufkirchen, Germany
acetic acid	$C_2H_4O_2$	64-19-7	Merck KGaA, Darmstadt, Germany
α-acetolactic acid (α-acetolactate)	$C_5H_8O_4$	71698-08-3	Forschungszentrum Jülich GmbH, IBG-1, synthesised and purified by T. Sehl in 2010
acetoin (racemic)	$C_4H_8O_2$	513-86-0	Sigma-Aldrich Chemie GmbH, Traufkirchen, Germany
acetone	C_3H_6O	67-64-1	Sigma-Aldrich Chemie GmbH, Traufkirchen, Germany

substance	molecular formula	CAS №	manufacturer
acetonitrile (HPLC grade)	C_2H_3N	75-05-8	Merck KGaA, Darmstadt, Germany
agar-agar	$C_{12}H_{18}O_9$	9002-18-0	Sigma-Aldrich Chemie GmbH, Traufkirchen, Germany
agarose	$C_{12}H_{18}O_9$	9012-36-6	Merck KGaA, Darmstadt, Germany
ampicillin sodium salt	$C_{16}H_{18}N_3NaO_4S$	69-52-3	Carl Roth GmbH & Co. KG, Karlsruhe, Germany
L-(+)-arabinose	$C_5H_{10}O_5$	5328-37-0	Sigma-Aldrich Chemie GmbH, Traufkirchen, Germany
benzaldehyde	C_7H_6O	100-52-7	Sigma-Aldrich Chemie GmbH, Traufkirchen, Germany
benzoin (racemic)	$C_{14}H_{12}O_2$	119-53-9	Sigma-Aldrich Chemie GmbH, Traufkirchen, Germany
(*R*)-benzoin	$C_{14}H_{12}O_2$	5928-66-5	Forschungszentrum Jülich GmbH, IBG-1, synthesised and purified by T. Sehl in 2015
bovine serum albumin (BSA)	-	9048-46-8	Sigma-Aldrich Chemie GmbH, Traufkirchen, Germany
Calcium chloride	$CaCl_2x2\ H_2O$	10035-04-8	Merck KGaA, Darmstadt, Germany
chloramphenicol	$C_{11}H_{12}Cl_2N_2O_5$	56-75-7	Merck KGaA, Darmstadt, Germany
Coomassie® Brilliant Blue G-250	$C_{47}H_{48}N_3NaO_7S_2$ (sodium-salt)	6104-58-1	Sigma-Aldrich Chemie GmbH, Traufkirchen, Germany
GelPilot 5x DNA Loading Dye	-	-	Qiagen, Hilden, Germany
D-glucose	$C_6H_{12}O_6$	50-99-7	Merck KGaA, Darmstadt, Germany
glycerol	$C_3H_8O_3$	56-81-5	Sigma-Aldrich Chemie GmbH, Traufkirchen, Germany
dimethyl sulfoxide (DMSO)	$(CH_3)_2SO$	67-68-5	Sigma-Aldrich Chemie GmbH, Traufkirchen, Germany
dipotassium phosphate	K_2HPO_4	7758-11-4	Carl Roth GmbH & Co. KG, Karlsruhe, Germany
ethanol	C_2H_6O	64-17-5	Carl Roth GmbH & Co. KG, Karlsruhe, Germany
ethidium bromide	$C_{21}H_{20}BrN_3$	1239-45-8	Sigma-Aldrich Chemie GmbH, Traufkirchen, Germany
ethyl acetate	$C_4H_8O_2$	141-78-6	Sigma-Aldrich Chemie GmbH, Traufkirchen, Germany
EDTA	$C_{10}H_{14}N_2Na_2O_8$ *x* $2H_2O$	6381-92-6	Merck KGaA, Darmstadt, Germany
FastRuler High Range DNA Ladder	-	-	Thermo Fisher Scientific Inc., Waltham, USA
flavin adenine dinucleotide (FAD)	$C_{27}H_{33}N_9O_{15}P_2$	146-14-5	Sigma-Aldrich Chemie GmbH, Traufkirchen, Germany
glycerol	$C_6H_8O_3$	56-81-5	Carl Roth GmbH & Co. KG, Karlsruhe, Germany

substance	molecular formula	CAS №	manufacturer
hydrochloric acid	HCl	7647-01-0	Merck KGaA, Darmstadt, Germany
3-hydroxypyruvate, lithium salt	$C_3H_3LiO_4$ x H_2O	3369-79-7	Sigma-Aldrich Chemie GmbH, Traufkirchen, Germany
(*R*)-HPP	$C_9H_{10}O_2$	65646-06-2	Forschungszentrum Jülich GmbH, IBG-1, synthesised and purified by J. Kulig in 2012
(*S*)-HPP	$C_9H_{10}O_2$	65646-07-3	Forschungszentrum Jülich GmbH, IBG-1, synthesised and purified by A. Jakob-Linnert in 2016
imidazole	$C_3H_4N_2$	288-32-4	Carl Roth GmbH & Co. KG, Karlsruhe, Germany
isopropanol	C_3H_8O	67-63-0	Merck KGaA, Darmstadt, Germany
IPTG	$C_9H_{18}O_5S$	367-93-1	Carl Roth GmbH & Co. KG, Karlsruhe, Germany
kanamycin sulphate	$C_{18}H_{36\text{-}37}N_{4\text{-}5}O_{10\text{-}11}$ *x* H_2O_4S	70560-51-9	Carl Roth GmbH & Co. KG, Karlsruhe, Germany
D-lactose	$C_{12}H_{22}O_{11}$	63-42-3	Merck KGaA, Darmstadt, Germany
magnesium chloride	$MgCl_2$	7786-30-3	Sigma-Aldrich Chemie GmbH, Traufkirchen, Germany
manganese sulphate heptahydrate	$MgSO_4$ *x* 7 H_2O	10034-99-8	Merck KGaA, Darmstadt, Germany
4-methyl morpholine	$C_5H_{11}NO$	109-02-4	Sigma-Aldrich Chemie GmbH, Traufkirchen, Germany
methyl *tert*-butyl ether (MTBE)	$C_5H_{12}O$	1634-04-4	Merck KGaA, Darmstadt, Germany
NuPAGE 4 x SDS sample buffer	-	-	Thermo Fisher Scientific Inc., Waltham, USA
NuPAGE 20 x MES SDS running buffer	-	-	Thermo Fisher Scientific Inc., Waltham, USA
NuPAGE 10 x sample reducing agent	-	-	Thermo Fisher Scientific Inc., Waltham, USA
n-octane	C_8H_{18}	111-65-9	Fluka, Steinheim, Germany
PAGE Ruler, prestained protein ladder	-	-	Thermo Fisher Scientific Inc., Waltham, USA
n-pentanal	$C_5H_{10}O$	110-62-3	Sigma-Aldrich Chemie GmbH, Traufkirchen, Germany
peptone (from casein)	-	91079-40-2	Carl Roth GmbH & Co. KG, Karlsruhe, Germany
(*R*)-PAC	$C_9H_{10}O_2$	1798-60-3	Forschungszentrum Jülich GmbH, IBG-1, synthesised and purified by T. Sehl in 2016
(*S*)-PAC	$C_9H_{10}O_2$	53439-91-1	Forschungszentrum Jülich GmbH, IBG-1, synthesised and purified by Z. Maugeri in 2016
phosphoric acid	H_3O_4P	7664-38-2	Carl Roth GmbH & Co. KG, Karlsruhe, Germany

substance	molecular formula	CAS №	manufacturer
potassium chloride	KCl	7447-40-7	AppliChem, Darmstadt, Germany
potassium dihydrogen phosphate	KH_2PO_4	7778-77-0	Carl Roth GmbH & Co. KG, Karlsruhe, Germany
propanal	C_3H_6O	123-38-6	Sigma-Aldrich Chemie GmbH, Traufkirchen, Germany
2-propanol	C_3H_8O	67-63-0	Merck KGaA, Darmstadt, Germany
pyruvic acid (pyruvate)	$C_3H_4O_3$	127-17-3	Merck KGaA, Darmstadt, Germany
Simply Blue Safe Stain	-	-	Thermo Fisher Scientific Inc., Waltham, USA
sodium chloride	NaCl	7647-14-5	Merck KGaA, Darmstadt, Germany
sodium hydroxide	NaOH	1310-73-2	Merck KGaA, Darmstadt, Germany
tetracycline	$C_{22}H_{24}N_2O_8$	60-54-8	AppliChem, Darmstadt, Germany
2,3,5-triphenyl tetrazolimchloride	$C_{19}H_{15}ClN_4$	298-96-4	AppliChem, Darmstadt, Germany
Tris-acetate-EDTA-buffer (TAE)	-	-	Sigma-Aldrich Chemie GmbH, Traufkirchen, Germany
Tris	$C_4H_{11}NO_3$	77-86-1	Merck KGaA, Darmstadt, Germany
triethanolamine	$C_6H_{15}NO_3$	102-71-6	Sigma-Aldrich Chemie GmbH, Traufkirchen, Germany
thiamine diphosphate (ThDP)	$C_{12}H_{18}N_4O_7P_2S$	154-87-0	AppliChem, Darmstadt, Germany
yeast extract	-	8013-01-2	Carl Roth GmbH & Co. KG, Karlsruhe, Germany

5.1.3 Commercial enzymes and enzyme kits

Table 5-3:List of enzymes and enzyme kits

Enzyme	Catalogue №	Manufacturer
Polymerases		
Phusion High-Fidelity DNA Polymerase Kit	F553S	Thermo Fisher Scientific Inc., Waltham, USA
KOD Hot Start Polymerase Kit	7108-5	Novagen, Merck KGaA, Darmstadt, Germany
Restriction endonucleases		
DpnI – FastDigest	FD1703	Thermo Fisher Scientific Inc., Waltham, USA
NdeI – FastDigest	FD0583	Thermo Fisher Scientific Inc., Waltham, USA
XhoI – FastDigest	FD0694	Thermo Fisher Scientific Inc., Waltham, USA
NcoI – FastDigest	FD0574	Thermo Fisher Scientific Inc., Waltham, USA
FastDigest 10x buffer		Thermo Fisher Scientific Inc., Waltham, USA
FastDigest 10x green buffer		Thermo Fisher Scientific Inc., Waltham, USA
Other		
Rapid DNA Ligation Kit	K1422	Thermo Fisher Scientific Inc., Waltham, USA
lysozyme from hen egg white	L6876	Sigma-Aldrich Chemie GmbH, Traufkirchen, Germany

5.1.4 Plasmids

Table 5-4: List of plasmids. Plasmid maps and gene sequences including information on point mutations are given in the appendix.

	gene	vector	restriction sides	His_6-tag	promotor	resistance	size
*Pp*YerE	*ilvB*	pET28a (+)	*NdeI, BamHI*	N-terminal	T7	kanamycin	7040 bp
*Ec*TK	*tktA*	pET22b (+)	*NdeI, XhoI*	C-terminal	T7	ampicillin	7356 bp
*Pf*BAL	*bznB*	pET28a (+)	*NcoI, XhoI*	C-terminal	T7	kanamycin	6922 bp

5.1.5 Primer

Table 5-5: Primer sequences and annealing temperatures for site-directed mutagenesis of *Pp*YerE. Non-matching base pairs are displayed in lower case letters

substitution	primer sequence		annealing temperature
I23A	sense:	GTATGGGTTTGAGTTG gct GGTGGAATGATTAC	57 °C
	anti-sense:	GTAATCATTCCACC agc CAACTCAAACCCATAC	
I23G	sense:	GTATGGGTTTGAGTTG ggt GGTGGAATGATTAC	57 °C
	anti-sense:	GTAATCATTCCACC acc CAACTCAAACCCATAC	
L476A in *Pp*YerE wt	sense:	GAATAACCATTCT gcg GGCATGGTACGAGG	55 °C
	anti-sense:	CCTCGTACCATGCC cgc AGAATGGTTATTC	
L476A in *Pp*YerE V479A	sense:	GAATAACCATTCT gcg GGCATGGCGCGAGG	61 °C
	anti-sense:	CCTCGCGCCATGCC cgc AGAATGGTTATTC	
L476A in *Pp*YerE V479G	sense:	GAATAACCATTCT gcg GGCATGGGCCGAGG	61 °C
	anti-sense:	CCTCGGCCCATGCC cgc AGAATGGTTATTC	
L476G in *Pp*YerE wt	sense:	GAATAACCATTCT ggc GGCATGGTACGAGG	55 °C
	anti-sense:	CCTCGTACCATGCC gcc AGAATGGTTATTC	
L476G in *Pp*YerE V479A	sense:	GAATAACCATTCT ggc GGCATGGCGCGAGG	57 °C
	anti-sense:	CCTCGCGCCATGCC gcc AGAATGGTTATTC	
L476G in *Pp*YerE V479G	sense:	GAATAACCATTCT ggc GGCATGGGCCGAGG	57 °C
	anti-sense:	CCTCGGCCCATGCC gcc AGAATGGTTATTC	
V479A	sense:	CCATTCTTTGGGCATG Gcg CGAGGTTTCCAGG	62 °C
	anti-sense:	CCTGGAAACCTCG cgC CATGCCCAAAGAATG	
V479G	sense:	CCATTCTTTGGGCATG Ggc CGAGGTTTCCAGG	61 °C
	anti-sense:	CCTGGAAACCTCG gcC CATGCCCAAAGAATG	
Q483X/ T494X	sense:	GCATGGGCCGAGGTTTC ndt GAAATGTATTTTGAGGGAAGAAAC TCCTCT ndT TACTGGAACGGATACAC	65 °C
	anti-sense:	GTGTATCCGTTCCAGTA Ahn AGAGGAGTTTCTTCCCTCAAAATA CATTTC ahn GAAACCTCGGCCCATGC	

Table 5-6: Primer sequences and annealing temperatures for the deletion of 48 bp from the *ilvB* gene encoding for *Pp*YerE. Non-matching base pairs are displayed in lower case letters.

	primer Sequence		annealing temp. 1	annealing temp. 2
PCR 1	sense:	ACGGATACACATCACAATTCAAAAAAATCGGGGAGG	57 °C	65 °C
	anti-sense:	tccagtaagTGCCCAAAGAATGGTTATTCATAACG		
PCR 2	sense:	ttctttgggcACTTACTGGAACGGATACACATCAC	57 °C	65 °C
	anti-sense:	TGGTTATTCATAACGATTGTCAGGATCGGGAGCTTATC		

Table 5-7: Primer sequences and annealing temperatures for the amplification of the *tktA* gene encoding for *Ec*TK before ligation into a pET22b (+) vector. Non-matching base pairs are displayed in lower case letters, introduced restriction sites are underlined.

	primer sequence	added restriction site	annealing temp. 1	annealing temp. 2
sense	gcctgtctcatATGTCCTCACGTAAAG AGCTTGC	*NdeI*	55 °C	63 °C
anti-sense	ccaccacgctcgagCAGCAGTTCTTTT GCTTTCG	*XhoI*	55 °C	63 °C

Table 5-8: Primer sequences and annealing temperatures for site-directed mutagenesis of *Ec*TK. Non-matching base pairs are displayed in lower case letters.

substitution	primer sequence		annealing temperature
H26A	sense:	CAAATCCGGT gcg CCGGGTGCCCCTATG	65 °C
	anti-sense:	ATAGGGGCACCCGG cgc ACCGGATTTGGC	
H26W	sense:	GAAAGCCAAATCCGG tgg GCCGGGTGCCCCTATG	60 °C
	anti-sense:	CCATAGGGGCACCCGG cca ACCGGATTTGGCTTTC	
H26Y	sense:	GCCAAATCCGGT tAt CCGGGTGCCCCTATG	60 °C
	anti-sense:	CATAGGGGCACCCGG aTa ACCGGATTTGGC	
I189A	sense:	GTATTTCT gcg GATGGTCACGTTGAAGGCTGGTTCAC	65 °C
	anti-sense:	GACCATC cgc AGAAATACCGTTGTCATCGTAGAATGC	
I189G	sense:	CAACGGTATTTCT ggC GATGGTCACGTTG	62 °C
	anti-sense:	CAACGTGACCATC Gcc AGAAATACCGTTG	
I189V	sense:	GTATTTCT gTg GATGGTCACGTTGAAGGCTGGTTCAC	63 °C
	anti-sense:	GACCATC cAc AGAAATACCGTTGTCATCGTAGAATGC	
H261A	sense:	CCACGACTCC gcg GGTGCGCCGCTGG	68 °C
	anti-sense:	AGCGGCGCACC cgc GGAGTCGTGG	
H261F	sense:	GTACCCACGACTCC ttt GGTGCGCCGCTGG	62 °C
	anti-sense:	CAGCGGCGCACC aaa GGAGTCGTGGGTAC	
H261G	sense:	ACGACTCC ggC GGTGCGCCGCTGGGCGACGCTGAAATTG	68 °C
	anti-sense:	GCGCACC Gcc GGAGTCGTGGGTACCGGCTTTGTTCG	
H261L	sense:	GTACCCACGACTCC Ctg GGTGCGCCGCTGG	62 °C
	anti-sense:	CAGCGGCGCACC caG GGAGTCGTGGGTAC	
H261S	sense:	CCACGACTCC tcg GGTGCGCCGCTGG	68 °C
	anti-sense:	CAGCGGCGCACC cga GGAGTCGTGG	
H261V	sense:	GTACCCACGACTCC gtt GGTGCGCCGCTGG	68 °C
	anti-sense:	CAGCGGCGCACC aac GGAGTCGTGGGTAC	
L382A	sense:	GGTTCTGCTGAC gca GCGCCGTCTAACC	60 °C
	anti-sense:	GGTTAGACGGCGC tgc GTCAGCAGAACC	
F434A	sense:	GTACACCTCCACC gcC CTGATGTTCGTG	58 °C
	anti-sense:	CGAACATCAG Ggc GGTGGAGGTGTACG	
F434L	sense:	CGTACACCTCCACC cTg CTGATGTTC	53 °C
	anti-sense:	CCACGAACATCAG cAg GGTGGAGGTGTACG	
D489E	sense:	GGTCTGGGCGAA GAa GGCCCGACTCAC	60 °C
	anti-sense:	GTGAGTCGGGCC tTC TTCGCCCAGACC	

Table 5-9: Primer sequences and annealing temperatures for site-directed mutagenesis of *Pf*BAL. Non-matching base pairs are displayed in lower case letters

substitution	primer sequence		annealing temperature
H29F	sense:	GGCCTGCACGGCGCG ttT ATCGATACGATTTTTC	63 °C
	anti-sense:	GAAAAATCGTATCGAT Aaa CGCGCCGTGCAGG	
A480H	sense:	CCAAAGCTGGGGG cat ACATTGCATTTCC	58 °C
	anti-sense:	GGAAATGCAATGT atg CCCCCAGCTTTGG	

5.1.6 *Escherichia coli* strains

Table 5-10: *E. coli* strains used for plasmid amplification and gene expression.

purpose	strain	genotype	source
plasmid amplification	DH5α	F– Φ80*lac*ZΔM15 Δ (*lac*ZYA-*arg*F) U169 *rec*A1 *end*A1 *hsd*R17 (rK–, mK+) *pho*A *sup*E44 λ– *thi*-1 *gyr*A96 *rel*A1	Invitrogen, Carlsbad USA
gene expression	BL21 (DE3) (Studier and Moffatt, 1986)	F- *omp*T *hsdS*$_B$ (r_B-m_B-) *gal dcm lon* (DE3)	Invitrogen, Carlsbad USA

5.1.7 Media

LB-medium

LB-medium (Bertani, 1951) was used for the cultivation of *E. coli* before the extraction of plasmid from the respective culture (chapter 5.2.1), for the production and transformation of chemically competent cells (chapter 5.2.7 and 5.2.8) and for the pre-cultures in the course of heterologous gene expression (chapter 5.3.1). All components (Table 5-11) were dissolved in ddH_2O and autoclaved. Further, agar plates were prepared from LB-medium by addition of 15 g·L^{-1} agar before autoclaving. If not stated otherwise, the medium was always supplemented either with 100 mg·L^{-1} ampicillin or with 50 mg·L^{-1} kanamycin.

Table 5-11: Composition of LB-medium

component	concentration
peptone (from casein)	10 g·L^{-1}
yeast extract	5 g·L^{-1}
NaCl	10 g·L^{-1}

AI-medium

AI-medium (Studier, 2005) was used for the main culture during heterologous gene expression in *E. coli* BL21 (DE3) (chapter 5.3.1). The media components, KP_i-buffer, glucose, lactose and glycerol were dissolved in ddH_2O and autoclaved separately before they were mixed according to Table 5-12. If not stated otherwise, the medium was always supplemented either with 100 mg·L^{-1} ampicillin or with 100 mg·L^{-1} kanamycin.

Table 5-12:Composition of AI-medium (Studier, 2005)

	concentration	volume	final concentration
media components		795 mL	
peptone (from casein)	15 $g \cdot L^{-1}$		12 $g \cdot L^{-1}$
yeast extract	30 $g \cdot L^{-1}$		24 $g \cdot L^{-1}$
KP_i-buffer pH 7		90 mL	90 mM
KH_2PO_4	53 $g \cdot L^{-1}$		
K_2HPO_4	106 $g \cdot L^{-1}$		
glucose	50 $g \cdot L^{-1}$	10 mL	0.5 $g \cdot L^{-1}$
lactose	20 $g \cdot L^{-1}$	100 mL	2 $g \cdot L^{-1}$
glycerol	100%	5 mL	0.5 % (v/v)

5.1.8 Buffer

Table 5-13: Composition of hybridisation buffer. pH 7.4 was adjusted with HCl.

component	concentration
Tris	40 mM
NaCl	400 mM
EDTA	4 mM

Table 5-14: Composition of TAE-buffer. pH 8 was adjusted with HCl.

component	concentration
Tris	40 mM
acetic acid	18 mM
EDTA	1 mM

Table 5-15: Composition of buffers for protein purification. The pH was adjusted with NaOH or H_3PO_4. All buffers were filtrated and degassed before use.

	***Pp*YerE**	***Ec*TK**	***Pf*BAL**
equilibration buffer			
molarity KP_i [mM]	50	50	50
pH	7.5	7.5	7.5
ThDP [mM]	0.1	0.1	0.1
$MgCl_2 \cdot 6\ H_2O$ [mM]	2.5	2.5	2.5
FAD [mM]	0.05	-	-
NaCl [mM]	300	300	300
washing buffer 1			
molarity KP_i [mM]	50	50	50
pH	7.5	7.5	7.5
ThDP [mM]	0.1	0.1	0.1
$MgCl_2 \cdot 6\ H_2O$ [mM]	2.5	2.5	2.5
FAD [mM]	0.05	-	-
NaCl [mM]	300	300	300
imidazole [mM]	50	20	50
elution buffer			
molarity KP_i [mM]	50	50	50
pH	7.5	7.5	7.5
ThDP [mM]	0.1	0.1	0.1
$MgCl_2 \cdot 6\ H_2O$ [mM]	2.5	2.5	2.5
FAD [mM]	0.05	-	-
NaCl [mM]	300	300	300
imidazole [mM]	300	125	250
washing buffer 2			
molarity KP_i [mM]	50	50	50
pH	7.5	7.5	7.5
ThDP [mM]	0.1	0.1	0.1
$MgCl_2 \cdot 6\ H_2O$ [mM]	2.5	2.5	2.5
FAD [mM]	0.05	-	-
NaCl [mM]	300	300	300
imidazole [mM]	300	250	250
desalting buffer			
molarity KP_i [mM]	50	10	10
pH	7.5	7	7.8
ThDP [mM]	0.1	0.1	0.1
$MgCl_2 \cdot 6\ H_2O$ [mM]	2.5	2.5	2.5
FAD [mM]	0.05	-	-

Table 5-16: Reaction buffer for biotransformations. The pH was adjusted with KOH or H_3PO_4. * No FAD was added to the buffer used for the screenings of the *Pp*YerE libraries.

	***Pp*YerE** aromatic acceptors	***Pp*YerE** aliphatic acceptors	***Pp*YerE** ketone acceptors	***Ec*TK**	***Pf*BAL**
molarity KP_i [mM]	50	100	100	100	50
pH	8	8	7	7	7.8
ThDP [mM]	0.5	2.4	2.4	2.4	0.1
$MgCl_2 \cdot 6\ H_2O$ [mM]	3	3	3	3	2.5
FAD [mM]	-	0.05*	0.05*	-	-

5.2 Molecular biological methods

5.2.1 DNA-purification

Extraction of plasmid DNA from E. coli DH5α

The *E. coli* strain DH5α was used to amplify plasmids for example for storage in a plasmid collection or to repair DNA containing nicks, for example in the process of site-directed mutagenesis. In order to isolate the plasmids from *E. coli* DH5α first a single colony was picked and cultivated in 5-10 µL LB-medium (Table 5-11) with an appropriate antibiotic at 37 °C and 150 rpm for 6-16 h. Cells from a 4 ml culture were pelleted by centrifugation. For the following plasmid extraction, the QIAprep Spin Minprep Kit (Qiagen) was used. With this kit, the cells are disrupted by alkaline lysis (Birnboim and Doly, 1979). After neutralisation of the lysate and separation of the cell debris by centrifugation the supernatant was transferred to a spin column containing a silica membrane. The plasmid DNA is adsorbed on the silica membrane in the presence of high salt concentrations (Vogelstein and Gillespie, 1979). Thus, DNA was eluted by applying an elution buffer with low salt concentration. The kit was used according to manufacturer's information with the following changes: The centrifugation speed in all DNA- binding and -eluting steps was reduced to 5000 g. In these steps, the centrifugation time was increased to 2 min. Further, samples were incubated at 37 °C for 10 min after elution buffer was added to the column. Plasmids were stored at -20 °C with a concentration of at least 100 $ng \cdot \mu L^{-1}$.

Purification of PCR products

After each PCR, the product was purified using spin-filters in order to remove excessive primers, dNTP's and the polymerase. For that purpose, the MinElute PCR Purification Kit (Qiagen) was used according to the manufacture's information with the same changes stated above for the QIAprep Spin Minprep Kit. Afterwards, the DNA-concentration was measured spectrophotometrically (chapter 5.2.2) and the purified product was used for digestions with restriction endonucleases (chapter 5.2.4).

Purification of DNA-fragments by agarose gel electrophoresis

After digestion of DNA-molecules with restriction endonucleases, the desired fragment was separated from other fragments by agarose gel electrophoresis.

To prepare the gel a suspension of 1 % (w/v) agarose powder in TAE-buffer (Table 5-14) was heated until the powder was fully dissolved. Subsequently, the solution was filled in a cast, where the gel

hardened upon cooling down to room temperature. Wells for sample loading were created with a comb. After the gel was fully polymerised, it was submerged in TAE-buffer in an electrophoresis tank.

Samples needed no addition of DNA loading dye, as FD-green buffer was used for the digestion (chapter 5.2.4), which allowed immediate loading of the reaction mixture on the gel. The separation was carried out at 120 V for 45 min. For visualisation of the DNA-bands under UV-light the gel was stained with 0.25 $mg \cdot L^{-1}$ ethidium bromide solution for 10 min. Background staining was removed by washing in water before the gel was exposed to UV-light.

The part of the gel containing the desired DNA-fragment was cut out of the gel and the DNA was extracted using the QIAquick Gel Extraction Kit (Qiagen) according to the manufacture's information with the same changes stated above for the QIAprep Spin Minprep Kit. The purified DNA-fragment was then used for a DNA-ligation (chapter 5.2.5).

5.2.2 Measurement of DNA concentration

The concentration of the DNA after purification as described in 5.2.1 was determined UV-spectrophotometrically via the absorption of the aromatic rings of the DNA bases at 260 nm. The measurements were performed in a 2 µL-scale using a NanoDrop microvolume spectrophotometer (Peqlab). Elution buffer of the respective kit used for the DNA preparation served as a control before the measurement. The concentration was calculated from the optical density, assuming a concentration of 50 $ng \cdot \mu L^{-1}$ at an OD_{260} of 1 for double stranded DNA. Additionally, the samples were checked for impurities of protein or RNA by measuring the absorption at 280 nm and 230 nm, respectively.

5.2.3 PCR

Amplification of DNA fragments

To insert a gene into a new vector construct the respective gene sequence was first amplified by PCR using primers that flank the respective sequence. The 3'-end of the primers was homologue to the template sequence with an overlap of 10-15 bp. The 5'-ends contained the restriction sites for two different restriction endonucleases. Thus, during the PCR the restriction sites were added to the amplified sequence, which enables digestion with the respective endonucleases followed by ligation with a vector backbone (chapters 5.2.4 and 5.2.5). The reactions were performed with the Phusion High-Fidelity DNA Polymerase (Thermo Fisher Scientific) in a 50 µL scale. The composition and the temperature profile of the reaction are given in Table 5-17 and Table 5-18, respectively.

Table 5-17: PCR composition for the amplification of DNA fragments

component	volume [µL]
template (plasmid DNA)	variable (50 ng)
5x Phusion buffer	10
sense-primer (10 µM)	2.5
antisense-primer (10 µM)	2.5
dNTPs (10 mM)	1
Phusion polymerase	0.5
sterile ddH_2O	filled up to 50 µL

Table 5-18: PCR temperature profile for the amplification of DNA fragments

step	temperature [°C]	time [s]	cycles
initial denaturation	98	30	
denaturation	98	10	
annealing	See 5.1.5	30	5
elongation	72	30 per kb	
denaturation	98	10	
annealing	See 5.1.5	30	25
elongation	72	30 per kb	
final elongation	72	600	
storage	15	-	

Site-directed mutagenesis

Site-directed mutagenesis is a method for the targeted exchange of DNA codons. It was performed with a PCR-based method using synthetic mutagenic primers containing the codon for the desired amino acid exchange and the KOD Hot Start Polymerase Kit (Novagene) (Hemsley et al., 1989). The primer pair was designed such that at least ten nucleotides were homologous to the template DNA before and after the mutation. PCRs were performed in a 50 µL scale according to the conditions in Table 5-19 and Table 5-20. During the PCR the complete plasmid was amplified. Afterwards the DNA-template was removed by *Dpn*I digestion (chapter 5.2.4).

Table 5-19: PCR composition for site-directed mutagenesis

component	volume [µL]
template (plasmid DNA)	variable (150 ng)
10x KOD buffer	5
sense-primer (10 µM)	2.5
antisense-primer (10 µM)	2.5
dNTPs (2 mM)	5
KOD polymerase	1
sterile ddH_2O	filled up to 50 µL

Table 5-20: PCR temperature profile for site-directed mutagenesis

step	temperature [°C]	time [s]	cycles
initial denaturation	95	120	
denaturation	95	20	
annealing	See 5.1.5	30	18
elongation	72	30 per kb	
final elongation	72	600	
storage	15	-	

Site-saturation mutagenesis

Site-saturation mutagenesis follows the same principle as site-directed mutagenesis but allows the simultaneous and randomised insertion of differing codons at the targeted position. For this purpose, degenerate primers containing a NDT-codons were used. Those are a mixture of primers with randomised codons at the positions of the NDT codons, in which all nucleotides can occur at the position

of N and adenine, thymine or guanine can be found at the position of D. Therefore, the codons for twelve proteogenic amino acids could randomly be inserted by one PCR. In this work site-saturation mutagenesis was targeted to two positions that were 30 bp apart. Both codons were mutated concurrently, using one primer pair with two NDT-codons. The PCR conditions corresponded to a site-directed mutagenesis (see Table 5-19 and Table 5-20).

Ligation-free cloning

Ligation-free cloning was used to delete a 48 bp long sequence from the *ilvB* gene that encodes for *Pp*YerE (see chapter 3.1.4). In two separate PCR reactions, the entire plasmid was amplified except of the sequence to be deleted. The primers were designed in such a way that a non-binding overhang was added to one end of the PCR product, which was homologous to the sequence on the other side of the deletion (approximately 15 bp overlapping sequence). As a result, the two PCR products could be hybridised to form a circular plasmid (Tillett and Neilan, 1999).

The PCR conditions are given in Table 5-21 and Table 5-22. After the PCR the products were purified by agarose gel electrophoresis (see chapter 5.2.1). Subsequently, the hybridisation was carried out according to Table 5-23 and Table 5-24 before *E. coli* DH5α were transformed with the product (see chapter 5.2.8)

Table 5-21: PCR composition for ligation-free cloning

component	volume [µL]
template (plasmid DNA)	variable (75 ng)
5x Phusion buffer	10
sense-primer (10 µM)	2.5
antisense-primer (10 µM)	2.5
dNTPs (10 mM)	1
Phusion polymerase	0.5
sterile ddH_2O	filled up to 50 µL

Table 5-22: PCR temperature profile for ligation-free cloning

step	temperature [°C]	time [s]	cycles
initial denaturation	98	30	
denaturation	98	20	
annealing	57	30	5
elongation	72	150	
denaturation	98	20	
annealing	65	30	25
elongation	72	150	
final elongation	72	600	
storage	15	-	

Table 5-23: Composition of the hybridisation reaction

component	volume [µL]
4x hybridisation buffer (Table 5-13)	6.25
PCR-product 1	variable (90 ng)
PCR product 2	variable (90 ng)
sterile ddH_2O	filled up to 25 µL

Table 5-24: Temperature profile for the hybridisation reaction

temperature [°C]	time [min]	cycles
95	3	
65	2	4
25	15	
15	-	

5.2.4 DNA- restriction

Preparative digestion

To link DNA fragments via ligation, compatible ends of the fragments are required, which were generated by digestion with restriction endonucleases. To ensure directional incorporation of DNA fragments into a vector backbone, two different endonucleases were used that create cohesive ends. For the selection of restriction endonucleases it is essential that the respective restriction site is present only once in the DNA molecule, which is the case for all restriction sites within the multiple cloning site of the commercially available vectors used in this work. For gene sequences that were supposed to be inserted into a vector, the respective restriction sites were added during amplification by PCR (chapter 5.2.3).

The composition for a preparative digestion is summarised in Table 5-25. The batches were incubated at 37 °C for at least 3 h. Subsequently, the desired fragments were separated from other fragments and agarose gel electrophoresis and purified from the gel (chapter 5.2.1)

Table 5-25: Composition of the preparative digestion of vectors or PCR products with restriction endonucleases

component	volume [µL]
DNA	variable (up to 1µg)
FD-green buffer	3
endonuclease 1	1.5
endonuclease 2	1.5
ddH_2O	filled up to 30 µL

DpnI-digestion

In order to remove the template plasmid after the PCR for site-directed mutagenesis or site-saturation mutagenesis the samples were treated with the restriction endonuclease *Dpn*I. *DpnI* recognises and cuts the sequence 5'-GATC-3' given that the adenosine is methylated (Lacks and Greenberg, 1975). The template plasmid was isolated from an *E. coli* strain containing a deoxyadenosine (dam) methylase, which is responsible for methylation of the adenosine in the 5'-GATC-3' sequence. Thus, the template plasmid is methylated and in contrast to the PCR-product cleaved by *Dpn*I. The composition of a *Dpn*I

digestion is summarised in Table 5-26. In case the total DNA-amount exceeded 1µg, samples where diluted before the digestion. The restriction was carried out at 37 °C for 3-5 h. Subsequently, the samples were used to transform chemically competent *E. coli* DH5α or *E. coli* BL21 (DE3) for site-directed or site-saturation mutagenesis, respectively. (Table 5-10, chapter 5.2.8)

Table 5-26: Composition of the digestion with *DpnI* for site directed mutagenesis

component	volume [µL]
PCR-product	17
FD buffer	2
FD-*Dpn*I	1

5.2.5 DNA-Ligation

DNA-ligation was used to insert a gene into a vector backbone. Between the DNA-strands a phosphodiester bond is formed catalysed by a DNA-ligase. Insert and backbone must have compatible cohesive ends. This was achieved by restriction of both DNA-molecules with the same restriction endonucleases, followed by purification of the desired fragments via agarose gel electrophoresis (chapters 5.2.4 and 5.2.1).

For the ligation the Rapid DNA Ligation Kit (Thermo Fisher Scientific), which contains T4 DNA ligase and a 5x ligation buffer, was applied. For one reaction 1 µL of T4-DNA ligase and 4 µL of ligation buffer were used. The amount of the vector backbone was adjusted to 30 ng in a total reaction volume of 20 µL. The insert was used in a 3.5-fold molar excess compared to the backbone. After mixing of all components the reaction was incubated at room temperature for 30 min. Afterwards, the ligase was inactivated by incubation at 70°C for 10 min and the reaction was used for the transformation of *E. coli* DH5α (Table 5-10, chapter 5.2.8).

5.2.6 DNA-Sequencing

The sequence of all plasmids created by site-directed mutagenesis or ligation of DNA-fragment was confirmed by DNA-sequencing. Further, selected mutants from the site-saturated mutagenesis were sequenced to identify mutations responsible for a certain phenotype. In order to screen a higher number of plasmids for the successful insertion of a point mutation by site-directed mutagenesis (usually four to six plasmids per mutation), a primer that binds between 50 bp and 500 bp upstream of the designated mutation was used for the sequencing. All plasmid selected for the following work steps, such as heterologous gene expression or further mutagenesis steps, were additionally sequenced over the full length of the respective gene using primers that bind to the T7-promotor and the T7-terminator, respectively. The sequencing was carried out by the company LGC-Genomics (Berlin, Germany) using the chain-termination methods according to Sanger (Sanger et al., 1977). Following the requirements of the company, samples were diluted with autoclaved ddH_2O to a DNA-concentration of 100 ng·µL^{-1}.

5.2.7 Production of chemically competent *E. coli* cells

Chemically competent *E. coli* cells were produced according to the $CaCl_2$-method (Hanahan, 1983). A pre-culture of 20 mL LB-medium (Table 5-11) was inoculated with the respective *E. coli* strain and

cultivated at 37°C and 750rpm in a 100-mL baffled Erlenmeyer flask overnight. Subsequently, 1 ml of the pre-culture was transferred to 100 mL LB-medium in a 500 mL baffled Erlenmeyer flask and incubated at 37 °C and 150 rpm. After an OD_{600} of 0.7 was reached, the culture was transferred to cooled 50 mL centrifuge tubes and incubated on ice for 10 min. Subsequently, the cells were pelleted by centrifugation at 2365 x*g* and 4°C for 10 min and the supernatant was discarded. The pellets were resuspended in 30 mL sterile, ice-cold $MgCl_2$-$CaCl_2$ solution (80 mM and 20 mM, respectively) and again pelleted under the same conditions. Finally, the pellets were suspended in 2 mL sterile, ice-cold 100 mM $CaCl_2$-solution before 0.5 mL glycerol was added. Aliquots of the cell suspension were frozen in liquid nitrogen and stored at -80°C.

5.2.8 Transformation of *E. coli*

In order to transform *E. coli* an aliquot of chemically competent cells (chapter 5.2.7) was thawed on ice. Plasmid DNA (100 ng) was added to 50 µL of competent cells and incubated on ice for 20 min. Subsequently, the cells were treated with a heat shock by incubation at 42 °C for 1 min. Samples were incubated on ice for five minutes before 1 mL LB-medium (Table 5-11) was added. The cells were cultivated at 37°C and 750 rpm in a ThermoMixer® (Eppendorf) for 1 h. Afterward 50 µL of the sample was plated on LB-agar plates containing a suitable antibiotic. This enables the application of an antibiotic resistance gene on the respective plasmid as a selectable marker for a successful transformation. The plate was either cultivated at 37 °C over night or at room temperature for three days.

When samples of a *Dpn*I digestion (chapter 5.2.4) were used for the transformation, lower transformation efficiency was expected, because the plasmid- DNA is nicked and not in its supercoiled form. Therefore, two steps of the protocol were adjusted: 1. 400 ng instead of 100 ng plasmid DNA was added to the competent cells; 2. Before plating on agar plates, the cells were separated from the medium by centrifugation. The supernatant was removed, and the cells were resuspended in 50 µL medium that was fully plated on the agar plate.

5.3 Protein biochemical methods

5.3.1 Gene expression in *E. coli* BL21 (DE3)

For heterologous enzyme production the respective genes, which were encoded on pET-vectors in a T7-expression system, were expressed in *E. coli* BL21 (DE3) (Table 5-10). After transformation with the respective plasmid (chapter 5.2.8), a single colony was picked and transferred to 20-50 µL LB-medium (Table 5-11) containing the respective antibiotic in an Erlenmeyer flask with baffles. The filling volume of the Erlenmeyer flask did not exceed 20 % of the total flask volume. This pre-culture was incubated at 37°C and 150 rpm overnight. For the main culture 0.4-1 L AI-medium (Table 5-12) were inoculated with the pre-culture to an OD_{600} of 0.1 and cultivated in Erlenmeyer flasks with baffles at 37 °C and 90 rpm. After 3 h the temperature was lowered to 20°C. The cells were harvested after 24 h by centrifugation at 14300 x*g* and 4°C for 30 min. The supernatant was discarded, and the cell pellet was stored at -20 °C.

5.3.2 Cell disruption

Cell lysates for protein purification or for enzyme assays with crude cell extracts were obtain by cell disruption via sonication. 0.1-0.2 $g \cdot mL^{-1}$ wet cells were suspended in equilibration buffer (Table 5-15) or reaction buffer (Table 5-16) for purification or enzyme assays, respectively. The sonication was executed with a U200S/H sonicator and sonotrode S3 for volumes up to 20 mL or SD14 for higher volumes (Hielscher). The cells were treated with ultrasound at 70 % amplitude and 0.5 s cycle in ten intervals of 60 s with 30 s breaks in between. During the whole time of the cell disruption the sample was kept on ice. Subsequently, the cell debris was removed by centrifugation at 43670 x*g* and 4 °C for 30 min.

5.3.3 Protein purification

As all enzyme variants were fused to a hexahistidine tag the purification of the variants form crude cell extracts could be performed by immobilised metal ion affinity chromatography, utilising the formation of chelate complexes between immobilised nickel ions and the non-protonated nitrogen of the histidine side chain. The purification was supported by Äkta purifier system (GE Healthcare) using 1 mL or 5 mL Ni-NTA Superflow Cartridges (Qiagen). For all purification steps 50 mM KP_i buffer, pH 7.5, containing 300 mM NaCl, 0.1 ThDP 2.5 $MgCl_2$ was used. For the purification of *Pp*YerE additionally 50 µM FAD was added. Minor differences in the purification of *Pp*YerE, *Ec*TK, and *Pf*BAL are summarised in Table 5-27. After equilibration of the column with five column volumes of equilibration buffer, the crude cell extract (chapter 5.3.2) was applied to the column. The protein concentration at the column outlet was monitored via the absorption at 280 nm. After the signal reached the baseline, unspecifically bound proteins were eluted with washing buffer, which contained a low concentration of imidazole. Subsequently, the bound enzyme variant was eluted by an increase of the imidazole concentration. The eluate was collected in smaller fractions, which were pooled according to the protein content. Between two purifications the column was washed with at least five column volumes of buffer containing 250-300 mM imidazole, to ensure that no residual protein was bound to the column. Before storage or latest after four purifications the column was flushed with ddH_2O until the conductivity reached its baseline. Subsequently, one column volume of 0.5 M NaOH was applied before the column was again washed with ddH_2O until the baseline of the conductivity was reached. The column was stored in 20 % ethanol at 4 °C.

Table 5-27: Summary of conditions that differed during the protein purification of *Pp*YerE, *Ec*TK, and *Pf*BAL.

	***Pp*YerE**	***Ec*TK**	***Pf*BAL**
volume of applied crude cell extract	40 mL	7 mL	7 mL
column volume	5 mL	1 mL	1 mL
flow	1.5 $mL \cdot min^{-1}$	1 $mL \cdot min^{-1}$	1 $mL \cdot min^{-1}$
imidazole concentration washing	50 mM	20 mM	50 mM
imidazole concentration elution	300 mM	125 mM	250 mM
fractionation volume	2 mL	1 mL	1 mL
pH of desalting buffer	7.5	7.2	7.8

Desalting of the collected eluate after IMAC was conducted by size-exclusion chromatography using PD-10 desalting columns (GE-Healthcare) according to the manufacturer's gravity protocol.

5.3.4 Lyophilisation

For storage after the purification, water was removed from the protein eluates by lyophilisation. For this purpose, the collected eluate after the size-exclusion chromatography was frozen in a sealed crystallising dish at -20 °C. If the protein concentration exceeded 1 $mg \cdot mL^{-1}$, the solution was diluted in desalting buffer, beforehand (Table 5-15). After the solution was thoroughly frozen, the sealing foil was perforated, and the water was removed by sublimation in an Alpha 1-4 LD plus lyophiliser (Christ) at 0.1 mbar at -42 °C for two days. The thus obtained white powder was stored at -20°C.

5.3.5 Protein determination

The protein concentration was determined according to Bradford (Bradford, 1976). This assay is based on the shift of the absorbance of Coomassie Brilliant Blue G2500 from 465 m to 595 nm due to binding of protein to the dye.

100 µL sample were mixed with 900 µL Bradford reagent (Table 5-28) and incubated at room temperature for 10 min. Subsequently, the absorbance at 595 nm was measured. The concentration was calculated from the absorbance using a calibration curve that was prepared with bovine serum albumin (BSA)

Table 5-28: Bradford reagent - the Coomassie was first dissolved in the ethanol before the phosphoric acid was added and the solution was stirred for 1 h. Subsequently, the ddH_2O was added and the solution was boiled up. After cooling down, particles where removed by filtration. The reagent was stored under light exclusion at room temperature.

component	amount
Coomassie Brilliant Blue G-250	100 mg
ethanol	50 mL
phosphoric acid (85 %)	100 mL
ddH_2O	850 mL

5.3.6 SDS-polyacrylamide gel electrophoresis (SDS-PAGE)

SDS-PAGE is a method to separate proteins based on their molecular weight (Laemmli, 1970). It was used to check the soluble production of a target protein in *E. coli* BL21 (DE3) and to monitor the progress of the protein purification. To control the protein production, the OD_{600} of the *E. coli* culture was adjusted to 10 before the cells were disrupted by sonication (chapter 5.3.2). To monitor the progress of the purification the protein concentration was adjusted to 0.5 $mg \cdot mL^{-1}$. For the sample preparation 19.5 µL cell lysate or protein solution were mixed with 7.5 µL sample buffer and 3 µL reducing agent (NuPAGE). The sample was incubated at 98 °C for 10 min. During this step, the proteins in the sample are unfolded by heat, DTT from the reducing agent, which reduces disulphide bridges, and SDS from the sample buffer which binds to the proteins and creates a negative charge that is proportional to the molecular mass of the respective protein. For the separation 10 µL sample were loaded onto a commercially available 4-12% Bis-Tris gels (NuPAGE). The separation took place at 200 V, 100 mA, and 15 W (maximum values) in MES SDS running buffer (NuPAGE) for 1 h. In order to visualise the bands, the gel was stained in Simply Blue Safe Stain (Thermo Fisher Scientific) at room temperature for 1 h and subsequently washed in water to remove background coloration.

5.3.7 Biotransformations

PpYerE-catalysed reactions

*Pp*YerE variants were characterised regarding the carboligation of pyruvate with the acceptor aldehydes benzaldehyde, n-pentanal, and propanal. Selected variants were furthermore tested with the ketones butan-2-one, hexan-2-one and hexan-3,4-dion. The reactions were performed with purified and lyophilised enzyme and additionally with crude cell extracts for the aliphatic acceptor aldehydes and biotransformations with the deletion variant PpYerE ΔM478-S493. The semi-automated screening of *Pp*YerE libraries is described in chapter 5.3.8.

Lyophilised enzyme variants were dissolved in reaction buffer (Table 5-16) and the protein concentration was measured (chapter 5.3.5) and adjusted to 1 $mg \cdot mL^{-1}$. Crude cell extracts were prepared by sonication of a 50 % (w/v) wet cell suspension in reaction buffer as described in chapter 5.3.2. Subsequently, the total protein concentration of the CCE was as well adjusted. The substrates were dissolved in reaction buffer and the pH was adjusted according to the reaction conditions. The reaction was started upon mixing of the enzyme solution or the CCE with the substrate solution and incubated at 30 °C. The final concentrations are summarised in Table 5-29, typical reaction volumes were 300 µL. Samples were taken in a time frame between 0.5 h and 24 h and analysed by chiral phase HPLC (acceptor: benzaldehyde, see chapter 5.4.2) or chiral phase GC-MS (acceptor: aliphatic aldehydes and ketones, see chapter 5.4.3).

Table 5-29: Composition of *Pp*YerE catalysed carboligations. The buffer composition is given in Table 5-16

component	final concentration
PAC synthesis	
*Pp*YerE variant	1 mg·mL^{-1}
pyruvate	50 mM
benzaldehyde	20 mM
PAC synthesis with deletion variant	
*Pp*YerE ΔM478-S493	10 mg·mL^{-1} total protein concentration CCE
pyruvate	25 mM
benzaldehyde	10 mM
3-HH synthesis	
*Pp*YerE variant	1 mg·mL^{-1} purified
	or 10 mg·mL^{-1} total protein concentration CCE
pyruvate	50 mM
n-pentanal	50 mM
3-HP synthesis	
*Pp*YerE variant	1 mg·mL^{-1} purified
	or 10 mg·mL^{-1} total protein concentration CCE
pyruvate	50 mM
propanal	50 mM
HMH synthesis	
*Pp*YerE variant	1 mg·mL^{-1}
pyruvate	50 mM
n-hexan-2-one	20 mM
HMP synthesis	
*Pp*YerE variant	1 mg·mL^{-1}
pyruvate	50 mM
butan-2-one	20 mM
EHH synthesis	
*Pp*YerE variant	1 mg·mL^{-1}
pyruvate	50 mM
hexan-3,4-dion	20 mM

EcTK-catalysed reactions

With the *Ec*TK variants the formation from DHH and DHP from pyruvate as donor substrate and n-pentanal and propanal, respectively, as acceptor substrates was investigated. All reactions were performed with purified and lyophilised enzyme in reaction buffer (Table 5-16). The enzyme concentration was adjusted after protein determination according to chapter 5.3.5. All substrates were as well dissolved in reaction buffer and the pH of the substrate solution was adjusted before mixing with the enzyme solution. The final concentrations are shown in Table 5-30. Typical reaction volumes were between 0.3 mL and 1.2 mL. The reactions were incubated at 25 °C. Samples were usually taken after 1 h and 3 h and analysed by chiral phase GC-MS as described in chapter 5.4.3.

Table 5-30: Composition of *Ec*TK catalysed carboligations. The buffer composition is given in Table 5-16.

component	final concentration
DHH-synthesis	
*Ec*TK variant	0.9 mg·mL^{-1}
3-hydroxpyruvate (HPA)	50 mM
n-pentanal	50 mM
DHP-synthesis	
*Ec*TK variant	0.9 mg·mL^{-1}
3-hydroxypyruvate (HPA)	100 mM
propanal	100 mM

PfBAL-catalysed reactions

The carboligation potential and stereoselectivity of the *Pf*BAL variants were characterised concerning the self-ligation of two benzoin molecules to benzoin as well as the mixed carboligation of benzaldehyde and acetaldehyde to HPP. The reactions were carried out with purified and lyophilised enzymes, which were dissolved in reaction buffer (Table 5-16) and the concentration was adjusted after protein determination according to (chapter 5.3.5). The substrates were dissolved in reaction buffer and the pH was adjusted before addition of the enzyme solution or the crude cell extract. The final concentrations are given in Table 5-31. Typical reaction volumes were 500 µL. After incubation at 22 °C samples for chiral HPLC analysis (see chapter 5.4.2) were taken after 15 min and 22 min for benzoin synthesis and HPP-synthesis, respectively.

Table 5-31: Composition of *Pf*BAL catalysed carboligations. The buffer composition is given in Table 5-16

component	final concentration
benzoin-synthesis (self-ligation)	
*Pf*BAL variant	0.1 mg·mL^{-1} purified
benzaldehyde	25 mM
HPP-synthesis (mixed ligation)	
*Pf*BAL variant	0.1 mg·mL^{-1} purified
benzaldehyde	12.5 mM
acetaldehyde	25 mM

5.3.8 Robotic platform assisted screening of enzyme variant libraries

In order to screen libraries of variants with combined amino acid exchanges at two to three positions, a robot assisted screening system describes by Westphal et al. (Westphal et al., 2013a) was applied. The libraries were either constructed by site-saturation mutagenesis or combined site-directed mutageneses with several amino acid exchanges at each position. In the case of site-saturation mutagenesis, the whole reaction mixture after the PCR and the *Dpn*I-digestion was used to transform chemically competent *E. coli* (BL21) DE3 (chapter 5.2.8) and all colonies were picked to inoculate pre-cultures. In case of combined site-directed mutageneses different aliquots of competent cells were transformed with the respective plasmids separately and three colonies per plasmid were picked for pre-cultures. Additionally, a control for the background reaction of the crude cell extract was always included. To prepare the crude cell extract for this control, *E. coli* BL21 (DE3) cells were transformed with the pET28a (+) empty

vector. For the pre-cultures, 600 µL LB-medium (Table 5-11) in a 96- deep well plate (Nerbe) were inoculated with a single colony, sealed with an air -permeable, sterile membrane and cultivated at 30 °C and 800 rpm over night.

For the main culture 10 µL of each well was transferred to 1.5 mL AI-medium (Table 5-12) in flower plates (M2P-labs) sealed with an air permeable, sterile membrane (AeraSeal^{TM}, EXCEL Scientific Inc.) and cultivated at room temperature and 850 rpm (TiMix, Edmund Bühler GmbH) for 48 h. The following steps were performed semi-automated using a TECAN robotic system (Freedom EVO 200). 700 µL of each culture were transferred to a 96-deep well plate and the cells were pelleted by centrifugation at 2683 *x*g for 3 min (centrifuge Rotana 46RSC, Hettich). After 620 µL of the supernatant were discarded, the cells were disrupted by freezing at -20 °C for 1 h followed by suspension in 420 µL of the respective reaction buffer (Table 5-16) containing 1 mg·mL^{-1} lysozyme (Sigma-Aldrich) and incubation at 30°C and 800 rpm for 1 h. The cell debris was separated by centrifugation at 2683 *x*g for 10 min and 250 µL of the supernatants were transferred to a fresh 96-deep well plate, respectively. Carboligation reactions were started by addition of 250 µL reaction buffer with the respective substrates resulting in final substrate concentrations as specified in chapter 5.3.7. The reaction plates were covered with a silicon cap-mat (Nerbe Plus). After incubation at 30 °C and 500 rpm overnight, samples were analysed by the TTC-assay (chapter 5.4.1), chiral phase HPLC (chapter 5.4.2) and/or chiral phase GC (chapter 5.4.3).

5.3.9 Incubation of (*S*)-DHH with *Ec*TK variants

To investigate the time dependent decline of the *ee* with *Ec*TK variant F434A (see chapter 3.2.6), (*S*)-DHH was incubated with TK variants and the *ee*-value was followed. For this purpose (*S*)-DHH was synthesised from HPA and n-pentanal using the highly *S*-selective *EcTK* variant D469E (Smith et al., 2008). The synthesis was performed in 2.5 mL scale using reaction conditions described in Table 5-30. After 1 h the enzyme was removed from the reaction solution by filtration using Centricon® centrifugal filter units according to the manufacturer's protocol (Merck Millipore, MWCO: 30 kDa). To prevent that HPA competes with DHH as a potential donor substrate, excess HPA was subsequently removed from the flow through, using a quaternary amine functionalised MP-carbonate resin (cation exchanger, Biotage) (Smith et al., 2006a). The resin (1 g) was first saturated with *Ec*TK reaction buffer (Table 5-16). After residual buffer was removed, the (*S*)-DHH solution was added and incubated in an overhead shaker for 1 h. Afterwards, the resin was removed by sedimentation and purified *Ec*TK variant was added to the (*S*)-DHH solution without any further purification. Samples were analysed by GC-MS as described in chapter 5.4.3.

5.4 Analytical methods

5.4.1 TTC-assay

The TTC-assay was used for fast, colorimetric detection of α-hydroxy ketones, which reduce the colourless 2,3,5-triphenyl tetrazoliumchloride (TTC) to the corresponding red-coloured formazan dye (Breuer et al., 2002). The assay was performed in 96-well microtiter plates. 100 µL sample was mixed with 40 µL TTC-solution (Table 5-32). Samples were diluted 1:10 before addition of the TTC-solution,

if necessary. The red coloration was measured via the absorption at 510 nm using the Infinite M200 microtiter plate reader (Tecan).

When the TTC-assay was used the monitor *Ec*TK catalysed reactions, residual HPA had to be removed before the assay was conducted, because it can as well reduce tetrazoliumchloride and create a red coloration. HPA was removed using MP Carbonate adsorber beads (Biorad), which adsorb negatively charged molecules (Smith et al., 2006a).

The removal of HPA was performed in 250 µL scale in microtiter plates. The adsorber (40 mg) was filled into each well and 225 µL Tris/HCl buffer (50 mM, pH 7.2) was added. As KP_i-buffer hampered the adsorption, reaction buffer could not be used for this step. Subsequently, a 25 µL sample was added to the adsorber suspension and incubated at room temperature and 700 rpm for 2 h. After that the beats were allowed to settle and the supernatant was used for the TTC-assay as described above.

Table 5-32: Composition of the TTC-solution

component	amount
2,3,5-triphenyl tetrazoliumchloride (sodium salt)	10 mg
ethanol	1.75 mL
NaOH (1M)	7.5 mL
ddH_2O	0.75 mL

5.4.2 Chiral phase HPLC

*Studies on PpYerE**

Chiral phase HPLC analysis of the reaction products was performed with an Agilent Technologies 1100 Series HPLC equipped with an analytical Chiralpak IE column (Diacel cooperation, length: 250 mm, inner diameter: 4.6 mm, particle size: 5 µm). Samples were diluted 1:5 in acetonitrile containing 0.04 $\mu L \cdot mL^{-1}$ 4-methoxybenzaldehyde as internal standard, centrifuged to remove potential precipitate, and 10 µL were injected. For the mobile phase, a gradient of acetonitrile in Millipore water was applied, starting with 35 vol % acetonitrile for 7 min followed by an increase of acetonitrile to 60 vol % within 1 min and 6 min of 60 vol % acetonitrile. Subsequently, the acetonitrile was decreased to 35 vol % within 1 min and kept constant for additional 3 min. The flow rate was set to 0.9 $mL \cdot min^{-1}$. The peaks were assigned using reference compounds: (*S*)- and (*R*)-PAC were detected at 210 nm at 6.4 min and 7.2 min, respectively. (*R*)-2-HPP, benzaldehyde and benzoin were detected at 254 nm at 7.5 min, 9.6 min and 12.6 min, respectively. The HPLC was only calibrated with reference compounds for the characterisation of selected *Pp*YerE variants and not for initial screenings.

Studies on PfBAL

The *Pf*BAL variants were characterised concerning the self-ligation of benzaldehyde to benzoin and the mixed carboligation of acetaldehyde and benzaldehyde to HPP. Additionally, the formation of benzoin and PAC was studied in the mixed carboligations. All reaction products were analysed on an Agilent Technologies 1260 Infinity HPLC using an analytical Chiralpak IE column (Diacel cooperation, length: 250 mm, inner diameter: 4.6 mm, particle size: 5 µm).

*This paragraph was taken from the manuscript Loschonsky *et. al* (submitted to ChemBioChem, see appendix 7.4) with minor changes.

Samples of the benzoin synthesis were diluted 1:25 in a 1:1 mixture of acetonitrile and Millipore water, potential precipitate was removed by centrifugation and 10 µL were applied to the HPLC analysis. All product peaks were detected at 250 nm and assigned via reference compounds. Using an isocratic elution profile with 50 vol % acetonitrile in ddH_2O and a flow rate of 1 mL·min^{-1}, the retention times were: 5.3 min benzaldehyde, 6.6 min (*S*)-benzoin, and 7.3 min (*R*)-benzoin. The products of the mixed carboligation were analysed as described above for the studies on *Pp*YerE. On the 1260 Infinity HPLC system the retention times were: (*S*)-PAC 5.9 min; (*R)*-PAC 6.4 min, (*S*)-HPP 6.9 min; (*R*)-HPP 7.3 min; benzaldehyde 8.9 min; benzoin 13.1 min. Acetaldehyde and acetoin were not determined.

5.4.3 Chiral phase GC-MS

The carboligation reactions with aliphatic acceptor aldehydes were analysed with chiral phase GC, using a Trace 1310 system (Agilent) equipped with a CP-Chirasil Dex CB column (Agilent, length: 25 m, inner diameter: 0.25 mm, film: 0.25 µm) and coupled to an ISQLT Single Quadrupole Mass Spectrometer (Agilent) as detector. Samples were extracted in the same volume of ethyl acetate containing 0.1 % octane as internal standard. 1 µL of the organic phase was applied to the analysis. The operating parameter of the GC and the MS are summarised in Table 5-33. The temperature profiles of the GC-oven were dependent on the studied reaction and are given in Table 5-34 together with the analyte retention times that were found for these conditions. As no references for the *Pp*YerE products 3-HH, 3-HP, and EHH were available, the peaks were assigned based on their mass fragmentation patterns. The identity of 3-HH and 3-HP was additionally confirmed by NMR-spectroscopy (chapter 5.6) and the configuration at the chiral centre was determined by CD-spectroscopy (chapter 5.4.5). Racemic reference compounds for the peak identification and calibration of the TK products DHH and DHP were synthesised as described in chapter 5.5. The configuration at the chiral centre was determined using products of biotransformations with the literature described *Ec*TK variants H26Y (*R*-selective) and D469E (*S*-selective) (Smith et al., 2008).

Table 5-33: Operating parameter for the GC-MS system

	setting
GC-parameter	
injection volume	1 µL
inlet temperature	210 °C
carrier gas	helium
split flow	23 mL·min^{-1}
split ratio	15
purge flow	5 mL·min^{-1}
FID-parameter	
temperature	250 °C
air flow	350 mL·min^{-1}
makeup gas flow	40 mL·min^{-1}
hydrogen flow	35 mL·min^{-1}
MS-parameter	
transfer line temperature	210 °C
ionisation type	EI
ion source temperature	200 °C
mass range	29-200 amu
scan time	0.2 sec
detector gain	5·10^{4}

Table 5-34: Temperature profiles of the applied GC-MS methods and retention times of the respective analytes for these methods.

	temperature profile	**analyte**	**retention time**
*Pp*YerE	50 °C, 1 min	n-pentanal	4.1 min
catalysed reactions	2 °C/min, 25 min (→ 100°C)	octane	5.2 min
	20 °C/min, 4.5 min (→ 190 °C)	hexan-3,4-dion	7.7 min
	190 °C, 2 min	(*R*)-3-HP	12.3 min
		(*S*)-3-HP	13.9 min
		(*R*)-3-HH	22.5 min
		(*S*)-3-HH	24.7 min
		EHH enantiomer 1	27.8 min
		EHH enantiomer 2	28.3 min
*Ec*TK	50 °C starting temperature	n-pentanal	3.5 min
catalysed reactions	5 °C/min, 28 min (→ 190 °C)	octane	4.5 min
	190 °C, 5 min	(*R*)-DHP	18.2 min
		(*S*)-DHP	18.4 min
		(*R*)-DHH	21.8 min
		(*S*)-DHH	22.0 min

5.4.4 ^{1}H- and ^{13}C-NMR*

For *Ec*TK carboligation products DHH and DHP, ^{1}H-NMR was used to confirm the identity and determine the purity of chemically synthesised, racemic references (chapter 5.5). 14 mg synthesised reference compound and 10 mg maleic acid as internal standard were dissolved in 750 µL deuterated DMSO with 0.03 % TMS. The purity of the reference compound was determined from the ratio of the maleic acid proton peak area and the average area of peaks from the reference compound protons.

For the carboligation products of *Pp*YerE, 3-HH and 3-HP, no readily applicable protocol for the chemical synthesis of reference compounds was available. Further, purification of the products proved to be difficult, as especially 3-HP was very volatile and evaporated upon removal of the organic solvent. Therefore, both products were synthesised enzymatically, and NMR-spectra were recorded with only minimal follow up purification. Reactions were performed in 100 mM potassium phosphate buffer, pH 7.6, containing 0.1 mM ThDP, 3 mM $MgCl_2$ and 2 mg·mL^{-1} *Pp*YerE. The final substrate concentrations were 300 mM pyruvate and 150 mM propanal for the formation of 3-HP and 150 mM pyruvate and 150 mM pentanal for the formation of-3HH. After incubation at 30 °C and 1000°rpm (ThermoMixer®, Eppendorf) for 2 h, 4 mL samples were extracted three times with 4 mL diethyl ether. The organic fractions were pooled and dried over $MgSO_4$. Subsequently, 750 µL D_2O with 0.05 % 3-(trimethylsilyl)propionic 2,2,3,3 d4 acid was added and the diethyl ether was evaporated at atmospheric pressure and room temperature.

All ^{1}H- and ^{13}C-NMR spectra were recorded on an Advance DRX 600 MHz instrument (Bruker) operating at 600 and 150 MHz for ^{1}H and ^{13}C acquisitions, respectively. The spectra are shown in the appendix chapter 7.3.

5.4.5 CD-spectroscopy*

The absolute configuration at the C3-atom was determined by CD-spectroscopy analogously to spectra obtained from similar compounds with unambiguously assigned absolute configuration. As *E. coli* BL21 (DE3) cells produced 3-HH and 3-HP from pyruvate and n-pentanal and propanal, respectively, with high enantiomeric excess (*ee*: 98%) (see chapter 3.1.6), samples for CD spectroscopy were prepared by whole cell biotransformations using *E. coli* BL21 (DE3). Reactions were performed in 100 mM KP_i buffer, pH 7.6, containing 0.1 mM ThDP and 3 mM $MgCl_2$ with 200 mg·mL^{-}1 wet cells. The final substrate concentrations were 150 mM pyruvate and 150 mM n-pentanal for the formation of 3-HH and 300 mM pyruvate and 150 mM propanal for the formation of 3-HP. After 1 h and 2 h incubation at 30 °C and 1000°rpm (ThermoMixer®, Eppendorf) the cells were separated by centrifugation. 500 µL of the supernatant was extracted three times with 500 µL diethyl ether. Subsequently, the pooled organic fractions were mixed with 400 µL buffer and the diethyl ether was evaporated at atmospheric pressure and room temperature. Spectra were recorded on a J-1100 CD-spectrometer (Jasco) at 20 °C in a 2 mm cuvette with three accumulations. Product formation was confirmed by chiral phase GC-MS as described in chapter 5.4.3.

*These chapters were partly taken from the manuscript Loschonsky *et. al* (submitted to ChemBioChem, see appendix 7.4) with minor changes.

Figure 5-1 shows that the reaction products of both biotransformations give rise to a positive CD band at 272 nm. According to Vinogradov et al. (Vinogradov et al., 2005) (*R*)-3-HP is characterised by a negative CD-band. Therefore, the 3-HP obtained with non-transformed *E. coli* BL21(DE3) contains the *S*-enantiomer in excess. For 3-HH no CD reference spectrum is available in literature, but the absolute configuration can be concluded by analogy to the CD spectra of 3-HP as well as (*R*)-acetoin and (*R*)-4-hydroxy-3-hexanone, which both show negative CD-maxima at 270 nm (Vinogradov et al., 2005). Hence, also for 3-HH the *S*-enantiomer was formed in excess.

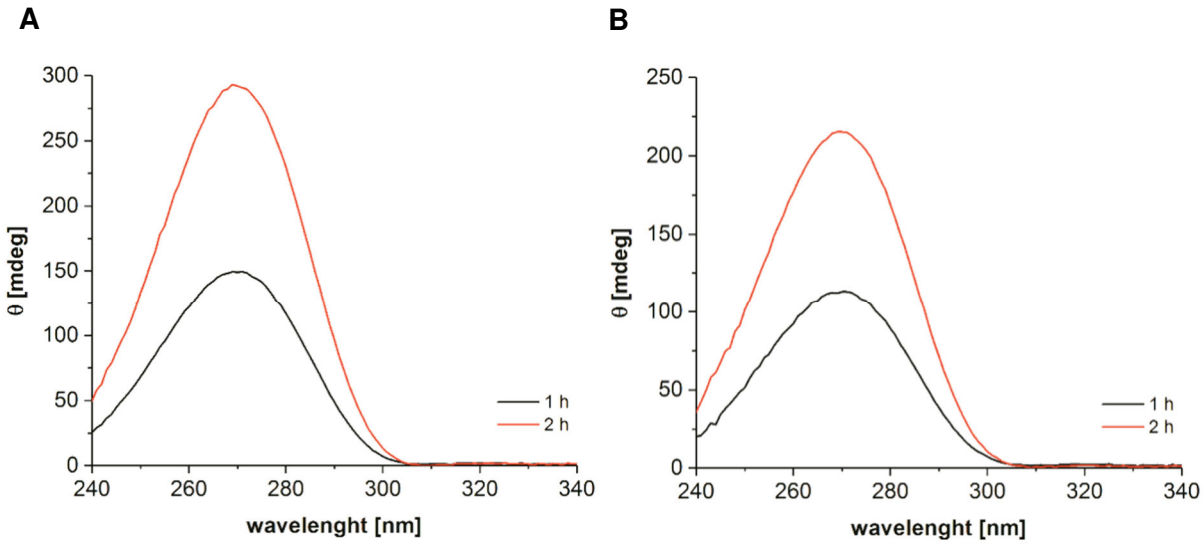

Figure 5-1: CD-spectra of 3-hydroxyheptan-2-one (3-HH) (A) and 3-hydroxypentan-2-one (3-HP) (B) produced in whole cell biotransformations of pyruvate and n-pentanal and propanal, respectively, with *E. coli* BL21 (DE3) as described above. The increase of the ellipticity (θ) between 1 h and 2 h corresponded to the increase of the peak area that was determined in parallel by GC-MS, confirming that the observed CD band was a result of 3-HH or 3-HP formation.

5.5 Chemical synthesis of dihydroxy ketones as reference compounds

Racemic 1,3-dihydroxyheptan-2-one (DHH) and 1,3-dihydroxypentan-2-one (DHP) were synthesised as described by Hailes and co-workers (Galman et al., 2012; Smith et al., 2006b). HPA (3 mmol), n-pentanal (3 mmol, DHH synthesis) or propanal (3 mmol, DHP synthesis) and 4-methylmorpholine (3 mmol) were dissolved in 60 mL desalted water. The pH was adjusted to 8 with hydrochloric acid. After stirring at room temperature for 24 h the reaction solution was extracted three times with 100 mL ethyl acetate. The organic phase was dried over $MgSO_4$ and concentrated by evaporation. The dihydroxy ketones were purified by gravity flow column chromatography (column: 30 g silica gel, height: 11 cm, outer diameter: 3cm) using a mixture of ethyl acetate and petrol ether (1:1) as mobile phase. The crystals obtained after evaporation of the solvent were washed with diethyl ether and analysed by ^{1}H-NMR.

5.6 Characteristics of the molecules synthesised in this thesis

The possible products of the mixed carboligation of acetaldehyde and benzaldehyde – 2-hydroxypropiophenone (HPP), phenylacetylcarbinol (PAC), and benzoin – were extensively characterised in previous studies (Beigi et al., 2016; Demir et al., 2002; Gocke, 2007; Sehl et al., 2012; Westphal et al., 2014b) and available as reference compounds and were therefore not again characterised by GC-MS and NMR.

5.6.1 3-Hydroxyheptan-2-one (3-HH)

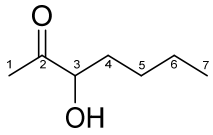

GC-MS:
R_t = 22.5 min, m/z (%): 130 (0.4) $[M]^+$, 87 (34) $[C_5H_{11}O]^+$, 69 (100) $[C_5H_9]^+$, 57 (21) $[C_4H_9]^+$, 43 (75) $[C_2H_3O]^+$, 41 (19) $[C_3H_5]^+$
R_t = 24.7 min, m/z (%): (%): 130 (0.4) $[M]^+$, 87 (34) $[C_5H_{11}O]^+$, 69 (100) $[C_5H_9]^+$, 57 (21) $[C_4H_9]^+$, 43 (75) $[C_2H_3O]^+$, 41 (19) $[C_3H_5]^+$

^{1}H-NMR: (600 MHz, D_2O): δ= 0.87-0.93 ppm (t, J=7 Hz, 3H, C^7H_3); 1.26-1.42 ppm (m, 4H, $C^6H_2C^5H_2$); 1.6-1.67 ppm (m, 1H, C^4HH); 1.8-1.87 ppm (m, 1H, C^4HH), 2.22-2.24 ppm (s, 3H, C^1H_3); 4.32-4.36 ppm (dd, J=8 Hz and 4 Hz, 1H, C^3HOH) (see appendix, Figure 7-4)

^{13}C-NMR: (150 MHz, D_2O): δ= 13.08 ppm (C^7); 21.72 ppm (C^6); 25.22 ppm (C^1); 26.37 ppm (C^5); 31.90 ppm (C^4); 76.89 ppm (C^3); 215.56 ppm (C^2) (see appendix, Figure 7-5)

5.6.2 3-Hydroxypentan-2-one (3-HP)

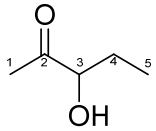

GC-MS:
R_t = 12.3 min, m/z (%): 102 (1.7) $[M]^+$, 59 (100) $[C_3H_7O]^+$,43 (47) $[C_2H_3O]^+$, 41 (35) $[C_3H_5]^+$, 31 (40) $[CH_3O]^+$
R_t = 13.9 min, m/z (%):102 (1.7) $[M]^+$, 59 (100) $[C_3H_7O]^+$,43 (49) $[C_2H_3O]^+$, 41 (37) $[C_3H_5]^+$, 31 (44) $[CH_3O]^+$

^{1}H-NMR: (600 MHz, D_2O): δ= 0.9-0.95 ppm (t, J=7.5 Hz, 3H, C^5H_3); 1.64-1.73 ppm (m, 1H, C^4HH); 1.84-1.93 ppm (m, 1H, C^4HH); 2.22-2.24 ppm (s, 3H, C^1H_3); 4.29-4.34ppm (dd, J=7.3 Hz and 4.5 Hz, 1H, C^3HOH) (see appendix, Figure 7-6)

^{13}C-NMR: (150 MHz, D_2O): δ= 8.35 ppm (C^5); 25.25 ppm (C^4); 25.52 ppm (C^1); 77.92 ppm (C^3); 215.33 ppm (C^2) (see appendix, Figure 7-7)

5.6.3 3-Ethyl-3-hydroxyhexan-2,4-dion (EHH)

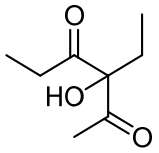

GC-MS:

R_t = 27.8 min, m/z (%): 158 (0.2) $[M]^+$, 116 (36) $[C_6H_{12}O_2]^+$, 102 (92), $[C_5H_{10}O_2]^+$, 87 (63) $[C_4H_7O_2]^+$, 57 (100) $[C_3H_5O]^+$, 43 (75) $[C_2H_3O]^+$, 29 (19) $[C_2H_5]^+$

R_t = 28.3 min, m/z (%): 158 (0.2) $[M]^+$, 116 (39) $[C_6H_{12}O_2]^+$, 102 (95), $[C_5H_{10}O_2]^+$, 87 (64) $[C_4H_7O_2]^+$, 57 (100) $[C_3H_5O]^+$, 43 (72) $[C_2H_3O]^+$, 29 (20) $[C_2H_5]^+$

5.6.4 1,3-Dihydroxyheptan-2-one (DHH)

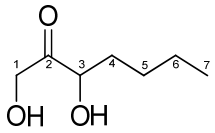

Isolated Yield (of chemical synthesis, chapter 5.5): 25 %

Purity (determined by ^{1}H-NMR with maleic acid as internal standard): 99 %

GC-MS:

R_t = 21.8 min, m/z: 146 $[M]^+$, 129 $[C_7H_{13}O_2]^+$,87 $[C_5H_{11}O]^+$, 85 $[C_5H_9O]^+$, 43 $[C_3H_7]^+$, 41 $[C_3H_5]^+$, 31$[CH_3O]^+$

R_t = 22.0min, m/z (%): 146 $[M]^+$, 129 $[C_7H_{13}O_2]^+$,87 $[C_5H_{11}O]^+$, 85 $[C_5H_9O]^+$, 43 $[C_3H_7]^+$, 41 $[C_3H_5]^+$, 31$[CH_3O]^+$

^{1}H-NMR: (600 mHZ, DMSO): δ =0.84-0.88ppm (t, J=7 Hz, 3H, C^7H_3); 1.21-1.34 ppm (m, 4H, C^5H_2-C^6H_2); 1.41-1.49 ppm (m, 1H, C^4HH); 1.55-1.62 ppm (m, 1H, C^4HH); 2.48-2.52 (s, DMSO); 3.99-4.03 ppm (dd, J=4.3 Hz and 8.2 Hz, 1H, C^3HOH); 4.29-4.32 ppm (s, 2H, C^1H_2OH); 6.26-6.29 ppm (s, maleic acid) (see appendix, Figure 7-8)

5.6.5 1,3-Dihydroxypentan-2-one (DHP)

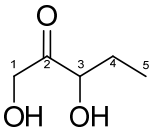

Isolated Yield (of chemical synthesis, chapter 5.5): 17 %

Purity (determined by ^{1}H-NMR with maleic acid as internal standard): 96 %

GC-MS:

R_t = 18.3 min, m/z: 118 $[M]^+$, 101 $[C_5H_9O_2]^+$,59 $[C_3H_7O]^+$ and $[C_2H_3O_2]^+$, 57 $[C_3H_5O]^+$, 43 $[C_3H_7]^+$, 41 $[C_3H_5]^+$, 31$[CH_3O]^+$

R_t = 18.6 min, m/z: 118 $[M]^+$, 101 $[C_5H_9O_2]^+$,59 $[C_3H_7O]^+$ and $[C_2H_3O_2]^+$, 57 $[C_3H_5O]^+$, 43 $[C_3H_7]^+$, 41 $[C_3H_5]^+$, 31$[CH_3O]^+$

^{1}H-NMR: (600 mHZ, DMSO): δ= 0.83-0.88 ppm (t, J=7.4 Hz, 3H, C^5H_3); 1.44-1.53 ppm (m, 1H, C^4HH); 1.59-1.67 ppm (m, 1H, C^4HH), 2.49-2.52 ppm (s, DMSO); 3.94-3.98 ppm (dd, J=4,7 Hz and 7,7 Hz; 1H; C^3HOH); 4.29-4.31 ppm (d; J= 4.3 Hz, 2H, C^1H_2OH); 6.26-6.29 ppm (s, maleic acid) (see appendix, Figure 7-9)

6 LITERATURE

Abdoul-Zabar, J., Sorel, I., Hélaine, V., Charmantray, F., Devamani, T., Yi, D., de Berardinis, V., Louis, D., Marlière, P., Fessner, W.-D., Hecquet, L., 2013. Thermostable Transketolase from *Geobacillus stearothermophilus*: Characterization and Catalytic Properties. Adv. Synth. Catal. 355, 116–128.

Abdoul Zabar, J., Lorillière, M., Yi, D., Saravanan, T., Devamani, T., Nauton, L., Charmantray, F., Hélaine, V., Fessner, W.-D., Hecquet, L., 2015. Engineering a Thermostable Transketolase for Unnatural Conversion of (2*S*)-Hydroxyaldehydes. Adv. Synth. Catal. 357, 1715–1720.

Anastas, P., Zimmerman, J., 2007. Design Through the 12 Principles of Green Engineering. IEEE Eng. Manag. Rev. 35, 16–16.

Andrews, F.H., Tom, A.R., Gunderman, P.R., Novak, W.R.P., McLeish, M.J., 2013. A bulky hydrophobic residue is not required to maintain the V-conformation of enzyme-bound thiamin diphosphate. Biochemistry 52, 3028–3030.

Asztalos, P., Parthier, C., Golbik, R., Kleinschmidt, M., Hübner, G., Weiss, M.S., Friedemann, R., Wille, G., Tittmann, K., 2007. Strain and Near Attack Conformers in Enzymic Thiamin Catalysis: X-ray Crystallographic Snapshots of Bacterial Transketolase in Covalent Complex with Donor Ketoses Xylulose 5-phosphate and Fructose 6-phosphate, and in Noncovalent Complex with Acceptor Aldo. Biochemistry 46, 12037–12052.

Baierl, A., Theorell, A., Mackfeld, U., Marquardt, P., Hoffmann, F., Moers, S., Nöh, K., Buchholz, P.C.F., Pleiss, J., Pohl, M., 2018. Towards a Mechanistic Understanding of Factors Controlling the Stereoselectivity of Transketolase. ChemCatChem. doi:10.1002/cctc.201800299

Baraibar, Á.G., von Lieres, E., Wiechert, W., Pohl, M., Rother, D., 2014. Effective Production of (*S*)-α-Hydroxy ketones: An Reaction Engineering Approach. Top. Catal. 57, 401–411.

Baykal, A., Chakraborty, S., Dodoo, A., Jordan, F., 2006. Synthesis with good enantiomeric excess of both enantiomers of α-ketols and acetolactates by two thiamin diphosphate-dependent decarboxylases. Bioorg. Chem. 34, 380–393.

Beigi, M., Gauchenova, E., Walter, L., Waltzer, S., Bonina, F., Stillger, T., Rother, D., Pohl, M., Müller, M., 2016. Regio- and Stereoselective Aliphatic-Aromatic Cross-Benzoin Reaction: Enzymatic Divergent Catalysis. Chem. - A Eur. J.

Beigi, M., Waltzer, S., Fries, A., Eggeling, L., Sprenger, G.A., Müller, M., 2013. TCA Cycle Involved Enzymes SucA and Kgd, as well as MenD: Efficient Biocatalysts for Asymmetric C–C Bond Formation. Org. Lett. 15, 452–455.

Beigi, M., Waltzer, S., Zarei, M., Müller, M., 2014. New Stetter reactions catalyzed by thiamine diphosphate dependent MenD from *E. coli*. J. Biotechnol. 191, 64–68.

Berheide, M., Kara, S., Liese, A., 2015. Reversibility of asymmetric catalyzed C–C bond formation by benzoylformate decarboxylase. Catal. Sci. Technol. 5, 2418–2426.

Berman, H.M., Westbrook, J., Feng, Z., Gilliland, G., Bhat, T.N., Weissig, H., Shindyalov, I.N., Bourne, P.E., 2000. The protein data bank. Nucleic Acids Res. 28, 235–242.

Bertani, G., 1951. Studies on lysogenesis - I. The mode of phage liberation by lysogenic *Escherichia coli*. J. Bacteriol. 62, 293–300.

Birnboim, H.C., Doly, J., 1979. A rapid alkaline extraction procedure for screening recombinal plasmid DNA. Nucleic Acids Res. 7, 1513–1523.

Bommarius, A.S., 2015. Biocatalysis: A Status Report. Annu. Rev. Chem. Biomol. Eng. 6, 319–345.

Bornscheuer, U.T., 2016. Biocatalysis: Successfully Crossing Boundaries. Angew. Chemie - Int. Ed. 55, 4372–4373.

Bradford, M.M., 1976. A rapid and sensitive method for the quantitation of microgram quantities of protein utilizing the principle of protein-dye binding. Anal. Biochem. 72, 248–254.

Brandt, G.S., Nemeria, N., Chakraborty, S., McLeish, M.J., Yep, A., Kenyon, G.L., Petsko, G.A., Jordan, F., Ringe, D., 2008. Probing the active center of benzaldehyde lyase with substitutions and the pseudosubstrate analogue benzoylphosphonic acid methyl ester. Biochemistry 47, 7734–7743.

Breslow, R., 1958. On the Mechanism of Thiamine Action. IV. 1 Evidence from Studies on Model Systems. J. Am. Chem. Soc. 80, 3719–3726.

Breslow, R., 1957. Rapid Deuterium Exchange in Thiazolium Salts. J. Am. Chem. Soc. 79, 1762–1763.

Breuer, M., Pohl, M., Hauer, B., Lingen, B., 2002. High-throughput assay of (*R*)-phenylacetylcarbinol synthesized by pyruvate decarboxylase. Anal. Bioanal. Chem. 374, 1069–1073.

Buchholz, P., Vogel, C., Reusch, W., Pohl, M., Rother, D., Spieß, A.C., Pleiss, J., 2016. BioCatNet: A Database System for the Integration of Enzyme Sequences and Biocatalytic Experiments. ChemBioChem 17, 2093–2098.

Burton, S.G., Cowan, D.A., Woodley, J.M., 2002. The search for the ideal biocatalyst. Nat. Biotechnol. 20, 37–45.

Bykova, I.A., Solovjeva, O.N., Meshalkina, L.E., Kovina, M. V., Kochetov, G.A., 2001. One-Substrate Transketolase-Catalyzed Reaction. Biochem. Biophys. Res. Commun. 280, 845–847.

Cahn, R.S., Ingold, C., Prelog, V., 1966. Specification of Molecular Chirality. Angew. Chemie Int. Ed. English 5, 385–415.

Cázares, A., Galman, J.L., Crago, L.G., Smith, M.E.B., Strafford, J., Ríos-Solís, L., Lye, G.J., Dalby, P.A., Hailes, H.C., 2010. Non-α-hydroxylated aldehydes with evolved transketolase enzymes. Org. Biomol. Chem. 8, 1301–1309.

Chen, H., Guo, Z., Liu, H., 1998. Biosynthesis of Yersiniose: Attachment of the Two-Carbon Branched-Chain Is Catalyzed by a Thiamine Pyrophosphate-Dependent Flavoprotein. J. Am. Chem. Soc. 120, 11796–11797.

Chipman, D., Barak, Z., Schloss, J. V., 1998. Biosynthesis of 2-aceto-2-hydroxy acids: acetolactate synthases and acetohydroxyacid synthases. Biochim. Biophys. Acta - Protein Struct. Mol. Enzymol. 1385, 401–419.

Costantini, A., Pala, M.I., Compagnoni, L., Colangeli, M., 2013. High-dose thiamine as initial treatment for Parkinson's disease. BMJ Case Rep. 1–4.

Costelloe, S.J., Ward, J.M., Dalby, P.A., 2008. Evolutionary Analysis of the TPP-Dependent Enzyme Family. J. Mol. Evol. 66, 36–49.

Davids, T., Schmidt, M., Böttcher, D., Bornscheuer, U.T., 2013. Strategies for the discovery and engineering of enzymes for biocatalysis. Curr. Opin. Chem. Biol. 17, 215–220.

Demir, A.S., Dünnwald, T., Iding, H., Pohl, M., Müller, M., 1999. Asymmetric benzoin reaction catalyzed by benzoylformate decarboxylase. Tetrahedron Asymmetry 10, 4769–4774.

Demir, A.S., Pohl, M., Janzen, E., Müller, M., 2001. Enantioselective synthesis of hydroxy ketones through cleavage and formation of acyloin linkage. Enzymatic kinetic resolution via C–C bond cleavage. J. Chem. Soc. Perkin Trans. 1 633–635.

Demir, A.S., Sesenogule, Ö., Eren, E., Hosrik, B., Pohl, M., Janzen, E., Kolter, D., Feldmann, R.,

Dünkemann, P., Müller, M., 2002. Enantioselective Synthesis of α-Hydroxy Ketones via Benzaldehyde Lyase-Catalyzed C-C Bond Formation Reaction. Adv. Synth. Catal. 344, 96–103.

Demuynck, C., Bolte, J., Hecquet, L., Dalmas, V., 1991. Enzyme catalyzed synthesis of carbohydrates: Synthetic potential of transketolase. Tetrahedron Lett. 32, 5085–5088.

Duggleby, R.G., 2006. Domain Relationships in Thiamine Diphosphate-Dependent Enzymes 39, 550–557.

Dünkelmann, P., Kolter-Jung, D., Nitsche, A., Demir, A.S., Siegert, P., Lingen, B., Baumann, M., Pohl, M., Müller, M., 2002. Development of a Donor−Acceptor Concept for Enzymatic Cross-Coupling Reactions of Aldehydes: The First Asymmetric Cross-Benzoin Condensation. J. Am. Chem. Soc. 124, 12084–12085.

Dünnwald, T., Demir, A.S., Siegert, P., Pohl, M., Müller, M., 2000. Enantioselective Synthesis of (*S*)-2-Hydroxypropanone Derivatives by Benzoylformate Decarboxylase Catalyzed C−C Bond Formation. European J. Org. Chem. 2000, 2161–2170.

Effenberger, F., Null, V., Ziegler, T., 1992. Preparation of Optically Pure L-2-Hydroxyaldehydes with Yeast Transketolase. Tetrahedron Lett. 33, 5157–5160.

Engel, S., Vyazmensky, M., Berkovich, D., Barak, Z., Chipman, D.M., 2004. Substrate range of acetohydroxy acid synthase I from *Escherichia coli* in the stereoselective synthesis of alpha-hydroxy ketones. Biotechnol. Bioeng. 88, 825–831.

Engel, S., Vyazmensky, M., Geresh, S., Barak, Z., Chipman, D.M., 2003. Acetohydroxyacid synthase: A new enzyme for chiral synthesis of *R*-phenylacetylcarbinol. Biotechnol. Bioeng. 83, 833–840.

Esakova, O.A., Meshalkina, L.E., Kochetov, G.A., Golbik, R., 2009. Halogenated pyruvate derivatives as substrates of transketolase from *Saccharomyces cerevisiae*. Biokhimiya 74, 1518–1523.

Faber, K., 2011. Biotransformations in Organic Chemistry, 6th ed. Springer Berlin Heidelberg, Berlin, Heidelberg.

Fiedler, E., Golbik, R., Schneider, G., Tittmann, K., Neef, H., König, S., Hübner, G., 2001. Examination of Donor Substrate Conversion in Yeast Transketolase. J. Biol. Chem. 276, 16051–16058.

Fiedler, E., Thorell, S., Sandalova, T., Golbik, R., König, S., Schneider, G., 2002. Snapshot of a key intermediate in enzymatic thiamin catalysis: Crystal structure of the alpha-carbanion of (alpha,beta-dihydroxyethyl)-thiamin diphosphate in the active site of transketolase from *Saccharomyces cerevisiae*. Pnas 99, 591–595.

Firth, A.E., Patrick, W.M., 2008. GLUE-IT and PEDEL-AA : new programmes for analyzing protein diversity in randomized libraries. Nucleic Acids Res. 36, 281–285.

Flechner, A., Dressen, U., Westhoff, P., Henze, K., Schnarrenberger, C., Martin, W., 1996. Molecular characterization of transketolase (EC 2.2.1.1) active in the Calvin cycle of spinach chloroplasts. Plant Mol. Biol. 32, 475–484.

Frank, R.A.W., Leeper, F.J., Luisi, B.F., 2007. Structure, mechanism and catalytic duality of thiamine-dependent enzymes. Cell. Mol. Life Sci. 64, 892–905.

Galman, J.L., Steadman, D., Bacon, S., Morris, P., Smith, M.E.B., Ward, J.M., Dalby, P.A., Hailes, H.C., 2010. α,α′-Dihydroxyketone formation using aromatic and heteroaromatic aldehydes with evolved transketolase enzymes. Chem. Commun. 46, 7608–7610.

Galman, J.L., Steadman, D., Haigh, L.D., Hailes, H.C., 2012. Investigating the reaction mechanism and organocatalytic synthesis of α,α′-dihydroxy ketones. Org. Biomol. Chem. 10, 2621–2628.

Gelman, A., Carlin, J.B., Stern, H.S., Rubin, D.B., 2013. Bayesian Data Analysis, 3rd ed. Chapman &

Hall/CRC Texts in Statistical Science.

Gerhards, T., Mackfeld, U., Bocola, M., von Lieres, E., Wiechert, W., Pohl, M., Rother, D., 2012. Influence of organic solvents on enzymatic asymmetric carboligations. Adv. Synth. Catal. 354, 2805–2820.

Gibson, G.E., Hirsch, J.A., Fonzetti, P., Jordan, B.D., Cirio, R.T., Elder, J., 2016. Vitamin B1 (thiamine) and dementia. Ann. N. Y. Acad. Sci. 1367, 21–30.

Giovannini, P.P., Fantin, G., Massi, A., Venturi, V., Pedrini, P., 2011. Enzymatic diastereo- and enantioselective synthesis of α-alkyl-α,β-dihydroxyketones. Org. Biomol. Chem. 9, 8038–8045.

Gocke, D., 2007. New and optimised thiamine diphosphate (ThDP)-dependent enzymes for carboligation - Creation of a toolbox for chiral 2-hydroxy ketones (Dissertation). Heinrich-Heine-Universität Düsseldorf.

Gocke, D., Graf, T., Brosi, H., Frindi-Wosch, I., Walter, L., Müller, M., Pohl, M., 2009. Comparative characterisation of thiamin diphosphate-dependent decarboxylases. J. Mol. Catal. B Enzym. 61, 30–35.

Gocke, D., Kolter, G., Müller, M., Pohl, M., 2010. Entwicklung einer Enzymplattform für die biokatalytische C-C-Verknüpfung. Chemie Ing. Tech. 82, 81–86.

Gocke, D., Nguyen, C.L., Pohl, M., Stillger, T., Walter, L., Müller, M., 2007. Branched-Chain Keto Acid Decarboxylase from *Lactococcus lactis* (KdcA), a Valuable Thiamine Diphosphate-Dependent Enzyme for Asymmetric C-C Bond Formation. Adv. Synth. Catal. 349, 1425–1435.

Gocke, D., Walter, L., Gauchenova, E., Kolter, G., Knoll, M., Berthold, C.L., Schneider, G., Pleiss, J., Müller, M., Pohl, M., 2008. Rational Protein Design of ThDP-Dependent Enzymes—Engineering Stereoselectivity. ChemBioChem 9, 406–412.

González, B., Vicuña, R., 1989. Benzaldehyde lyase, a novel thiamine PPi-requiring enzyme, from *Pseudomonas fluorescens* biovar I. J. Bacteriol. 171, 2401–5.

Gorshkova, R.P., Zubkov, V.A., Isakov, V. V., Ovodov, Y.S., 1984. Yersiniose, a new branched-chain sugar. Carbohydr. Res. 126, 308–312.

Hailes, H.C., Rother, D., Müller, M., Westphal, R., Ward, J.M., Pleiss, J., Vogel, C., Pohl, M., 2013. Engineering stereoselectivity of ThDP-dependent enzymes. FEBS J. 280, 6374–6394.

Hammer, S.C., Knight, A.M., Arnold, F.H., 2017. Design and evolution of enzymes for non-natural chemistry. Curr. Opin. Green Sustain. Chem. 7, 23–30.

Hanahan, D., 1983. Studies on Transformation of *Escherichia coli* with Plasmids. J. Mol. Biol. 166, 557–580.

Hawkins, C.F., Borges, A., Perham, R.N., 1989. A common structural motif in thiamin pyrophosphate-binding enzymes. FEBS Lett. 255, 77–82.

Hecquet, L., Bolte, J., Demuynck, C., 1993. New Assays for Transketolase. Biosci. Biotechnol. Biochem. 57, 2174–2176.

Hegeman, G.D., 1966. Synthesis of the enzymes of the mandelate pathway by *Pseudomonas putida*. I. Synthesis of enzymes by the wild type. J. Bacteriol. 91, 1140–54.

Hemsley, A., Arnheim, N., Toney, M.D., Cortopassi, G., Galas, D.J., 1989. A simple method for site-directed mutagenesis using the polymerase chain reaction. Nucleic Acids Res. 17, 6545–6551.

Hibbert, E.G., Senussi, T., Costelloe, S.J., Lei, W., Smith, M.E.B., Ward, J.M., Hailes, H.C., Dalby, P.A., 2007. Directed evolution of transketolase activity on non-phosphorylated substrates. J.

Biotechnol. 131, 425–432.

Hibbert, E.G., Senussi, T., Smith, M.E.B., Costelloe, S.J., Ward, J.M., Hailes, H.C., Dalby, P.A., 2008. Directed evolution of transketolase substrate specificity towards an aliphatic aldehyde. J. Biotechnol. 134, 240–245.

Hildebrandt, G., Klavehn, W., 1934. Manufacture of Laevo-1-phenyl-2-methylaminopropanol-1.

Hilvert, D., 2013. Design of Protein Catalysts. Annu. Rev. Biochem. 82.

Hinrichsen, P., Gomez, I., Vicuña, R., 1994. Cloning and sequencing of the gene encoding benzaldehyde lyase from *Pseudomonas fluorescens* biovar I. Gene 144, 137–138.

Hobbs, G.R., Lilly, M.D., Turner, N.J., Ward, J.M., Willets, A.J., Woodley, J.M., 1993. Enzyme-catalysed carbon–carbon bond formation: use of transketolase from *Escherichia coli*. J. Chem. Soc., Perkin Trans. 1 1, 165–166.

Hoffmann, F., 2016. Studies of the Stereoselectivity of *E. coli* Transketolase (Master thesis). Ludwigs-Maximilians-Universität München.

Hönig, M., Sondermann, P., Turner, N.J., Carreira, E.M., 2017. Enantioselective Chemo- and Biocatalysis: Partners in Retrosynthesis. Angew. Chemie Int. Ed. 56, 8942–8973.

Horecker, B.L., 2002. The pentose phosphate pathway. J. Biol. Chem. 277, 47965–47971.

Horecker, B.L., 1953. The metabolism of pentose phosphate. J. Cell. Comp. Physiol. 41, 137–164.

Horecker, B.L., Smyrniotis, P.Z., 1953. The coenzmye function of thiamine pyrophosphate in pentose phosphate metabolism. J. Am. Chem. Soc. 75, 1009–1010.

Hoyos, P., Sinisterra, J.-V., Molinari, F., Alcántara, A.R., Domínguez de María, P., 2010. Biocatalytic strategies for the asymmetric synthesis of alpha-hydroxy ketones. Acc. Chem. Res. 43, 288–299.

Huang, C.Y., Chang, A.K., Nixon, P.F., Duggleby, R.G., 2001. Site-directed mutagenesis of the ionizable groups in the active site of *Zymomonas mobilis* pyruvate decarboxylase: Effect on activity and pH dependence. Eur. J. Biochem. 268, 3558–3565.

Hübner, G., Tittmann, K., Killenberg-Jabs, M., Schäffner, J., Spinka, M., Neef, H., Kern, D., Kern, G., Schneider, G., Wikner, C., Ghisla, S., 1998. Activation of thiamin diphosphate in enzymes. Biochim. Biophys. Acta - Protein Struct. Mol. Enzymol. 1385, 221–228.

Huisman, G.W., Collier, S.J., 2013. On the development of new biocatalytic processes for practical pharmaceutical synthesis. Curr. Opin. Chem. Biol. 17, 284–292.

Iding, H., Dünnwald, T., Greiner, L., Liese, A., Müller, M., Siegert, P., Grötzinger, J., Demir, A.S., Pohl, M., 2000. Benzoylformate Decarboxylase from *Pseudomonas putida* as Stable Catalyst for the Synthesis of Chiral 2-Hydroxy Ketones. Chem. - A Eur. J. 6, 1483–1495.

Jiang, M., Cao, Y., Guo, Z.-F., Chen, M., Chen, X., Guo, Z., 2007. Menaquinone Biosynthesis in Escherichia coli : Identification of 2-Succinyl-5-enolpyruvyl-6-hydroxy-3-cyclohexene-1-carboxylate as a Novel Intermediate and Re-Evaluation of MenD Activity. Biochemistry 46, 10979–10989.

Kern, D., Kern, G., Neef, H., Tittmann, K., Killenberg-jabs, M., Wikner, C., Schneider, G., Hu, G., 1997. How Thiamine Diphophate Is Activated in Enzymes 275, 67–70.

Kerns, J.C., Gutierrez, J.L., 2017. Thiamin. Adv. Nutr. An Int. Rev. J. 8, 395–397.

Kluger, R., Tittmann, K., 2008. Thiamin Diphosphate Catalysis: Enzymic and Nonenzymic Covalent Intermediates. Chem. Rev. 108, 1797–1833.

Kneen, M.M., Pogozheva, I.D., Kenyon, G.L., McLeish, M.J., 2005. Exploring the active site of benzaldehyde lyase by modeling and mutagenesis. Biochim. Biophys. Acta - Proteins Proteomics 1753, 263–271.

Knoll, M., Müller, M., Pleiss, J., Pohl, M., 2006. Factors Mediating Activity, Selectivity, and Substrate Specificity for the Thiamin Diphosphate-Dependent Enzymes Benzaldehyde Lyase and Benzoylformate Decarboxylase. ChemBioChem 7, 1928–1934.

Kobori, Y., Myles, D.C., Whitesides, G.M., 1992. Substrate specificity and carbohydrate synthesis using transketolase. J. Org. Chem. 57, 5899–5907.

Kochetov, G.A., Sevostyanova, I., 2005. Binding of the Coenzyme and Formation of the Transketolase Active Center. IUBMB Life (International Union Biochem. Mol. Biol. Life) 57, 491–497.

Kokova, M., Zavrel, M., Tittmann, K., Spiess, A.C., Pohl, M., 2009. Investigation of the carboligase activity of thiamine diphosphate-dependent enzymes using kinetic modeling and NMR spectroscopy. J. Mol. Catal. B Enzym. 61, 73–79.

König, S., Spinka, M., Kutter, S., 2009. Allosteric activation of pyruvate decarboxylases. A never-ending story? J. Mol. Catal. B Enzym. 61, 100–110.

Kutter, S., Weiss, M.S., Wille, G., Golbik, R., Spinka, M., König, S., 2009. Covalently bound substrate at the regulatory site of yeast pyruvate decarboxylases triggers allosteric enzyme activation. J. Biol. Chem. 284, 12136–12144.

Lacks, S., Greenberg, B., 1975. A Deoxyribonuclease of *Diplococcus pneumoniae* Specific for Methylated DNA. J. Biol. Chem. 250, 4060–4066.

Laemmli, U.K., 1970. Cleavage of Structural Proteins during the Assembly of the Head of Bacteriophage T4. Nature 227, 680–685.

Lehwald, P., Richter, M., Röhr, C., Liu, H., Müller, M., 2010. Enantioselective Intermolecular Aldehyde-Ketone Cross-Coupling through an Enzymatic Carboligation Reaction. Angew. Chemie Int. Ed. 49, 2389–2392.

Leuthardt, F., Nielsen, H., 1952. Phosphorylation Biologique de La Thiamine. Helv. Chim. Acta 35, 1196–1209.

Li, Y., Cirino, P.C., 2014. Recent advances in engineering proteins for biocatalysis. Biotechnol. Bioeng. 111, 1273–1287.

Lindqvist, Y., Schneider, G., 1993. Thiamin diphosphate dependent ezymes: transketolase, pyruvate oxidase and pyruate decarboxylase. Curr. Opin. Struct. Biol. 3, 896–901.

Lindqvist, Y., Schneider, G., Ermler, U., Sundstrom, M., 1992. Three-dimensional structure of transketolase, a thiamine diphosphate dependent enzyme, at 2.5 A resolution. EMBO J. 11, 2373–2379.

Lingen, B., Grötzinger, J., Kolter, D., Kula, M.-R., Pohl, M., 2002. Improving the carboligase activity of benzoylformate decarboxylase from *Pseudomonas putida* by a combination of directed evolution and site-directed mutagenesis. Protein Eng. Des. Sel. 15, 585–593.

Lingen, B., Kolter-Jung, D., Dünkelmann, P., Feldmann, R., Grötzinger, J., Pohl, M., Müller, M., 2003. Alteration of the Substrate Specificity of Benzoylformate Decarboxylase from *Pseudomonas putida* by Directed Evolution. ChemBioChem 4, 721–726.

Littlechild, J., Turner, N.J., Hobbs, G., Lilly, M., Rawas, A., Watson, H., 1995. Crystallization and preliminary X-ray crystallographic data with *Escherichia coli* transketolase. Acta Crystallogr. Sect. D Biol. Crystallogr. 51, 1074–1076.

Lorillière, M., De Sousa, M., Bruna, F., Heuson, E., Gefflaut, T., de Berardinis, V., Saravanan, T., Yi, D., Fessner, W.-D., Charmantray, F., Hecquet, L., 2017. One-pot, two-step cascade synthesis of naturally rare <scp>l</scp> -erythro (3S,4S) ketoses by coupling a thermostable transaminase and transketolase. Green Chem. 19, 425–435.

Loschonsky, S., 2014. Untersuchungen zur C–C-Bindungsknüpfungs und C–C-Bindungsspaltungs-Aktivität des Thiamindiphosphat-abhängigen Enzyms Cyclohexan-1,2-dion Hydrolase (Dissertation). Albert-Ludwigs-Universität Freiburg.

Marquardt, P., 2015. Untersuchungen zu Enantioselektivität der *Escherichia coli* K12-Transketolase (Master thesis). Fachhochschule Aachen.

Marsden, S.R., Gjonaj, L., Eustace, S.J., Hanefeld, U., 2017. Separating Thermodynamics from Kinetics-A New Understanding of the Transketolase Reaction. ChemCatChem 9, 1808–1814.

Mitschke, L., Parthier, C., Schröder-Tittmann, K., Coy, J., Lüdtke, S., Tittmann, K., 2010. The crystal structure of human transketolase and new insights into its mode of action. J. Biol. Chem. 285, 31559–31570.

Moers, S., 2017. Varianten der *E. coli* Transketolase zur Untersuchung der Stereoselektivität (Master thesis). Rheinisch-Westfälische Technische Hochschule Aachen.

Mücke, U., König, S., Hübner, G., 1995. Purification and Characterisation of Pyruvate Decarboxylase from Pea Seeds (*Pisum sativum* cv. Miko). Biol. Chem. Hoppe. Seyler. 376, 111–118.

Müller, M., 2014. Enzymatic Synthesis of Tertiary Alcohols. ChemBioEng Rev. 1, 14–26.

Muller, Y.A., Lindqvist, Y., Schulz, G.E., Jordan, F., Schneider, G., 1993. A thiamin diphosphate binding fold revealed by comparison of the crystal structures of transketolase, pyruvate oxidase and pyruvate decarboxylase. Structure 95–103.

Neuser, F., Zorn, H., Berger, R.G., 2000. Generation of Odorous Acyloins by Yeast Pyruvate Decarboxylases and Their Occurrence in Sherry and Soy Sauce. J. Agric. Food Chem. 48, 6191–6195.

Ni, Y., Holtmann, D., Hollmann, F., 2014. How Green is Biocatalysis? To Calculate is To Know. ChemCatChem 6, 930–943.

Nikkola, M., Lindqvist, Y., Schneider, G., 1994. Refined Structure of Transketolase from *Saccharomyces cerevisiae* at 2.0A resolution. J. Mol. Biol. 238, 387–404.

Nilsson, U., Hecquet, L., Gefflaut, T., Guerard, C., Schneider, G., 1998. Asp477 is a determinant of the enantioselectivity in yeast transketolase. FEBS Lett. 424, 49–52.

Nilsson, U., Meshalkina, L., Lindqvist, Y., Schneider, G., 1997. Examination of Substrate Binding in Thiamin Diphosphate- dependent Transketolase by Protein Crystallography and Site-directed Mutagenesis. J. Biol. Chem. 272, 1864–1869.

Otte, K.B., Hauer, B., 2015. Enzyme engineering in the context of novel pathways and products. Curr. Opin. Biotechnol. 35, 16–22.

Patrick, W.M., Firth, A.E., 2005. Strategies and computational tools for improving randomized protein libraries. Biomol. Eng. 22, 105–112.

Payongsri, P., Steadman, D., Hailes, H.C., Dalby, P.A., 2015. Second generation engineering of transketolase for polar aromatic aldehyde substrates. Enzyme Microb. Technol. 71, 45–52.

Payongsri, P., Steadman, D., Strafford, J., MacMurray, A., Hailes, H.C., Dalby, P.A., 2012. Rational substrate and enzyme engineering of transketolase for aromatics. Org. Biomol. Chem. 10, 9021–9029.

Pohl, M., Gocke, D., Müller, M., 2010. Thiamine-Based Enzymes for Biotransformations, in: Crabtree, R.H. (Ed.), Handbook of Green Chemistry. Wiley-VCH Verlag GmbH & Co. KGaA, Weinheim, Germany, pp. 75–114.

Pohl, M., Grötzinger, J., Wollmer, A., Kula, M., 1994. Reversible Dissociation and Unfolding of Pyruvate Decarboxylase from Zymomonas mobilis. Eur. J. Biochem. 224, 651–661.

Pohl, M., Siegert, P., Mesch, K., Bruhn, H., Grotzinger, J., 1998. Active site mutants of pyruvate decarboxylase from *Zymomonas mobilis* . A site-directed mutagenesis study of L112, I472, I476, E473 and N482. Eur. J. Biochem. 257, 538–546.

Poliakoff, M., Licence, P., 2007. Sustainable technology: green chemistry. Nature 450, 810–812.

Porter, J.L., Rusli, R.A., Ollis, D.L., 2016. Directed Evolution of Enzymes for Industrial Biocatalysis. ChemBioChem 17, 197–203.

Racker, E., Haba, G.D. LA, Leder, I.G., 1953. Thiamine pyrophosphate, a coenzyme of transketolase. J. Am. Chem. Soc. 75, 1010–1011.

Rahmen, N., Schlupp, C.D., Mitsunaga, H., Fulton, A., Aryani, T., Esch, L., Schaffrath, U., Fukuzaki, E., Jaeger, K.-E., Büchs, J., 2015. A particular silent codon exchange in a recombinant gene greatly influences host cell metabolic activity. Microb. Cell Fact. 14, 156.

Raj, K.C., Ingram, L.O., Maupin-Furlow, J.A., 2001. Pyruvate decarboxylase: a key enzyme for the oxidative metabolism of lactic acid by Acetobacter pasteurianus. Arch. Microbiol. 176, 443–451.

Ranoux, A., Hanefeld, U., 2013. Improving Transketolase. Top. Catal. 56, 750–764.

Reetz, M.T., Carballeira, J.D., Peyralans, J., Höbenreich, H., Maichele, A., Vogel, A., 2006. Expanding the Substrate Scope of Enzymes: Combining Mutations Obtained by CASTing. Chem. - A Eur. J. 12, 6031–6038.

Reetz, M.T., Kahakeaw, D., Lohmer, R., 2008. Addressing the Numbers Problem in Directed Evolution. ChemBioChem 9, 1797–1804.

Rother neé Gocke, D., Kolter, G., Gerhards, T., Berthold, C.L., Gauchenova, E., Knoll, M., Pleiss, J., Müller, M., Schneider, G., Pohl, M., 2011. *S*-Selective Mixed Carboligation by Structure-Based Design of the Pyruvate Decarboxylase from *Acetobacter pasteurianus*. ChemCatChem 3, 1587–1596.

Sanger, F., Nicklen, S., Coulson, A.R., 1977. DNA sequencing with chain-terminating. Proc. Natl. Acad. Sci. U. S. A. 74, 5463–5467.

Saravanan, T., Junker, S., Kickstein, M., Hein, S., Link, M.K., Ranglack, J., Witt, S., Lorillière, M., Hecquet, L., Fessner, W.-D., 2017a. Donor Promiscuity of a Thermostable Transketolase by Directed Evolution: Efficient Complementation of 1-Deoxy-d-xylulose-5-phosphate Synthase Activity. Angew. Chemie - Int. Ed. 56, 5358–5362.

Saravanan, T., Reif, M.-L., Yi, D., Lorillière, M., Charmantray, F., Hecquet, L., Fessner, W.-D., 2017b. Engineering a thermostable transketolase for arylated substrates. Green Chem. 19, 481–489.

Schenk, G., Layfield, R., Candy, J.M., Duggleby, R.G., Nixon, P.F., 1997. Molecular Evolutionary Analysis of the Thiamine-Diphosphate-Dependent Enzyme, Transketolase. J. Mol. Evol. 44, 552–572.

Schneider, G., Lindqvist, Y., 1998. Crystallography and mutagenesis of transketolase: mechanistic implications for enzymatic thiamin catalysis. Biochim. Biophys. Acta - Protein Struct. Mol. Enzymol. 1385, 387–398.

Schneider, G., Lindqvist, Y., 1993. Enzymatic Thiamine Catalysis: Mechanistic Implications from the

Three-Dimensional Structure of Transketolase. Bioorg. Chem. 21, 109–117.

Schörken, U., Sprenger, G.A., 1998. Thiamin-dependent enzymes as catalysts in chemoenzymatic syntheses. Biochim. Biophys. Acta - Protein Struct. Mol. Enzymol. 1385, 229–243.

Sehl, T., Bock, S., Marx, L., Maugeri, Z., Walter, L., Westphal, R., Vogel, C., Menyes, U., Erhardt, M., Müller, M., Pohl, M., Rother, D., 2017. Asymmetric synthesis of (S)-phenylacetylcarbinol – closing a gap in C–C bond formation. Green Chem. 19, 380–384.

Sehl, T., Hailes, H.C., Ward, J.M., Menyes, U., Pohl, M., Rother, D., 2014. Efficient 2-step biocatalytic strategies for the synthesis of all nor(pseudo)ephedrine isomers. Green Chem. 16, 3341–3348.

Sehl, T., Maugeri, Z., Rother, D., 2015. Multi-step synthesis strategies towards 1,2-amino alcohols with special emphasis on phenylpropanolamines. J. Mol. Catal. B Enzym. 114, 65–71.

Sehl, T., Simon, R.C., Hailes, H.C., Ward, J.M., Schell, U., Pohl, M., Rother, D., 2012. TTC-based screening assay for ω-transaminases: A rapid method to detect reduction of 2-hydroxy ketones. J. Biotechnol. 159, 188–194.

Sevostyanova, I.A., Solovjeva, O.N., Kochetov, G.A., 2004. A hitherto unknown transketolase—catalyzed reaction. Biochem. Biophys. Res. Commun. 313, 771–774.

Sheldon, R.A., 2016. Biocatalysis and Green Chemistry, in: Green Biocatalysis. John Wiley & Sons, Inc, Hoboken, NJ, pp. 1–15.

Sheldon, R.A., Pereira, P.C., 2017. Biocatalysis engineering: the big picture. Chem. Soc. Rev. 46, 2678–2691.

Shukla, V.B., Kulkarni, P.R., 2000. L -Phenylacetylcarbinol (L -PAC): biosynthesis and industrial applications. World J. Microbiol. Biotechnol. 16, 499–506.

Singleton, C.K., Wang, J.J.L., Shan, L., Martin, P.R., 1996. Conserved residues are functionally distinct within transketolases of different species. Biochemistry 35, 15865–15869.

Smith, M.E.B., Hibbert, E.G., Jones, A.B., Dalby, P.A., Hailes, H.C., 2008. Enhancing and Reversing the Stereoselectivity of *Escherichia coli* Transketolase via Single-Point Mutations. Adv. Synth. Catal. 350, 2631–2638.

Smith, M.E.B., Kaulmann, U., Ward, J.M., Hailes, H.C., 2006a. A colorimetric assay for screening transketolase activity. Bioorg. Med. Chem. 14, 7062–7065.

Smith, M.E.B., Smithies, K., Senussi, T., Dalby, P.A., Hailes, H.C., 2006b. The First Mimetic of the Transketolase Reaction. European J. Org. Chem. 2006, 1121–1123.

Stainer, R.Y., Ornston, L.N., 1973. The β-Ketoadipate Pathway, in: Advances in Microbial Physiology. Academic Press, pp. 89–151.

Stewart, A., 1990. Observations on Induced Thiamine (Vitamin B1) Deficiency in Man. J. Nutr. Med. 1, 73–74.

Steyn-Parvé, E.P., 1952. Partial Purification and Properties of Thiaminokinase from Yeast. Biochim. Biophys. Acta 8, 310–324.

Strafford, J., Payongsri, P., Hibbert, E.G., Morris, P., Batth, S.S., Steadman, D., Smith, M.E.B., Ward, J.M., Hailes, H.C., Dalby, P.A., 2012. Directed evolution to re-adapt a co-evolved network within an enzyme. J. Biotechnol. 157, 237–245.

Studier, F.W., 2005. Protein production by auto-induction in high-density shaking cultures. Protein Expr. Purif. 41, 207–234.

Studier, F.W., Moffatt, B.A., 1986. Use of Bacteriophage T7 RNA Polymerase to Direct Selective High-level Expression of Cloned Genes. J. Mol. Biol. 189, 113–130.

Sukumaran, J., Hanefeld, U., 2005. Enantioselective C-C bond synthesis catalysed by enzymes. Chem. Soc. Rev. 34, 530–542.

Tang, S.L.Y., Smith, R.L., Poliakoff, M., 2005. Principles of green chemistry: PRODUCTIVELY. Green Chem. 7, 761.

Tillett, D., Neilan, B. a, 1999. Enzyme-free cloning: a rapid method to clone PCR products independent of vector restriction enzyme sites. Nucleic Acids Res. 27, e26.

Truppo, M.D., 2017. Biocatalysis in the Pharmaceutical Industry: The Need for Speed. ACS Med. Chem. Lett. 8, 476–480.

Tsou, A.Y., Ransom, S.C., Gerlt, J.A., Buechter, D.D., Babbitt, P.C., Kenyon, G.L., 1990. Mandelate pathway of *Pseudomonas putida*: sequence relationships involving mandelate racemase, (*S*)-mandelate dehydrogenase, and benzoylformate decarboxylase and expression of benzoylformate decarboxylase in *Escherichia coli*. Biochemistry 29, 9856–9862.

Ukai, T., Tanaka, R., Dokawa, T., 1943. A new catalyst for acyloin condensation. J. Pharm. Soc. Jpn 63, 296–300.

van den Bergh, E.R.E., Baker, S.C., Raggers, R.J., Terpstra, P., Woudstra, E.C., Dijkhuizen, L., Meijer, W.G., 1996. Primary structure and phylogeny of the calvin cycle enzymes transketolase and fructosebisphosphate aldolase of *Xanthobacter flavus*. J. Bacteriol. 178, 888–893.

van der Schaft, P.H., de Goede, H., ter Burg, N., 1997. Bakers yeast reduction of 2,3-pentanedion to natural 3-hydroxy-2-pentanone, in: Taylor, A.J., Mottram, D.S. (Eds.), Flavour Science: Recent Developments. Elsevier, pp. 134–137.

Vinogradov, M., Kaplun, A., Vyazmensky, M., Engel, S., Golbik, R., Tittmann, K., Uhlemann, K., Meshalkina, L., Barak, Z., Hübner, G., Chipman, D.M., 2005. Monitoring the acetohydroxy acid synthase reaction and related carboligations by circular dichroism spectroscopy. Anal. Biochem. 342, 126–133.

Vinogradov, V., Vyazmensky, M., Engel, S., Belenky, I., Kaplun, A., Kryukov, O., Barak, Z., Chipman, D.M., 2006. Acetohydroxyacid synthase isozyme I from *Escherichia coli* has unique catalytic and regulatory properties. Biochim. Biophys. Acta - Gen. Subj. 1760, 356–363.

Vogel, C., Pleiss, J., 2014. The modular structure of ThDP-dependent enzymes. Proteins Struct. Funct. Bioinforma. 82, 2523–2537.

Vogel, C., Widmann, M., Pohl, M., Pleiss, J., 2012. A standard numbering scheme for thiamine diphosphate-dependent decarboxylases. BMC Biochem. 13, 24–33.

Vogelstein, B., Gillespie, D., 1979. Preparative and analytical purification of DNA from agarose. Proc. Natl. Acad. Sci. U. S. A. 76, 615–619.

Wachtmeister, J., Jakoblinnert, A., Rother, D., 2016. Stereoselective Two-Step Biocatalysis in Organic Solvent: Toward All Stereoisomers of a 1,2-Diol at High Product Concentrations. Org. Process Res. Dev. 20, 1744–1753.

Weinstock, O., Sella, C., Chipman, D.M., Barak, Z., 1992. Properties of subcloned subunits of bacterial acetohydroxy acid synthases. J. Bacteriol. 174, 5560–6.

Werther, T., Zimmer, A., Wille, G., Golbik, R., Weiss, M.S., König, S., 2010. New insights into structure-function relationships of oxalyl CoA decarboxylase from *Escherichia coli*. FEBS J. 277, 2628–2640.

Westphal, R., 2013. Tailor-made thiamine-diphosphate-dependent enzymes for *S*-selective carboligation - Complementation of the alpha-hydroxy ketone platform (Dissertation). Heinrich-Heine-Universität Düsseldorf.

Westphal, R., Hahn, D., Mackfeld, U., Waltzer, S., Beigi, M., Widmann, M., Vogel, C., Pleiss, J., Müller, M., Rother, D., Pohl, M., 2013a. Tailoring the *S*-Selectivity of 2-Succinyl-5-enolpyruvyl-6-hydroxy-3-cyclohexene-1-carboxylate Synthase (MenD) from *Escherichia coli*. ChemCatChem 5, 3587–3594.

Westphal, R., Jansen, S., Vogel, C., Pleiss, J., Müller, M., Rother, D., Pohl, M., 2014a. MenD from *Bacillus subtilis*: A Potent Catalyst for the Enantiocomplementary Asymmetric Synthesis of Functionalized α-Hydroxy Ketones. ChemCatChem 6, 1082–1088.

Westphal, R., Vogel, C., Schmitz, C., Pleiss, J., Müller, M., Pohl, M., Rother, D., 2014b. A tailor-made chimeric thiamine diphosphate dependent enzyme for the direct asymmetric synthesis of (*S*)-benzoins. Angew. Chemie - Int. Ed. 53, 9376–9379.

Westphal, R., Waltzer, S., Mackfeld, U., Widmann, M., Pleiss, J., Beigi, M., Müller, M., Rother, D., Pohl, M., 2013b. (*S*)-Selective MenD variants from *Escherichia coli* provide access to new functionalized chiral α-hydroxy ketones. Chem. Commun. 49, 2061–2063.

Widmann, M., Radloff, R., Pleiss, J., 2010. The Thiamine diphosphate dependent Enzyme Engineering Database: A tool for the systematic analysis of sequence and structure relations. BMC Biochem. 11, 9.

Wikner, C., Meshalkina, L., Nilsson, U., Bäckström, S., Lindqvist, Y., Schneider, G., 1995. His103 in Yeast Transketolase is Required for Substrate Recognition and Catalysis. Eur. J. Biochem. 233, 750–755.

Wikner, C., Nilsson, U., Meshalkina, L., Udekwu, C., Lindqvist, Y., Schneider, G., 1997. Identification of Catalytically Important Residues in Yeast Transketolase. Biochemistry 36, 15643–15649.

Wilcocks, R., Ward, O.P., 1992. Factors Affecting 2-Hydroxypropiophenone Formation by Benzoylformate Decarboxylase from *Pseudomonas putida*. Biotechnol. Bioeng. 39, 1058–1063.

Williams, R.D., Mason, H.L., Wilder, R.M., Smith, B.F., 1940. Observations on induced thiamine (vitamin b1) deficiency in man. Arch. Intern. Med. 66, 785–799.

Wohlgemuth, R., 2009. C2-Ketol elongation by transketolase-catalyzed asymmetric synthesis. J. Mol. Catal. B Enzym. 61, 23–29.

Wolfenden, R., Snider, M.J., 2001. The Depth of Chemical Time and the Power of Enzymes as Catalysts. Acc. Chem. Res. 34, 938–945.

Woodley, J.M., 2013. Protein engineering of enzymes for process applications. Curr. Opin. Chem. Biol. 17, 310–316.

Yi, D., Devamani, T., Abdoul-Zabar, J., Charmantray, F., Helaine, V., Hecquet, L., Fessner, W.-D., 2012. A pH-Based High-Throughput Assay for Transketolase: Fingerprinting of Substrate Tolerance and Quantitative Kinetics. ChemBioChem 13, 2290–2300.

Yi, D., Saravanan, T., Devamani, T., Charmantray, F., Hecquet, L., Fessner, W.-D., 2015. A thermostable transketolase evolved for aliphatic aldehyde acceptors. Chem. Commun. 51, 480–483.

Zhou, C., Saravanan, T., Lorillière, M., Wei, D., Charmantray, F., Hecquet, L., Fessner, W.-D., Yi, D., 2017. Second-Generation Engineering of a Thermostable Transketolase (TK_{gst}) for Aliphatic Aldehyde Acceptors with Either Improved or Reversed Stereoselectivity. ChemBioChem 18, 455–459.

7 APPENDIX

7.1 Overview over the stereoselectivites and yields with all *Ec*TK variants

Table 7-1: Overview over the stereoselectivities and yields for the formation of 1,3-dihydroxyheptan-2-one (DHH) and 1,3-dihydroxypentan-2-one (DHP) with all *Ec*TK variants investigated in the course of this thesis. The yields are given relative to the yield obtained with wildtype *Ec*TK under the same reactions conditions and refer to the product formed in the course of the reactions as assigned by GC without any product purification. Reaction conditions: 100 mM KP_i-buffer pH 7, 2.4 mM ThDP, 3 mM $MgCl_2$ and 0.9 mg·mL^{-1} *Ec*TK variant. The donor substrate 3-hydroxypyruvate (HPA) and the acceptor substrates n-pentanal and propanal were always used equimolar with final concentrations of 50 mM and 100 mM for n-pentanal and propanal, respectively. Samples were incubated at 25°C for 3 h before analysis via chiral phase GC. Variants highlighted in bold are discussed in detail in chapter 3.2.

***Ec*TK variant**	**DHH-synthesis acceptor: n-pentanal**		**DHP-synthesis acceptor: propanal**	
	***ee*-value**	**rel. yield**	***ee*-value**	**rel. yield**
wildtype	**87 % (*S*)**	**100 %**	**53 % (*S*)**	**100 %**
I189A	**22 % (*S*)**	**37 %**	**1 % (*R*)**	**9 %**
I189G	**48 % (*S*)**	**40 %**	**62 % (*S*)**	**24 %**
I189V	**41 % (*S*)**	**47 %**	**14 % (*S*)**	**7 %**
I189A/H261A	**31 % (*S*)**	**32 %**	**7 % (*S*)**	**20 %**
I189A/H261G	**42 % (*S*)**	**56 %**	**6 % (*S*)**	**8 %**
I189A/H261V	**80 % (*S*)**	**243 %**	**7 % (*S*)**	**20 %**
I189G/H261A	**20 % (*S*)**	**38 %**	**8 % (*S*)**	**8 %**
I189G/H261G	**56 % (*S*)**	**77 %**	**9 % (*S*)**	**8 %**
I189G/H261V	**81 % (*S*)**	**237 %**	**23 % (*S*)**	**19 %**
I189V/H261A	**26 % (*S*)**	**47 %**	**4 % (*R*)**	**20 %**
I189V/H261V	**77 % (*S*)**	**367 %**	**17 % (*S*)**	**72 %**
H26A/I189G/H261V	10 % (*S*)	20 %	34 % (*R*)	9 %
L382A	**97 % (*S*)**	**541 %**	**90 % (*S*)**	**150 %**
I189A/L382A	85 % (*S*)	237 %	67 % (*S*)	16 %
F434A	**33 % (*S*)**	**646 %**	**63 % (*S*)**	**27 %**
F434L	**57 % (*S*)**	**499 %**	**56 % (*S*)**	**143 %**
I189A/F434A	37 % (*S*)	211 %	31 % (*S*)	18 %
I189A/F434L	50 % (*S*)	75 %	13 % (*S*)	17 %
L382A/F434A	**61 % (*S*)**	**507 %**	**27 % (*S*)**	**136 %**
L382A/F434L	**13 % (*S*)**	**387 %**	**10 % (*S*)**	**5 %**
I189A/L382A/F434A	49 % (*R*)	167 %	10 % (*S*)	3 %
I189A/L382A/F434L	38 % (*S*)	70 %	27 % (*R*)	12 %
H26A	**11 % (*R*)**	**351 %**	**71 % (*R*)**	**96 %**
H26W	24 % (*S*)	106 %	3 % (*R*)	16 %
H26Y	**94 % (*R*)**	**154 %**	**95 % (*R*)**	**52 %**
H261A	**62 % (*S*)**	**91 %**	**18 % (*S*)**	**26 %**
H261F	**31 % (*S*)**	**73 %**	**3 % (*S*)**	**20 %**
H261G	**51 % (*S*)**	**73 %**	**9 % (*S*)**	**15 %**
H261L	**52 % (*S*)**	**92 %**	**48 % (*S*)**	**11 %**
H261V	**61 % (*S*)**	**100 %**	**2 % (*R*)**	**36 %**
H26A/H261A	57 % (*S*)	59 %	13 % (*S*)	18 %
H26A/H261F	**9 % (*R*)**	**17 %**	**2 % (*R*)**	**4 %**
H26A/H261L	**23 % (*S*)**	**30 %**	**14 % (*S*)**	**5 %**
H26Y/H261A	**0 %**	**7 %**	**9 % (*S*)**	**2 %**
H26Y/H261F	4 % (*R*)	7 %	6 % (*S*)	5 %
D469E	**92 % (*S*)**	**617 %**	**77 % (*S*)**	**163 %**
H26A/D469E	**44 % (*S*)**	**195 %**	**45 % (*R*)**	**34 %**
H261A/D469E	**74 % (*S*)**	**105 %**	**17 % (*S*)**	**18 %**
H26Y/D469E	18 % (*R*)	64 %	85 % (*R*)	19 %

7.2 Sequences

pMP39-1: *Pseudomonas protegens* YerE (*Pp*YerE) gene (*ilvB*) in pET28a (+) (restriction sites: *Nde*I, *BamH*I)

Gene sequence

ATGGGCAGCAGCCATCATCATCATCATCACAGCAGCGGCCTGGTGCCGCGCGGCAGCCATATGAAAGC
CTCGGATGCAGTAGCAAAAATTCTTGCAGATAATAATGTTCTGTATGGGTTTGAGTTGATTGGTGGAA
TGATTACTCACCTAGTAGATAGTATTAATCTATTAGGTAAGACCAAGTTGGTTTCAATGCACCATGAA
CAAGGCGCCGCCTTTGCTGCATCTGCAGTATCTCGAGTAACCCACCACAAGACTCTGGGGTTAGCCCT
TGCAACCAGCGGCCCTGGTGCGACCAACTTGATCACTGGCATTGCAGACTGCTGGCTTGATAGCCACC
CCTGCATTTTCCTGACAGGTCAAGTCAACACCCATGAGCTAAAAGGCAAAAGGGACATTCGTCAGCAG
GGTTTTCAGGAACTGGATAGCGTAGCCTTGGTCACCAGTATTACCAAATATGCCTATCAGATTAAAAG
CGCAGATGAGTTGGTACCCTGTTTGCGAAAAGCGATCCAGATCGCTAAAGAAGGACGCCCCGGCCCAG
TATTACTTGATATTCCAATGGATATACAAAGAGCAGACATCGACGAAGCCCTGCTCAACAATCCTATG
ACTCCAGAGCCTAAAGTCCAACGCCCTTCAATAGCTATGAGTGATCTGGACTTTATAATAAATAAACT
TCAGAACGCAAAAAAACCACTCCTGCTAATTGGAGGTGGGGCTGTCAACAGTTCAGGCTTTCAGAAGT
GGCTAGAACAGATTGAGCTCAGAGGCATCCCCTATGTAGCCAGCTTAAAGGGGGCCGAAAAAATAAAA
GCCAGCGACCTATACTTGGGAATGCTTGGCGCCTATGGCACTAGGGCAGCCAACCACGCTGTGCAAAA
CTGTGATTTGTTGCTGGTACTGGGAAGTCGAATGGATGTACGTCAGACTGGAGCACAACCAGAAGACT
TCGCTCGGAACGCCGAAATCATTCAGATAGACTTGCAGGAAGGGCAGCTAAACAATCGTGTCATTGCC
GACTTTTCATACCAAATTGAACTGAGCGAGTATTTTTCCCGATTCTCCCCATTGCAAATACCCGTCAA
CAATGACTGGAGCGTCTGGACTGCATTATTGAAAGAGAAGTTCAGAGTAACTTTTATTGACGAATATA
CCACTTGGAACCTCAGCCCCTTTGGCTTGTTCACCCAACTGAATAAACTAACAGAGAGGGTAGCACTG
GATTACATTTTGGATGTAGGCAACAACCAGATGTGGGCTGCACATACATTACGCCTCAACGCCCAACA
AGCCATGCATCACTCTGGCGGCCTGGGCAGCATGGGGTTTGCAATACCTGCTGCAATTGGCGCGTGCT
ACGCAGGAAAGAAGCCAATCATTGTCATTACTGGTGATGGTGGTGCGCAGCTGAATATCCAAGAGTTG
GACATTATCGCAAGAGATAAGCTCCCGATCCTGACAATCGTTATGAATAACCATTCTTTGGGCATGGT
ACGAGGTTTCCAGGAAATGTATTTTGAGGGAAGAAACTCCTCTACTTACTGGAACGGATACACATCAC
AATTCAAAAAAATCGGGGAGGCCTACCGCGTCGAATCAAAAACCATAATAAGTATGCAAGCTTTTAGC
TCTGCACTGGAAAGCTTTCTGGAATCGCCTCGTCCGCTGCTATTGGAAGTATCTATGTCCGATGCTAG
GGAGTGCCGACCAAGACTTGAATATGGCAGGGCCATTGACCAGCAATCACCCCGACACGATGGATAA

Amino acid sequence

MGSSHHHHHHSSGLVPRGSHMKASDAVAKILADNNVLYGFELIGGMITHLVDSINLLGKTKLVSMHHE
QGAAFAASAVSRVTHHKTLGLALATSGPGATNLITGIADCWLDSHPCIFLTGQVNTHELKGKRDIRQQ
GFQELDSVALVTSITKYAYQIKSADELVPCLRKAIQIAKEGRPGPVLLDIPMDIQRADIDEALLNNPM
TPEPKVQRPSIAMSDLDFIINKLQNAKKPLLLIGGGAVNSSGFQKWLEQIELRGIPYVASLKGAEKIK
ASDLYLGMLGAYGTRAANHAVQNCDLLLVLGSRMDVRQTGAQPEDFARNAEIIQIDLQEGQLNNRVIA
DFSYQIELSEYFSRFSPLQIPVNNDWSVWTALLKEKFRVTFIDEYTTWNLSPFGLFTQLNKLTERVAL
DYILDVGNNQMWAAHTLRLNAQQAMHHSGGLGSMGFAIPAAIGACYAGKKPIIVITGDGGAQLNIQEL
DIIARDKLPILTIVMNNHSLGMVRGFQEMYFEGRNSSTYWNGYTSQFKKIGEAYRVESKTIISMQAFS
SALESFLESPRPLLLEVSMSDARECRPRLEYGRAIDQQSPRHDG

Plasmid map

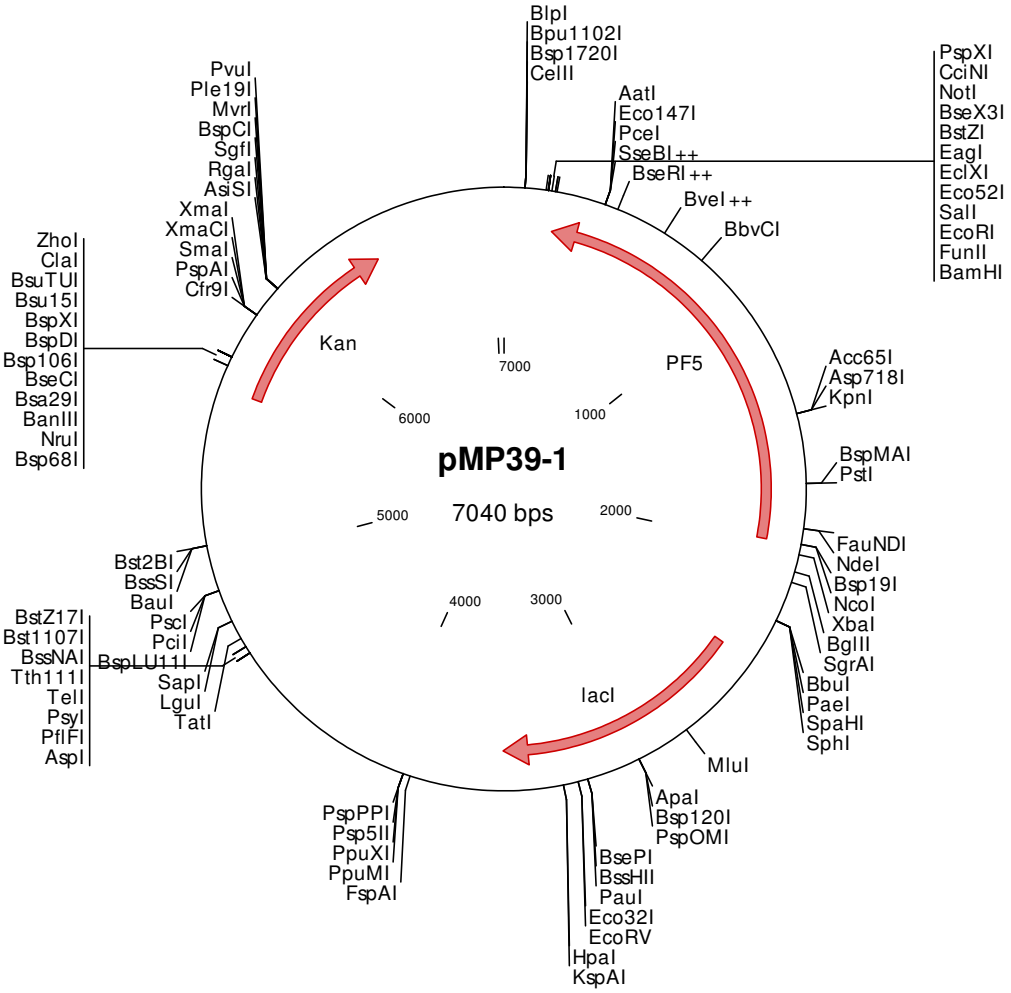

Figure 7-1: Plasmid map of pMP39-1: pET28a(+) vector with the *ilvB* gene encoding for *Pp*YerE inserted via *NdeI* and *BamHI* restriction

Mutagenesis

Table 7-2: Codon exchanges during site directed mutagenesis of *Pp*YerE. Amino acid positions refer to the original *Pp*YerE sequence, codon numbers referee to the open reading frame including the N-terminal His-tag and a linker sequence.

plasmid name	substitutions	codon №	№ of first bp	wt codon	inserted codon
pMP39-1	none (wt)	-	-	-	-
pMP39-2	V479G	499	1495	GTA	GGC
pMP39-3	V479A	499	1495	GTA	GCG
pMP39-4	Q483X	503	1507	CAG	NDT
	T494X	514	1540	ACT	NDT
pMP39-5	deletion ΔM478-S493	Δ498-513	Δ1492-1539	-	-
pMP39-6	L476G	496	1486	TTG	GGC
pMP39-7	L476G	496	1486	TTG	GGC
	V479G	499	1495	GTA	GGC
pMP39-8	L476G	496	1486	TTG	GGC
	V479A	499	1495	GTA	GCG
pMP39-9	L476A	496	1486	TTG	GCG
pMP39-10	L476A	496	1486	TTG	GCG
	V479G	499	1495	GTA	GGC

plasmid name	substitutions	codon №	№ of first bp	wt codon	inserted codon
pMP39-11	L476A	496	1486	TTG	GCG
	V479A	499	1495	GTA	GCG
pMP39-12	I23G	43	127	ATT	GGT
pMP39-13	I23G	43	127	ATT	GGT
	V479G	499	1495	GTA	GGC
pMP39-14	I23G	43	127	ATT	GGT
	V479A	499	1495	GTA	GCG
pMP39-15	I23G	43	127	ATT	GGT
	L476G	496	1486	TTG	GGC
pMP39-16	I23G	43	127	ATT	GGT
	L476G	496	1486	TTG	GGC
	V479G	499	1495	GTA	GGC
pMP39-17	I23G	43	127	ATT	GGT
	L476G	496	1486	TTG	GGC
	V479A	499	1495	GTA	GCG
pMP39-18	I23G	43	127	ATT	GGT
	L476A	496	1486	TTG	GCG
pMP39-19	I23G	43	127	ATT	GGT
	L476A	496	1486	TTG	GCG
	V479G	499	1495	GTA	GGC
pMP39-20	I23G	43	127	ATT	GGT
	L476A	496	1486	TTG	GCG
	V479A	499	1495	GTA	GCG
pMP39-21	I23A	43	127	ATT	GCT
pMP39-22	I23A	43	127	ATT	GCT
	V479G	499	1495	GTA	GGC
pMP39-23	I23A	43	127	ATT	GCT
	V479A	499	1495	GTA	GCG
pMP39-24	I23A	43	127	ATT	GCT
	L476G	496	1486	TTG	GGC
pMP39-25	I23A	43	127	ATT	GCT
	L476G	496	1486	TTG	GGC
	V479G	499	1495	GTA	GGC
pMP39-26	I23A	43	127	ATT	GCT
	L476G	496	1486	TTG	GGC
	V479A	499	1495	GTA	GCG
pMP39-27	I23A	43	127	ATT	GCT
	L476A	496	1486	GTA	GCG
pMP39-28	I23A	43	127	ATT	GCT
	L476A	496	1486	TTG	GCG
	V479G	499	1495	GTA	GGC
pMP39-29	I23A	43	127	ATT	GCT
	L476A	496	1486	TTG	GCG
	V479A	499	1495	GTA	GCG

pMP32-1: *Escherichia coli* transketolase (*Ec*TK) gene (*tktA*) in pET22b (+) (restriction sites: *Nde*I, *Xho*I)

Gene Sequence

ATGTCCTCACGTAAAGAGCTTGCCAATGCTATTCGTGCGCTGAGCATGGACGCAGTACAGAAAGCCAA
ATCCGGTCACCCGGGTGCCCCTATGGGTATGGCTGACATTGCCGAAGTCCTGTGGCGTGATTTCCTGA
AACACAACCCGCAGAATCCGTCCTGGGCTGACCGTGACCGCTTCGTGCTGTCCAACGGCCACGGCTCC
ATGCTGATCTACAGCCTGCTGCACCTCACCGGTTACGATCTGCCGATGGAAGAACTGAAAAACTTCCG
TCAGCTGCACTCTAAAACTCCGGGTCACCCGGAAGTGGGTTACACCGCTGGTGTGGAAACCACCACCG
GTCCGCTGGGTCAGGGTATTGCCAACGCAGTCGGTATGGCGATTGCAGAAAAAACGCTGGCGGCGCAG
TTTAACCGTCCGGGCCACGACATTGTCGACCACTACACCTACGCCTTCATGGGCGACGGCTGCATGAT
GGAAGGCATCTCCCACGAAGTTTGCTCTCTGGCGGGTACGCTGAAGCTGGGTAAACTGATTGCATTCT
ACGATGACAACGGTATTTCTATCGATGGTCACGTTGAAGGCTGGTTCACCGACGACACCGCAATGCGT
TTCGAAGCTTACGGCTGGCACGTTATTCGCGACATCGACGGTCATGACGCGGCATCTATCAAACGCGC
AGTAGAAGAAGCGCGCGCAGTGACTGACAAACCTTCCCTGCTGATGTGCAAAACCATCATCGGTTTCG
GTTCCCCGAACAAAGCCGGTACCCACGACTCCCACGGTGCGCCGCTGGGCGACGCTGAAATTGCCCTG
ACCCGCGAACAACTGGGCTGGAAATATGCGCCGTTCGAAATCCCGTCTGAAATCTATGCTCAGTGGGA
TGCGAAAGAAGCAGGCCAGGCGAAAGAATCCGCATGGAACGAGAAATTCGCTGCTTACGCGAAAGCTT
ATCCGCAGGAAGCCGCTGAATTTACCCGCCGTATGAAAGGCGAAATGCCGTCTGACTTCGACGCTAAA
GCGAAAGAGTTCATCGCTAAACTGCAGGCTAATCCGGCGAAAATCGCCAGCCGTAAAGCGTCTCAGAA
TGCTATCGAAGCGTTCGGTCCGCTGTTGCCGGAATTCCTCGGCGGTTCTGCTGACCTGGCGCCGTCTA
ACCTGACCCTGTGGTCTGGTTCTAAAGCAATCAACGAAGATGCTGCGGGTAACTACATCCACTACGGT
GTTCGCGAGTTCGGTATGACCGCGATTGCTAACGGTATCTCCCTGCACGGTGGCTTCCTGCCGTACAC
CTCCACCTTCCTGATGTTCGTGGAATACGCACGTAACGCCGTACGTATGGCTGCGCTGATGAAACAGC
GTCAGGTGATGGTTTACACCCACGACTCCATCGGTCTGGGCGAAGACGGCCCGACTCACCAGCCGGTT
GAGCAGGTCGCTTCTCTGCGCGTAACCCCGAACATGTCTACATGGCGTCCGTGTGACCAGGTTGAATC
CGCGGTCGCGTGGAAATACGGTGTTGAGCGTCAGGACGGCCCGACCGCACTGATCCTCTCCCGTCAGA
ACCTGGCGCAGCAGGAACGAACTGAAGAGCAACTGGCAAACATCGCGCGCGGTGGTTATGTGCTGAAA
GACTGCGCCGGTCAGCCGGAACTGATTTTCATCGCTACCGGTTCAGAAGTTGAACTGGCTGTTGCTGC
CTACGAAAAACTGACTGCCGAAGGCGTGAAAGCGCGCGTGGTGTCCATGCCGTCTACCGACGCATTTG
ACAAGCAGGATGCTGCTTACCGTGAATCCGTACTGCCGAAAGCGGTTACTGCACGCGTTGCTGTAGAA
GCGGGTATTGCTGACTACTGGTACAAGTATGTTGGCCTGAACGGTGCTATCGTCGGTATGACCACCTT
CGGTGAATCTGCTCCGGCAGAGCTGCTGTTTGAAGAGTTCGGCTTCACTGTTGATAACGTTGTTGCGA
AAGCAAAAGAACTGCTGCTCGAGCACCACCACCACCACCACTGA

Amino acid sequence

MSSRKELANAIRALSMDAVQKAKSGHPGAPMGMADIAEVLWRDFLKHNPQNPSWADRDRFVLSNGHGS
MLIYSLLHLTGYDLPMEELKNFRQLHSKTPGHPEVGYTAGVETTTGPLGQGIANAVGMAIAEKTLAAQ
FNRPGHDIVDHYTYAFMGDGCMMEGISHEVCSLAGTLKLGKLIAFYDDNGISIDGHVEGWFTDDTAMR
FEAYGWHVIRDIDGHDAASIKRAVEEARAVTDKPSLLMCKTIIGFGSPNKAGTHDSHGAPLGDAEIAL
TREQLGWKYAPFEIPSEIYAQWDAKEAGQAKESAWNEKFAAYAKAYPQEAAEFTRRMKGEMPSDFDAK
AKEFIAKLQANPAKIASRKASQNAIEAFGPLLPEFLGGSADLAPSNLTLWSGSKAINEDAAGNYIHYG
VREFGMTAIANGISLHGGFLPYTSTFLMFVEYARNAVRMAALMKQRQVMVYTHDSIGLGEDGPTHQPV
EQVASLRVTPNMSTWRPCDQVESAVAWKYGVERQDGPTALILSRQNLAQQERTEEQLANIARGGYVLK
DCAGQPELIFIATGSEVELAVAAYEKLTAEGVKARVVSMPSTDAFDKQDAAYRESVLPKAVTARVAVE
AGIADYWYKYVGLNGAIVGMTTFGESAPAELLFEEFGFTVDNVVAKAKELLLEHHHHHH

Plasmid map

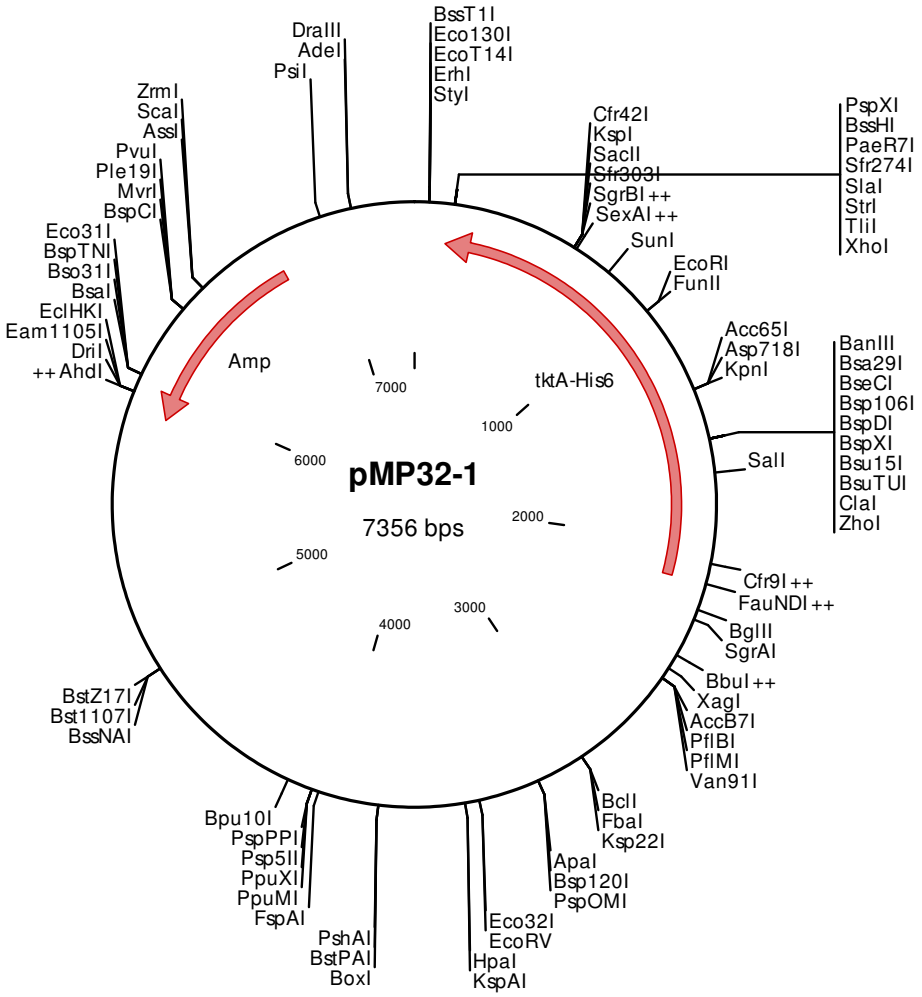

Figure 7-2: Plasmid map of pMP32-1: pET22b(+) vector with the *tktA* gene encoding for *Ec*TK inserted via *NdeI* and *XhoI* restriction

Mutagenesis

Table 7-3:Codon exchanges during site directed mutagenesis of *Ec*TK.

plasmid name	substitutions	codon №	№ of first bp	wt codon	inserted codon
pMP32-1	none (wt)	-	-	-	-
pMP32-2	I189G	189	565	ATC	GGC
pMP32-3	I189G	189	565	ATC	GGC
	H261V	261	781	CAC	GTT
pMP32-4	H26A	26	76	CAC	GCG
pMP32-5	H26Y	26	76	CAC	TAT
pMP32-7	H261A	261	781	CAC	GCG
pMP32-8	D469E	469	1405	GAC	GAA
pMP32-9	H26A	261	76	CAC	GCG
	D469E	469	1405	GAC	GAA
pMP32-10	H26A	26	76	CAC	GCG
	H261A	261	781	CAC	GCG
pMP32-11	H26Y	26	76	CAC	TAT
	H261A	261	781	CAC	GCG

plasmid name	substitutions	codon №	№ of first bp	wt codon	inserted codon
pMP32-12	H261A	26	781	CAC	GCG
	D469E	469	1405	GAC	GAA
pMP32-13	H26A	26	76	CAC	GCG
	H261A	261	781	CAC	GCG
	D469E	469	1405	GAC	GAA
pMP32-14	H26Y	26	76	CAC	TAT
	H261S	261	781	CAC	TCG
pMP32-15	H261S	261	781	CAC	TCG
	D469E	469	1405	GAC	GAA
pMP32-16	H26A	26	76	CAC	GCG
	H261S	261	781	CAC	TCG
	D469E	469	1405	GAC	GAA
pMP32-17	H261S	261	781	CAC	TCG
pMP32-18	F434A	434	1300	TTC	GCC
pMP32-19	H261L	261	781	CAC	CTG
pMP32-20	H261F	261	781	CAC	TTT
pMP32-21	H26A	26	76	CAC	GCG
	H261L	261	781	CAC	CTG
pMP32-22	H26A	26	76	CAC	GCG
	H261F	261	781	CAC	TTT
pMP32-23	I189A	189	565	ATC	GCG
pMP32-24	I189V	189	565	ATC	GTG
pMP32-25	I189G	189	565	ATC	GGC
	H261A	261	781	CAC	GCG
pMP32-26	I189A	189	565	ATC	GCG
	H261A	261	781	CAC	GCG
pMP32-27	I189V	189	565	ATC	GTG
	H261A	261	781	CAC	GCG
pMP32-28	H261V	261	781	CAC	GTT
pMP32-29	I189A	189	565	ATC	GCG
	H261V	261	781	CAC	GTT
pMP32-30	I189V	189	565	ATC	GTG
	H261V	261	781	CAC	GTT
pMP32-31	H261G	261	781	CAC	GGC
pMP32-32	I189G	189	565	ATC	GGC
	H261G	261	781	CAC	GGC
pMP32-33	I189A	189	565	ATC	GCG
	H261G	261	781	CAC	GGC
pMP32-34	I189V	189	565	ATC	GTG
	H261G	261	781	CAC	GGC
pMP32-35	H26Y	26	76	CAC	TAT
	H261F	261	781	CAC	TTT
pMP32-36	H26A	26	76	CAC	GCG
	I189G	189	565	ATC	GGC
	H261V	261	781	CAC	GTT

plasmid name	substitutions	codon №	№ of first bp	wt codon	inserted codon
pMP32-37	H26Y	26	76	CAC	TAT
	D469E	469	1405	GAC	GAA
pMP32-38	I189A	189	565	ATC	GCG
	F434A	434	1300	TTC	GCC
pMP32-39	H26W	26	76	CAC	TGG
pMP32-40	L382A	382	1144	CTG	GCA
pMP32-41	I189A	189	565	ATC	GCG
	L382A	382	1144	CTG	GCA
pMP32-42	F434L	434	1300	TTC	CTG
pMP32-43	I189A	189	565	ATC	GCG
	L382A	382	1144	CTG	GCA
	F434A	434	1300	TTC	GCC
pMP32-44	L382A	382	1144	CTG	GCA
	F434L	434	1300	TTC	CTG
pMP32-45	I189A	189	565	ATC	GCG
	F434L	434	1300	TTC	CTG
pMP32-46	I189A	189	565	ATC	GCG
	L382A	382	1144	CTG	GCA
	F434L	434	1300	TTC	CTG
pMP32-47	L382A	382	1144	CTG	GCA
	F434A	434	1300	TTC	GCC

pMP03.1_RW1: *Pseudomonas fluorescens* benzaldehyde lyase (*Pf*BAL) gene (*bznB*) in pET28a (+) (restriction sites: *Nco*I, *Xho*I)

Gene sequence

ATGGCGATGATTACAGGCGGCGAACTGGTTGTTCGCACCCTAATAAAGGCTGGGGTCGAACATCTGTT
CGGCCTGCACGGCGCGCATATCGATACGATTTTTCAAGCCTGTCTCGATCATGATGTGCCGATCATCG
ACACCCGCCATGAGGCCGCCGCAGGGCATGCGGCCGAGGGCTATGCCCGCGCTGGCGCCAAGCTGGGC
GTGGCGCTGGTCACGGCGGGCGGGGGATTTACCAATGCGGTCACGCCCATTGCCAACGCTTGGCTGGA
TCGCACGCCGGTGCTCTTCCTCACCGGATCGGGCGCGCTGCGTGATGATGAAACCAACACGTTGCAGG
CGGGGATTGATCAGGTCGCGATGGCGGCGCCCATTACCAAATGGGCGCATCGGGTGATGGCAACCGAG
CATATCCCACGGCTGGTGATGCAGGCGATCCGCGCCGCGTTGAGCGCGCCACGCGGGCCGGTGTTGCT
GGATCTGCCGTGGGATATTCTGATGAACCAGATTGATGAGGATAGCGTCATTATCCCCGATCTGGTCT
TGTCCGCGCATGGGGCCAGACCCGACCCTGCCGATCTGGATCAGGCTCTCGCGCTTTTGCGCAAGGCG
GAGCGGCCGGTCATCGTGCTCGGCTCAGAAGCCTCGCGGACAGCGCGCAAGACGGCGCTTAGCGCCTT
CGTGGCGGCGACTGGCGTGCCGGTGTTTGCCGATTATGAAGGGCTAAGCATGCTCTCGGGGCTGCCCG
ATGCTATGCGGGGCGGGCTGGTGCAAAACCTCTATTCTTTTGCCAAAGCCGATGCCGCGCCAGATCTC
GTGCTGATGCTGGGGGCGCGCTTTGGCCTTAACACCGGGCATGGATCTGGGCAGTTGATCCCCCATAG
CGCGCAGGTCATTCAGGTCGACCCTGATGCCTGCGAGCTGGGACGCCTGCAGGGCATCGCTCTGGGCA
TTGTGGCCGATGTGGGTGGGACCATCGAGGCTTTGGCGCAGGCCACCGCGCAAGATGCGGCTTGGCCG
GATCGCGGCGACTGGTGCGCCAAAGTGACGGATCTGGCGCAAGAGCGCTATGCCAGCATCGCTGCGAA
ATCGAGCAGCGAGCATGCGCTCCACCCCTTTCACGCCTCGCAGGTCATTGCCAAACACGTCGATGCAG
GGGTGACGGTGGTAGCGGATGGTGCGCTGACCTATCTCTGGCTGTCCGAAGTGATGAGCCGCGTGAAA
CCCGGCGGTTTTCTCTGCCACGGCTATCTAGGCTCGATGGGCGTGGGCTTCGGCACGGCGCTGGGCGC
GCAAGTGGCCGATCTTGAAGCAGGCCGCCGCACGATCCTTGTGACCGGCGATGGCTCGGTGGGCTATA
GCATCGGTGAATTTGATACGCTGGTGCGCAAACAATTGCCGCTGATCGTCATCATCATGAACAACCAA
AGCTGGGGGGCGACATTGCATTTCCAGCAATTGGCCGTCGGCCCCAATCGCGTGACGGGCACCCGTTT
GGAAAATGGCTCCTATCACGGGGTGGCCGCCGCCTTTGGCGCGGATGGCTATCATGTCGACAGTGTGG
AGAGCTTTTCTGCGGCTCTGGCCCAAGCGCTCGCCCATAATCGCCCCGCCTGCATCAATGTCGCGGTC
GCGCTCGATCCGATCCCGCCCGAAGAACTCATTCTGATCGGCATGGACCCCTTCGCACTCGAGCACCA
CCACCACCACCACTGA

Amino acid sequence

MAMITGGELVVRTLIKAGVEHLFGLHGAHIDTIFQACLDHDVPIIDTRHEAAAGHAAEGYARAGAKLG
VALVTAGGGFTNAVTPIANAWLDRTPVLFLTGSGALRDDETNTLQAGIDQVAMAAPITKWAHRVMATE
HIPRLVMQAIRAALSAPRGPVLLDLPWDILMNQIDEDSVIIPDLVLSAHGARPDPADLDQALALLRKA
ERPVIVLGSEASRTARKTALSAFVAATGVPVFADYEGLSMLSGLPDAMRGGLVQNLYSFAKADAAPDL
VLMLGARFGLNTGHGSGQLIPHSAQVIQVDPDACELGRLQGIALGIVADVGGTIEALAQATAQDAAWP
DRGDWCAKVTDLAQERYASIAAKSSSEHALHPFHASQVIAKHVDAGVTVVADGALTYLWLSEVMSRVK
PGGFLCHGYLGSMGVGFGTALGAQVADLEAGRRTILVTGDGSVGYSIGEFDTLVRKQLPLIVIIMNNQ
SWGATLHFQQLAVGPNRVTGTRLENGSYHGVAAAFGADGYHVDSVESFSAALAQALAHNRPACINVAV
ALDPIPPEELILIGMDPFALEHHHHHH

Plasmid map

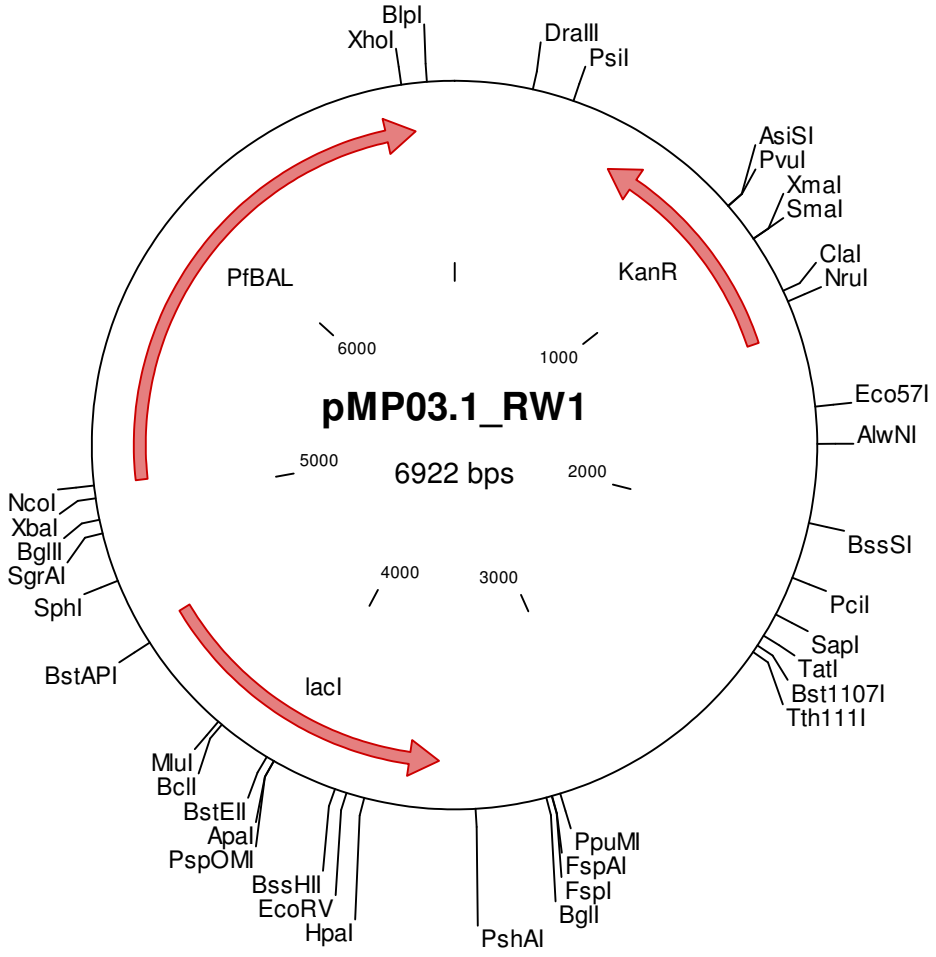

Figure 7-3: Plasmid map of pMP03.1_RW1: pET28a(+) vector with the *bznB* gene encoding for *Pf*BAL inserted via *NcoI* and *XhoI* restriction

Mutagenesis

Table 7-4: Codon exchanges during site directed mutagenesis of *Pf*BAL

plasmid name	substitutions	codon №	№ of first bp	wt Codon	inserted codon
pMP03.1_RW1	none (wt)	-	-	-	-
pMP03.1_ABa1	A480H	480	1438	GCG	CAT
pMP03.1_ABa2	H29F	29	85	CAT	TTT
pMP03.1_ABa2	H29F	29	85	CAT	TTT
	H480A	480	1438	GCG	CAT

7.3 NMR-Spectra

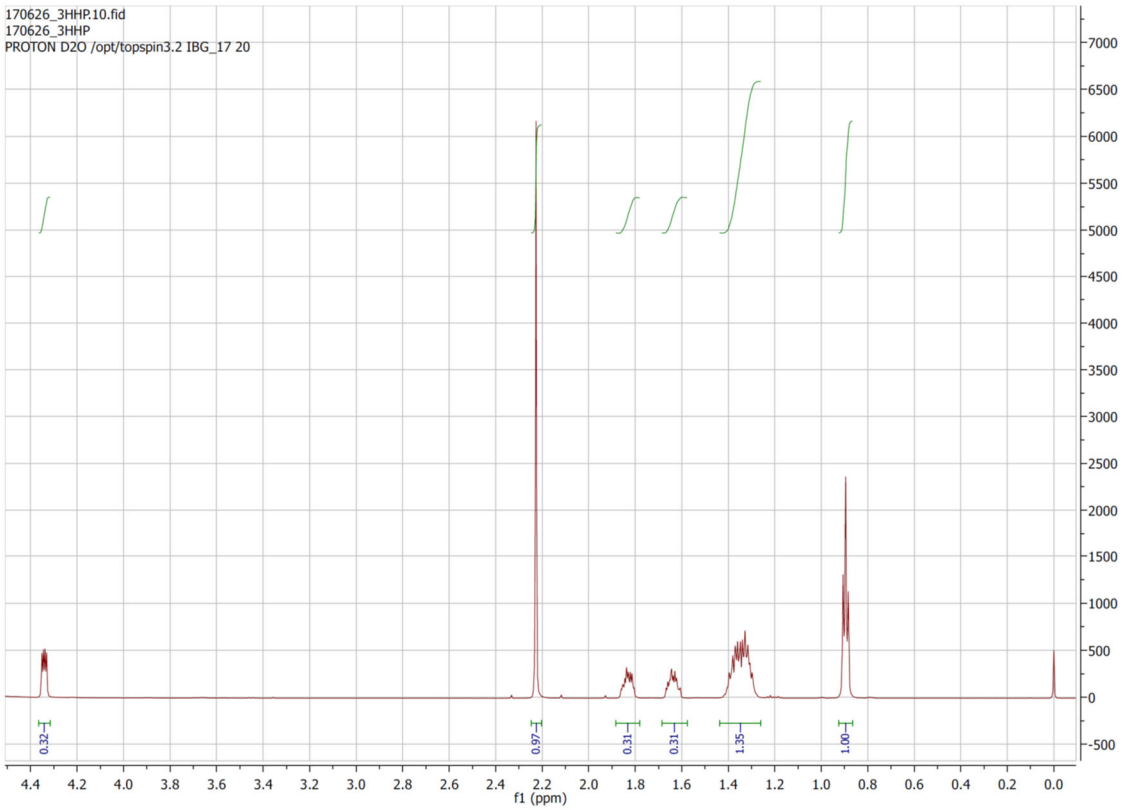

Figure 7-4: ^{1}H-NMR of 3-hydroxyheptan-2-one (3-HH) produced with wildtype *Pp*YerE as described in chapter 5.4.4. Spectra were recorded in D_2O on an Advance DRX instrument (Bruker) operating at 600 MHz

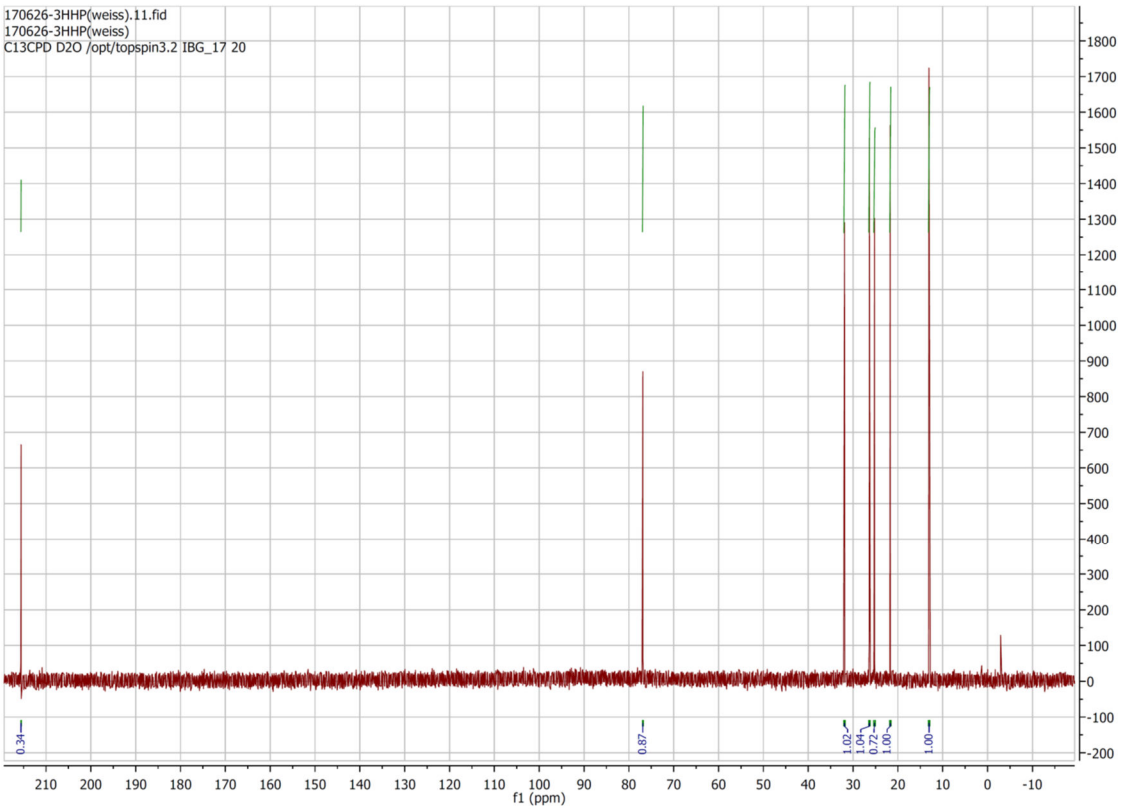

Figure 7-5: ^{13}C-NMR of 3-hydroxyheptan-2-one (3-HH) produced with wildtype *Pp*YerE as described in chapter 5.4.4. Spectra were recorded in D^2O on an Advance DRX instrument (Bruker) operating at 150 MHz

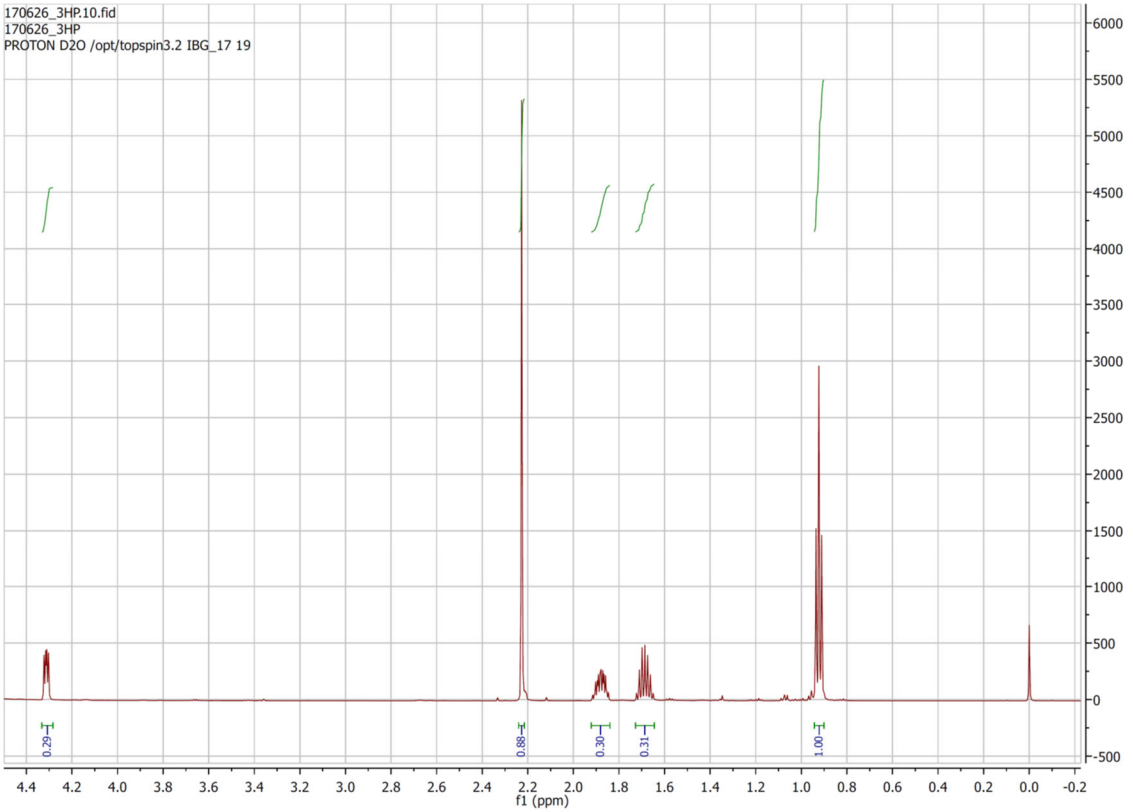

Figure 7-6: ^{1}H-NMR of 3-hydroxypentan-2-one (3-HP) produced with wildtype *Pp*YerE as described in chapter 5.4.4. Spectra were recorded in D_2O on an Advance DRX instrument (Bruker) operating at 600 MHz

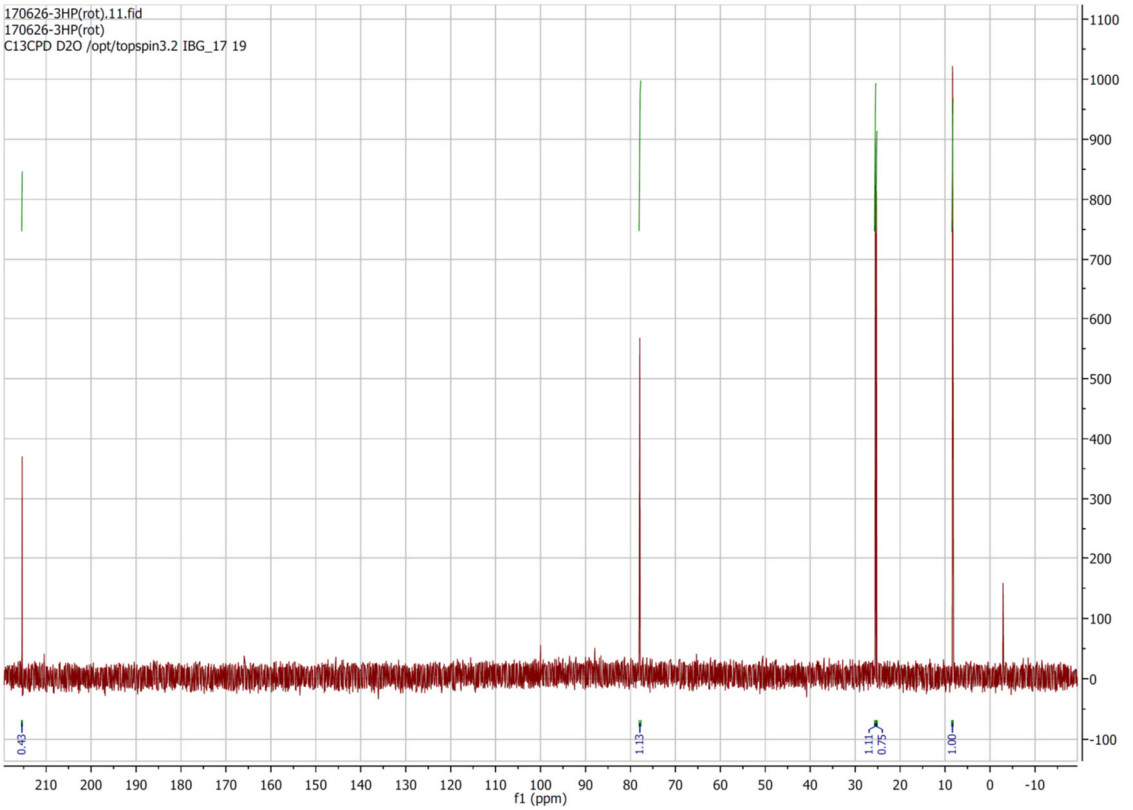

Figure 7-7: ^{13}C-NMR of 3-hydroxypentan-2-one (3-HP) produced with wildtype *Pp*YerE as described in chapter 5.4.4 Spectra were recorded in D_2O on an Advance DRX instrument (Bruker) operating at 150 MHz

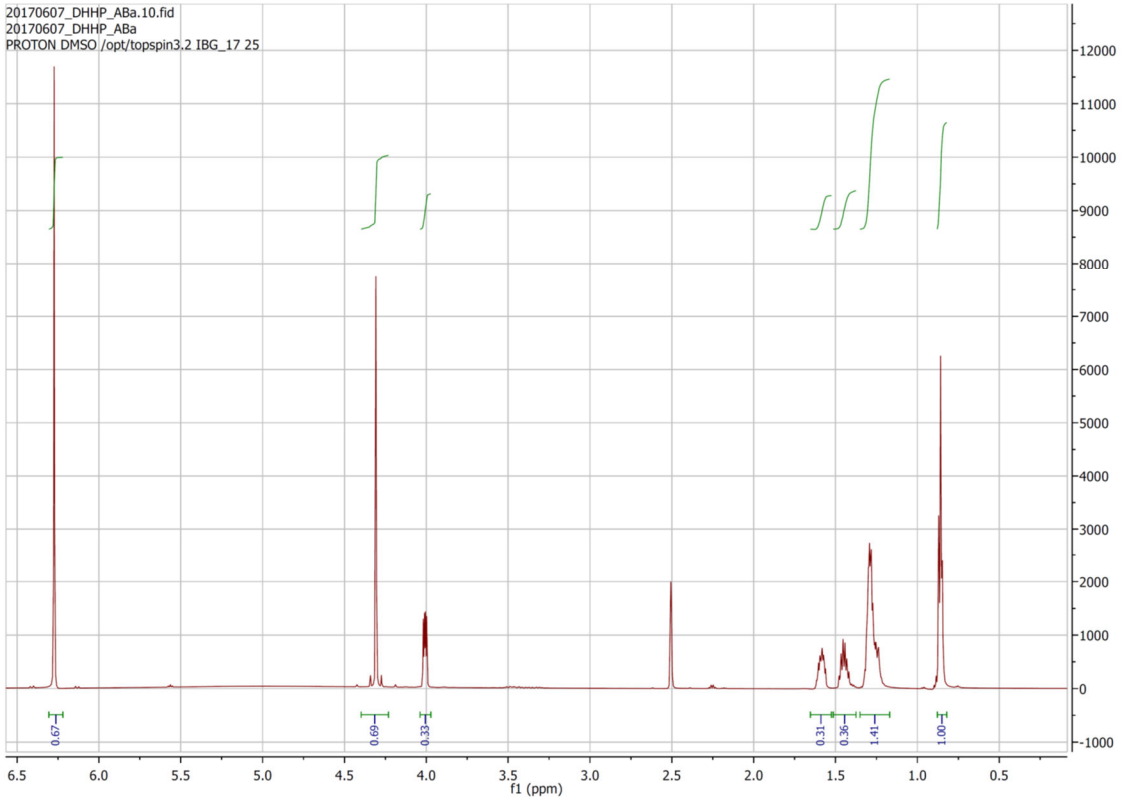

Figure 7-8: ^{1}H-NMR spectrum of 1,3-dihydroxy-2-heptanone (DHH) with maleic acid as internal standard. DHH was synthesised as described in chapter 5.5. Spectra were recorded in DMSO on an Advance DRX instrument (Bruker) operating at 600 MHz.

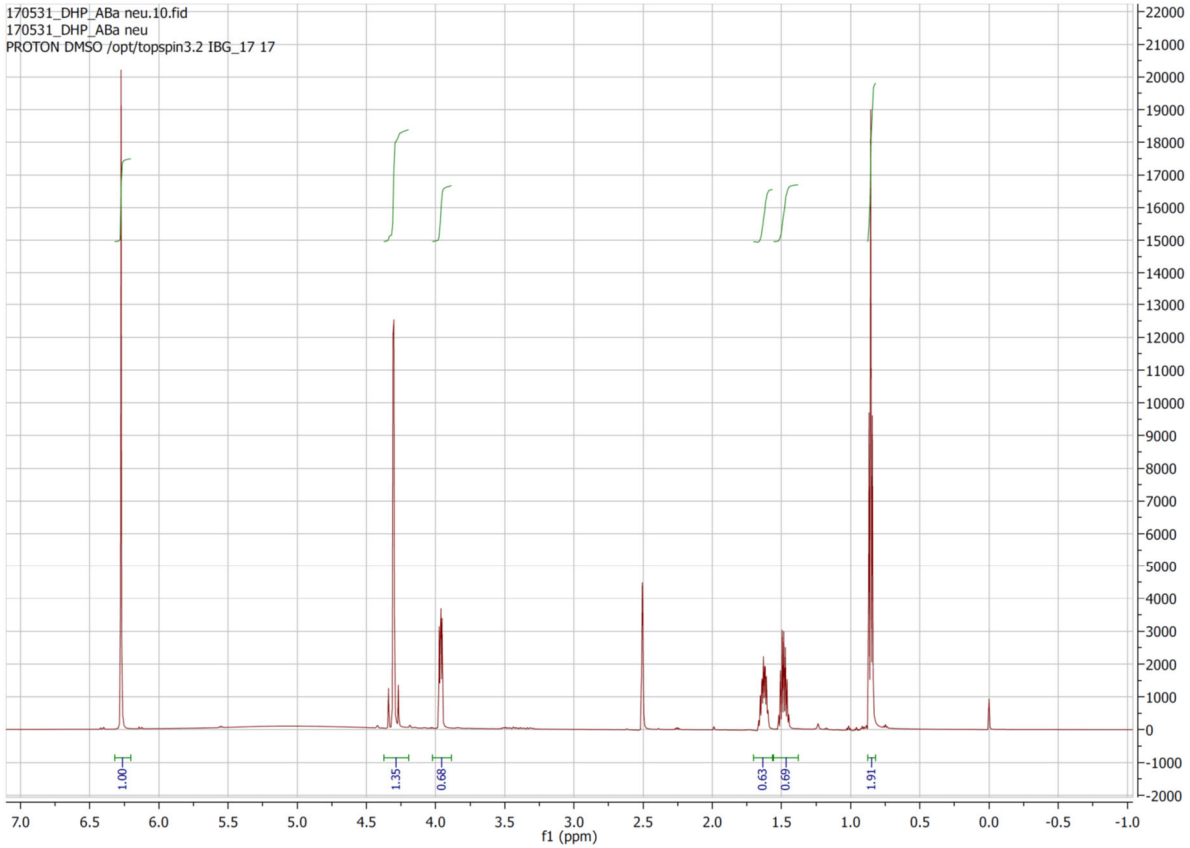

Figure 7-9: ^{1}H-NMR spectrum of 1,3-dihydroxypentan-2-one (DHP) with maleic acid as internal standard. DHP was synthesised as described in chapter 5.5. Spectra were recorded in DMSO on an Advance DRX instrument (Bruker) operating at 600 MHz.

7.4 Publications

Baierl, A., Theorell, A., Mackfeld, U., Marquardt, P., Hoffmann, F., Moers, S., Nöh, K., Buchholz, P.C.F., Pleiss, J., Pohl, M., 2018. Towards a Mechanistic Understanding of Factors Controlling the Stereoselectivity of Transketolase. ChemCatChem. doi:10.1002/cctc.201800299

Own contribution:

I planned, conducted, and analysed experiments regarding the evaluation of the stereoselectivity model for transketolases, which I developed in the course of this thesis based on an existing model for ThDP-dependent decarboxylases, and wrote the manuscript. The experiments included the design, production, and purification of the *Ec*TK variants, the characterisation of the respective variants in biotransformations, and the analysis of the reaction products. Further, I supervised the students P. Marquardt, F. Hoffmann, and S. Moers, who supported the project in the course of their master theses.

Loschonsky, S., Steitz, J. P., Baierl, A., Wiesli, L., Richter, M., Pohl, M., Schneider, G., Dobritzsch, D., Müller, M. Structural and mutagenesis studies of the thiamine-dependent, ketone-accepting YerE from *Pseudomonas protegens*, submitted to ChemBioChem

Own contribution:

I conducted the mutagenesis studies, including the design, production, and purification of *Pp*YerE variants, the characterisation of the respective variants in biotransformations, and the analysis of the reaction products, and wrote the respective chapters in the manuscript.

7.5 Conference contributions

Poster: Westphal, R., Vogel, C., Baierl, A. (presenting author), Pleiss, J., Müller, M. Pohl, M., Rother, D. (2014) A tailor-made pyruvate decarboxylase for the direct asymmetric synthesis of (*S*)-benzoins, *The 8th International Conference on Thiamine: From Catalysis to Pathology, Liege, Belgium, 23 May 2014 - 26 May 2014*

Poster: Baierl, A., Marquardt, P., Vogel, C., Pleiss, J., Hailes, H., Müller, M., Pohl, M. (2015) Investigations on the structural basis of transketolase stereoselectivity, *Biotrans 2015, Wien, Austria, 26 Jul 2015 - 30 Jul 2015*

Talk: Pohl, M. (presenting author), Rother, D., Westphal, R., Baierl, A., Vogel, C., Pleiss, J., Müller, M. (2015) Tailored Enantiocomplementary Carboligases, *Biotrans 2015, Wien, Österreich, 26 Jul 2015 - 30 Jul 2015*

Poster: Baierl, A., Hoffmann, F., Fademrecht, S., Pleiss, J., Hailes, H., Müller, M., Pohl, M. (2016) Structure-function-relationship of ThDP-dependent enzymes: investigations on regio- and stereoselectivity, *Gordon Research Conference "Biocatalysis", Biddeford, ME, USA, 10 Jul 2016 - 15 Jul 2016*

Poster: Baierl, A., Hoffmann, F., Fademrecht, S., Pleiss, J., Hailes, H., Müller, M., Pohl, M. (2016) Structure-function studies on the chemo- and stereoselectivity of ThDP-dependent enzymes, *ProcessNet 2016, Aachen, Germany, 12 Sep 2016 - 15 Sep 2016*

7.6 List of Figures

7.7 List of Tables